Incorporation of Nickel into Synthetic Goethites and the Stabilisation of Mineral Precursor Phases - Implications for Natural Systems

by

Rachel L Norman

Doctoral Thesis

Submitted in partial fulfilment of the requirements
for the award of
Doctor of Philosophy of Loughborough University

April 2014

Abstract

Over 70% of the Earth's economically recoverable nickel (Ni) resides in laterite ore deposits, however they account for less than half of the current global nickel production. During laterization, nickel and other soluble ions are taken into solution before re-precipitating within iron oxide minerals in the limonite zone, or as serpentines and other phyllosilicates in the layers below this zone. It is these laterite deposits that show the greatest potential for low energy, environmentally conscious processing.

The major host of nickel in the limonite zone is the iron-oxyhydroxide mineral goethite, α-FeOOH, where up to 4 mol% Ni has been reported in natural specimens, and even higher levels in synthetic samples (5.5 mol%). The Ni is assumed to be incorporated in the crystal structure of the goethite, but previous characterisation work only demonstrated a weak to moderate correlation of mineral structure change with the nickel content in goethite.

Mining companies working on the extraction and recovery of nickel from the limonite zone of lateritic deposits have noticed that the ease with which nickel can be extracted varies greatly; goethite rich ores that appear to have similar mineralogies/geologies can display extreme variation in their leachability. It is not clear why the ores behave in this way, but in order for extraction techniques and subsequent recovery of nickel to be improved, the reasons behind this variability need to be understood.

The lateritic ore materials from which nickel is extracted are generally made up of a number of different mineral phases. The multiphase nature of the samples means that characterisation of the goethite-type phases from these materials is challenging. To simplify the system and allow the association of Ni into goethite and/or other iron oxyhydroxide phases to be studied in a controlled environment, a synthetic study was carried out. Ni-bearing goethites have been synthesised at a series of different temperatures and characterised by a range of analytical techniques including PXRD, IR, Raman, TGA, ICP-OES, SEM and TEM. It was found that a second phase, ferrihydrite, co-existed with the goethites, the proportion of which increased at lower synthesis temperatures and with increasing amounts of Ni.

Ferrihydrite is known to be a precursor phase in the formation of goethite, but its poorly crystalline nature makes it difficult to identify using standard characterisation techniques such as PXRD. The introduction of Ni to the system increases the stability of the ferrihydrite phase, inhibiting its transformation to goethite. It is believed that some of the Ni thought to be incorporated into goethite could actually reside in an undetected

ferrihydrite phase, which could account for the differences observed in the leachability of natural materials. Characterisation techniques were investigated to try and determine a simple way to identify ferrihydrite in these systems, which could ideally be used in the field to identify the presence of ferrihydrite in goethite rich ore materials. Thermal analysis proved to be particularly promising as a technique which could be used to identify ferrihydrite rich deposits before extraction, enabling the most efficient and environmentally conscious metal recovery process for each deposit to be identified.

In order to investigate the way in which Ni partitions itself between structural incorporation into goethite and association with a secondary ferrihydrite phase, a new washing technique was developed using EDTA, which is capable of selectively removing the ferrihydrite phase whilst leaving the goethite intact. This investigation suggests that a maximum of ~2.5 mol% of Ni is structurally incorporated into goethite, regardless of how much is added during the synthesis. Any excess nickel, above that which is substituted into the goethite structure, was found to be associated with the poorly crystalline ferrihydrite phase.

Despite being considered a metastable phase, the increased stability of ferrihydrite resulting from the presence of Ni suggests that it may persist in laterite deposits within geological systems. If ferrihydrite is indeed present in nickeliferous laterites, it may be a significant host for Ni, and potentially many other critical elements. Based on the methodology developed whilst studying synthetic samples, a characterisation program for materials from lateritic ore deposits was conducted to investigate the presence of ferrihydrite in natural systems.

From the research presented and discussed in this thesis, proof of the presence or absence of ferrihydrite in laterite systems, causing variations in the leachability of the ore materials, could not be conclusively established. The thermal analysis technique developed here successfully identified and quantified ferrihydrite in the presence of goethite in synthetic systems, and showed great potential when used to characterise the lateritic goethite samples, certainly suggesting that ferrihydrite could be present in these natural ore materials. With further refinement of the methodology, to enable a larger range of sample types to be accurately analysed, TGA is a technique which could be used as a screening tool for laterite ores.

Acknowledgements

I would like to begin by thanking Loughborough University, the Natural History Museum and European Nickel for funding and running this PhD research project. Particular thanks go to my supervisors from the Natural History Museum, Paul Schofield and Richard Herrington, for their helpful insight and support, and Sandie Dann for all of her assistance and encouragement at Loughborough University.

I would like to thank all of the friends I have made along the way in the Chemistry Department – especially Rob, Joe, Andy, James, Tom, Simon, Chris, Neil and Dr Kelly, who not only provided me with assistance in the lab, but also made it such an enjoyable place to work. A huge thanks has to go to Pauline King, who kept the lab running smoothly, was always on hand to provide assistance and training, and taught me so much - it definitely wouldn't have been possible without you! I am also grateful to Stuart and Marion for the help they provided, and Jens at the NHM for all of his help with PXRD.

Whilst completing my PhD I was fortunate to hold a subwarden position in Royce Hall. I would like to thank Mark King, his family, and the other subwardens for making it such an enjoyable place to live over the past four years.

Thank you to my parents and family – I may not have always shown it but I am hugely grateful for the support (and money!) you have provided me with during my time at Loughborough. I wouldn't be where I am now without your help.

To the soon-to-be Dr Stephen Pendleton; thank you for being 'you'. Thanks for being there, for your assistance with work related things (especially the radiochemistry) and generally just for all the fun things we managed to do outside of our PhDs.

My final (and biggest) thank you has to go to Caroline Kirk – not only for being a fantastic supervisor, but also for becoming a great friend over the last few years. None of this would have been possible without your help and encouragement, and I can't thank you enough.

Contents

Chapter 3. Synthesis and Characterisation of Goethite and its Precursors

Chapter 4. The Removal of Secondary Phases from Goethite

Chapter 5. Incorporation of Foreign Cations into Goethite

Chapter 1.

Introduction

1.1. Introduction

Nickel (Ni) is an extremely important metallic element which is a key component in many industrial and consumer products. It makes up 0.008% of the Earth's crust (the 25th most abundant element[1]) and when the deeper core of the Earth is included, nickel becomes more abundant and is the fifth most common element behind iron, oxygen, silicon and magnesium.[2, 3]

The demand for nickel has risen rapidly in recent years, from under 200 ktpa in 1950, to over 1200 ktpa in 2003, and is growing at an average of 4% pa.[4] The demand for nickel stems from the large number of exploitable properties it possesses, see Figure 1.1.[5] It has relatively low thermal and electrical conductivities, high resistance to corrosion and oxidation, excellent strength and toughness at elevated temperatures, is capable of being magnetized, and readily forms alloys with a range of other metals.[6]

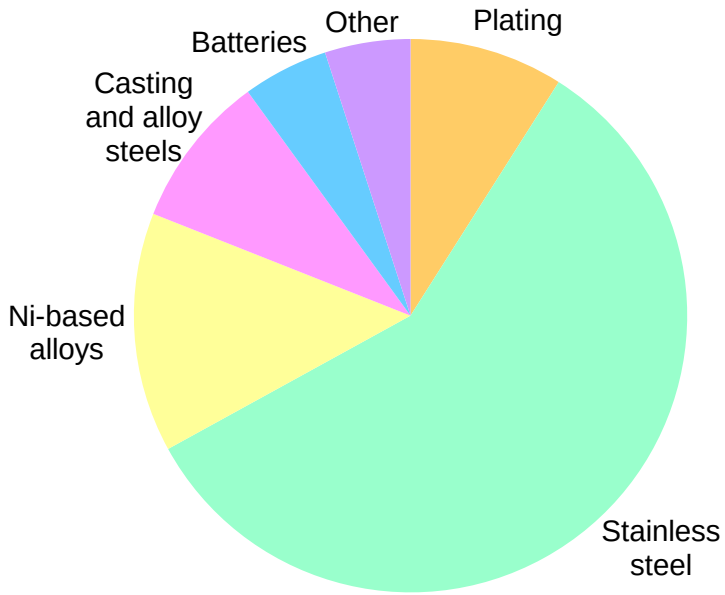

Figure 1.1: The major uses of nickel. [5]

Nickel-containing alloys are valued in industry for their superior combinations of toughness, strength, and corrosion resistance, and their ability to retain these properties at extreme temperatures. These nickel alloys are also used in the manufacture of coins and magnets. Nickel is used as a plating material to provide both corrosion-resistant and decorative finishes on items, and as a catalyst in several important reactions including the

hydrogenation of vegetable oils. It is also a key part of many rechargeable battery systems used in electronics, transport and emergency power supply.

Approximately 70% of the world's known land based nickel deposits are found within nickel laterites.[7] These nickel laterites are formed by the intense weathering of ultramafic rocks. During the weathering process, nickel containing minerals (e.g. olivine, serpentine) are destroyed, leaving behind iron oxide deposits containing residual concentrations of nickel in what is known as the limonitic laterite zone.

Iron oxides, oxy-hydroxides and hydroxides are common compounds which are widespread in nature and easily synthesised in the laboratory. They play an important role in a whole range of disciplines including industrial chemistry, soil science, environmental chemistry and corrosion science. These iron oxides, hydroxides and oxy-hydroxides are introduced into the environment through the weathering of rocks, for example in the formation of laterite deposits described above.

There are a large number of different iron oxides/hydroxides/oxyhydroxides. This project focuses mainly on the iron oxyhydroxide mineral goethite, which is the major host of nickel in the limonitic laterite zone.[8] Goethite (α-FeOOH) is formed under the Earth's surface conditions, at ambient pressure and temperature and is one of the most common minerals found around the world. The abundance of goethite in soils, ores and sediments, as well as its exceptional reactivity gives the mineral a special importance.

Goethite is a poorly and imperfectly crystallised material, resulting in the ability for it to incorporate, fix and adsorb ions from migrating solutions. The amount of nickel which is present in natural goethite varies depending on the individual laterite source, but it is normally no more than 3 wt%. Goethite found in the laterites of Çaldağ, Turkey, contain a maximum nickel concentration of 3%, although the average is much lower (1.14%).[7] Although laterite deposits, and specifically the goethite that resides within them, are an extremely important source of nickel, the precise way in which nickel is associated with goethite; the proportion of it which is incorporated into the lattice, adsorbed onto the surface or associated with the goethite in some other way, is not yet fully understood.[8, 9]

Nickel can be extracted from these laterite deposits through acid leaching (described in more detail later), but these ores, which may be from the same area and appear similar in nature, have been shown to display huge amounts of variation in their leachability – the ease with which Ni can be recovered from them.[10] In order for the mining industry to improve the design of their leach technologies for particular laterites, and to understand the reasons behind the variations in the ease of extracting Ni from different deposits, it is

vital to understand the precise mineralogy of the nickel residence in these poorly structured iron oxides and oxyhydroxides. For the laterites to be successfully exploited, an accurate understanding of the nature of the mineral phases is required, as the leachability is partly dependent on characteristics including the specific polymorph, crystallinity, grain size and chemistry of the phase.[11]

1.2. The Iron Oxides

Iron is the fourth most abundant element by mass in the crust of the Earth.[12, 13] The sheer abundance of iron within the Earth means that iron oxides are widespread in nature and are present in almost all parts of the global system (see Figure 1.2).

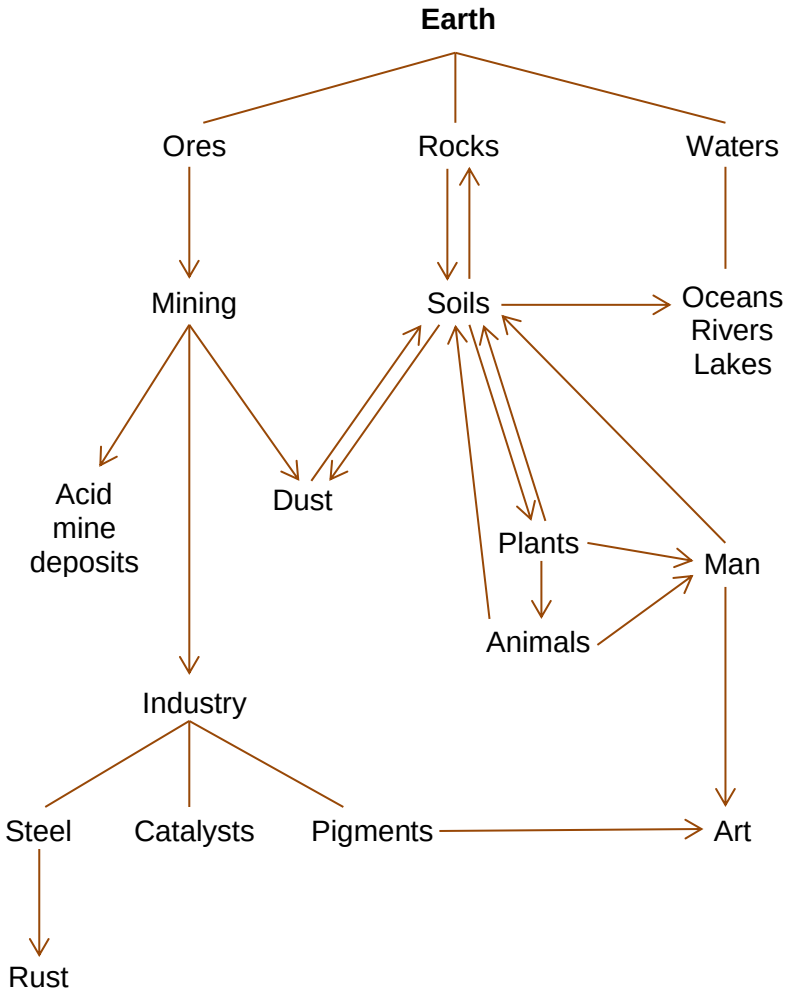

Figure 1.2: The relationship between iron oxides in the global system.[14]

There are two basic mechanisms which result in the formation of iron oxides and oxy-hydroxides.[14] The first is direct precipitation from Fe(II) or Fe(III) containing solutions, and the second route is by transformation of an iron oxide precursor. A schematic representation of the major formation and transformation pathways is shown in Figure 1.3.

Although the iron-oxyhydroxide mineral goethite will be the main focus of this thesis, as it is believed to be the major host of nickel in limonitic laterite ores, other iron oxy-hydroxides may also be present so these will be briefly discussed.

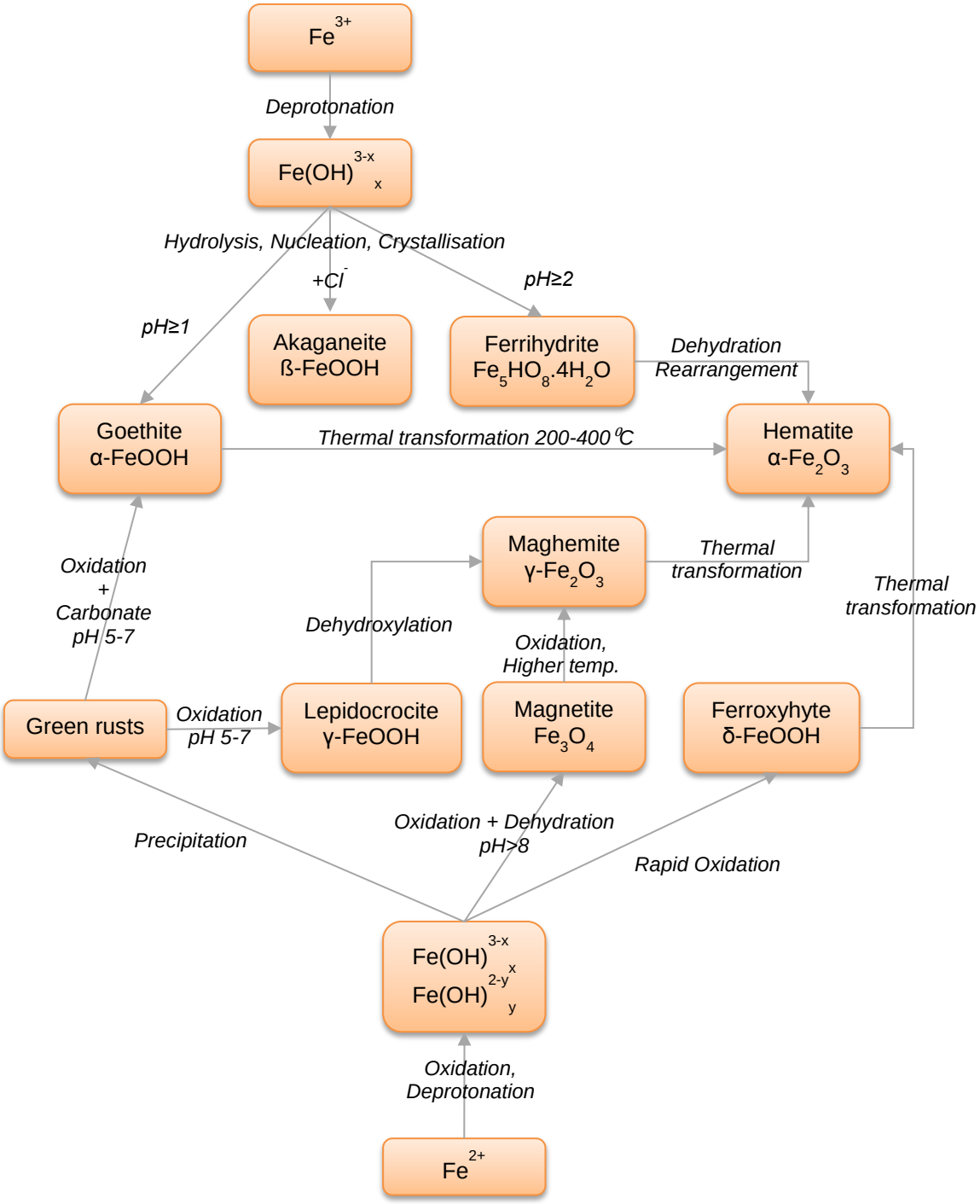

Figure 1.3: Schematic representation of the formation and transformation pathways of some common iron oxides. [14]

1.2.1. Structure and Characteristics of the Iron Oxyhydroxides

There are five iron-oxyhydroxide polymorphs, described in Table 1.1, although not all of these are naturally occurring mineral phases. All of the different iron oxyhydroxide forms consist of a basic structural unit of the $FeO_3(OH)_3$ octahedron, but the way in which they are linked results in each polymorph exhibiting a different crystal structure. In all of the FeOOH polymorph structures only half of the octahedral sites are filled with Fe^{3+}.

Ferrihydrite, although not a polymorph of goethite, is also described in this section as it is a precursor in the formation of goethite and plays an important role in this research project.

Table 1.1: Structural information of the FeOOH polymorphs, (esds shown in parentheses where available).

Compound Name	Crystallographic System	Space Group	Unit Cell Dimensions (Å)			
			a	***b***	***c***	***α, β, γ***
Goethite [15]	Orthorhombic	*Pbnm*	4.602 (3)	9.952 (4)	3.021 (2)	
Akaganeite (naturally occurring) [16]	Monoclinic	*I*2/*m*	10.56	3.031	10.513	β= 90.24
Akaganeite (synthetic)	Tetragonal	*I*4/*m*	10.535	-	3.030	
Lepidocrocite [17]	Orthorhombic	*Cmcm*	3.873 (2)	12.520 (6)	3.071 (6)	
Feroxyhyte δ'-FeOOH (naturally occurring)[24]	Hexagonal	*P*3*m*1	2.94	2.94	4.56	
δ-FeOOH (synthetic)[18]	Hexagonal	*P*3*m*1	2.95	2.95	4.53	
High pressure FeOOH (ε-FeOOH) [25]	Orthorhombic	$P2_1nm$	4.594 (1)	4.4540 (9)	3.0001 (8)	

Goethite

The mineral goethite, α-FeOOH, was first described in 1806 and crystallises with the diaspore structure (α-AlOOH) which is based on hexagonal close packing of anions. Goethite crystals that are in the μm size range are usually yellow, but as the particle size decreases to approximately 0.01μm the crystals change to a dark brown colour. The goethite structure consists of double chains of $FeO_3(OH)_3$ octahedra, adjacent to double chains of vacant sites. The double chains of $FeO_3(OH)_3$ are formed by edge sharing, and are linked to adjacent double chains by corner sharing. This arrangement of double

chains and vacant sites results in 2x1 'tunnels' which are crossed by hydrogen bonds, see Figure 1.4.[9, 14] Goethite has an orthorhombic unit cell and was initially described as having the space group *Pbnm*, but this has now been reassigned to *Pnma*.[19] For ease of comparison of results in this thesis with other published works, the original setting, Pbnm, will be used.

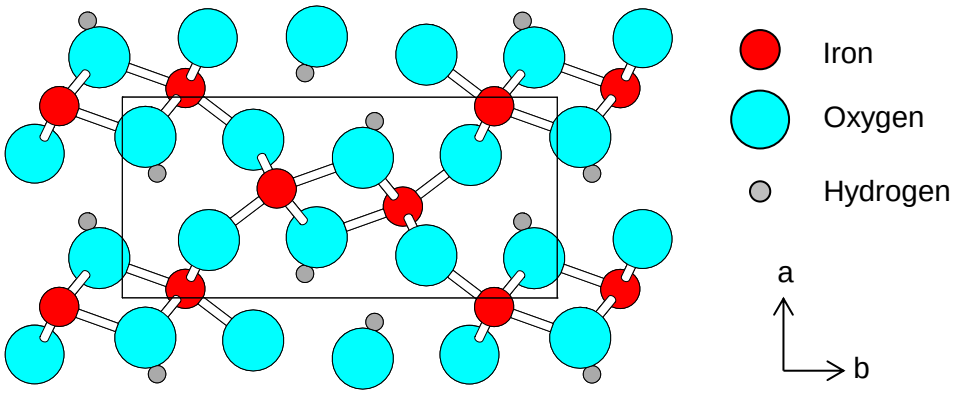

Figure 1.4: Crystal structure of goethite, *ab* projection.

Akaganeite

Akaganeite, β-FeOOH, is named after the Akagané mine in Japan where it was first discovered.[20] It doesn't occur often in nature and is found in chloride/fluoride containing environments such as hot brines and in rust from marine environments. Akaganeite has the hollandite structure ($BaMn_8O_{16}$) based on body centred cubic packing of anions, and the structure itself has a partially occupied (~30%) halide site. Akaganeite crystals are brown to bright yellow in colour. The structure of akaganeite, shown in Figure 1.5, is made up of double chains of edge shared $FeO_3(OH)_3$ octahedra running parallel to the *b* direction, which share corners with adjacent chains.[21] The unit cell formula can be written as $(X, H_2O)^{2-}Fe_8(O, OH)_{16}$, where $X=Cl^-$ or F^-. This results in 2x2 'tunnels' in the akaganeite structure which are stabilised by variable amounts of extra framework halide anions.[22] The halide content varies (usually 1-7%), and although it can be reduced, is impossible to extract all of the halide ions without inducing collapse of the akaganeite structure to goethite or hematite.[14] Natural akaganeite samples are reported as having a monoclinic unit cell, whereas synthetic samples have a tetragonal unit cell.

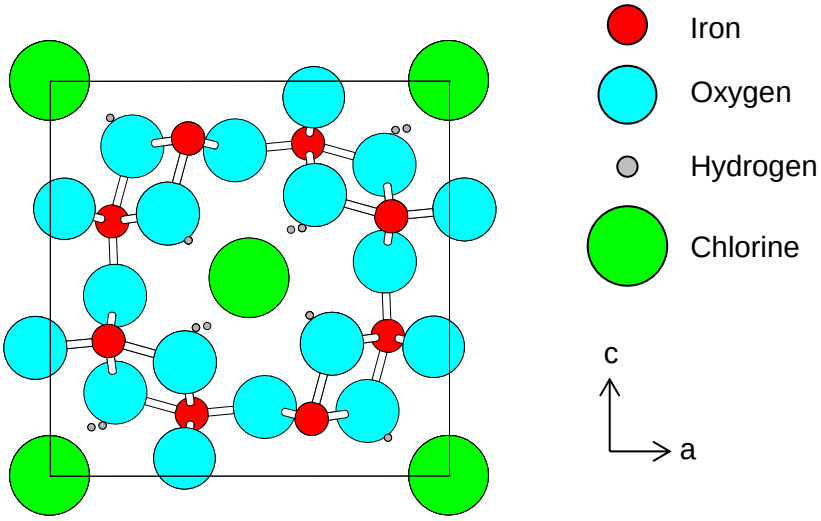

Figure 1.5: Crystal structure of akaganeite, *ac* projection.

Lepidocrocite

Lepidocrocite occurs in soils, rocks and rust and is often an oxidation product of Fe^{2+}. It has the boehmite (γ-AlOOH) structure which is based on cubic close packing of anions. The colour of lepidocrocite changes from bright orange for the larger crystals to dark brownish-orange for crystals of a smaller size. Unlike akaganeite and goethite which have 'tunnel' structures, in lepidocrocite the double bands of the octahedra share edges to form zig-zag layers running parallel to the *c* direction, connected to one another by hydrogen bonds, see Figure 1.6. These layers are separated by double rows of empty octahedral sites, the sheets being held together purely by hydrogen bonds. The mineral has an orthorhombic crystal structure and although initially given the space group *Cmcm* (as presented here), has now been reassigned to *Bbmm.* [14, 23]

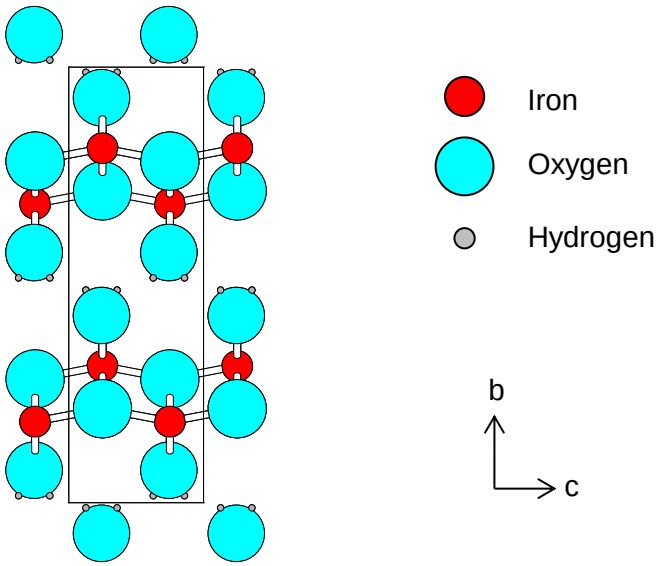

Figure 1.6: Crystal structure of lepidocrocite, *bc* projection.

δ-FeOOH and Feroxyhyte (δ'-FeOOH)

Naturally occurring feroxyhyte, δ'-FeOOH, is a rare, poorly crystalline material which is stable at the bottom of the ocean under high pressure and low temperature conditions. It spontaneously transforms into goethite when exposed to air. The synthetic analogue, δ-FeOOH, is isostructural with $Fe(OH)_2$ and has a hexagonal unit cell.[24]

High pressure FeOOH (ε-FeOOH)

This polymorph is a synthetic compound, made by the hydrothermal conversion of hematite, α-Fe_2O_3, in NaOH at 400°C and a pressure of 8Gpa. High pressure FeOOH is isostructural with InOOH and consists of single chains of $Fe(O,OH)_6$ octahedra running along the *c* direction, linked by edges and joined to adjacent chains by corner sharing. The structure of this compound was initially determined to have the space group $P2_1/c$, but more detailed analysis using X-ray and neutron diffraction revealed that the compound has an orthorhombic crystal system with the space group $P2_1nm$.[25, 26, 27]

Ferrihydrite

Ferrihydrite is a poorly ordered and thermodynamically unstable iron oxide phase. [14, 28] Although not strictly a polymorph of goethite, ferrihydrite is usually the first phase to precipitate from the rapid hydrolysis of Fe(III) solutions before recrystallising to form the more stable iron oxide phases, goethite or hematite. [28, 29] The occurrence of ferrihydrite on Earth is wide ranging; it is found in waters, sediments and soils, mine wastes and as a corrosion product of iron and steel. [28]

Despite the prevalence of ferrihydrite, there is still no consensus on its crystal structure, or even a single widely accepted chemical formula for the phase. [30,31] Published chemical formulae for ferrihydrite include: $Fe_5HO_8{\cdot}4H_2O$, [32] $5Fe_2O_3{\cdot}9H_2O$,[29] $Fe_6(O_4H_3)_3$, [33] $Fe_2O_3.2FeOOH{\cdot}6H_2O$ [34] and $Fe_{4.5}(O, OH, H_2O)_{12}$.[35] Definitive determination of the structure of ferrihydrite has been hindered by its nano-crystalline nature, variable water content and lack of long range order. [36] Most of the disagreement when considering its structure revolves around the local environment of the iron and the possible presence of multiple structural phases. [30]

Even with the lack of consensus, several structural models for 6-line ferrihydrite have been proposed. One of the most widely cited models, proposed by Towe and Bradley (1967), suggested a defective hematite-like structure with Fe in pairs of face sharing octahedral sites, periodic stacking faults and molecular water.[32]

Eggleton and Fitzpatrick (1988) proposed a model where two sheets of octahedrally coordinated Fe were connected by two sheets with mixed octahedral-tetrahedral iron, with the cations randomly distributed over the sites.[35] This model resulted in 36% of the Fe found in 6-line ferrihydrite being tetrahedrally coordinated. However, later work using synchrotron techniques disputed the presence of tetrahedral Fe, and reported that essentially all of the Fe in the interior of 6-line ferrihydrite crystals was octahedrally coordinated.[37]

Drits *et al.* (1993) proposed that all natural and synthetic ferrihydrites are multi-component phases comprised of defect free and defective ferrihydrite mixed with ultra-dispersed hematite.[38]

Zhao *et al.* (1994) found, using XAFS, that the bulk structure of a commercially available ferrihydrite catalyst was FeOOH-like, with octahedral symmetry.[39] However it also contained a significant amount (up to 25%) of Fe ions at the surface in lower coordination sites. This leads to the theory that there are, in essence, two structural aspects to ferrihydrite; the bulk 'core' of the structure and the surface.

More recently, Michel *et al.* (2007) proposed a single phase model for ferrihydrite, structurally similar to a natural alumina hydrate akdalaite ($Al_{10}O_{14}(OH)_2$) with the ideal formula $Fe_{10}O_{14}(OH)_2$, where 20% of the Fe was in tetrahedral sites.[30]

1.2.2. The Formation of Goethite

Goethite is formed naturally by a number of different methods and is one of the most thermodynamically stable iron oxides at ambient temperature, resulting in it being either the first iron oxide to form, or the end member of many transformations.[14] It can be formed by the direct precipitation of a soluble Fe(III) species, oxidation and hydrolysis of an Fe(II) salt solution, or by dissolution/recrystallisation of a solid precursor. The mode of crystallisation can affect the crystal morphology, surface area, degree of crystallinity, extent of substitution by foreign cations and water content of the product obtained.

In primary rocks, most of the iron is located in iron silicates (e.g. pyroxenes - $(Mg, Fe)_2Si_2O_6$, olivines - $(Mg, Fe)_2SiO_4$) and also in sulfides (e.g. pyrite - FeS_2). During weathering processes, the silicates are decomposed by oxidation and hydrolysis reactions to form the limonitic laterite zone, which consists largely of goethite. Examples of these decomposition reactions are shown in Equation 1.1 and Equation 1.2.

Equation 1.1: Goethite from an olivine

$$Fe_2SiO_{4\,(s)} + ½\ O_{2\,(g)} + 3\ H_2O_{\,(l)} \rightarrow 2\ \alpha\text{-}FeOOH_{\,(s)} + H_4SiO_{4\,(aq)}$$

Equation 1.2: Goethite from pyrite

$$4\ FeS_{2\,(s)} + 15\ O_{2\,(g)} + 10\ H_2O_{\,(l)} \rightarrow 4\ \alpha\text{-}FeOOH_{\,(s)} + 8\ H_2SO_{4\,(aq)}$$

Naturally occurring goethite often contains a number of different foreign metal cations in addition to iron, such as chromium, manganese, cobalt, aluminum and nickel. These cations are incorporated into goethite during the weathering processes and sometimes are present in large enough amounts to warrant commercial extraction.[40]

One of the most widely applied technologies for the extraction of metals from laterite ore deposits is leaching, both at high and low temperatures.[41, 42] The success and/or viability of the leaching process is very much related to the physical characteristics of the goethite ore material and consequently properties such as particle size, surface area and crystallinity can be as important as the residence of the target metals, such as Ni, themselves.[4] For example, the leaching behaviour of goethite is known to be affected by particle size, as shown by Aaltonen *et al.* (2003) where crushing laterite ores in a mill before the leaching process was shown to enable leaching of the metals at significantly lower temperatures and pressures due to changes in the crystal structure brought about

by the milling process.[43] Furthermore it was shown that both substitution by foreign cations and the crystallinity of the goethite phase can affect the leaching behaviour, as the presence of minor elements was shown to affect the dissolution of iron.[44]

The application of leaching technologies in metal extraction from laterite ores is further complicated by the fact that the physical properties of naturally occurring goethite in lateritic deposits vary as a function of depth, for example decreasing goethite crystallinity is often observed with increasing depth.[45] Furthermore, the physical properties of goethite can vary laterally within the same stratigraphic unit in a laterite deposit, with goethite found in well drained and poorly drained areas of lateritic profiles exhibiting different levels of crystallinity.[45]

1.3. The Occurrence of Nickel

Although a large number of nickel bearing minerals have been identified, very few contain nickel in high enough quantities for them to be industrially significant (e.g. for commercial exploitation). There are two main types of ore deposits from which nickel is economically exploitable; laterite deposits, where the main nickel-bearing minerals are garnierite and nickeliferous limonite, and magmatic sulfide deposits, where the major nickel hosts are pentlandite, pyrrohotite and pyrite (see Table 1.2).[46, 47, 48]

Table 1.2: The most common nickel-bearing minerals found in economic deposits.[42]

Mineral Name	Group	Formula	Example Deposits
Pentlandite	Sulfide	$(Fe,Ni)_9S_8$	Noril'sk, Russia. Bushveld, South Africa. Voisey's Bay, Canada. Kambalada, Western Australia
Ni replacement in **pyrrhotite**	Sulfide	$Fe_{1-x}S_x$	Noril'sk, Russia. Bushveld, South Africa. Voisey's Bay, Canada. Kambalada, Western Australia.
Millerite	Sulfide	NiS	Silver Swan, Western Australia. Sudbury, Canada.
Siegenite	Sulfide	$(Ni,Co)_3S_4$	Siegen, Germany. Jachymov, Czech Republic.
Niccolite	Nickel Arsenide	NiAs	Cobalt, Ontario. Widgiemooltha Dome and Kambalda, Western Australia.
Garnierite	Hydrous nickel silicate (serpentine)	$(NiMg)_3Si_2O_5(OH)_4$	New Caledonia. Sulawesi, Indonesia. Cerro Matoso, Columbia.
Nickeliferous **limonite**	Hydroxide	(Fe,Ni)O(OH)	New Caledonia. Sulawesi, Indonesia. Euboea, Greece.
Nickeliferous **goethite**	Hydrated oxide	(Fe,Ni)O(OH)	Koniambo Massif, New Caledonia.

Of the estimated 64 Mt of economically recoverable nickel in land based deposits, over 70% resides in lateritic deposits, located mainly in tropical areas such as New Caledonia, Brazil, Cuba and Indonesia. The remaining Ni resources occur in magmatic sulfide ores, located mainly in Canada and Russia, see Figure 1.7.[46]

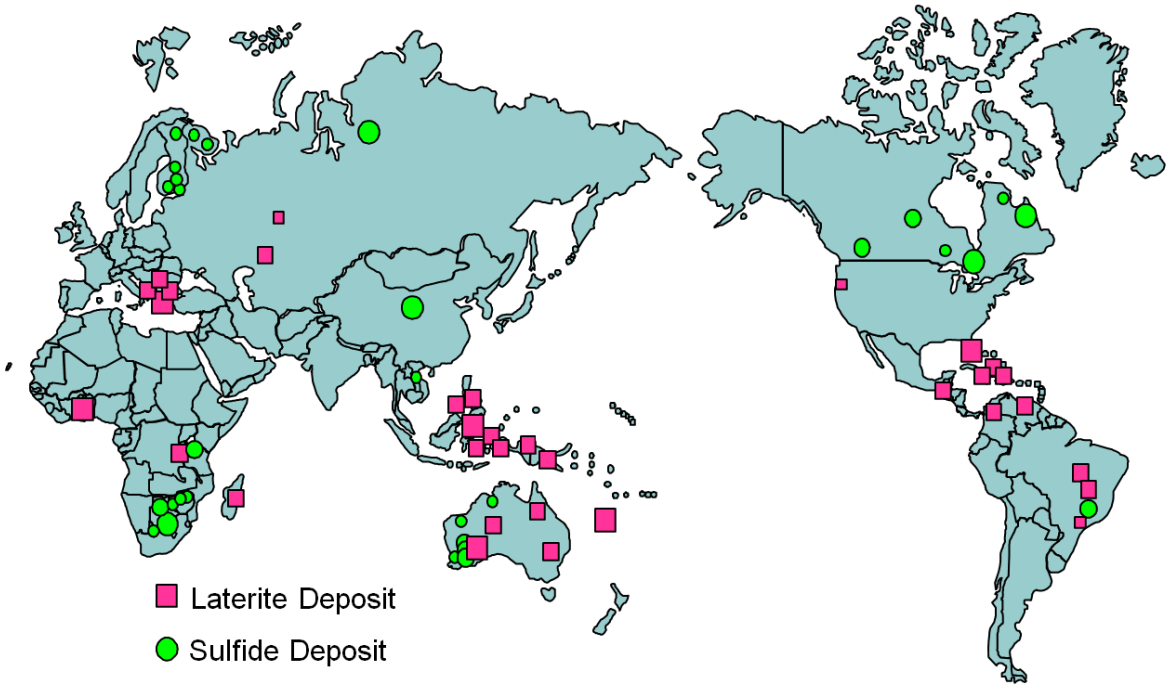

Figure 1.7: Distribution of laterite and sulfide deposits across the surface of the Earth.

Although the majority of nickel resides in laterite deposits, historically the bulk of Ni production has come from sulfide ores. In 1968, laterites supplied just 28% of the global Ni demand, increasing to 42% in 2003, and it was expected to increase to over 50% by 2012.[46] The low production levels arising from laterite ores in the past resulted from the more complex processing required to extract the Ni when compared to the processing methods used to extract Ni from sulfide ores.[4, 5, 49 50] However, the demand for Ni is still growing and the extraction of Ni from sulfide ores is becoming more challenging due to deeper drilling requirements and depleting reserves.[51] To enable a continued supply in the future, recovery of nickel from laterite ores is increasing.[11]

1.3.1. Nickel in Laterite Deposits

This project focuses on nickel residence in the limonite (iron-rich) zone of nickel laterite deposits. Laterites develop in humid, sub-tropical climates as a result of the intense weathering (and therefore leaching) of the underlying parent rock. The mechanism of leaching involves acid dissolving the host mineral lattice resulting in the more soluble ions being taken into solution, whilst leaving the more insoluble ions such as iron and aluminum behind.[47] Laterite type ores occur close to the surface of the Earth in layers that typically have depths ranging from 0-40 m.[6]

The mineralogical and chemical compositions of specific laterites are dependent on their parent rocks. Nickel rich laterites (which are also often cobalt rich too) occur as a result of prolonged tropical weathering of ultramafic rocks; these are igneous rocks with a low silica content, and high magnesium and iron contents. These ultramafic rocks contain trace amounts of nickel, for example in peridotites (e.g. olivine, general formula $(Mg, Fe)_2SiO_4$) and serpentinites (e.g. serpentine, general formula $(Mg, Fe)_3Si_2O_5(OH)_4$). During the laterization of these rocks, nickel and other soluble ions, are temporarily taken into solution before they re-precipitate with insoluble iron oxide minerals in the limonite zone, or as garnierite and other phyllosilicates (clays) in the rock layer below the laterite.[48, 52] A generalised laterite profile is shown in Figure 1.8.[53]

Common Name	Approximate Analysis (%)			
	Ni	Co	Fe	MgO
Red limonite	<0.8	<0.1	>50	<0.5
Yellow limonite	0.8-1.5	0.1-0.2	40-50	0.5-5
Transition	1.5-2	0.02-0.1	25-40	5-15
Saprolite/ Garnierite/ Serpentine	1.8-3	0.02-0.1	10-25	15-35
Fresh rock	0.3	0.01	5	35-45

Figure 1.8: A schematic laterite profile, with approximate elemental composition of the different zones.[53]

In lateritic nickel deposits, two kinds of ore need to be distinguished: limonite types and silicate types. Limonitic laterites are rich in aluminum and iron oxide ores, with an iron content in excess of 40 wt%. Literature discussing nickel laterites uses the phrase nickeliferous limonite ($(Fe, Ni)O(OH)\cdot nH_2O$) to describe a mixture of nickel containing hydrated iron (III) oxide deposits.[54] Goethite, (α-FeOOH) is the major nickel host in this region, and experimental studies have shown that natural goethite may contain nickel up to 3 wt%, although other iron oxides and oxy-hydroxides are often present in minor

amounts.[8, 55] The aluminum that is present in the limonitic region exists mainly in solid solution with iron in the goethite phase, although some is also found in the form of gibbsite ($Al(OH)_3$) and other aluminum oxide phases.[41]

Beneath the limonite zone lies the silicon and magnesium rich saprolite region. The saprolite region consists of two parts, a zone made up of hydrous magnesium silicate deposits, and a zone made up of clay silicate deposits. The hydrous Mg silicate deposits are mainly nickeliferous varieties of serpentine, talc, chlorite and sepiolite, often informally described as 'garnierite'. Garnierite is a general name used by mine geologists to describe an intimate mixture of two or more Ni-Mg hydrosilicates.[56] The clay silicate deposits are made up of Ni-rich smectites such as nontronite and saponite.[47]

1.3.2. The Association Between Nickel and Goethite

The association between nickel and goethite is well recognised, although the nature of this relationship remains unclear.[57] There are a number of different mechanisms which have been suggested to explain the way in which nickel is associated with goethite; isomorphous substitution of Ni for Fe into the goethite structure, association of Ni with an amorphous or poorly crystalline phase, nickel hydroxide intergrowths, or that Ni is weakly adsorbed to the crystalline goethite surface. [4, 58]

Ni is not believed to be accommodated in nickel hydroxide intergrowths, as microprobe and EDS analysis has shown a homogenous distribution of nickel in goethite.[57] Further studies by Singh *et al.* (2002) on the incorporation of small amounts of Ni into the goethite structure using EXAFS found no evidence that separate phases were forming as a result of the presence of foreign cations, suggesting that isomorphous substitution for Fe^{3+} by Ni^{2+} (up to 5.5 mol%) does occur.[9, 59] Carvalho *et al*. (2003) reported that using EXAFS data they had confirmed that Ni is associated with goethite via isomorphous substitution for Fe.[58]

It is not thought that significant quantities of Ni are associated with goethite via surface adsorption. Leaching experiments performed by Trolard *et al.* (1995) found that nickel is not adsorbed onto mineral surfaces, and Swamy *et al.* (2003) found the quantity of chemisorbed nickel on Indian laterite samples to be minimal. [60, 61] Swamy *et al.* (2003) used sequential leaching studies of laterite samples to report that most of the nickel was bound in the crystal lattice with some associated with amorphous goethite.[61]

1.4. Nickel Extraction Processes

Although there are a large number of mineral phases in which nickel is structurally incorporated, relatively few of them are abundant enough, or contain Ni in high enough quantities, to be industrially significant.[48] For nickel to be of commercial value, it needs to be extracted from the ore and purified in a process called extractive metallurgy. There are many different extraction methods employed to recover nickel, the process which is finally chosen being dependant on the characteristics of the specific nickel containing mineral phases that are present.

Typically, nickel bound within goethite is processed hydrometallurgically. This process uses aqueous solutions to extract metals/compounds from their ores. Leaching is one such method which causes chemical dissolution of the desired minerals in an aqueous solution. As different compounds have different dissolution rates, it is possible to separate the metals out.

Atmospheric (acid) heap leaching to extract nickel from limonitic laterite ores has been seen as a breakthrough in environmentally conscious extraction techniques, although the process is still in its infancy.[62, 63] This method of processing consumes little energy, has a low carbon footprint, uses simple equipment and has low capital costs when compared with the more traditional processing techniques (e.g. high pressure acid leaching).[4] Since the costs are so low when compared to the other processing methods, heap leaching may make some low-grade laterite ore deposits economically viable to process, however this is not without its challenges. [64] Nickel containing goethite in laterite ores shows a huge amount of variability in heap leaching performance as low-temperature leaching is strongly dependent on mineralogy. [64, 65]

Heap leach treatment of nickel laterites is generally used for oxide rich/clay poor ore types where the clay content is low enough to allow percolation of acid through the heap. The ore is ground and agglomerated and then stacked on top of impermeable plastic membranes. Over a three to four month period, acid is percolated over the heap resulting in 60-70% of the nickel/cobalt content being released into the acidic solution. This is then neutralised with limestone to produce a nickel/cobalt-hydroxide intermediate which is sent to a smelter for refining. Generally, this route of production is much cheaper than HPAL (high pressure acid leaching) as the process does not require the ore to be heated and pressurised in specialist equipment, although it is more limited in the types of ore which can be processed and a key issue is the kinetics of the reaction.[4, 54]

European Nickel demonstrated the viability of this technique at a plant in Çaldağ, Turkey, where recoveries of up to 72% have been recorded for both nickel and cobalt (a summary of the process is shown in Figure 1.9). The leach solution is collected in ponds and recirculated through the heaps to maximise the metal content. It is then pumped to the precipitation plant where the pH is raised to precipitate out the iron content, which is thickened and filtered before being disposed of as the only waste product from the process. Then the liquor from the iron thickener is treated by raising the pH further with soda ash to produce a nickel-cobalt hydroxide precipitate with a nickel content of above 30% that is filtered and packaged in bulk bags which are placed in containers for shipment.[66]

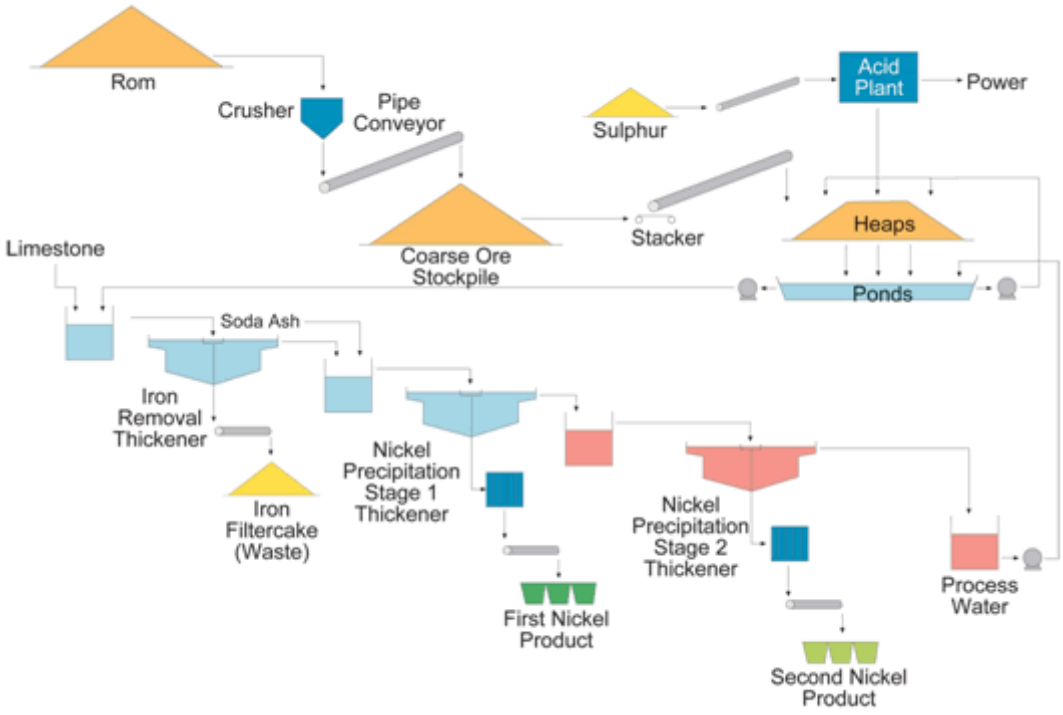

Figure 1.9: Simplified flow diagram of the heap leach process in operation at Çaldağ by European Nickel [66]

1.5. Summary and Aims of This Research

In recent years, the demand for nickel has risen rapidly, and with the many exploitable properties that nickel possesses, is only set to increase further. Historically, the majority of nickel produced came from sulfide deposits, however, extraction from this type of ore is expensive and often damaging to the environment, and due to depleting reserves is becoming more and more challenging. To ensure a continued supply in the future, recovery of nickel from laterite ores is increasing.

This research focuses on the extraction of nickel from the limonite zone of the laterite profile, where the major host of nickel is believed to be the iron oxyhydroxide mineral goethite (α-FeOOH). In this type of deposit, extraction of nickel can be achieved using atmospheric acid heap leaching, a low cost technique which is kinder to the environment than the traditional processing of sulfide deposits. In preliminary studies, mining groups have noticed that goethite rich ores, with apparently similar properties, can display extreme variation in their leachability (the ease with which Ni is extracted). It is not clear why the ores behave in this way, but in order for extraction techniques and subsequent recovery of nickel to be improved, the reasons behind this variability need to be understood.

The laterite systems in which goethite forms are complex. This work initially aims to investigate the formation of goethite synthetically, under different experimental conditions, both in the pure Fe form (FeOOH) and in the presence of nickel ($Fe_{1-x}Ni_xOOH$). This will help to establish the way in which nickel is associated with goethite – whether it is structurally incorporated into goethite via isomorphous substitution for iron, or associated, in some way, with a separate phase or phases. Research carried out by other groups and discussed earlier in this chapter suggests that nickel does not form a separate nickel hydroxide phase in this system, and the role that surface adsorption plays is believed to be minimal. For these reasons, structural incorporation and the possible presence of a poorly crystalline/amorphous (ferrihydrite) secondary phase are the modes of Ni association with goethite that will be investigated in more detail in this research project. It is possible that the synthetic Ni goethite samples prepared in this work will have a small amount of Ni adsorbed onto the surface of the goethite, rather than being structurally incorporated into the goethite or associated with the ferrihydrite phase. The effect or extent of adsorption will not be specifically investigated in this body of work.

By establishing the residence of nickel in these synthetic systems, it is hoped that the reasons behind the variation in leachability observed in natural samples can be explained. Characterisation techniques will be explored that could enable mining companies to

‘screen’ the ore before processing, possibly to pick materials more amenable to the heap leach process, or to tailor the extraction to the type of ore identified.

The aims of this research project can be summarised as follows:

1. Investigate how varying the experimental conditions used when synthesising goethite influences the formation products.
2. Investigate a range of characterisation techniques to assess their suitability for determining and quantifying the presence of ferrihydrite in mixed goethite/ferrihydrite systems.
3. Develop a technique to remove associated ferrihydrite from synthetic goethite samples, whilst ensuring the goethite itself remains unaffected.
4. Investigate the effect of adding nickel to the goethite synthesis procedure to determine the effect that the presence of nickel has on the formation of goethite and/or secondary phases.
5. Investigate the residency of nickel in natural laterite samples to consider reasons for the variations in leachability that are observed.

1.6. References

1 Çaldağ Nikel, http://caldagnikel.com.tr/en/index.php, last accessed August 2013.

2 Nickel Institute, www.nickelinstitute.org, 'Nickel and its Uses', last accessed August 2013.

3 J. H. Weber, Nickel and Nickel Alloys – An Overview, Encyclopedia of Materials Science and Technology, (2001) 6145.

4 R.G. McDonald, B.I. Whittington, *Hydrometallurgy*, (2008) **91**, 35-55.

5 G.M. Mudd, *Ore Geology Reviews*, (2010) **38**, 9-26.

6 R.R. Moskalyk, A.M. Alfantazi, *Minerals Engineering*, (2002) **15**, 593-605.

7 R. Thorne, R. Herrington, S. Roberts, *Mineralium Deposita*, (2009) **44**, 581-595.

8 N.W. Brand, C.R.M. Butt, M. Elias, *Journal of Australian Geology & Geophysics*, (1998) **17**, 81-88.

9 B. Singh, D. Sherman, R.J. Gilkes, M.A. Wells, J.F.W. Mosselmans, *Clay Minerals*, (2002) **37**, 639-649.

10 S. A. Gleeson, R. J. Herrington, J. Durango, C. A. Velasquez, G. Koll, *Economic Geology,* (2004) **99**, 1197-1213.

11 J.C.Ø. Andersen, G.K. Rollinson, B. Snook, R. Herrington, R.J. Fairhurst, *Minerals Engineering*, (2009) **22**, 1119-1129.

12 RSC Advancing the Chemical Sciences, *Visual Elements Periodic Table – Iron,* http://www.rsc.org/periodic-table/element/26/iron, last accessed September 2013.

13 P. A. Frey, G. H. Reed, *ACS Chemical Biology*, (2012) **7**, 1477-1481.

14 U. Schwertmann, R.M. Cornell, *The iron oxides: structure, properties, reactions, occurrences and uses* (Wiley & Sons, 2006).

15 C.F. Sampson, *Acta Crystallographica*, (1969) **B25**, 1683.

16 J.E. Post, V.F. Buchwald, *American Mineralogist*, (1991) **76**, 272-277.

17 H. Christenses, A.N. Christensen, *Acta Chemica Scandinavica*, (1978) **A32**, 87-88.

18 M.H. Francombe, H.P. Rooksby, *Clay Minerals Bulletin*, (1959) **4**, 1-14.

19 F. Gaboriaud, J. J. Ehrhardt, *Geochimica et Cosmochimica Acta*, (2003) **67**, 967-983.

20 A.L. Mackay, *Mineralogical Magazine*, (1962) **33**, 270-280.

21 E. Paterson, R. Swaffield, D.R. Clark, *Thermochimica Acta*, (1982) **54**, 201-211.

22 J. Cai, J. Liu, Z. Gao, A. Navrotsky, S.L. Suib, *Chemistry of Materials*, (2001) **13**, 4395-4602.

23 G. Navarro, R. Acevedo, A. Soto, M. Herane, *Journal of Physics: Conference Series*, (2004) 134.

24 F.V. Chukhrov, B.B. Zvyagin, L.P. Yermilova, A.I. Gorshkov, *Mineralium Deposita*, (1976) **11**, 24.

25 A. Suzuki, *Physics and Chemistry of Minerals*, (2010) **37**, 153-157.

26 N.B. Bolotina, V.N. Molchanov, T.I. Dyuzheva, L.M. Lityagina, N.A. Bendeliani, *Crystallography Reports*, (2008) **53**, 960-965.

27 J. Chenavas, J.C. Joubert, J. Capponi, M. Marezio, *Journal of Solid State Chemistry*, (1973) **6**, 1-15.

28 J.L. Jambor, J.E. Dutrizac, *Chemical Reviews*, (1998) **98**, 2549-2585.

29 U. Schwertmann, R.M. Cornell, Iron Oxides in the Laboratory – Preparation and Characterization, (Wiley, 1991).

30 F.M. Michel, L. Ehm, S. M. Antao, P. L. Lee, P. J. Chupas, G. Liu, D. R. Strongin, M. A. A. Schoonen, B. L. Phillips, J. B. Parise, *Science*, (2007) **316**, 1726-1729.

31 W. Xu, D.B. Hausner, R. Harrington, P.L Lee, D.R Strongin, J.B. Parise, *American Mineralogist*, (2011) **96**, 513-520.

32 K. M. Towe, W. F. Bradley, *Journal of Colloid and Interface Science***,** (1967) **24**, 384.

33 F. V. Chukhrov, B. B. Zvyagin, A. I. Gorshkov, L. P. Yermilova, V. V. Balashova, *International Geology Review*, (1974) **16**, 1131.

34 J. D. Russell, *Clay Minerals*, (1979) **14**, 109.

35 R. A. Eggleton, R. W. Fitzpatrick, *Clays and Clay Minerals*, (1988) **36**, 111-124.

36 Y. Guyodo, S. K. Banerjee, R. L. Penn, D. Burleson, T. S. Berquo, T. Seda, P. Solheid, *Physics of the Earth and Planetary Interiors*, (2006) **154**, 222-233.

37 J. Zhao, F. E. Huggins, Z. Feng, F. Lu, N. Shah, G. P. Huffman, *Journal of Catalysis,* (1993) **143**, 499-509.

38 V. A. Drits, B. A. Sakharov, A. L. Salyn, A. Manceau, *Clay Minerals*, (1993) **28**, 185-207.

39 J. Zhao, F. E. Huggins, Z. Feng, G. P. Huffman, *Clays and Clay Minerals,* (1994) **42**, 737-746.

40 S. Krehula, S.Music, S. Popovic, *Journal of Alloys and Compounds*, (2005) **403**, 368-375.

41 D. Georgiou, V.G. Papangelakis, *Hydrometallurgy*, (1998) **49**, 23-46.

42 MineralsUK, Nickel mineral profile. British Geological Survey. www.mineralsUK.com, last accessed August 2013.

43 A. Aaltonen, K. Karpale, R. Malmström, *Method for recovering nickel and eventually cobalt by extraction from nickel-containing laterite ore*. 2003, World Patent 03/004709 A1.

44 R. Kumar, R. K. Ray, A. K. Biswas, *Hydrometallurgy,* (1990) **25**, 61–83.

45 R.A. Kühnel, H.J. Roorda, J.J. Steensma, *Clay and Clay Minerals*, (1975) **23**, 349-354.

46 Sudol, S., The thunder from down under: everything you wanted to know about laterites but were afraid to ask. Canadian Mining Journal. August 2005.

47 P. Freyssinet, C.R.M. Butt, R.C. Morris, P. Piantone, *Society of Economic Geologists*, (2005) 100th Anniversary Volume, 681-722.

48 S.J. Rosenberg, Nickel and Its Alloys, *Untied States Department of Commerce, National Bureau of Standards* 106, 1968.

49 A.D. Dalvi, W.G. Bacon, R.C. Osborne, PDAC 2004 International Convention – Trade Show & Investors Exchange, 2004.

50 G M. Mudd, Nickel Sulfide Versus Laterite : The Hard Sustainability Challenge. Remains. Proc. “48th Annual Conference of Metallurgists 2009.

51 D. Zhu, Y. Cui, S. Hapugoda, K. Vining, J. Pan, *Transactions of Nonferrous Metals Society of China*, (2012) **22**, 907-916.

52 A.M. Evans, An Introduction to Ore Geology, Second Edition (Blackwell Scientific Publications, 1987)

53 Direct Nickel: A breakthrough process for all types of nickel laterite, http://www.directnickel.com, accessed August 2013.

54 Y. Chang, X. Zhai, B. Li, Y. Fu, *Hydrometallurgy*, (2010) **101**, 84-87.

55 D.H. Rubisov, V.G. Papangelakis, *Hydrometallurgy*, (2000) **58**, 13-26.

56 J.A. Proenza, J.F. Lewis, S. Gali, E. Tauler, M. Labrador, J.C. Melgarejo, F. Longo, G. Bloise, *Macla*, (2008) **9,** 197-198.

57 M.L.M. De Carvalho-E-Silva, C.S.M. Partiti, J. Enzweiler, S. Petit, S.M. Netto, S.M.B De Oliveira, *Hyperfine Interactions*, (2002) **142**, 559-576.

58 M.L. Carvalho-E-Silva, A.Y. Ramos, H.C.N. Tolentino, J. Enzweiler, S.M. Netto, M.D.C.M. Alves, *American Mineralogist*, (2003) **88**, 876-882.

59 W. Stiers, U. Schwertmann, *Geochimica et Cosmochimica Acta,* (1985) **49**, 1909-1911.

60 F. Trolard, G. Bourrie, E. Jeanroy, A.J. Herbillon, H. Martin, *Geochimica et Cosmochimica Acta*, (1995) **59**, 1285-1297.

61 Y.V. Swamy, B.B. Kar, J.K. Mohanty, *Hydrometallurgy*, (2003) **69**, 89-98.

62 H. M. A. Hunter, R. J. Herrington, E. A. Oxley, *Minerals Engineering*, (2013) **54**, 100-109.

63 T. Norgate, S. Jahanshahi, *Minerals Engineering, (*2011) **24**, 698-707.

64 H. R. Watling, A. D. Elliot, H. M. Fletcher, D. J. Robinson, D. M. Sully, *Australian Journal of Earth Sciences: An International Geoscience Journal of the Geological Society of Australia, (*2011) **58**, 725-744.

65 X. Wang, R. G. McDonald, R. D. Hart, J. Li, A. van Riessen, *Hydrometallurgy*, (2013) **140**, 48-58.

66 European Nickel, http://www.enickel.co.uk/Caldag-Project/heap_leach_process, 'Heap Leach Process', accessed June 2010.

Chapter 2.

Synthesis and Characterisation Techniques

2.1. Synthesis Procedure

2.1.1. Synthesis of Un-Substituted Goethite

From an Fe (III) Precursor

Unless otherwise stated the following method has been used for all goethite syntheses – the reasons for this are discussed in Chapter 3. All samples were prepared in polyethylene flasks, as opposed to glass containers, to prevent any of the silicon from the glass dissolving in the highly alkaline solutions. Additionally, both the ageing time and synthesis temperature were varied (0h – 7d and 20-90°C) according to the needs of the specific experiment. The conditions used for each part of this work are stated in each section.

The method for the synthesis of pure (un-substituted) goethite (α-FeOOH) has been adapted from that described by Böhm (1925).[1] A 10 ml solution of 1M $Fe(NO_3)_3 \cdot 9H_2O$ (99+%, Acros) in distilled water was prepared. To this, 18 ml of 5M KOH (reagent grade, Fisher Scientific) solution was added, and immediately the solution was diluted to 200 ml with distilled water. The solution was held in a polyethylene flask for 7d at 70°C. Over this time period the initial red/brown suspension changed to a yellow/brown precipitate. The product was gravity filtered using Fisherbrand QL100 filter papers, washed with distilled water and left to dry at room temperature in air.

From an Fe (II) Precursor

An alternative synthesis method for producing goethite was also investigated, adapted from Schwertmann and Cornell (1991).[2] Here, goethite was prepared by dissolving 9.9g of $FeCl_2 \cdot 4H_2O$ (98%, Alfa Aesar), or 13.9g of $FeSO_4 \cdot 7H_2O$ (98+% Aldrich) in distilled water (which had previously been degassed for 30 minutes by bubbling N_2 through). This was mixed with a solution of $NaHCO_3$ (reagent grade, Fisher Scientific) in a polyethylene flask. Air was bubbled through the solution for 48h with constant stirring. Over this time period the solution changed from a green-blue colour to ochre. The product was filtered using Fisherbrand QL100 filter papers, washed with distilled water and left to dry in air at room temperature.

2.1.2. Synthesis of Metal Substituted Goethites ($Fe_{1-x}M_xOOH$)

Substituted goethites were prepared with the idealised formula ($Fe_{1-x}M_xOOH$), where M is a metal cation (M = Ni, Co, Cr, Mn, Al) and x is the level of substitution by that metal. Initially the full solid solution was investigated, with the nominal value of x_M = 0, 0.2, 0.4, 0.5, 0.6, 0.8 and 1. After this, smaller regions were investigated, to establish the solid solution limits. Because the main focus of this project was nickel residence in goethite, further adaptations (e.g. time and temperature) were made to the procedure to examine what effect these parameters had on the products formed (described in Chapter 5).

It is worth mentioning that where samples are described, for example, as "*x*% Ni goethite", this terminology is being used as a label, a way to describe the samples, and is based on the composition of the target product (not necessarily the composition of the actual product). Using this method of terminology in the text allows the individual samples to be distinguished from one another, and the actual (measured) Ni composition of each sample will be discussed where relevant.

Standard Synthesis Method (M = Ni, Co, Cr)

The standard synthesis method, described in section 2.1.1., from an Fe(III) precursor was used to prepare the nickel, cobalt and chromium substituted goethites. For the synthesis of these substituted goethites, the method used for the synthesis of pure goethite was adapted such that solutions of $Fe(NO_3)_3 \cdot 9H_2O$ and another metal nitrate were dissolved in the appropriate ratios (maintaining an initial total cation concentration of 1.0M) in 10 ml of distilled water. To this mixed solution, 18 ml of 5M KOH solution was added, and then immediately diluted to 200 ml with distilled water. The solution was held in a polyethylene flask for 7d at 70°C and the resulting product was collected as described previously.

The other metal salts used were $Ni(NO_3)_2 \cdot 6H_2O$ (99.999%, Aldrich), $Co(NO_3)_2 \cdot 6H_2O$ (98+%, Acros) and $Cr(NO_3)_3 \cdot 9H_2O$ (99%, Aldrich).

Alternative Synthesis Methods (M=Mn, Al)

To prepare manganese substituted goethites a synthesis method from the literature was used which is different to the standard method above.[3,4] Mixed $Fe(NO_3)_3 \cdot 9H_2O$ and $Mn(NO_3)_2 \cdot 4H_2O$ (98%, Alfa Aesar) solutions (in the appropriate ratios for the desired composition) were prepared in 50 ml of distilled water with a total cation concentration of 0.53M. 175 ml of 2M NaOH solution was added to each solution and they were then

diluted with 250 ml of 0.3M NaOH. The resulting solutions were stored at 60°C for 20d. After this time the resulting precipitates were filtered, washed with distilled water and dried at room temperature in air.

Aluminium substituted goethites were also prepared by a previously reported method.[2] Solutions of $Fe(NO_3)_3 \cdot 9H_2O$ and $Al(NO_3)_3 \cdot 9H_2O$ (97+%, Alfa Aesar) were mixed in the appropriate ratios and KOH solution was added. The resulting solutions were held in polyethylene flasks for 14d at 70°C, and shaken once a day. After this period the precipitates were filtered, washed and dried.

Nickel Specific Synthesis

As the focus of this research is mainly on nickel residence in goethite, nickel substituted goethites were prepared by both the Fe(II) synthesis route (as well as via the standard Fe(III) method described above). For the Fe(II) synthesis route, the appropriate ratios of $FeCl_2 \cdot 4H_2O$ (98%, Alfa Aesar) and $NiCl_2 \cdot 4H_2O$ (99.999%, Aldrich) were mixed as described previously in section 2.1.1. One set of samples was held at room temperature (as described in the original method) and another at 70°C.

All of the solid phases obtained from the above synthesis methods were characterised by XRD, and more in depth characterisation work (TGA, Raman, ICP-OES, SEM) was carried out on the Ni-substituted goethites.

2.1.3. Synthesis of Ferrihydrite

6-line ferrihydrite – 'Original Method' [2]

500 ml of distilled water in a polyethylene bottle was heated in an oven to 75°C, and 5g of $Fe(NO_3)_3 \cdot 9H_2O$ was added to it with rapid stirring. The solution was returned to the oven and left for a further 10-12 minutes. After this time period the bottle was removed from the oven and cooled rapidly in an ice bath. Once cooled, the solution was transferred to a dialysis membrane which was placed in a large container of salt water (changed twice daily). After ~3 days a ferrihydrite precipitate was collected from the membrane, filtered (by gravity) and washed with distilled water and finally with acetone. The ferrihydrite product was left to dry in a desiccator.

2-line ferrihydrite – 'Original Method' [2]

8g of $Fe(NO_3)_3 \cdot 9H_2O$ was dissolved in 100 ml of distilled water. Whilst stirring the solution vigorously, 66 ml of 1M KOH was added - the last 20 ml drop-wise with constant checking of the pH (which should be kept between 7-8). The resulting solution was left to stand for 15 minutes, before being collected by gravity filtration and washed thoroughly with distilled water. The solid ferrihydrite product was dried in an oven at 60°C overnight.

2-line Ferrihydrite - Citrate Method [5]

10M ammonia solution was added drop-wise (20 drops per minute) with constant stirring to 500 ml of 0.3M iron citrate solution until a pH of 12.0 was obtained. The resulting suspension was aged for 24h at 90°C. This suspension was then gravity filtered, washed with distilled water and dried at room temperature in air.

2-line ferrihydrite – 'Goethite Method'

For this synthesis of ferrihydrite, the method for forming goethite via an Fe(III) precursor was adapted so that a product was collected before goethite had a chance to form. A 10 ml solution of 1M $Fe(NO_3)_3 \cdot 9H_2O$ (99+%, Acros) in distilled water was prepared and 18 ml of 5M KOH (reagent grade, Fisher Scientific) solution was added, immediately diluting the solution to 200 ml with distilled water. The bottle was gently shaken to mix the red/brown suspension. The product was gravity filtered (within 5 minutes of addition of the KOH) using Fisherbrand QL100 filter papers, washed with distilled water and left to dry at room temperature in air.

2.2. Characterisation Techniques

2.2.1. Powder X-Ray Diffraction

Powder X-ray diffraction (PXRD) was used to identify the crystalline phases present in the synthesised samples and to assess the degree and nature of any impurities. In addition to phase identification, the technique can provide information about the crystal structure of the samples (unit cell parameters, atomic coordinates, site occupancies etc) and in this study refinements of the unit cell parameters were carried out with a view to assess the degree of substitution by foreign cations into the parent structure.

PXRD data were collected using three different diffractometers. At the Natural History Museum XRD data were collected using a Nonius PDS120 Powder Diffraction System with an INEL curved position sensitive detector (PSD). This detector permits the simultaneous measurement of diffracted X-ray intensities at all angles of 2θ across 120˚ whilst maintaining a static beam-sample-detector geometry. Cobalt $K_{\alpha 1}$ radiation was selected from the primary beam using a germanium 111 single-crystal monochromator, and horizontal and vertical slits were used to restrict the beam to a size of 0.24 by 5.0 mm respectively. Measurements were made in reflection geometry with the powder sample surface (mounted in a deep well) at angles of either 5 or 10° to the incident beam, depending upon the 2θ range and peak resolution required. Data were collected for 15 minutes for each sample and the angular range recorded was 5º - 120º (for a beam to sample angle of 5°) and 10-120° 2θ (for a beam to sample angle of 10°). NIST silicon powder SRM640 and silver behenate were used as external 2θ calibration standards and for linearization of the detector.

In order to carry out direct comparisons of the PXRD patterns collected for each of the samples, as well as employing PXRD as a technique to develop ferrihydrite identification/quantification techniques in Chapter 3, careful preparation of the samples prior to PXRD analysis was vital. The samples were initially crushed and then ground well (by hand) to a fine powder using a pestle and mortar. The finely ground powder was then packed into deep well sample holders which were rotated during data collection.

At Loughborough University, two different diffractometer set ups were used. Most of the data were collected using a Bruker D8 Discover Diffractometer in transmission geometry, Co $K_{\alpha 1}$ radiation, selected from a Ge 111 single crystal monochromator and a Braun linear position sensitive detector. The samples were ground to a fine powder in an agate pestle and mortar and a small amount mounted between two pieces of ‘Scotch Magic Tape’. The diffraction pattern for the scotch tape exhibits two small peaks at ~26.45 and ~ 29.50°,

shown in Figure 2.1. For phase identification, data were collected over the 2θ range 10-80˚ 2θ with a step size of 0.036° and a count time of 6s. NIST silicon powder was used as either an internal or external calibration standard.

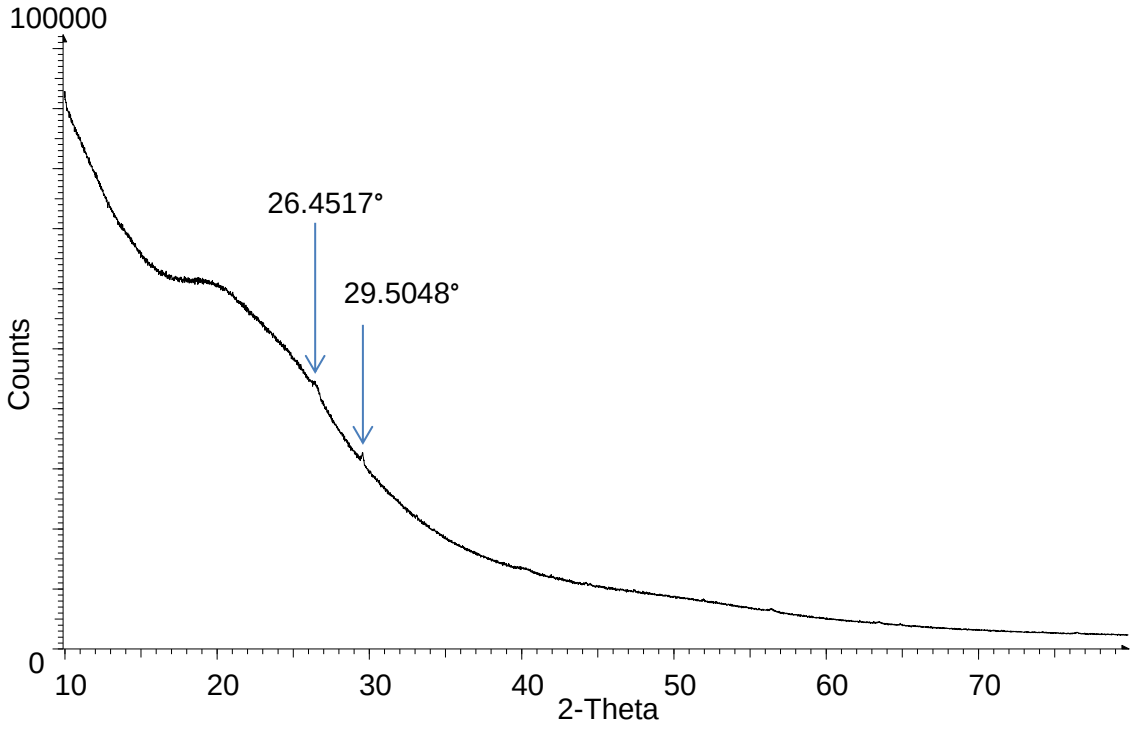

Figure 2.1: PXRD pattern for Scotch Magic Tape.

Alternatively, data were collected using a Bruker D8 Advance diffractometer in reflection geometry, Cu $K_{\alpha 1}$ radiation and a Braun linear position sensitive detector. For phase identification, data were collected over the 2θ range 10-60˚ 2θ with a step size of 0.036° and a count time of 6s per step.

For the purposes of phase identification, the PXRD data patterns were compared to known phases in the International Centre for Diffraction Data (ICDD) Powder Diffraction File (PDF) database using the search match software contained in the software suites WinXPow, or EVA.

Diffraction patterns were indexed and the unit cell parameters determined for the synthetic goethite samples using a least-squares refinement programme in the WinXPow software package. The expected peak positions of the most commonly identified phases found in this work are shown in Table 2.1.

Table 2.1: d-spacings and peak positions observed in PXRD patterns for goethite and ferrihydrite

Goethite [29-713] [6]			
d-spacing (Å)	2Theta position (°)		Miller index
	Co $K\alpha_1$	Cu $K\alpha_1$	
4.98	20.695	17.796	0 2 0
4.183	24.695	21.223	1 1 0
3.383	30.663	26.323	1 2 0
2.693	38.799	33.242	1 3 0
2.583	40.522	34.701	0 2 1
2.527	41.461	35.496	1 0 1
2.489	42.124	36.056	0 4 0
2.45	42.827	36.65	1 1 1
2.303	45.71	39.081	2 0 0
2.253	46.784	39.985	1 2 1
2.19	48.214	41.187	1 4 0
2.089	50.705	43.276	2 2 0
2.011	52.82	45.045	1 3 1
1.92	55.534	47.306	0 4 1
1.802	59.522	50.614	2 1 1
1.7728	60.604	51.508	1 4 1
1.7192	62.703	53.238	2 2 1
1.6906	63.888	54.212	2 4 0
1.6593	65.241	55.321	0 6 0
1.6037	67.802	57.413	2 3 1
1.5637	69.784	59.025	1 5 1
1.5614	69.901	59.121	1 6 0
1.5091	72.701	61.386	0 0 2
1.4675	75.111	63.324	3 2 0
1.4541	75.925	63.976	0 6 1
1.4207	78.042	65.667	1 1 2
1.3936	79.86	67.11	3 3 0
1.3694	81.566	68.459	3 0 1
1.359	82.324	69.057	1 7 0
1.3459	83.303	69.826	2 6 0
1.3173	85.535	71.572	1 3 2
1.2921	87.62	73.191	0 4 2
1.2654	89.963	74.997	3 3 1
1.2437	91.979	76.539	1 4 2
1.1994	96.451	79.918	3 4 1
1.1506	102.047	84.053	0 8 1
1.1445	102.805	84.605	4 1 0
1.1263	105.155	86.301	2 4 2

6-line ferrihydrite [29-712] [7]			
d-spacing (Å)	2Theta position (°)		Miller index
	Co $K\alpha_1$	Cu $K\alpha_1$	
2.5000	41.929	35.892	1 1 0
2.2100	47.750	40.797	2 0 0
1.9600	54.306	46.284	1 1 3
1.7200	62.671	53.211	1 1 4
1.5100	72.651	61.345	1 1 5
1.4800	74.368	62.728	1 0 6

2-line ferrihydrite [8]			
d-spacing (Å)	2Theta position (°)		Miller index
	Co $K\alpha_1$	Cu $K\alpha_1$	
2.59	40.32	34.57	1 1 0
1.49	73.67	62.14	3 0 0

2.2.2. Thermal Analysis (Simultaneous Thermo-Gravimetric Analysis (TGA)/Differential Scanning Calorimetry (DSC) Measurements)

Thermo-gravimetric analysis (TGA) is a technique where the mass of a sample is recorded as a function of temperature, in this case allowing for the water content of the goethite samples to be quantified. By examining the weight losses which occur over different temperature ranges as the sample is heated, TGA can provide information about the amount of adsorbed and structurally bound water present in the goethite samples. Furthermore, TGA can be used to explore the effect that variation of the synthesis conditions and chemical composition of the goethite phases has upon the water content in the samples.

Thermal analysis data were collected on a TA SDT Q600 instrument, capable of performing both TGA and differential scanning calorimetry (DSC) simultaneously. The advantage of this is that as well as measuring the weight loss associated with the degradation of a sample, the instrument can also measure exothermic or endothermic events which occur within the sample but have no associated weight change.

For thermal analysis measurements, a known weight of sample (5-15 mg) was loaded into an alumina crucible which was then placed inside the instrument on the balance arm. To carry out DSC measurements simultaneously, a reference material, in this case alumina powder (Al_2O_3), was loaded into an alumina crucible and placed on the reference arm which is located next to the sample arm, see Figure 2.2.

Initially, TGA/DSC data were collected on the goethite samples from ambient to 800°C with a temperature ramp of 10°C/min in a nitrogen atmosphere. Where a more accurate determination of the weight loss profile and a more precise distinction between structural OH and other types of associated water were required, TGA data were collected using an isothermal-stepwise method. In this case a heating rate of 5°C/min was used until the sample weight loss exceeded 0.2 wt%/min whereupon the temperature was held constant until the weight loss fell to less than 0.05 wt%/min. At this point, heating was resumed at the same ramp rate as that prior to the isothermal step (5°C/min). This methodology ensured that at any given temperature the mechanism responsible for the weight loss was completed before heating resumed.

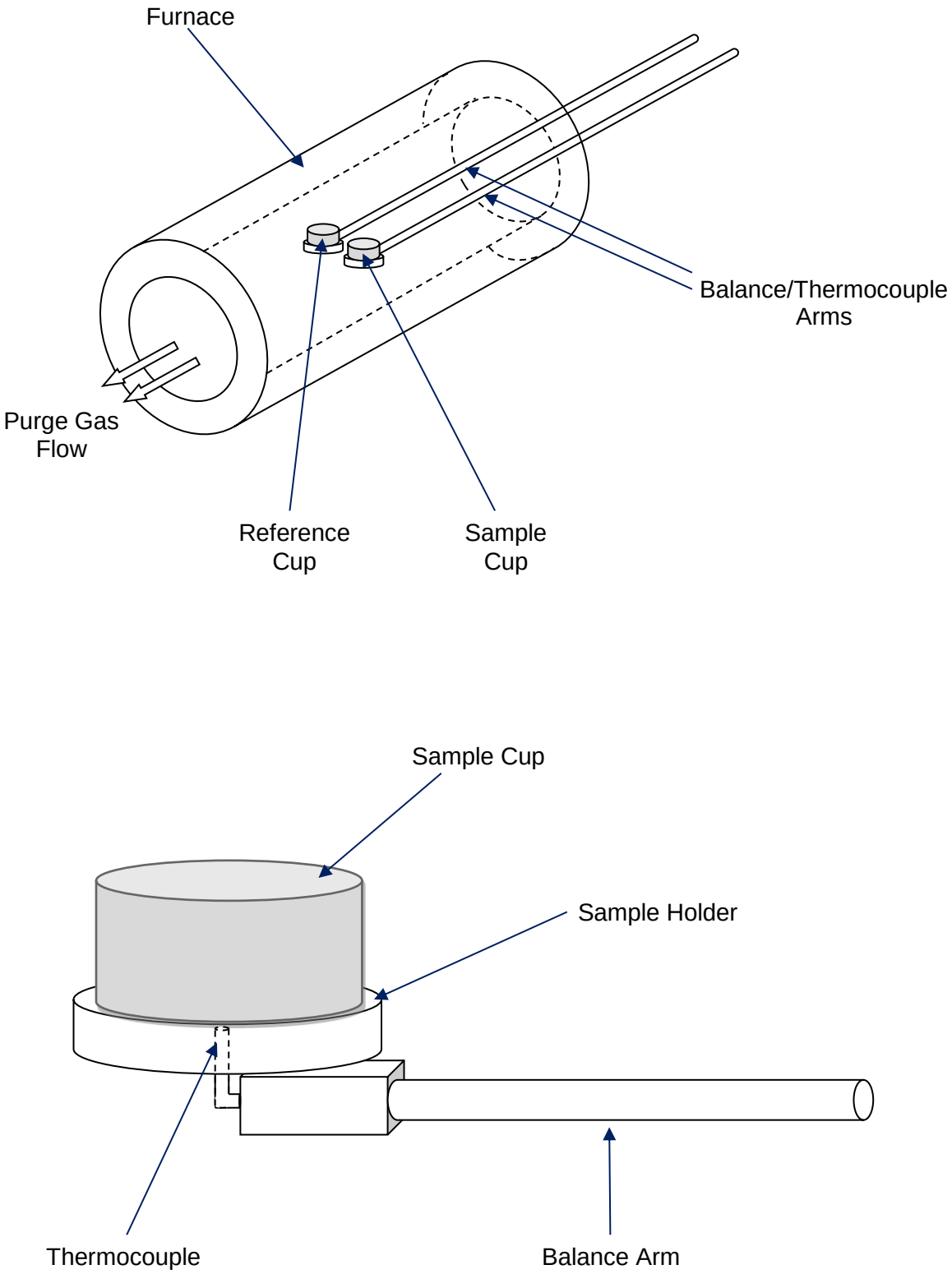

Figure 2.2: Schematic diagram of TGA instrumentation.

2.2.3. Inductively Coupled Plasma – Optical Emission Spectroscopy (ICP-OES)

Inductively coupled plasma optical emission spectroscopy (ICP-OES) is one of the most versatile methods of inorganic elemental analysis, allowing detection of elements at the ppm level. It uses a plasma torch to excite atoms and ions that then emit electromagnetic radiation at wavelengths characteristic of a particular element. The intensity of these emissions is indicative of the concentration of the element within the sample. ICP-OES was utilised in this project in order to investigate both the initial compositions of natural and synthetic goethite samples, as well as assessing the effectiveness of the EDTA washing technique that was developed by establishing exactly what was being removed from the goethite samples and in what proportions.

ICP-OES was performed on a Thermo Scientific iCAP 6000 series ICP Spectrometer fitted with a CETAC ASX-520 AutoSampler using the iTEVA Control Centre software package. The chemical composition of the solid samples was determined by dissolving 0.01 g of goethite in 2 ml of concentrated hydrochloric acid. 0.4 ml of this concentrated solution was then diluted to 25 ml using 1.75% nitric acid solution. Chemical analyses of the solutions resulting from the EDTA washing experiments was achieved by diluting 0.4 ml of the neat washing solution to 10 ml with 1.75% nitric acid.

For every batch of analyses that were performed, 10 elemental standards were prepared using the Primar-MS 28 Element Standard with concentrations ranging from 0 – 100 ppm. This allowed detection of Fe, Ni and K (an impurity resulting from the synthesis) in the synthetic samples, as well as analysing for the presence of a wide range of elements (e.g. Co, Mn, Mg) in the natural goethite samples.

For every set of samples that were analysed a set of blanks were prepared in order to determine the limit of detection (LOD) and limit of quantification (LOQ) for each analysis. When studying the solid goethite samples, the blanks consisted of 0.4 ml of concentrated HCl diluted to 25 ml in 1.75% nitric acid, and for the analysis of the EDTA washings the blanks were made by diluting 0.4 ml of 0.1M EDTA solution to 10 ml with 1.75% nitric acid.

Examples of the calibration graphs created from the elemental standards, and the calculations used to work out the LOD and LOQ are shown in Appendix 1.

2.2.4. Infra-Red (IR) Spectroscopy

IR Spectroscopy is a well-established method for rapid identification of the presence of goethite in both natural and synthetic samples. Additionally, it is also aids in the identification of impurity phases resulting from the syntheses, for example, a band at ~1400 cm^{-1} suggests the presence of a nitrate species whereas bands at ~1300 cm^{-1} and ~1500 cm^{-1} are indicative of carbonate.[2]

IR data were collected on the goethite powders between 4000-400 cm^{-1} using a Perkin Elmer Spectrum 100 FT-IR Spectrometer fitted with a universal attenuated total reflectance accessory (UATR). Obtaining IR spectra using an UATR accessory involves placing a sample (in this case the solid goethite in powdered form) on top of a crystal with a high refractive index (on this instrument diamond). An infrared beam from the instrument is passed into the accessory and up into the crystal. It is then reflected internally in the crystal, penetrating the sample by a few microns, before reflecting back towards the detector in the instrument. The UATR is a useful accessory to have on the IR instrument as it negates the need for any sample preparation, thus both simplifying the process and increasing the reproducibility of the spectra obtained from sample to sample. The expected band positions observed in the spectra for goethite and ferrihydrite are shown in Table 2.2.[9, 10]

Table 2.2: Expected IR bands observed for goethite and ferrihydrite.

Iron Phase	**Band position (cm^{-1})**
Goethite [9]	3660, 3484 (surface OH), 3140 (OH stretch), 892 (δ_{OH} in plane bend), 795 (γ_{OH} out of plane bend), 630 (Fe-O symmetric stretch parallel to *a*) and 449.
Ferrihydrite (evacuated) [10]	3615 (free surface OH groups), 3430 (OH stretch), 650 and 450 (bulk OH deformations).
Ferrihydrite (hydrated) [10]	3400 and 1635 (surface OH).

The OH bending bands at ~892 cm^{-1} and 795 cm^{-1}, and the Fe-O stretch at ~630 cm^{-1} are important diagnostic bands for goethite. Furthermore, the OH bending bands can be used to provide information about the crystallinity of the goethite phases as decreasing crystallinity causes the bands to broaden, the OH bending bands to shift to lower frequency, and the OH stretch to shift to a higher frequency.[9, 11]

2.2.5. Raman Spectroscopy

Raman spectroscopy is an extremely useful tool when characterising iron oxides as the various iron oxide phases display distinct Raman spectra, and the technique has been proven in its ability to distinguish the different iron oxides/oxy-hydroxides from one another by their individual Raman spectra.[12] The expected band positions observed in the Raman spectra for a number of iron oxides are shown in Table 2.3.

Table 2.3: Diagnostic Raman bands observed for some iron oxides/hydroxides.[12] The strongest bands are underlined.

Mineral	Wavenumbers of observed diagnostic bands (cm^{-1})					
Goethite	244	299	<u>385</u>	480	548	681
Ferrihydrite	370	510	<u>710</u>	1340		
Hematite	<u>225</u>	245	290-300	412	497	612
Maghemite	350	512	<u>665</u>	<u>730</u>		
Magnetite	310	540	<u>670</u>			

Raman spectra were acquired using a Horiba Jobin-Yvon LabRam HR system, with a solid-state laser at 1% power and a frequency of 632.817nm. The low laser power was used because of the challenging nature of the samples; poorly crystallised material (e.g. ferrihydrite) will rapidly transform under higher laser powers. To prepare the samples for analysis, they were ground to a fine powder in an agate pestle and mortar and a small amount pressed flat onto a glass microscope slide. Spectra were recorded over the range 100-1800 cm^{-1} for 2 cycles of 100s and analysed using the 'LabSpec' software package and Microsoft Excel.

2.2.6. Transmission Electron Microscopy (TEM)

TEM is a technique that was used in this work to enable the characterisation of goethite particle size and morphology. The high magnification imaging and high spatial resolution allow the particles to be observed in great detail. In this project, TEM was used to investigate the morphology of the goethite particles, as well as the purity and homogeneity of the synthetic products.

TEM analyses were performed on a JEOL 2000FX with the addition of a Gatan Erlangshen ES500W digital camera. Samples were prepared by grinding the goethite

samples to a powder in a pestle and mortar, before dispersing it in methanol using an ultrasonic bath. A drop of the resulting suspension was evaporated to dryness on a carbon-coated copper grid.

2.2.7. Electron Probe Micro Analysis (EPMA)

Electron probe microanalysis (EPMA) of the natural goethite samples was carried out on a Cameca SX100 instrument housed at the Natural History Museum in London. The instrument operated at 20kV, 20nA and the spot size for analysis was 1 µm. For analysis, the goethite samples were mounted in epoxy resin blocks, polished and carbon coated. The instrument was used for quantitative (point) analysis of areas within the samples. Images were captured in back-scattered electron (BSE) mode and areas for analyses were selected based on notable variations in contrast (pertaining to differences in elemental composition).

The instrument was fitted with wavelength dispersive X-ray crystal spectrometers to enable quantitative elemental point analysis of selected areas. The analysing crystals employed were: Ca on PET (Sp1), Mg, Al and Si on LTAP (Sp2), Ti, Cr and S on LPET (Sp3), Fe on LLIF (Sp5). The instrument was calibrated using: Mg on Mg_2SiO_4 (FOR), Al on Al_2O_3 (COR4), Si and Ca on $CaSiO_3$ (WOL4), S on $BaSO_4$ (BAR2), Ti on TiO_2 (RUT), Fe on Fe_2SiO_4 (FAY), and Cr on $FeCr_2O_4$ (CRO2).

2.2.8. Scanning Electron Microscopy (SEM)

For SEM analysis, carried out at the Natural History Museum, the goethite samples were made into 1mm thick pellets using a 13mm die set before being mounted onto stubs using araldite.

The elemental composition (Fe and Ni content) across the samples were analysed using a Zeiss Evo 15LS analytical SEM instrument, fitted with an energy dispersive X-ray detector, operating at 20kV.

Elemental maps (256x256 pixels) showing the distribution of Fe and Ni across the samples were collected using a high resolution Carl Zeiss Ultra Plus Field Emission SEM (FEG-SEM) fitted with an energy dispersive X-ray detector, operating at 8kV.

Collection and manipulation of the data was performed using Oxford Instruments INCA software package.

2.3. References

1 J. Böhm, Z. Anorg. *Zeitschrift für Anorganische und Allgemeine Chemie*, (1925) **149**, 203.

2 U. Schwertmann, R.M. Cornell, *Iron Oxides in the Laboratory – Preparation and Characterization,* (Wiley, 1991).

3 W. Stiers, U. Schwertmann, Geochimica et. Cosmochimica. Acta, (1985) **49**, 1909-1911.

4 R.M. Cornell, R. Giovanoli, *Clays and Clay Minerals*, (1987) **35**, 11-20.

5 K. Rout, M. Mohapatra, S. Anand, *Dalton Transactions,* (2012) **41**, 3302.

6 International Centre for Diffraction Data (ICDD) Powder Diffraction File (PDF) Card No. [29-713] Goethite.

7 International Centre for Diffraction Data (ICDD) Powder Diffraction File (PDF) Card No. [29-712] Ferrihydrite.

8 V.A. Drits, B.A. Sakharov, A.L. Salyn, A. Manceau, *Clay Minerals*, (1993) **28**, 185-207.

9 P. Cambier, *Clay Minerals,* (1986) **21**, 191-200.

10 J.D. Russell, *Clay Minerals,* (1979) **14**, 109.

11 P. Cambier, *Clay Minerals*, (1986) **21**, 201-210.

12 M. Hanesch, *Geophysical Journal International,* (2009) **177**, 941-948.

Chapter 3.
Synthesis and Characterisation of Goethite and its Precursors

3.1. Introduction

3.1.1 Goethite in Natural Systems

Goethite is formed naturally in a range of different environments and through a number of different pathways. Being one of the most thermodynamically stable iron oxides at ambient temperature, goethite can either be the first iron oxide to form in a geochemical system or be the end member of many transformations.[1] Goethite can be formed in aqueous systems by the direct precipitation of a soluble Fe(III) species (supplied by the dissolution of a solid precursor), oxidation and hydrolysis of an Fe(II) salt solution, or by hydrolysis of an Fe(III) salt solution.[1] The crystallisation pathway affects the physical nature of the product obtained, particularly its crystal morphology, surface area, degree of crystallinity and the extent of substitution by foreign cations.[2]

In primary ultramafic igneous rocks (the source of metalliferous laterite ore deposits), most of the iron is located in iron silicates such as pyroxenes (*(Mg,Fe)SiO_3)* and olivines (*(Mg,Fe)$_2SiO_4$*), or sulfides such as pyrite (*FeS_2*) and pyrrhotite (*$Fe_{1-x}S$*). [3, 4] To a lesser degree iron is also found in spinel oxides such as magnetite (*Fe_3O_4*) and chromite (*$FeCr_2O_4$*). During weathering processes the primary igneous minerals decompose by oxidation and hydrolysis reactions to form a limonitic zone (see Chapter 1), which consists largely of goethite. Examples of these decomposition reactions are shown in Equation 3.1 and Equation 3.2, below.

Equation 3.1: Goethite from an olivine.

$$Fe_2SiO_{4\,(s)} + ½\ O_{2\,(g)} + 3\ H_2O_{\,(l)} \rightarrow 2\ \alpha\text{-}FeOOH_{\,(s)} + H_4SiO_{4\,(aq)}$$

Equation 3.2: Goethite from pyrite.

$$4\ FeS_{2\,(s)} + 15\ O_{2\,(g)} + 10\ H_2O_{\,(l)} \rightarrow 4\ \alpha\text{-}FeOOH_{\,(s)} + 8\ H_2SO_{4\,(aq)}$$

Naturally occurring goethite usually contains a number of trace metal cation impurities, for example chromium, manganese, cobalt, aluminium, and nickel. These cations are incorporated into goethite during the weathering processes and if present in large enough amounts, may form economically viable ore deposits and warrant commercial extraction, e.g. Çaldağ and Cerro Matoso. [5, 6, 7]

3.1.2. Laboratory Synthesis Methods

A thorough description of the methods used to synthesise goethite in this project are described in Chapter 2. In general terms, synthetic goethite is usually prepared by one of two different methods, both of which mimic the natural processes which result in goethite formation.

The first synthesis method is direct precipitation from an Fe(II) solution, which involves the oxidative hydrolysis of Fe(II) solutions (commonly iron chloride or iron sulfate). This synthesis method is extremely versatile and is capable of producing a whole range of iron (oxy)hydroxides including goethite, lepidocrocite, magnetite, maghemite, ferrihydrite, hematite and feroxyhyte.[2] The particular oxide that forms is governed by the precise reaction conditions used - particularly the pH, temperature, rate of oxidation and concentration, and unless the reaction conditions are very carefully controlled a mixture of phases (rather than a single phase) usually results.[1]

The second synthesis method uses an Fe(III) starting solution. This is a two stage process involving the precipitation of a ferrihydrite precursor phase from an aqueous Fe(III) solution, followed by the transformation of this precursor into goethite, first described in 1925. [8] A freshly precipitated ferrihydrite phase is prepared by neutralising an Fe(III) salt solution (usually iron nitrate) with alkali (e.g. potassium hydroxide), a process which can take several days. In the presence of water, an Fe(III) salt dissociates to form the purple hexa-aqua ion, $Fe(H_2O)_6^{3+}$. The electropositive cation causes the H_2O ligands to act as acids, resulting in hydrolysis reactions. The process is stepwise, ending with all six ligands being deprotonated, and an example using iron (III) chloride is shown in Equation 3.3.

Equation 3.3: The formation of goethite from an Fe(III) starting material.

- $FeCl_{3\,(s)} + 6H_2O_{\,(l)} \rightarrow Fe(H_2O)_6^{3+}{}_{(aq)} + 3\,Cl^-_{\,(aq)}$
- $2\,Fe(H_2O)_6^{3+}{}_{(aq)} \rightarrow FeOOH_{(s)} + 3H^+_{\,(aq)} + 4H_2O_{\,(l)}$

As with the Fe(II) synthesis method, this process can be manipulated to produce a variety of products including hematite, akaganeite, goethite and ferrihydrite. The factors which most influence the resulting product are rate of hydrolysis, pH, temperature and concentration of Fe^{3+}. [46]

3.1.3 Ferrihydrite

Ferrihydrite, which until relatively recently was often inaccurately referred to as 'amorphous iron oxide', colloidal ferric hydroxide, $Fe(OH)_3$ or hydrous ferric oxide is a poorly ordered and thermodynamically unstable iron oxide phase.[1, 9] In the absence of foreign ions (which can alter the process – see Chapter 5), ferrihydrite is usually the first phase to precipitate from rapid hydrolysis of Fe(III) solutions.[2] The thermodynamic instability of ferrihydrite causes it to slowly recrystallise and form the more stable iron oxide phases, goethite or hematite, although under the right conditions lepidocrocite, magnetite and maghemite can also be formed.[9, 10]

The importance of ferrihydrite in metallurgical processing and the geochemical cycling of iron has, historically, probably been misjudged. The true abundance of it in modern natural environments is potentially underestimated, due largely to difficulties in identifying its presence in complex mixtures of mineral phases.[9]

The occurrence of ferrihydrite in natural systems is wide ranging. It has been identified as a preterrestrial component on meteorites and it is thought it may be a constituent of the soil on Mars.[11, 12, 13] On Earth, ferrihydrite is found in waters, sediments and soils, in mine wastes and as a corrosion product of iron and steel.[14, 15, 16, 17, 18, 19] Ferrihydrite also has industrial value, particularly as a catalyst in converting coal to liquid fuel and as an essential component in heavy-oil upgrading processes.[9]

Although ferrihydrite is poorly ordered, a continuum in structure from amorphous to partly crystalline does exist, and the ferrihydrite phases are commonly classified as either '2-line' (the least crystalline) or '6-line' (more crystalline) ferrihydrite, based on the number of broad reflections observed on a PXRD pattern, see Figure 3.1.[1, 43]

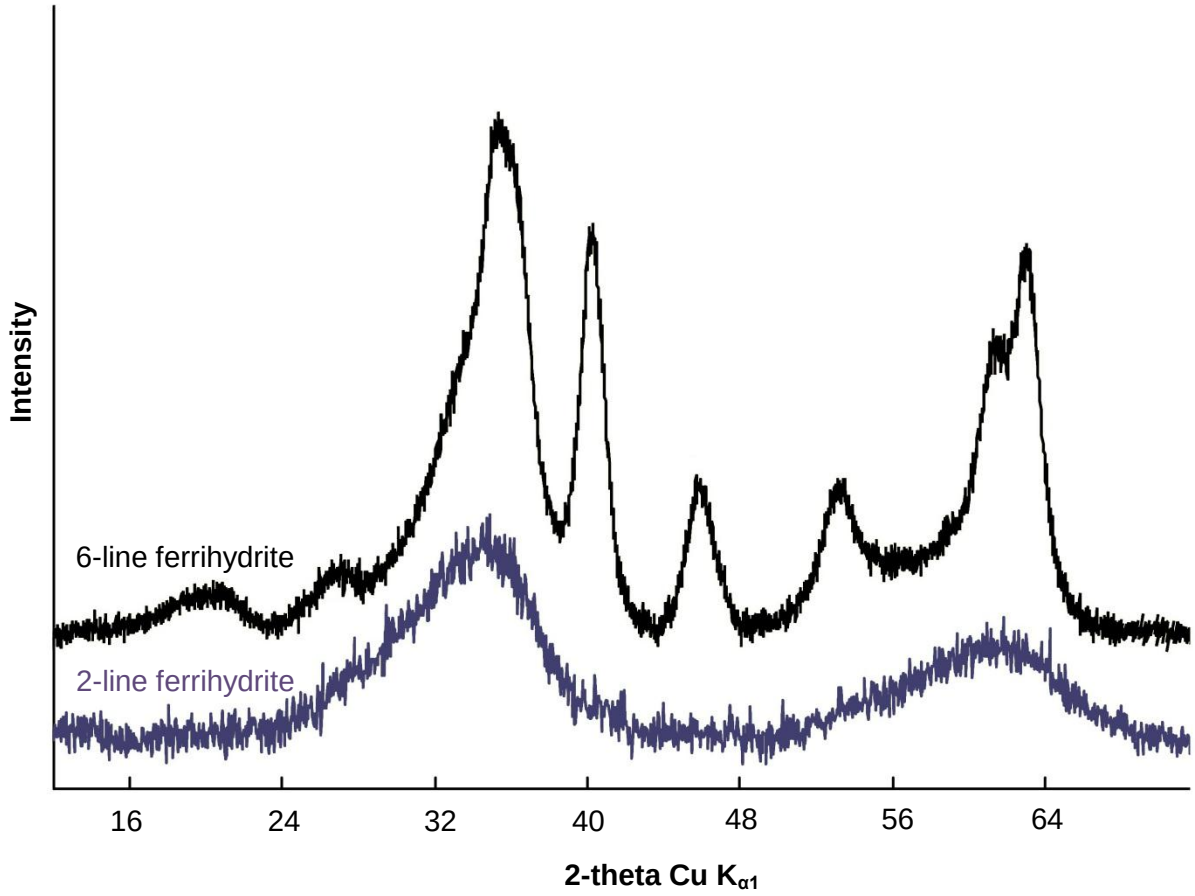

Figure 3.1: PXRD patterns for 6-line and 2-line ferrihydrite. (Adapted from [43])

The lack of long range order within the crystallites of ferrihydrite makes definitive identification challenging.[20] Later in this thesis, the presence (or absence) of ferrihydrite will need to be confirmed when in association with samples of goethite, further complicating the identification process. A number of techniques have been used previously to characterise the transformation of ferrihydrite to goethite such as oxalate extraction [21], X-ray diffraction [55], X-ray absorption spectroscopy [22], neutron diffraction [23], Mössbauer spectroscopy [24, 25], colorimetry and UV visible spectroscopy [26, 27], infrared spectroscopy [28, 55] and differential thermal analysis [29, 55]. Some of these techniques will be used later on in this work to try to identify ferrihydrite in the synthetic samples prepared here.

Structure and Composition

Despite its prevalence in natural systems and its industrial importance, definitive structural determination of ferrihydrite has been hindered by its nano-crystalline nature, variable water content and lack of long range order. [9, 30] Considerable attention has been given to

both the chemical and physical properties of ferrihydrite in previous research, however there is still no consensus on the crystal structure. [31] In addition to the lack of a conclusive structural model for ferrihydrite, there is also no single widely accepted chemical formula. [9, 50]

Chemical analyses, although usually a key component in the process of defining a general formula for a mineral, have not helped in the case of ferrihydrite, as the changeable water content results in a remarkable amount of variation in reports of the mineral formula. [9] Cismasu *et al.* (2011) found the water content (both adsorbed and structural) varied between 18 and 29.6 wt% for a number of naturally occurring ferrihydrite samples. [32] Published chemical formulae for ferrihydrite include: $Fe_5HO_8 \cdot 4H_2O$,[44] $5Fe_2O_3 \cdot 9H_2O$,[2] $Fe_6(O_4H_3)_3$,[33] $Fe_2O_3.2FeOOH \cdot 6H_2O$ [34] and $Fe_{4.5}(O, OH, H_2O)_{12}$. [42] When considering the structure of ferrihydrite, most of the disagreement revolves around the local environment of iron and the possible presence of multiple structural phases. [31]

The Transformation of Ferrihydrite

Due to its metastable nature, ferrihydrite will slowly transform to the more stable iron oxides. In a non-aqueous environment, there is general agreement that dry heating of ferrihydrite will result in its transformation to hematite. This has been investigated using thermal analysis, where a single exothermic peak is observed in the DTA trace at ~415°C, which is reported to result from the conversion of ferrihydrite to hematite, or from energy released during the recrystallization of hematite. [44, 50] Eggleton and Fitzpatrick (1988) observed two endotherms in the DTA trace (~350 and ~440°C) which they suggested resulted from a 2-step transformation process of ferrihydrite upon heating: firstly the conversion of ferrihydrite to maghemite, and secondly the transformation of maghemite to hematite. [42] Reports of maghemite as a conversion product of ferrihydrite have been published previously, but only in the presence of organic matter. [35] Prasad and Sitakara Rao (1984) also reported the presence of dual exothermic peaks, but they attributed the first to the conversion from ferrihydrite to hematite, and the higher temperature peak to the crystallisation of hematite. [36]

In an aqueous environment, and in the absence of foreign cations, ferrihydrite gradually transforms to either hematite, via dehydration and internal rearrangement of the ferrihydrite phase, or goethite. [9, 37] Two alternative mechanisms have been suggested for the transformation of ferrihydrite to goethite in an aqueous environment. Firstly, a dissolution/re-precipitation mechanism, which can occur at both high and low pH ranges and is the most commonly occurring formation method. [38] The second formation method

is via an oriented aggregation mechanism; however this has only been demonstrated in biogenic ferrihydrite at ambient temperatures and near neutral pH. [39]

The principal product, goethite or hematite, that forms is largely dependent on the pH and temperature of the suspension.[1] Since goethite and hematite form by competing mechanisms the conditions which promote the formation of one phase will therefore be unfavourable to the formation of the other. Raising the temperature of the reaction promotes the formation of hematite over goethite, as this involves dehydration of the ferrihydrite phase.[1] Furthermore changing the pH affects the solubility and rate of dissolution of the ferrihydrite phase, in turn influencing the products that form. Over the pH range 2-12, maximum hematite formation is achieved at pH 7-8 as this is where ferrihydrite is the least soluble. As the pH increases towards 12 or decreases towards 4, the solubility and dissolution rate of ferrihydrite increases, hence the formation of goethite is favoured. [38]

The formation of goethite will be investigated in this chapter, and particular attention will be paid to the extent of ferrihydrite transformation to goethite, as well as examining characterisation techniques able to identify its presence.

3.2. Experimental Methods

Goethite and ferrihydrite were synthesised using the methods described in detail in Chapter 2. In order to investigate the use of multiple characterisation techniques to enable identification of ferrihydrite when in association with goethite, physical mixtures of the two phases were prepared. Goethite (produced from an Fe(III) precursor, 7d at 70°C) and ferrihydrite ('goethite method synthesis') were synthesised and then combined, by weight, to produce a range of 'standards' that could be characterised.

After the initial synthesis experiments, further investigation on the effects of temperature and time were carried out on the Fe(III) goethite synthesis method. The different synthesis temperatures studied were 20, 40, 70 and 90°C, and the synthesis durations ranged from 0h – 24h.

3.3. Results and Discussion

3.3.1. Characterisation of Ferrihydrite

As was mentioned in the previous section, the presence (or absence) of ferrihydrite is difficult to confirm, particularly when in complex mixtures with other iron oxide phases. In order to try and overcome this problem, work was carried out in order to identify characterisation technique(s) which can help to identify ferrihydrite in association with the goethites/Ni-goethites which will be the focus of the studies detailed later in this thesis.

Ferrihydrite samples (both 2 and 6-line variants) were synthesised according to the methodology described in Chapter 2 (briefly recapped in Table 3.1), and the phases formed were characterised by PXRD, see Table 3.2. Any modifications to the standard synthesis methods described in Table 3.1 are noted in the 'synthesis method' column of Table 3.2. Some of the diffraction patterns show a sharp peak at ~76° 2θ which results from the sample holder used to collect the PXRD data.

Table 3.1: Summary of ferrihydrite synthesis methods.

Synthesis Method	Target Product	Description of Method
A	6-line ferrihydrite – 'original method'. [2]	Heat 500 ml distilled water to 75°C, add 5g of $Fe(NO_3)_3 \cdot 9H_2O$ with rapid stirring. Return to oven for 10-12 minutes, then cool rapidly in an ice bath. Transfer solution to a dialysis membrane placed in a large container of salt water (change twice daily for 3 days).
B	2-line ferrihydrite – 'original method'. [2]	Dissolve 8g of $Fe(NO_3)_3 \cdot 9H_2O$ in 100 ml of distilled water. Add 66 ml of 1M KOH with vigorous stirring (the last 20 ml should be added drop-wise with constant checking of the pH (which should be kept between 7-8). Leave resulting solution to stand for 15 minutes.
C	2-line ferrihydrite – citrate method. [40]	Add 10M ammonia solution drop-wise with constant stirring to 500 ml of 0.3M iron citrate solution until a pH of 12.0 is obtained. Age resulting suspension for 24h at 90°C.
D	2-line ferrihydrite – goethite method	Mix 10 ml of 1M $Fe(NO_3)_3 \cdot 9H_2O$ in distilled water with 18 ml of 5M KOH. Immediately dilute the solution to 200 ml with distilled water.

Table 3.2: Phases identified by PXRD patterns in ferrihydrite syntheses.

Target Product	Synthesis Method (Described in more detail in Table 3.1)	Phases identified by PXRD	Figure
6-line ferrihydrite	A – original method.	Akaganeite	Figure 3.2
	A – original method. Modified to more dilute NaCl dialysis solution.	Akaganeite Ferrihydrite	
	A – original method. Modified to sodium bicarbonate dialysis solution.	6-line ferrihydrite	Figure 3.4
	A – original method. Modified to sodium hydroxide dialysis solution.	6-line ferrihydrite Goethite	
	A – original method. Repeat.	Ferrihydrite	Figure 3.3
2-line ferrihydrite	B - original method.	2-line ferrihydrite KNO_3	Figure 3.5
	C - citrate method.	2-line ferrihydrite	Figure 3.6
	D - 'goethite' method.	2-line ferrihydrite	

The synthesis of 6-line ferrihydrite had only limited success – many of the attempts resulted in the formation of akaganeite, β-FeOOH (Figure 3.2). This could have formed rather than ferrihydrite because akaganeite uses halide ions to stabilise its structure, which would have been present (as Cl^-) as the dialysis membrane was placed in a solution of NaCl.[41]

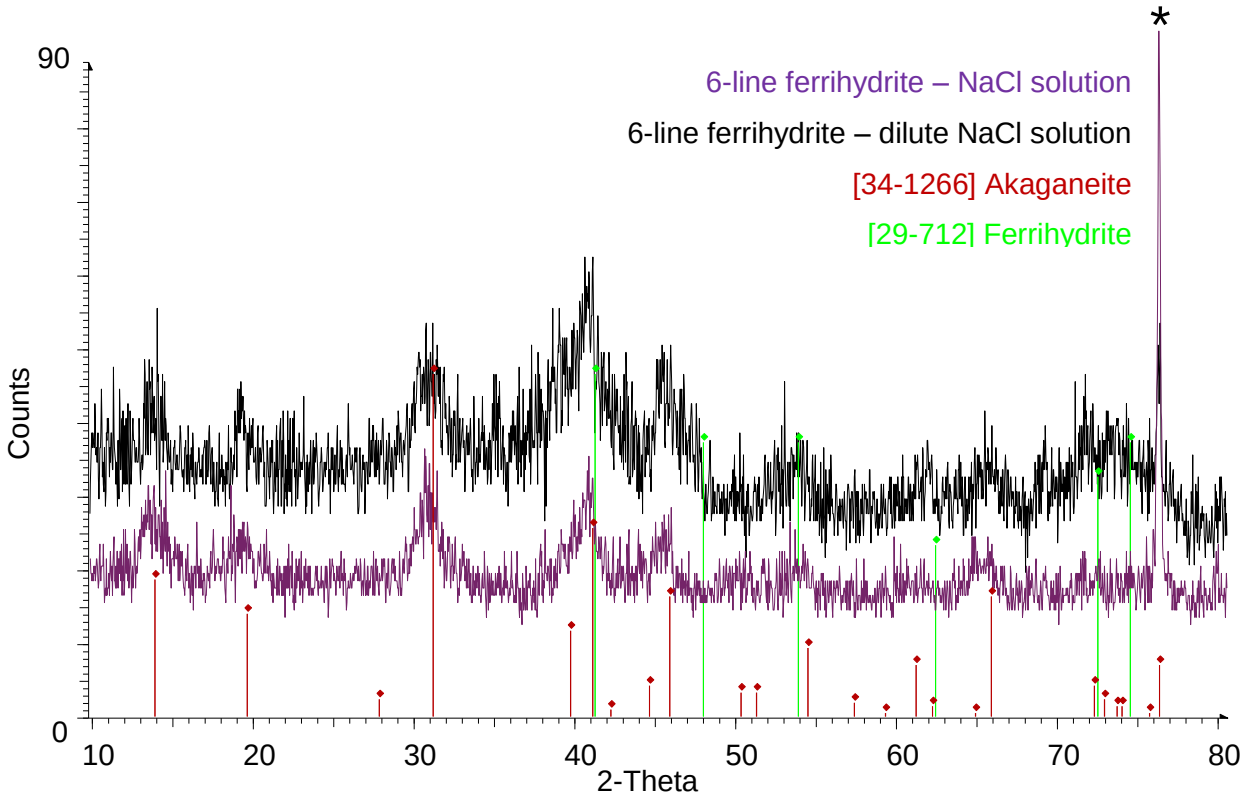

Figure 3.2: PXRD patterns of attempts to synthesise 6-line ferrihydrite using a NaCl dialysis solution. (Co $K_{\alpha 1}$ radiation, reflection from sample holder marked by *.)

One attempt at synthesising 6-line ferrihydrite through this method was successful, although the reasons for this working where previous attempts had failed are unknown, and the PXRD pattern is shown in Figure 3.3.

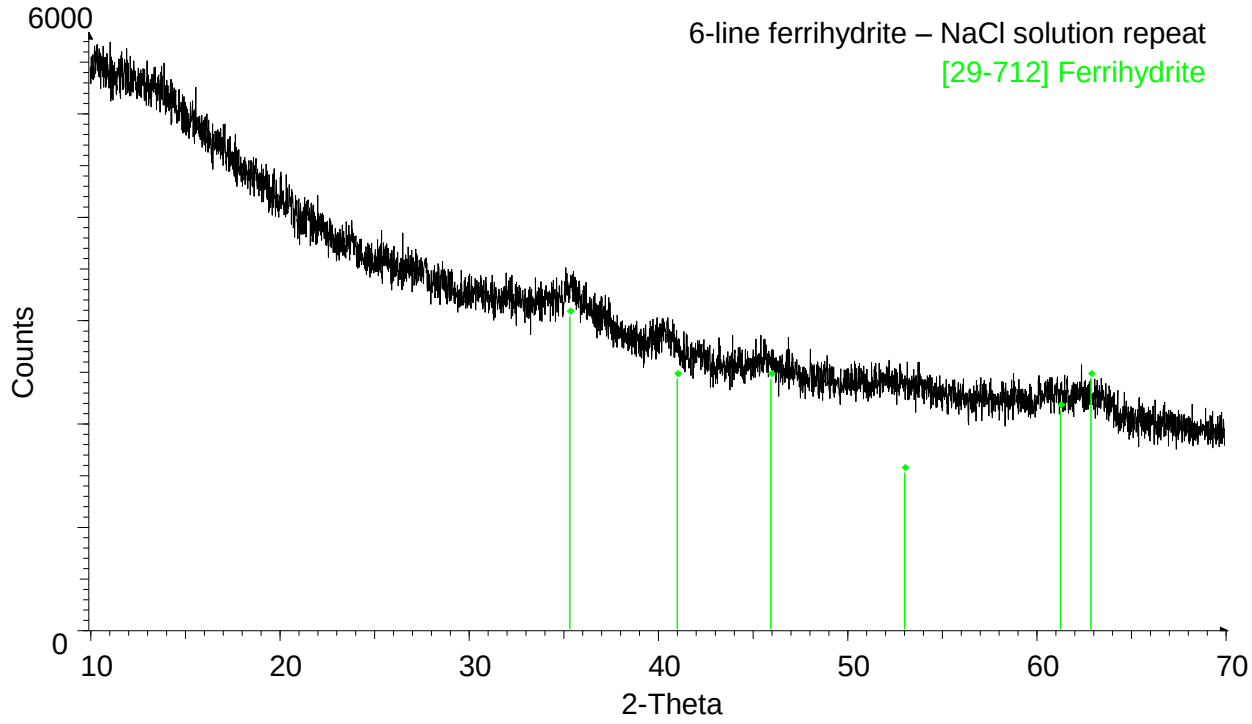

Figure 3.3: PXRD pattern of 6-line ferrihydrite. Data collected using Cu $K_{\alpha 1}$ radiation.

To try and prevent the formation of akaganeite over ferrihydrite, the synthesis procedure was modified so that either sodium bicarbonate or sodium hydroxide were used as the dialysis solution. In the syntheses using modified dialysis solutions, ferrihydrite was produced. The sodium bicarbonate method produced a very poorly crystalline ferrihydrite, whilst the sodium hydroxide resulted in a mixture of goethite and ferrihydrite (Figure 3.4). In the absence of chloride ions, akaganeite was not produced.

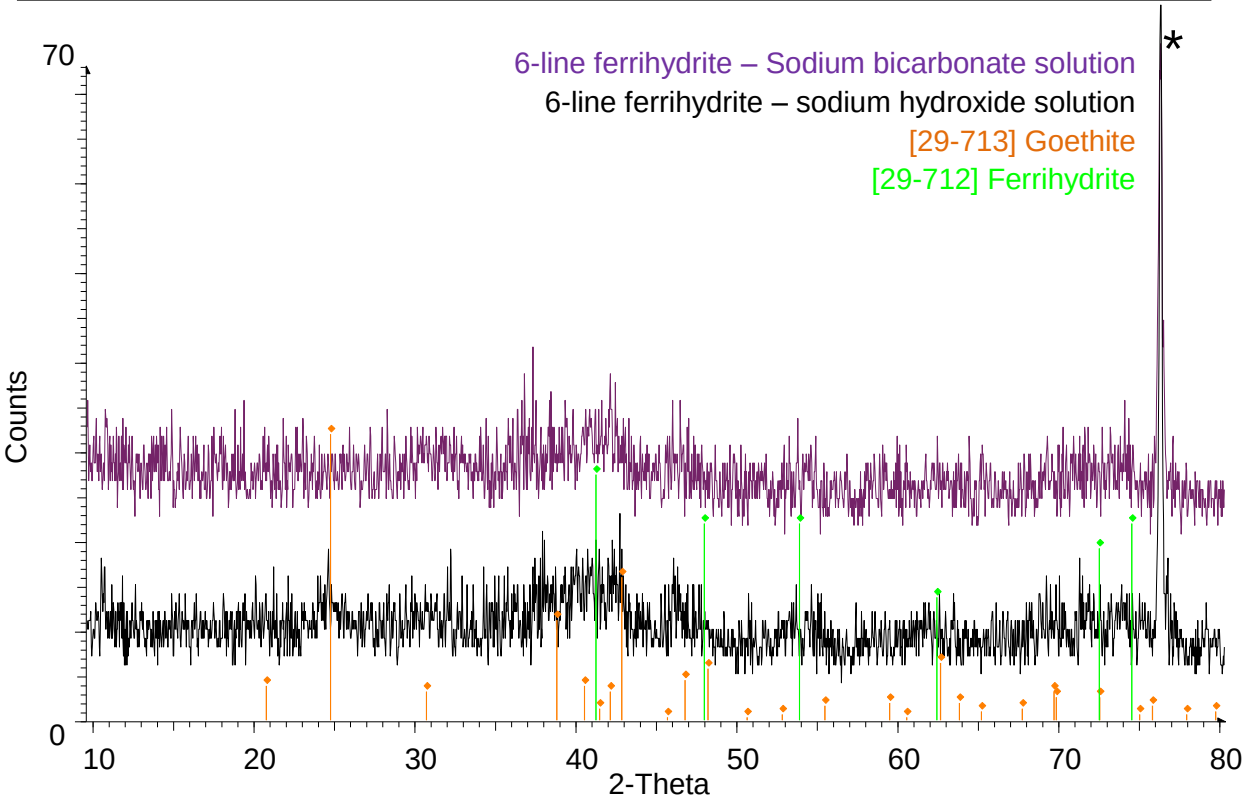

Figure 3.4: PXRD patterns of attempts to synthesise 6-line ferrihydrite using modified dialysis solutions. Data collected using Co $K_{\alpha 1}$ radiation, reflection resulting from sample holder marked by *.

The original 2-line ferrihydrite synthesis method (synthesis B in Table 3.1) produced ferrihydrite, as identified by the two broad peaks in the PXRD pattern (Figure 3.5), as well as a KNO_3 impurity phase.

The citrate and 'goethite' methods (C and D in Table 3.1) were successful in forming 2-line ferrihydrite, and the diffraction patterns obtained for the samples of ferrihydrite prepared via all three synthesis routes (B, C and D) are shown in Figure 3.6.

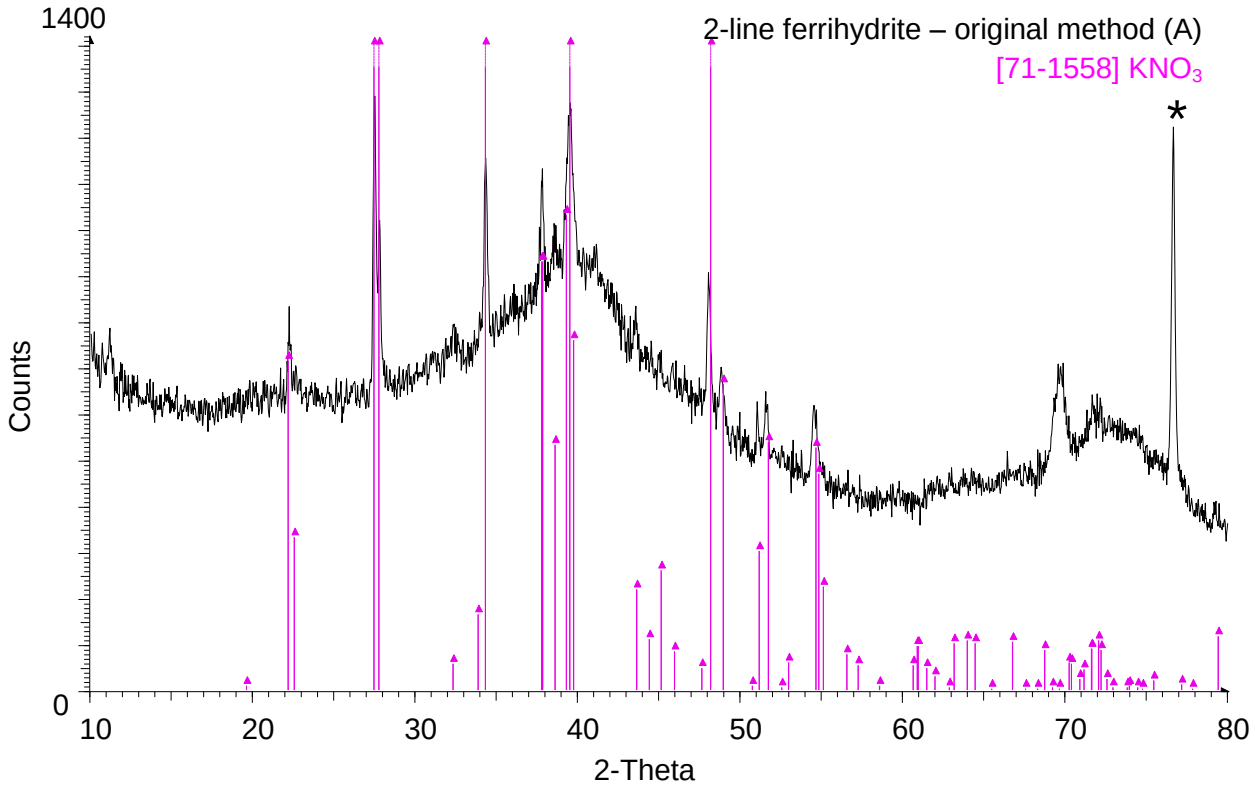

Figure 3.5: PXRD pattern of 2-line ferrihydrite (and KNO_3 impurity) synthesised by the original method. Data collected using Co $K_{\alpha 1}$ radiation, reflection resulting from sample holder marked by *.

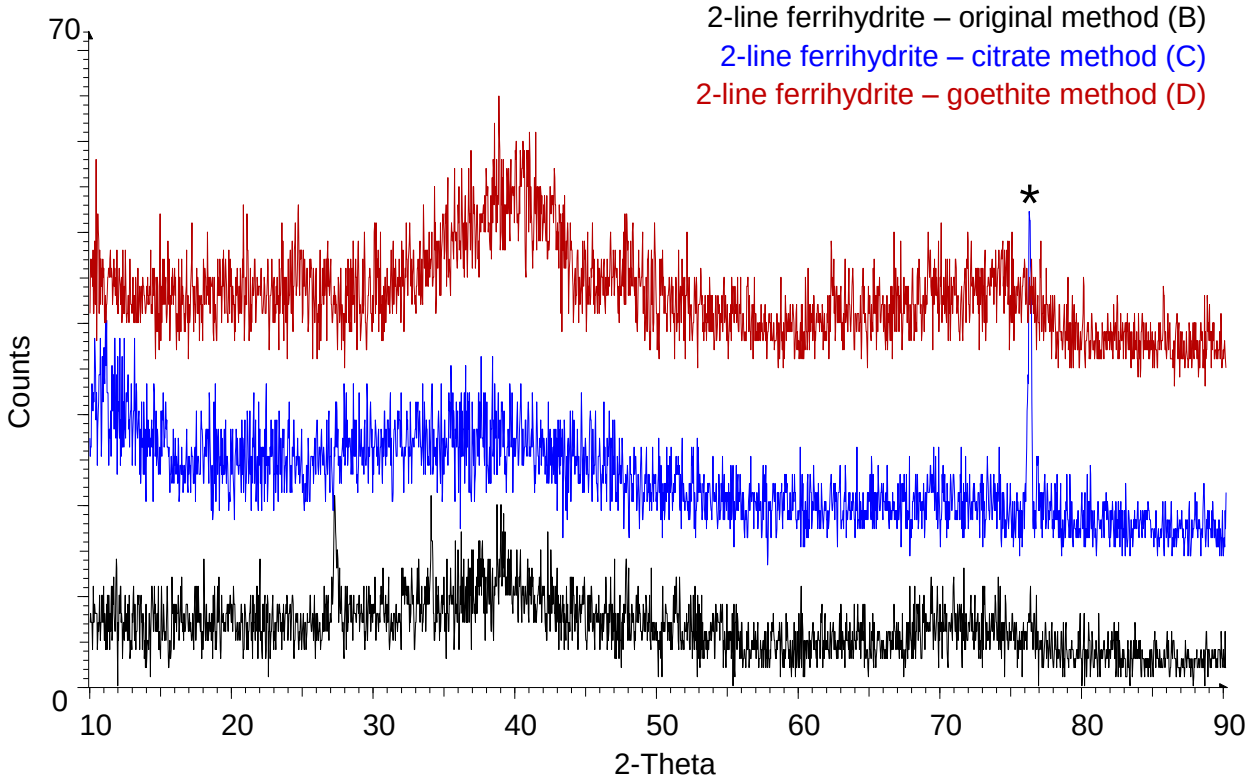

Figure 3.6: Comparison of the PXRD patterns of 2-line ferrihydrite synthesised by different methods. Data collected using Co $K_{\alpha 1}$ radiation, reflection resulting from sample holder marked by *.

After comparing all of the ferrihydrite products formed, the 'goethite method' 2-line ferrihydrite (Table 3.1, method D) was chosen as the ferrihydrite phase to use for characterisation work in the remainder of this project. Method D proved to be the most reproducible and this method was based on the synthetic procedure used to synthesise the goethite samples. Because of this, the ferrihydrite that is formed is likely to be the closest in structure, chemistry and particle size to that which may form alongside the synthetic goethite/M-substituted goethites discussed in the following chapters.

The *d*-spacings of the phase pure ferrihydrite phases formed through the different synthesis procedures were calculated and were found to be in good agreement with those found in the literature, shown in Table 3.3.

Table 3.3: Observed d-spacings of ferrihydrite synthesised in this work (shown in bold font) and compared to those from the literature (italic).

Sample	Observed *d*-spacing					
6-line ferrihydrite [42]	*2.52*	*2.23*	*1.98*	*1.72*	*1.51*	*1.46*
6-line ferrihydrite [43]	*2.51*	*2.25*	*1.98*	*1.73*	*1.481*	
6-line ferrihydrite [44]	*2.54*	*2.24*	*1.98*	*1.725*	*1.515*	*1.47*
Synthesis route A 6-line ferrihydrite (Figure 3.3)	**2.52**	**2.24**	**1.98**		**1.51**	**1.47**
Synthesis route A 6-line ferrihydrite using sodium bicarbonate solution (Figure 3.4)	**2.51**	**2.24**	**1.97**		**1.52**	**1.48**
Synthetic 2-line ferrihydrite [43]	*2.59*	*1.49*				
Synthetic 2-line ferrihydrite [44]	*2.55*	*1.47*				
Natural 2-line ferrihydrite [45]	*2.75*	*1.52*				
Synthesis route B 2-line ferrihydrite (Figure 3.6)	**2.64**	**1.53**				
Synthesis route C Citrate method 2-line ferrihydrite (Figure 3.6)	**2.71**	**1.56**				
Synthesis route D 'Goethite' method 2-line ferrihydrite (Figure 3.6)	**2.56**	**1.48**				

3.3.2. Synthesis of Goethite

Characterisation of the goethite samples by PXRD confirmed that all three of the synthetic methods which were attempted here (nitrate/chloride/sulfate starting materials) produced goethite, although the different synthetic routes resulted in products with varying crystallinities, shown in Figure 3.7.

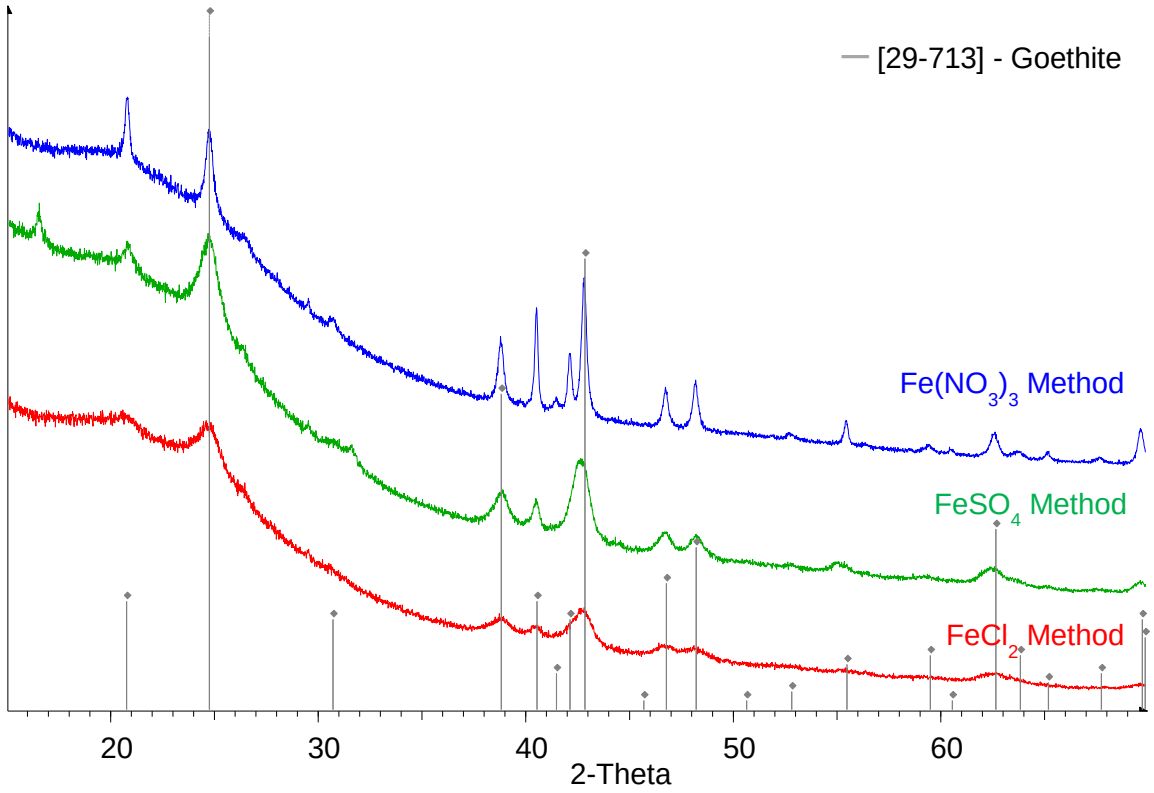

Figure 3.7: PXRD patterns collected using Co $K_{\alpha 1}$ radiation of goethite samples synthesised from different starting materials.

Analysis of the diffraction patterns shows that the goethite produced from the $Fe(NO_3)_3$ starting material appears to be the most crystalline, with relatively sharp, intense peaks. The goethite formed from the $FeSO_4$ starting material is less crystalline, with broader peaks and also contains an impurity phase, identified as lepidocrocite, probably formed as the rate of oxidation in the synthesis was too high.[2] The most poorly crystalline of the goethite samples was produced from the $FeCl_2$ method, where the peaks in the diffraction pattern are very broad and poorly defined.

The differences in the crystallinity of the samples observed in this work are supported by previous studies. Goethite crystals produced by the oxidation of Fe^{2+} solutions at ambient temperature and in neutral solution are reported to be much smaller and less well

developed than those formed in alkaline Fe^{3+} solutions.[1] It has been reported that goethite produced from the Fe(II) method has a surface area of about 80 m^2/g, compared to the more crystalline Fe(III) goethite which has a surface area of approximately 20 m^2/g .[2,46]

The unit cell parameters for each of the goethite samples were determined from refinement of the PXRD patterns (Figure 3.7) and are shown in Table 3.4. The refined unit cell parameters for the goethite prepared from $Fe(NO_3)_3$ are in good agreement with those reported in the literature.[47] The unit cell parameters for the $FeSO_4$ and $FeCl_2$ synthesis goethites are also close to the previously published values, however the refined unit cell parameters were calculated using a much smaller number of observed reflections, due to the poorly crystalline nature of the samples.

Table 3.4: Unit cell parameters for synthetic goethite samples prepared via different synthesis routes.

Name	Unit Cell Parameters			
	***a* (Å)**	***b* (Å)**	***c* (Å)**	**Volume (Å^3)**
Literature Goethite[47]	4.602 (3)	9.952 (4)	3.021 (2)	138.23 (1)
Goethite prepared from $Fe(NO_3)$	4.614 (2)	9.961 (3)	3.024 (2)	138.98 (6)
Goethite prepared from $FeSO_4$	4.627 (4)	9.948 (6)	3.033 (4)	139.60 (1)
Goethite prepared from $FeCl_2$	4.598 (9)	9.990 (2)	3.028 (5)	139.00 (3)

Of the goethite samples produced from the three synthesis routes described above, the most crystalline, identified by the sharpest and most intense, well defined peaks in the diffraction patterns, resulted from the $Fe(NO_3)_3$ synthesis. Furthermore, this synthesis method proved to be the most reproducible and consequently was chosen as the standard method to use for the rest of this project when synthesising goethite.

3.3.3. Characterisation of Physical Mixtures of Goethite and Ferrihydrite

Introduction

Ferrihydrite can be extremely difficult to characterise, especially when in the presence of other iron oxyhydroxide phases such as goethite, primarily due to its poor crystallinity. For the work presented in this thesis, it was imperative that the presence (or otherwise) of ferrihydrite in the goethite samples could be confirmed. In an attempt to increase the confidence with which ferrihydrite could be identified in the presence of goethite, and potentially to estimate the relative proportions of each phase that were present, mechanical mixtures of goethite and ferrihydrite were prepared and characterised by a number of techniques (e.g. PXRD, Raman, IR, TGA). The focus of the characterisation work was to identify any systematic changes that occurred in the datasets as the proportions of ferrihydrite and goethite in the sample were methodically altered. The data collected would then be used to try to plot calibration graphs, relating the datasets from the characterisation of the mixtures to the proportion of ferrihydrite present in the sample and hence providing a way of estimating the proportion of ferrihydrite that is present in the goethite samples prepared later in this thesis.

Samples of pure goethite and pure ferrihydrite were prepared by the chosen methods discussed previously in this chapter: goethite from $Fe(NO_3)_3$, 7d at 70°C and 2-line ferrihydrite from $Fe(NO_3)_3$. Once prepared the goethite and ferrihydrite samples were mixed (by weight) to form six different mixtures that varied systematically in the relative proportions of the two phases, from 0 wt% to 100 wt% ferrihydrite (Table 3.5), and characterised using microscopy, PXRD, TGA, IR and Raman spectroscopy.

The mixtures were produced by grinding the required amounts of goethite and ferrihydrite by hand in a pestle and mortar until the powder had a homogenous appearance (approximately 10 minutes). Optical microscopy (Figure 3.8) showed that at 50X magnification there was heterogeneity in the samples, highlighted by ‘clumps’ of ferrihydrite of ~10-40 μm in size. Although the manual preparation of goethite/ferrihydrite mixtures results in a product that is less homogenous than the chemically precipitated intergrowths that would form in natural environments, the majority of the characterisation techniques which will be tested use relatively large amounts of material and characterise the bulk of the sample, therefore the heterogeneity observed at smaller scales of analysis should not be a problem.

Table 3.5: Proportions of goethite and ferrihydrite in mixed samples. Actual wt% calculated from the exact proportions of goethite and ferrihydrite weighed out.

Target Wt%		Actual Wt%	
Goethite	**Ferrihydrite**	**Goethite**	**Ferrihydrite**
100	0	100.0	0.0
80	20	78.9	21.1
60	40	60.2	39.8
40	60	40.1	59.9
20	80	20.4	79.6
0	100	0.0	100.0

Optical Microscopy

Optical microscopy images (50X magnification) of the goethite/ferrihydrite mixtures are shown in Figure 3.8. The pure goethite sample (Figure 3.8a) appears as a homogenous, light coloured powder. As the proportion of ferrihydrite in the mixtures is increased, distinct black clumps are clearly visible in amongst the light coloured powder (e.g. Figure 3.8b and c).

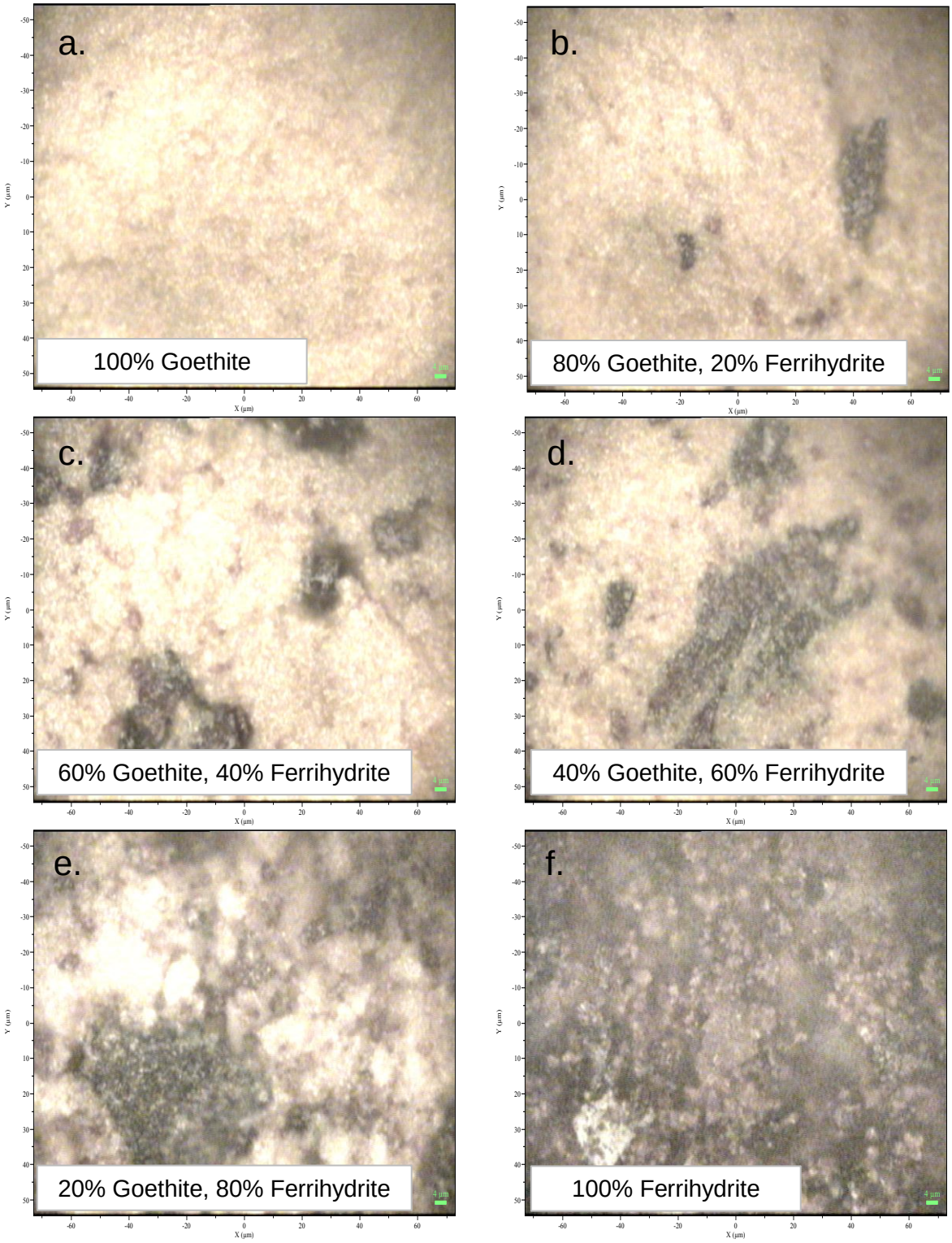

Figure 3.8: Images of the goethite/ferrihydrite mixtures, 50X magnification.

The amount of sample consisting of these black clumps increases as the amount of ferrihydrite within the mixtures rises, and the 100 wt% ferrihydrite sample (Figure 3.8f) comprises entirely of these black particles (the small white particle in the bottom left hand corner is thought to be dust which settled on the slide before analysis).

PXRD

PXRD patterns collected on the goethite/ferrihydrite mixtures show that, with the exception of the pure ferrihydrite sample, reflections attributed to goethite can be observed in all of the other samples (Figure 3.9). Furthermore, the relative intensity of these peaks increase as the proportion of goethite increases.

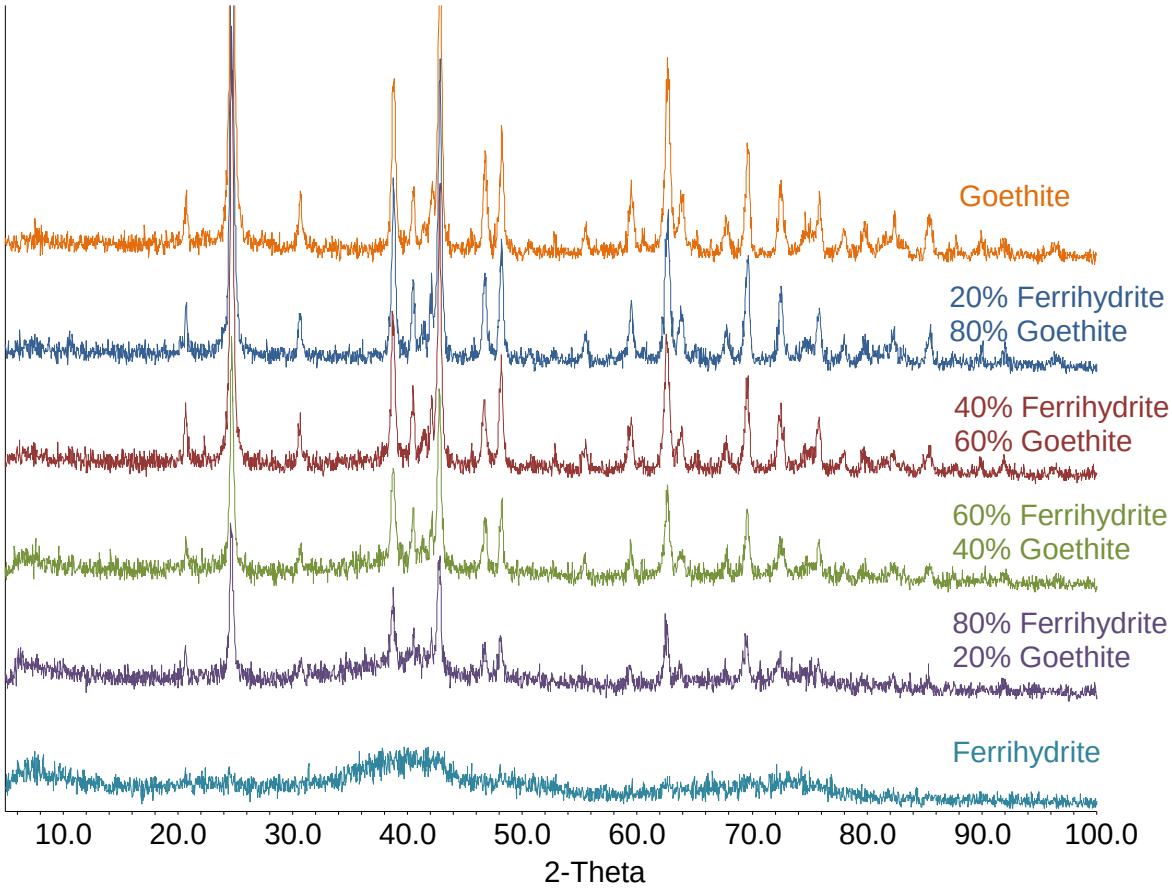

Figure 3.9: PXRD patterns for goethite/ferrihydrite mixtures. Data collected using Co $K_{\alpha 1}$ radiation.

In the 100% ferrihydrite sample there is a broad reflection around ~40° 2θ (Co $K_{\alpha 1}$ radiation), which is the main reflection for 2-line ferrihydrite (see section 3.3.1). This reflection overlaps the 130, 021, 101, 040 and 111 reflections of goethite, but nevertheless, it can be observed in the background PXRD profile of the other ferrihydrite rich samples (e.g. ≥60% ferrihydrite). The PXRD pattern of the pure goethite sample has a completely flat background profile in this region, and it is very similar to the background profiles in the PXRD patterns of the other goethite rich samples.

Although systematic changes can be observed in the PXRD patterns of the goethite/ferrihydrite series of samples shown in Figure 3.9, unless appreciable quantities

of ferrihydrite are present (≥60%) it becomes difficult to confirm the presence of ferrihydrite by eye alone, unless already aware of its presence.

One of the first observations made was that the intensity of the main goethite peak at ~24° 2θ (110) increases as the proportion of goethite in the sample increases. Furthermore, the background intensity at ~40° 2θ increases as the proportion of ferrihydrite in the sample increases. The intensities at each of these points (see Figure 3.10) were plotted against the proportion of ferrihydrite in the sample and are shown in Figure 3.11. There is strong correlation between the intensity of these reflections and the relative proportions of goethite/ferrihydrite in each mixture.

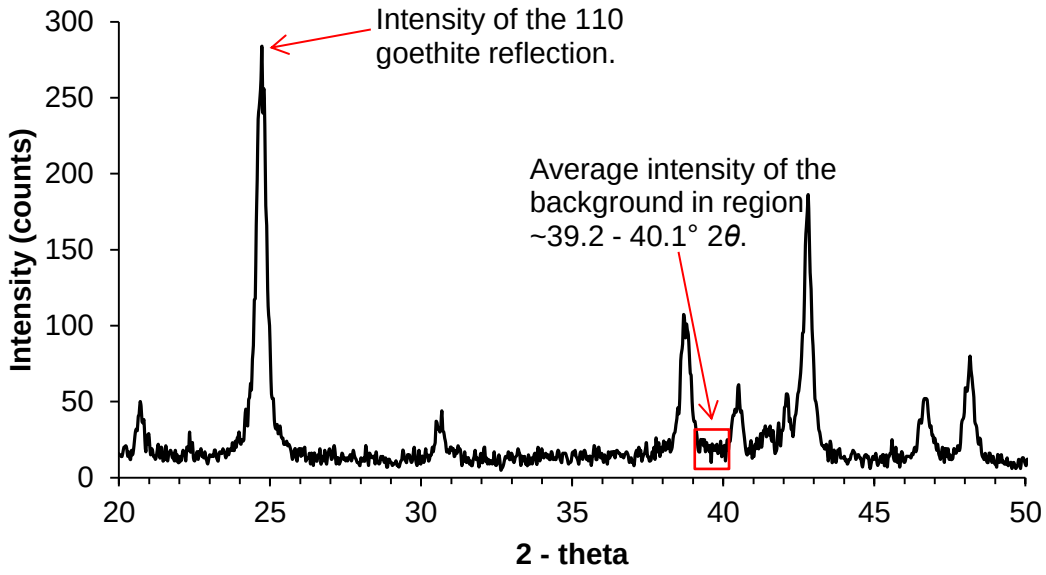

Figure 3.10: Areas where the intensity is being measured in PXRD patterns.

To ensure that the observations made with respect to the intensity of the different parts of the diffraction pattern were reproducible, a diffraction pattern was collected on the same sample six times. The intensity of the 110 goethite reflection and the average intensity of the background in the region ~39.2 - 40.1° 2θ were recorded for each repetition. Details of this reproducibility test are presented in Appendix 2. The results showed that in both intensity regions studied, the variation in intensity was less than 3% over repeated data collections.

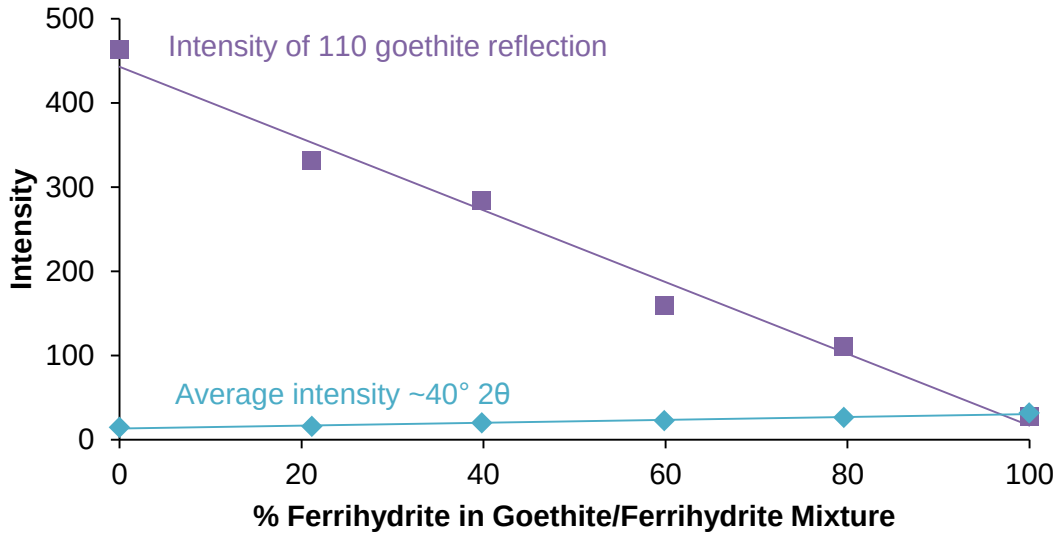

Figure 3.11: Relationship between intensities measured in the diffraction pattern of goethite/ferrihydrite mixtures and the proportion of ferrihydrite in the sample.

To be able to utilise this method to estimate the proportion of ferrihydrite that may be present in association with goethite in a sample, the ratio between the intensity of the main (110) goethite reflection and the intensity of the background at ~40° 2θ was plotted against the wt% ferrihydrite in a sample, see Figure 3.12. This method was chosen so to negate the impact that using different data collection times would have when obtaining the PXRD intensity data in the two regions.

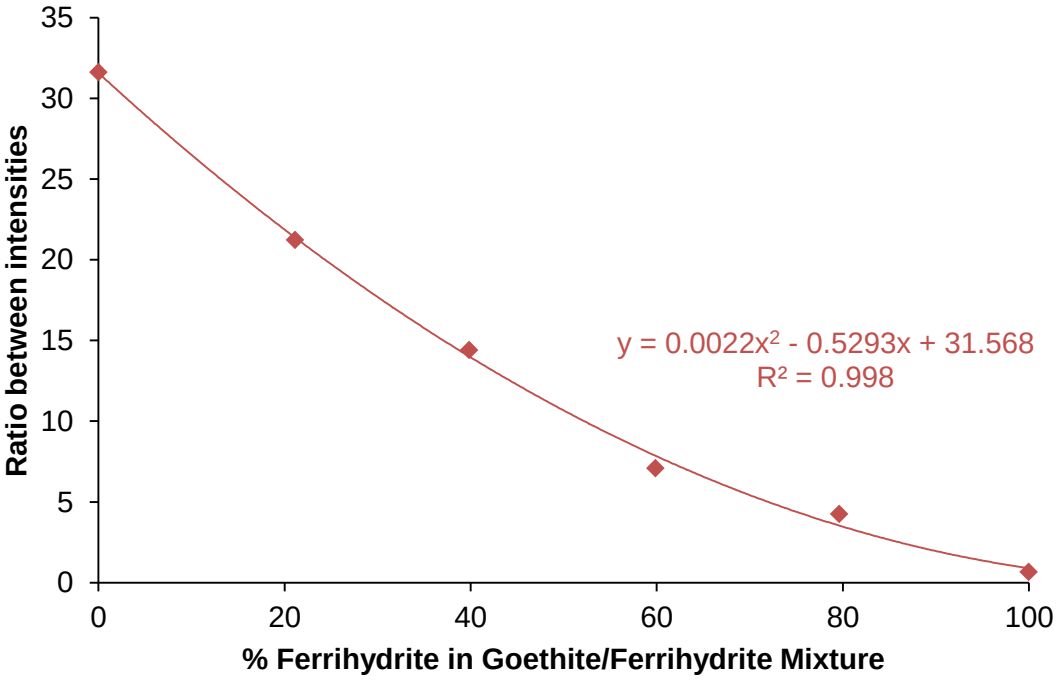

Figure 3.12: The relationship between the ratio of the intensities from PXRD data for goethite/ferrihydrite mixtures and the wt% ferrihydrite in each mixture.

By using the relationship between the intensities taken from the PXRD patterns and the proportion of ferrihydrite present in the samples, a line of best fit was plotted on to the data in Figure 3.12, see Equation 3.4. It was hoped that by using this equation, the proportion of ferrihydrite present in goethite samples studied later in this thesis could be estimated using their PXRD patterns.

Equation 3.4: The relationship between intensity ratios from PXRD patterns and the proportion of ferrihydrite present in a goethite/ferrihydrite mixture.

$$y = 0.0022x^2 - 0.5293x + 31.568$$

Where y = the ratio between intensities and x=wt% ferrihydrite

TGA

TGA weight loss profiles collected using an isothermal step-wise run type (see Chapter 2) were obtained for the goethite/ferrihydrite mixtures. The differences in both chemistry and atomic structure of goethite and ferrihydrite means that there should be distinct differences in the decomposition profiles of each phase (see Figure 3.13). By using the differences in the decomposition profiles, it was hoped that the presence (and subsequently proportion) of ferrihydrite could be determined.

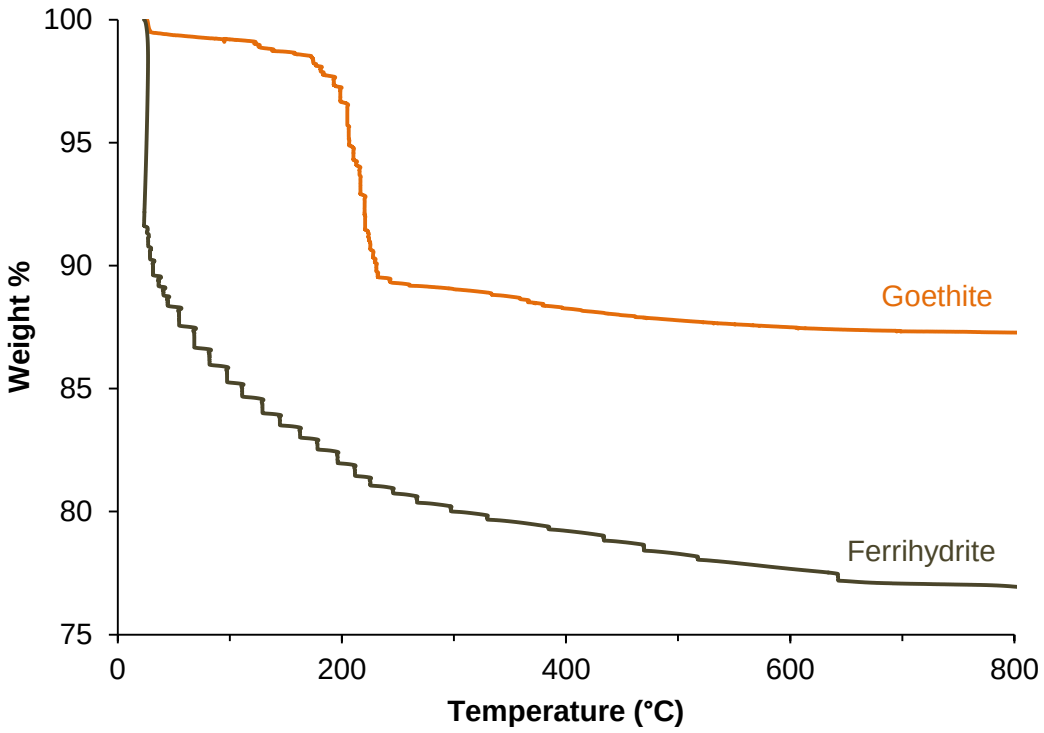

Figure 3.13: Comparison of the weight loss profiles of goethite and ferrihydrite.

Theoretically, in pure goethite, there should be a single weight loss event of 10.14%, occurring between 200-300°C resulting from the dehydroxylation of goethite to hematite, (see Equation 3.5). [48] The decomposition profile of the goethite prepared here is in agreement with the reported results, with the synthetic goethite exhibiting a weight loss of 10.13 wt%.

Equation 3.5: The dehydroxylation of goethite.

$$2FeOOH \rightarrow Fe_2O_3 + H_2O$$

Ferrihydrite begins to lose weight immediately as heat is applied, and has a rapid decomposition of approximately 20-25 wt% resulting in the formation of hematite. The rate of the weight loss decreases until the dehydration reaction is complete by ~700°C, although the majority of the decomposition occurs below 300°C (Figure 3.13).[42, 49, 50] The total measured weight loss for the decomposition of ferrihydrite can vary greatly from sample to sample due to its changeable water content. It has been reported that up to 15% of the total weight loss can result from surface adsorbed OH.[51] This results in difficulties in predicting a decomposition pathway as given for goethite (equation above).

The most immediate difference observed in the weight loss profiles for the goethite/ferrihydrite mixtures (shown in Figure 3.14), is the weight loss which occurs in each of the samples below 40°C, i.e. as soon as heating commences. In the pure goethite sample the weight loss in this region is negligible, yet as the proportion of ferrihydrite increases, the weight loss below 40°C also increases. This is a result of the large amounts of surface adsorbed OH that can be associated with ferrihydrite.

In order to establish how effective this technique could be in estimating the amount of ferrihydrite present in association with goethite samples, the weight loss profiles (Figure 3.14) were split into two different regions:

- Below 40°C – physically adsorbed surface water (goethite should display no/little weight loss).
- 150-400°C – the dehydroxylation of goethite to hematite.

The amount of weight lost in each of the samples from the two different temperature ranges (Figure 3.14 and Table 3.6) show a strong linear correlation between the weight lost in each of the temperature ranges described above and the goethite/ferrihydrite proportions, shown in Figure 3.15. The weight loss which occurs below 40°C increases linearly from 0.6 wt% for the pure goethite sample, to 11.0 wt% for the pure ferrihydrite sample. Conversely, the weight loss in the region 150-400°C, decreases linearly from 10.4 wt% for the pure goethite sample, to 4.3 wt% for the pure ferrihydrite sample. The weight loss data shows that even the 100% goethite sample has a very small (0.6 wt%) weight loss which occurs below 40°C, which is due to surface adsorbed OH associated with the goethite itself.

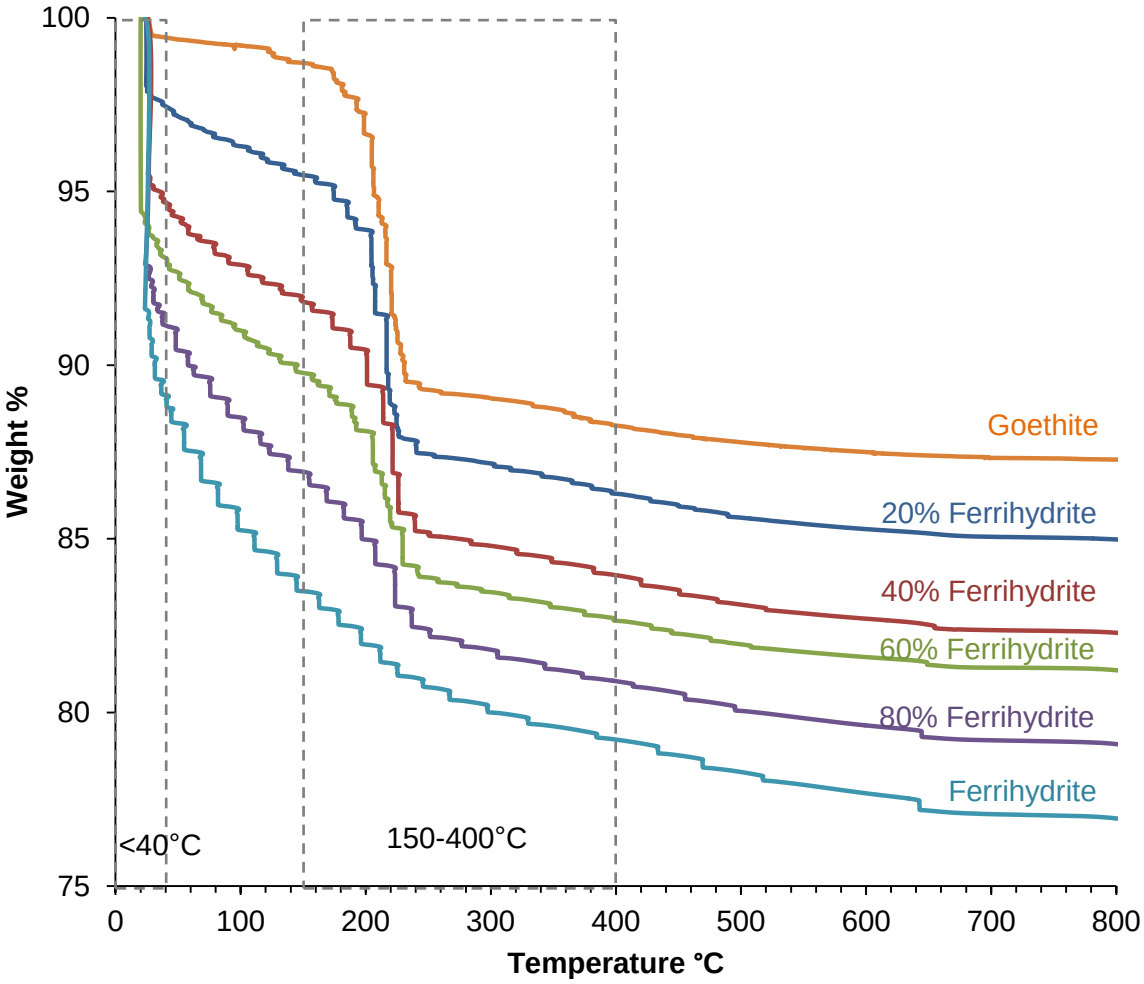

Figure 3.14: TGA weight loss profiles for goethite/ferrihydrite mixtures.

Table 3.6: Thermal analysis weight losses recorded for goethite/ferrihydrite mixtures.

Wt% Ferrihydrite in Goethite Sample	Wt% lost ≤40°C	Wt% lost 150-400°C
0.0	0.6	10.4
21.1	2.5	9.2
39.8	5.3	7.9
59.9	6.9	7.1
79.6	8.9	6.0
100.0	11.0	4.3

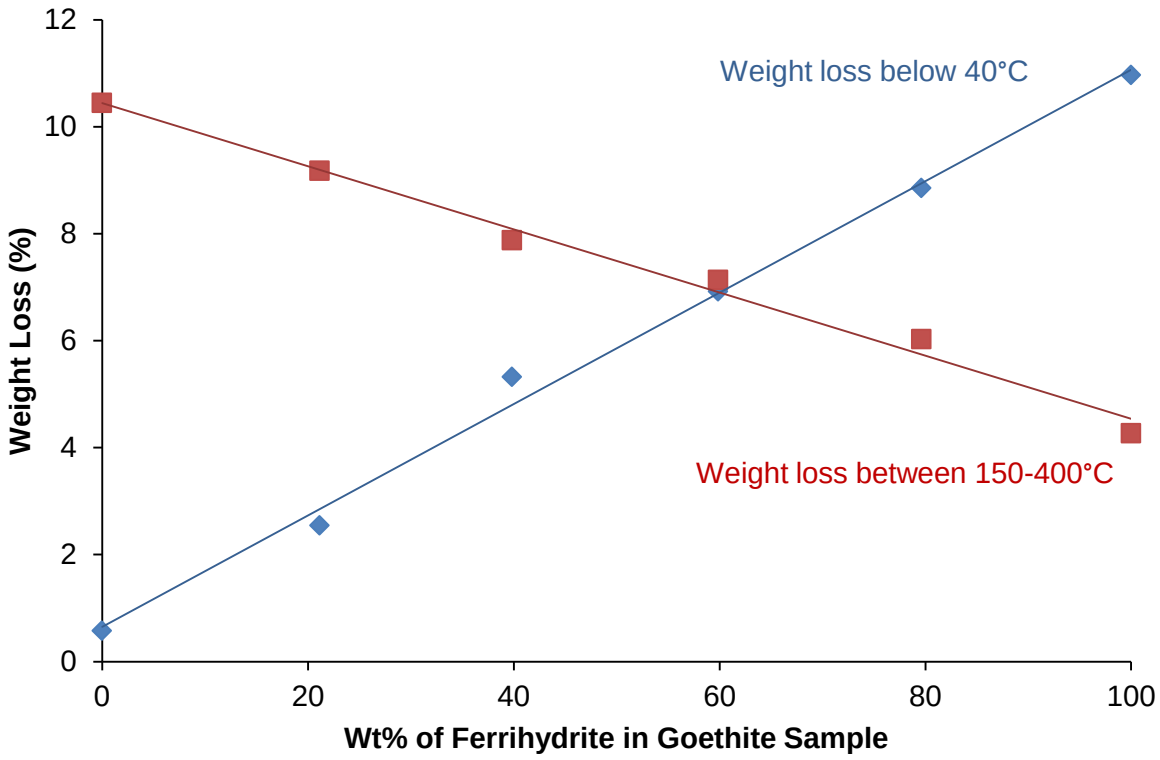

Figure 3.15: The relationship between the proportion of ferrihydrite in a ferrihydrite/goethite mixture and the weight loss which occurs in different temperature ranges.

The strong linear correlations observed in Figure 3.15 between the weight loss and wt% of ferrihydrite in the samples indicates that TGA could be utilised in both detection and quantification of ferrihydrite when associated with goethite samples. The equation of the trendline for the data relating the weight loss below 40°C to the amount of ferrihydrite in a sample is shown in Equation 3.6. The possible use of this for estimating the ferrihydrite content in real goethite samples will be investigated later in this chapter. The correlation of the weight loss below 40°C with the wt% ferrihydrite has been chosen rather than the correlation between the weight loss at 150-400°C with the wt% ferrihydrite because the former has no input from goethite, whereas the latter region has weight losses for both of the phases.

Equation 3.6: Relationship between the weight loss below 40°C and the wt% ferrihydrite in a goethite/ferrihydrite mixture (y = wt% loss, x = wt% ferrihydrite).

$$y = 0.1042x + 0.6475$$

To ensure the weight loss measurements were reproducible, TGA analysis was carried out on the same sample five times and the weight loss which occurred below 40°C was recorded. This repetition of analysis, presented in Appendix 3, showed that the technique produced reproducible results, with the weight loss occurring below 40°C varying by just 0.3 wt% across all samples, and the resulting estimation of ferrihydrite content for the samples, calculated using Equation 3.6, varying by less than 3 wt%.

IR Spectroscopy

IR spectroscopy can be used to differentiate between goethite and ferrihydrite using each minerals' characteristic IR bands. There are three important diagnostic bands used in the identification of goethite at ~892 cm^{-1}, 795 cm^{-1} and ~630 cm^{-1}.[52, 53] These bands should not be present in a pure ferrihydrite sample, where the only bands observed should be at ~3400 and ~1635 cm^{-1}.[44]

IR spectra for all six of the goethite/ferrihydrite mixtures were recorded and are shown in Figure 3.16. Goethite can be clearly identified in mixtures containing 20 wt% or more goethite and the positions of the bands observed are in good agreement with those identified above. Even the pure ferrihydrite sample has weak bands at ~892 and 795 cm^{-1}, suggesting that even in this sample, an amount of crystalline goethite is present, however the remainder of the spectrum matches that expected for ferrihydrite. In all cases there are a number of bands between ~1300-1600 cm^{-1} which result from adsorbed carbonate species, and physically adsorbed surface water. [2, 26, 54]

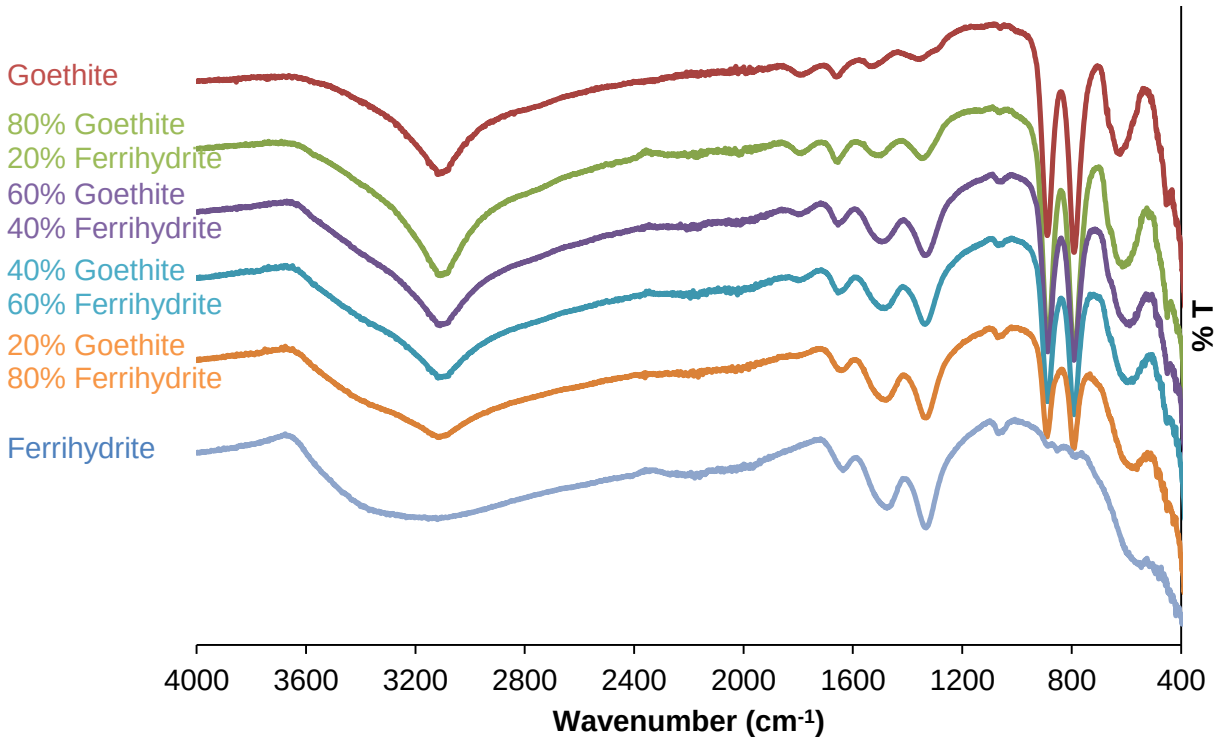

Figure 3.16: IR spectra recorded for goethite/ferrihydrite mixtures.

In an attempt to assess the potential for features in the IR spectra of goethite samples to be utilised in the identification and quantification of ferrihydrite association with goethite,

the positions of the diagnostic goethite bands were compared to one another and to the relative goethite/ferrihydrite proportions, shown in Table 3.7.

Table 3.7: IR band positions in goethite/ferrihydrite mixtures.

wt% ferrihydrite mixed with goethite	OH in plane (cm^{-1})	OH out of plane (cm^{-1})	Fe-O stretch (cm^{-1})
0.0	892	793.5	627.5
21.1	890.5	793.5	616.5
39.8	890.5	795	596
59.9	891.5	794.5	597
79.6	892	796	578.5
100.0	-	-	562.5

The only band where any correlation could be found between the position of that band and the goethite/ferrihydrite ratio was that of the Fe-O stretch (Figure 3.17). The position of this band decreases from 627.5 cm^{-1} for the pure goethite sample, to 562.5 cm^{-1} for the pure ferrihydrite sample, however the band becomes broader as the amount of ferrihydrite increases so the maxima become more difficult to identify, hence increasing the error.

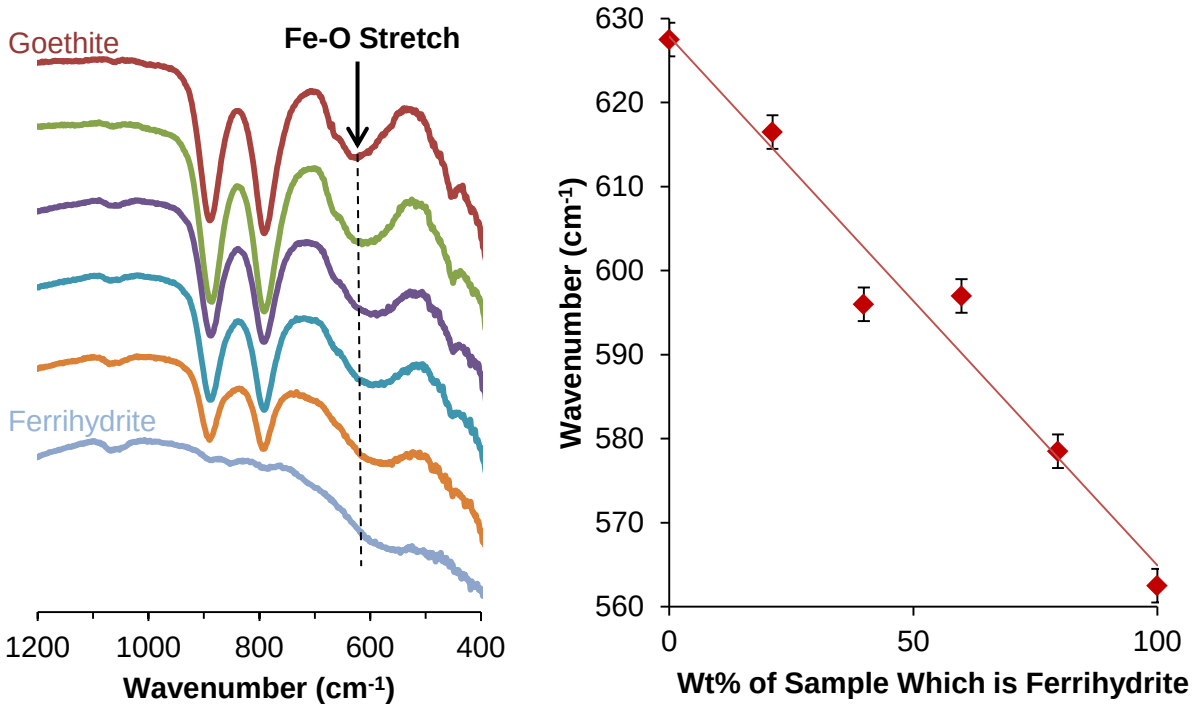

Figure 3.17: Relationship between the position of the Fe-O stretch and the proportion of ferrihydrite in a goethite sample.

The relationship between the intensities of the bands at ~3145 cm^{-1} (OH-stretching vibrations in goethite) and ~3410 cm^{-1} (absorbtion maximum of ferrihydrite OH groups) were also investigated (see Figure 3.18), as this has been the subject of previous work by Houben *et al.* (2001).[55]

The authors suggested the use of IR as an alternative to BET (Brunauer-Emmett-Teller theory) measurements in the estimation of specific surface area (SSA). Their premise was that, as ferrihydrite transforms to goethite the SSA decreases, so by knowing the SSA of an iron oxide sample, the proportions of ferrihydrite/goethite in that sample can be estimated. In an attempt to expand on the findings of Houben *et al.* the band positions and ratio between the bands of the goethite/ferrihydrite mixtures characterised in this section are shown in Table 3.8.

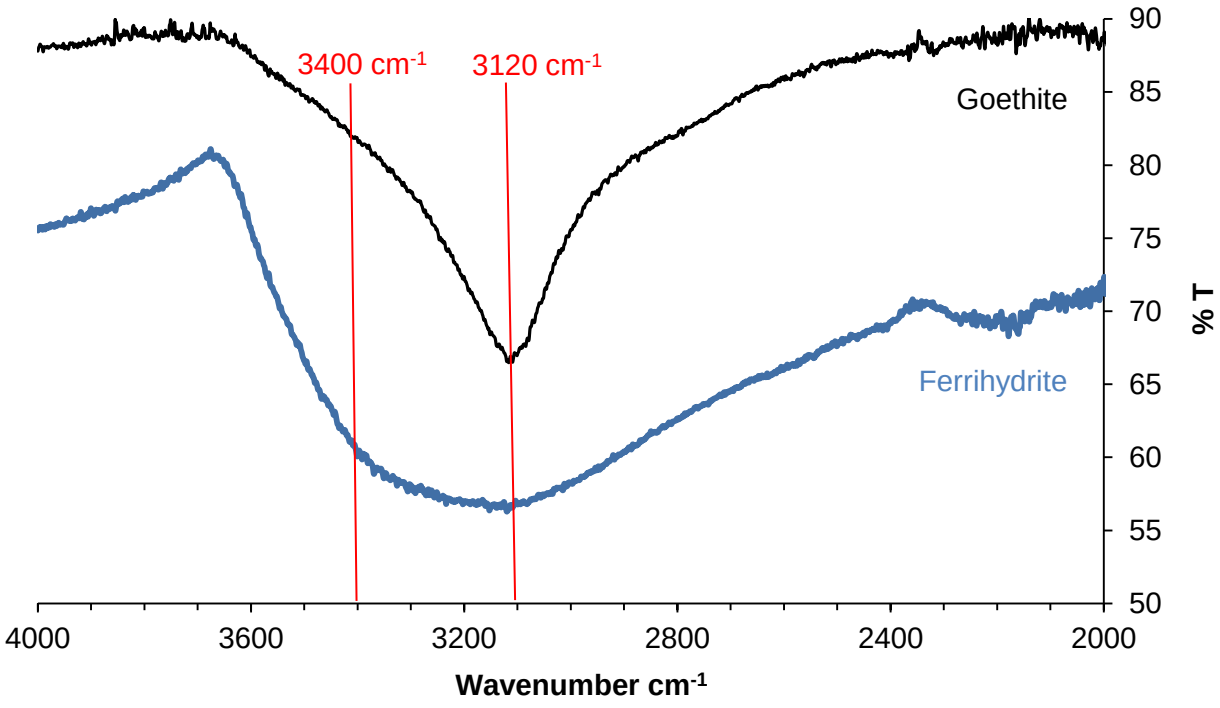

Figure 3.18: IR spectra of goethite (black) and ferrihydrite (blue).

Table 3.8: Band positions and ratio of bands at 3120 cm^{-1} and 3400 cm^{-1} in goethite/ferrihydrite mixtures.

Sample wt% Ferrihydrite	Intensity of band:		Ratio
	3120 cm^{-1}	3400 cm^{-1}	3400/(3400+3120)
0.0	56.4	77.3	0.58
21.1	57.0	83.2	0.59
39.8	52.4	73.4	0.58
59.9	70.2	74.8	0.52
79.6	65.2	76.0	0.54
100.0	56.4	60.2	0.52

When plotted (Figure 3.19), there does appear to be some correlation between the amount of ferrihydrite in the mixture and the ratio between the band positions, which agree with the results obtained by Houben *et al.* (2001), however there are not enough data points in this investigation to be wholly confident in the results. The previous authors concluded that the use of IR band ratios was not a viable technique for estimating the SSA (and hence ferrihydrite content) of goethite samples, because the band at ~3400 cm^{-1} depends largely on the amount of adsorbed water which is reported to be as high as 100 g kg^{-1} in air dried samples.[51, 55] The drying conditions can therefore have a huge impact on the intensity of this band and hence affect the correlation. For this reason, the ratio of the intensity of the OH group bands in goethite and ferrihydrite will not be used to attempt identification and/or quantification of ferrihydrite in this study.

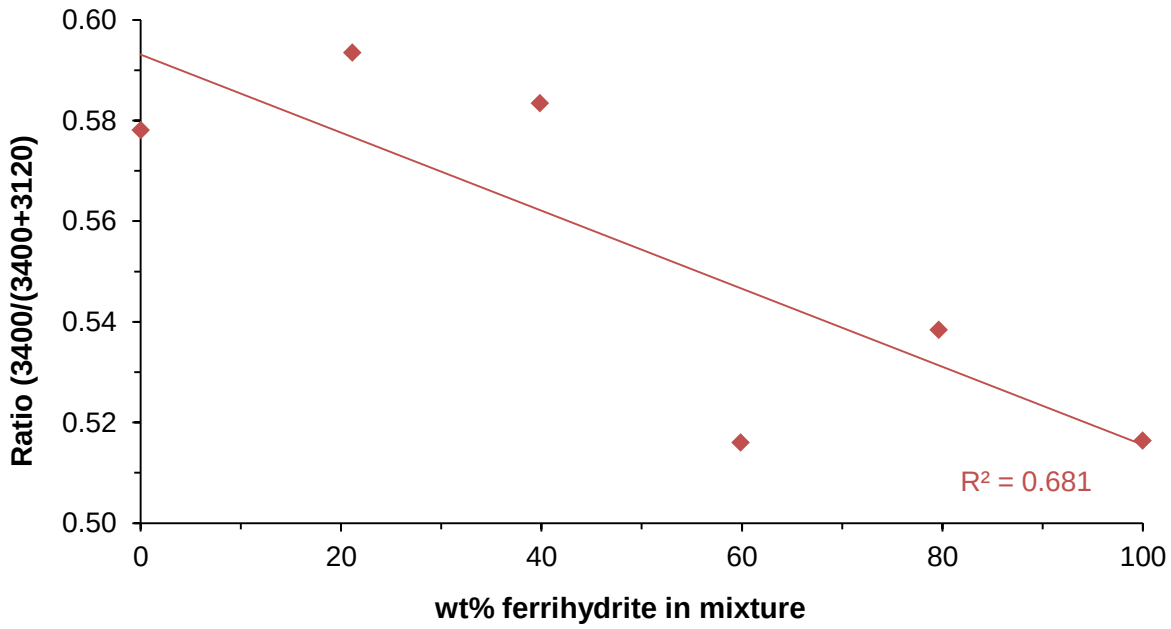

Figure 3.19: The relationship between wt% ferrihydrite in a goethite/ferrihydrite mixture and the ratio of IR bands.

The characterisation of the goethite/ferrihydrite mixtures using IR spectroscopy suggests that this isn't a particularly strong technique to use in order to identify the presence, or estimate the quantity, of ferrihydrite in association with goethite samples. However, the relationship between the position of the Fe-O stretch and the proportion of ferrihydrite in the sample (shown in Equation 3.7 and taken from Figure 3.17), will be used in section 3.3.4. to compare with the other techniques in estimating the proportion of ferrihydrite present in goethite samples.

Equation 3.7: The relationship between the position of the Fe-O stretch in the IR spectrum and the proportion of ferrihydrite in a goethite sample.

$$y = -0.6294x + 627.86$$

Where y = wavenumber of Fe-O band and x = wt% ferrihydrite

Raman Spectroscopy

Raman spectroscopy was carried out on the goethite/ferrihydrite mixtures to ascertain whether this was a technique which could be used in order to identify ferrihydrite associated with goethite, as the two phases have distinct bands in their respective spectra. Unfortunately, because the samples were just physical (hand prepared) mixtures of the two phases, both goethite and ferrihydrite type spectra were acquired for each of the mixed samples, depending on the exact spot that was analysed.

Figure 3.20 shows an example of the type of Raman spectra that were acquired from two different spots on the 80 wt% goethite/ 20 wt% ferrihydrite mixture. Two different types of spectra were obtained, one that was mainly ferrihydrite (although bands relating to goethite can also be observed) and one that could be attributed wholly to goethite. Data collected on all of the hand mixed goethite/ferrihydrite samples found them to be very heterogeneous and it was therefore concluded that a calibration graph could not be produced to allow the quantification of ferrihydrite proportions using Raman data.

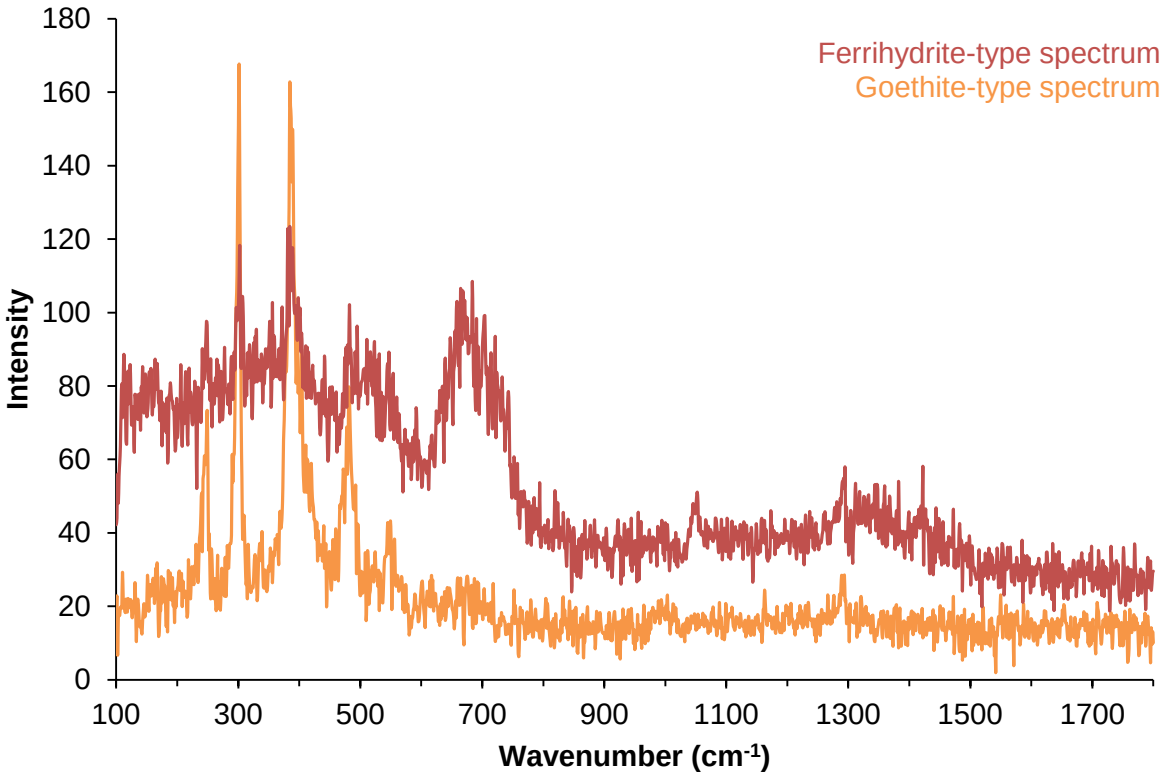

Figure 3.20: Two distinct types of Raman spectra acquired from characterisation of the 80 wt% goethite / 20 wt% ferrihydrite sample.

3.3.4. The Effect of Synthesis Time and Temperature on the Formation of Goethite

Introduction

The synthesis duration and temperature have a significant effect upon the formation of goethite (when produced via the Fe(III) route described in Chapter 2 and used throughout this thesis). As the synthesis time and/or temperature are varied, so the extent of transformation from the ferrihydrite precursor to goethite changes, and these variables can also affect other characteristics of the goethite samples produced such as crystallinity and morphology. [46, 56]

Schwertmann *et al.* (1985) investigated the effect of synthesis temperature on the characteristics of goethites produced from a ferrihydrite precursor. Their study varied the temperature between 4-90°C, and monitored the reaction over time, stopping it once less than 2% of the product was oxalate soluble (hence ensuring at least 98% conversion of ferrihydrite to goethite). They found that the duration of synthesis (to achieve an oxalate-soluble portion of less than 2%) decreased as the synthesis temperature was increased, from 68 days at 4°C, to 6 days at 70°C. [56]

In this section of work, goethite was synthesised at four different temperatures; ~20°C, 40°C, 70°C and 90°C, and left for time periods ranging from 0-24 hours, to monitor how both of these factors would affect the extent to which ferrihydrite transformed to the more stable goethite phase, and identify if there were any other differences in the characteristics of the goethite samples produced. Having previously explored (section 3.3.3) the potential of a number of characterisation techniques (e.g. PXRD, TGA) to quantify the proportions of goethite and ferrihydrite present in two-phase mixtures, it should be possible to estimate the extent of the transformation from ferrihydrite to goethite as a function of time and temperature.

PXRD

From examination of the PXRD patterns collected on the variable synthesis temperature/duration series of goethite samples described above, it can be seen that both the temperature and time period have a large impact on the extent of transformation. At the lower (≤40°C) syntheses (Figure 3.21 and Figure 3.22), even after 24 hours, the goethite produced is poorly crystalline, with broad peaks (and many that are not observed at all). The goethite produced from the higher (≥70°C) temperature syntheses (Figure

3.23 and Figure 3.24) are much more crystalline after 24 hours than the lower temperature samples, with intense, sharp peaks visible on the diffraction patterns.

In all cases, the first traces of goethite can be observed after ~3h – at a synthesis temperature of 90°C. There appears to be a well formed, crystalline product even after this short time period. The 90°C sample also contains traces of hematite in the samples with a synthesis time ≥11h (Figure 3.24).

These results suggest that the transformation of ferrihydrite to goethite is strongly affected by the synthesis temperature and duration; for example the sample prepared at 20°C still has a large proportion of ferrihydrite present after 24 hours, whereas those samples prepared at 70 and 90°C have completely transformed in this time period.

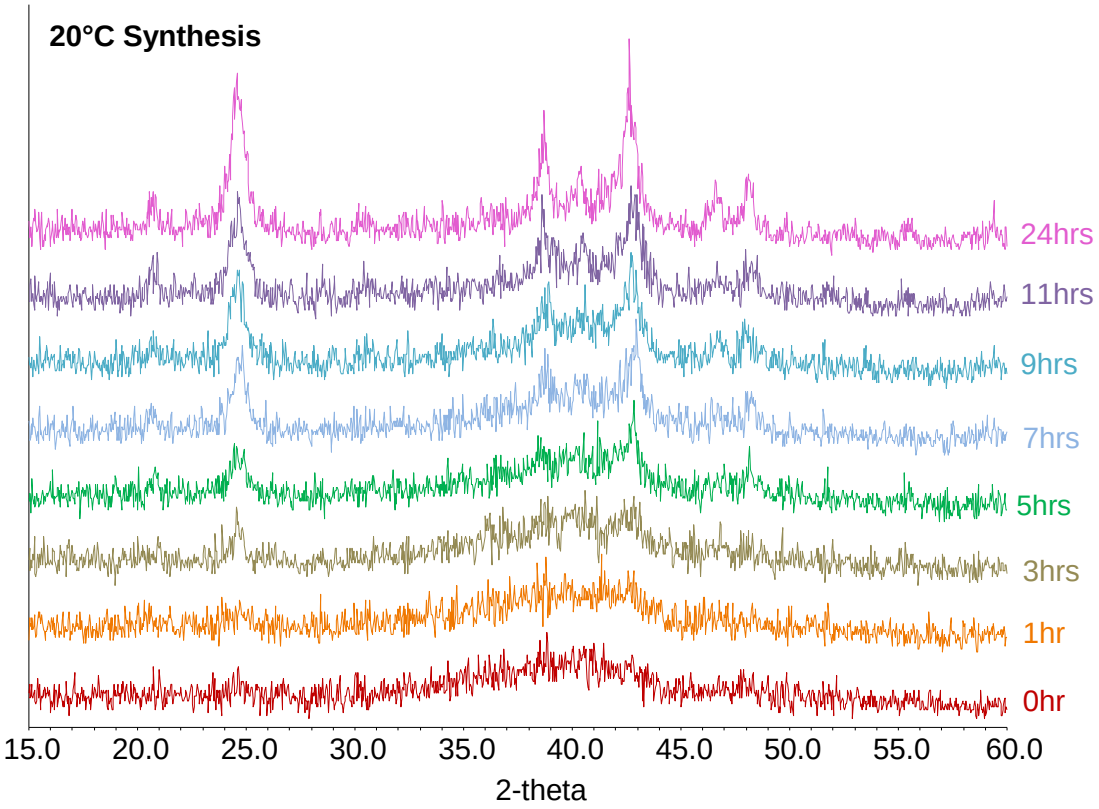

Figure 3.21: PXRD patterns showing the effect of synthesis duration on goethite prepared at 20°C.

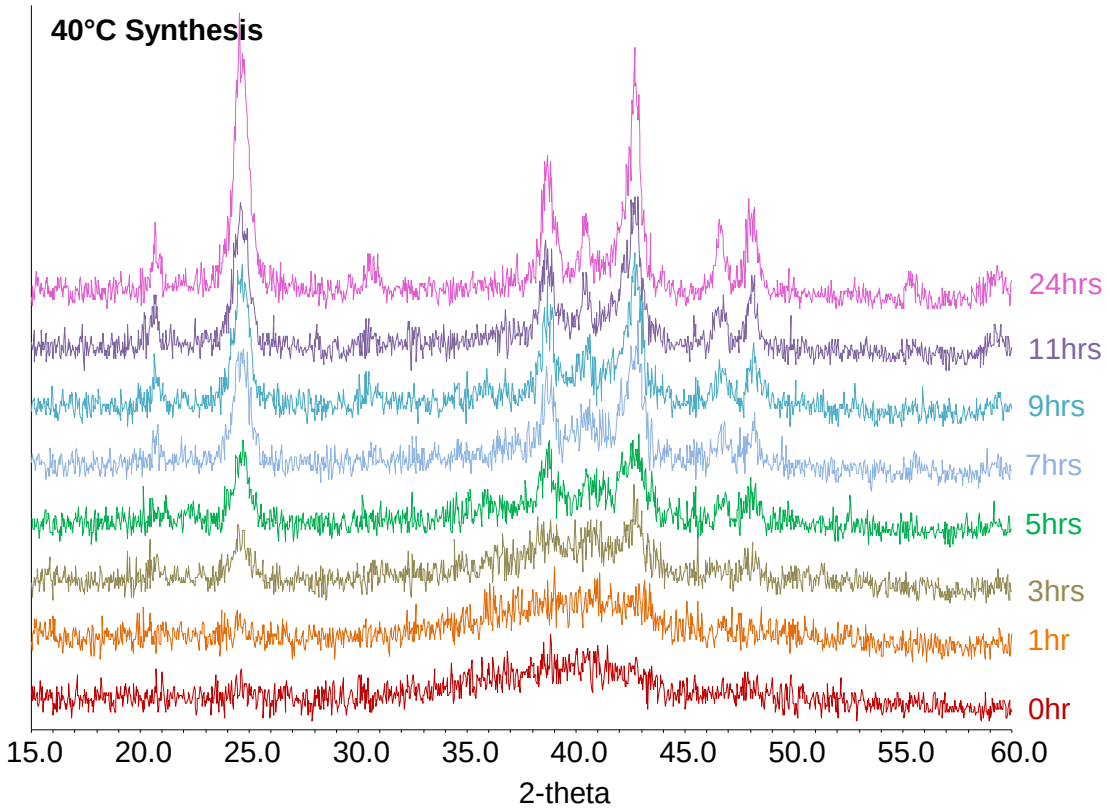

Figure 3.22: PXRD patterns showing the effect of synthesis duration on goethite prepared at 40°C.

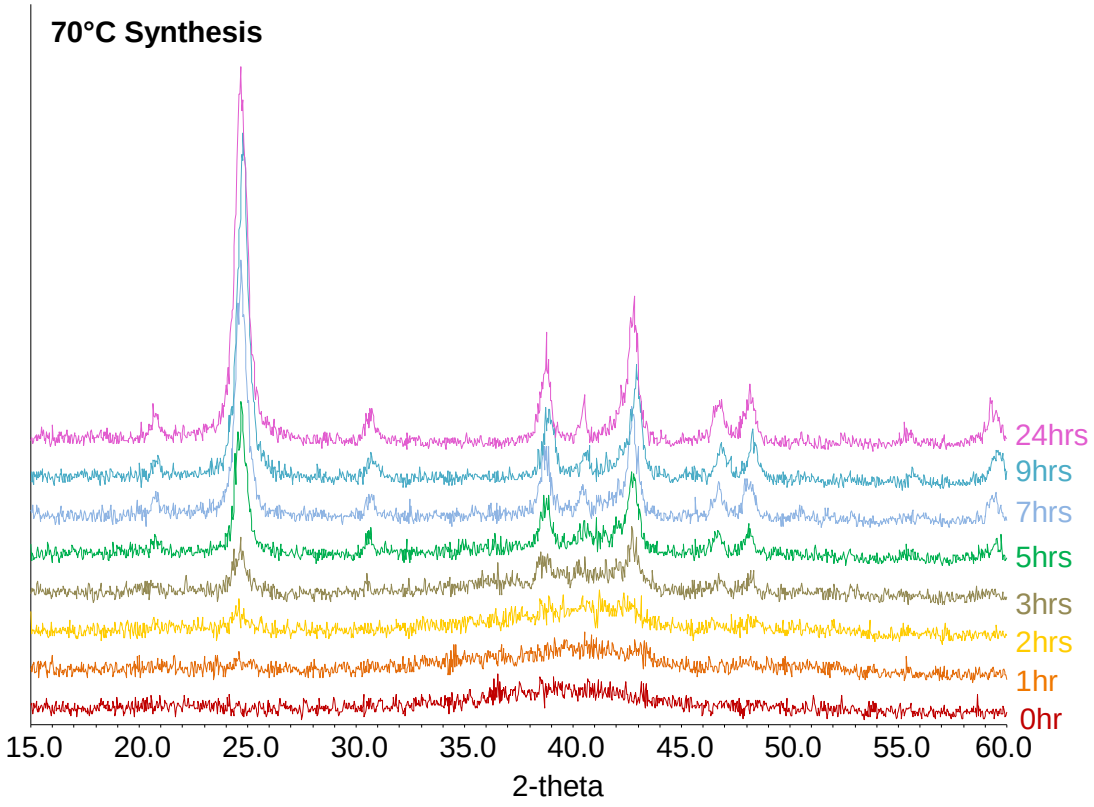

Figure 3.23: PXRD patterns showing the effect of synthesis duration on goethite prepared at 70°C.

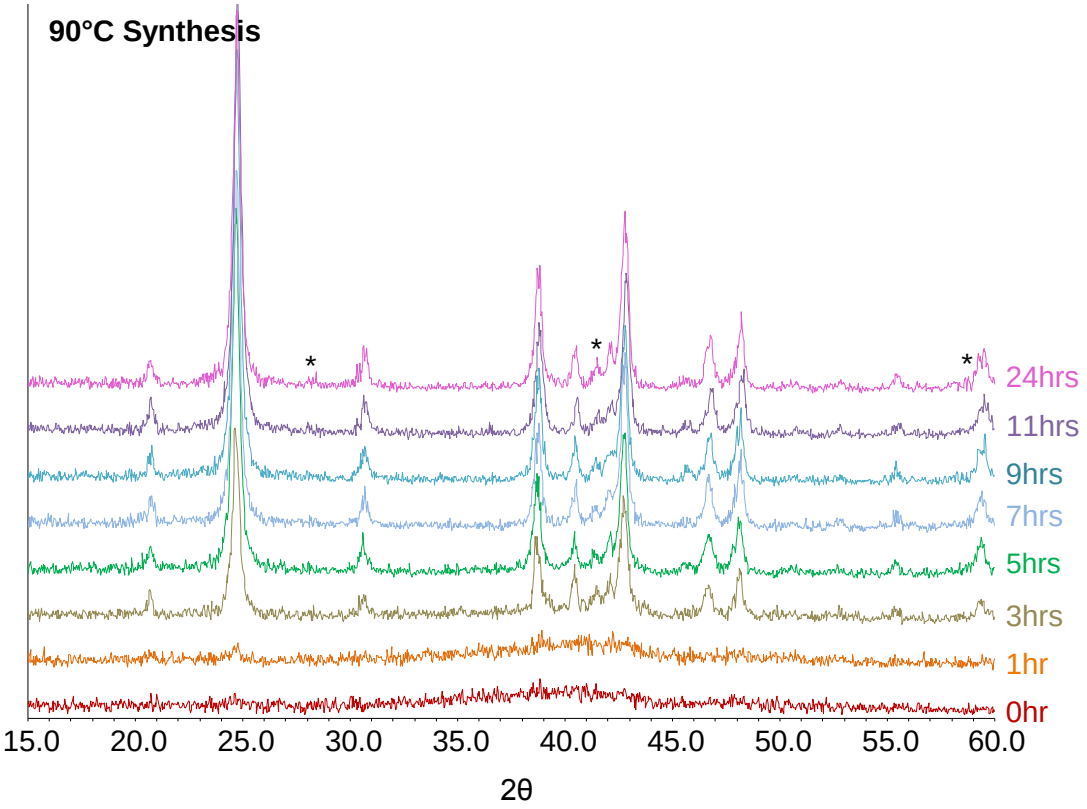

Figure 3.24: PXRD patterns showing the effect of synthesis duration on goethite prepared at 90°C. Hematite reflections marked by *.

Using the data collected in section 3.3.3., where characterisation techniques were investigated to allow identification and quantification of the relative proportions of ferrihydrite and goethite in physical mixtures, the extent of transformation of ferrihydrite to goethite as a function of both the synthesis temperature and time can be examined.

Earlier in this work, the relationship between the ratio of the intensities of the 110 goethite reflection (~24° 2θ) and the background around 40° 2θ with the proportion of ferrihydrite in a sample (Figure 3.12) was investigated and found to be a possible method of estimating the quantity of ferrihydrite present in association with a goethite sample. The intensities measured from the PXRD patterns (Figures 3.21-3.24) for the goethite samples synthesised at different temperatures and durations are shown in Table 3.9.

Table 3.9: Intensity measurements and ratios taken from PXRD data on goethite samples synthesised at different temperatures (grey boxes where data unavailable).

Synthesis Time (hrs)	20°C Synthesis			40°C Synthesis			70°C Synthesis			90°C Synthesis		
	Measured Intensity		Ratio	Measured Intensity		Ratio	Measured Intensity		Ratio	Measured Intensity		Ratio
	~24° 2θ	~40° 2θ		~24° 2θ	~40° 2θ		~24° 2θ	~40° 2θ		~24° 2θ	~40° 2θ	
0	21	22	1.0	21	22	1.0	15	23	0.7	20	22	0.9
1	21	23	0.9	20	23	0.9	22	24	0.9	22	22	1.0
2							31	23	1.3			
3	30	25	1.2	28	22	1.3	46	22	2.1	164	16	10.1
5	28	24	1.2	39	19	2.1	105	17	6.0	311	12	25.7
7	40	23	1.8	50	20	2.5	176	14	12.2	304	10	30.8
8							233	14	16.5			
9	43	23	1.9	59	21	2.8				367	10	38.5
11	47	23	2.1	60	20	3.1				371	10	38.9
24	65	21	3.1	105	17	6.1	251	11	23.0	321	11	29.9

Using Equation 3.4: $y = 0.0022x^2 - 0.5293x + 31.568$ (taken from the characterisation work carried out on goethite/ferrihydrite mixtures), the proportions of un-transformed ferrihydrite (wt%) remaining in each of the goethite samples was estimated, shown in Table 3.10 and Figure 3.25.

Table 3.10: Estimates, using PXRD data, of the amount of untransformed ferrihydrite (wt%) present in the goethite samples as a result of varying the synthesis temperature and duration.

Synthesis time (hours)	Synthesis Temperature			
	20°C	40°C	70°C	90°C
0	97	97	100	97
1	97	98	97	96
2			93	
3	95	94	88	52
5	95	88	67	12
7	90	85	45	2
8			33	
9	89	83		-12
11	88	81		-13
24	81	66	17	3

Examining the estimations shown in the table of the amount of untransformed ferrihydrite present in the samples, attention is drawn to the negative proportions for the wt%

ferrihydrite in the 9 and 11h syntheses at 90°C. This is clearly a downfall of the estimation technique and could be due to the presence of hematite in the samples which affects the relative intensities of the two points in the diffraction pattern being used for this analysis.

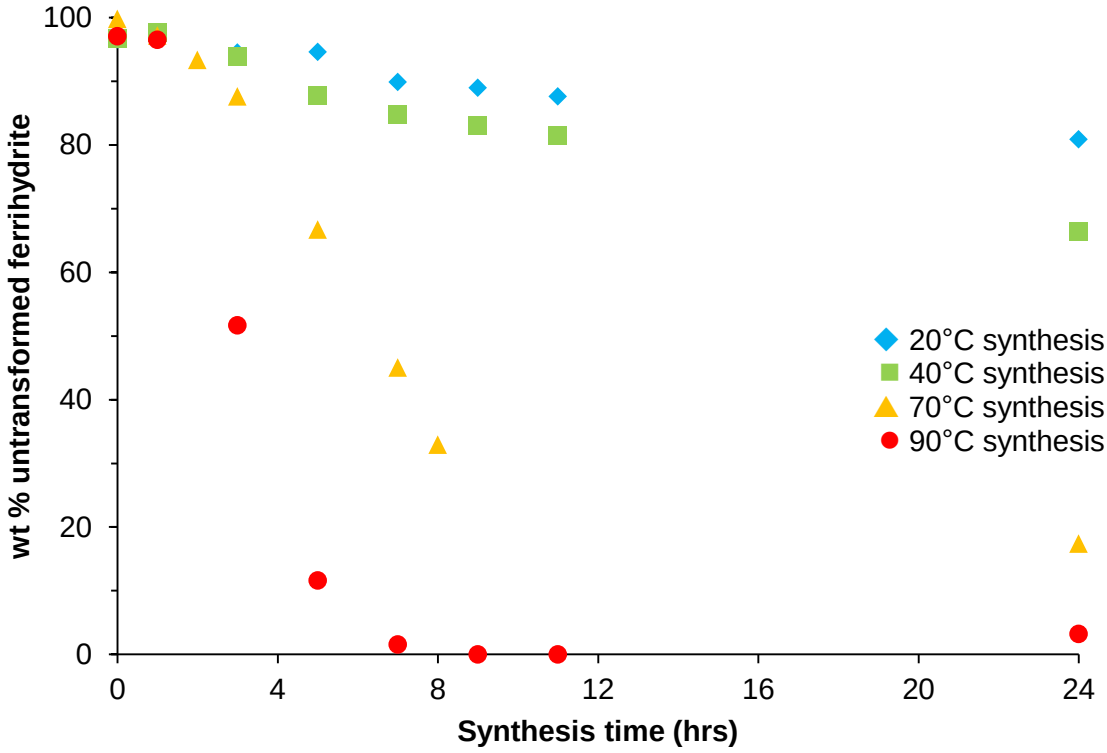

Figure 3.25: A plot of the proportion (wt%) of untransformed ferrihydrite in goethite samples after various synthesis durations. Negative estimates of ferrihydrite proportion in the 9 and 11h 90°C synthesis are shown as 0 wt% in this figure.

The proportions of ferrihydrite estimated to remain in the samples (Table 3.10) show the transformation of ferrihydrite to goethite occurs more quickly (based on the fact that less ferrihydrite is estimated to be present) the higher the synthesis temperature. For example, using this quantification technique it could be estimated that after 24 hours at 20°C, over 80 wt% of the sample is ferrihydrite, whereas at the 70°C synthesis temperature, just 17 wt% ferrihydrite remains.

TGA

In section 3.3.3., TGA was highlighted as a technique which appeared to have particular promise in identifying the presence of ferrihydrite in goethite samples. A strong correlation was observed in the data between the weight loss which occurred below 40°C as the samples were heated, and the proportion of ferrihydrite in the goethite/ferrihydrite mixtures. It was hoped this characterisation technique could be used to monitor the extent of transformation from ferrihydrite to goethite under the different synthesis conditions.

The weight loss profiles for each set of goethite samples (synthesis temperatures 20, 40, 70 and 90°C) are shown in Figures 3.26-3.29 and the weight losses which were measured below 40°C for each sample are shown in Table 3.11.

Table 3.11: Weight loss measured below 40°C from TGA profiles for goethites with variable synthesis conditions.

Synthesis Time (hrs)	Weight % lost below 40°C from TGA profiles:			
	20°C Synthesis	40°C Synthesis	70°C Synthesis	90°C Synthesis
0	11.0	11.0	11.0	11.0
1	10.4	10.0	9.8	10.2
2			9.7	
3	9.6	8.7	7.0	3.9
5	9.4	8.5	6.4	1.6
7	8.3	7.4	4.3	0.7
8			3.4	
9	7.6	6.7		0.6
11	7.4	5.9		0.4
24	6.0	3.8	1.2	0.4

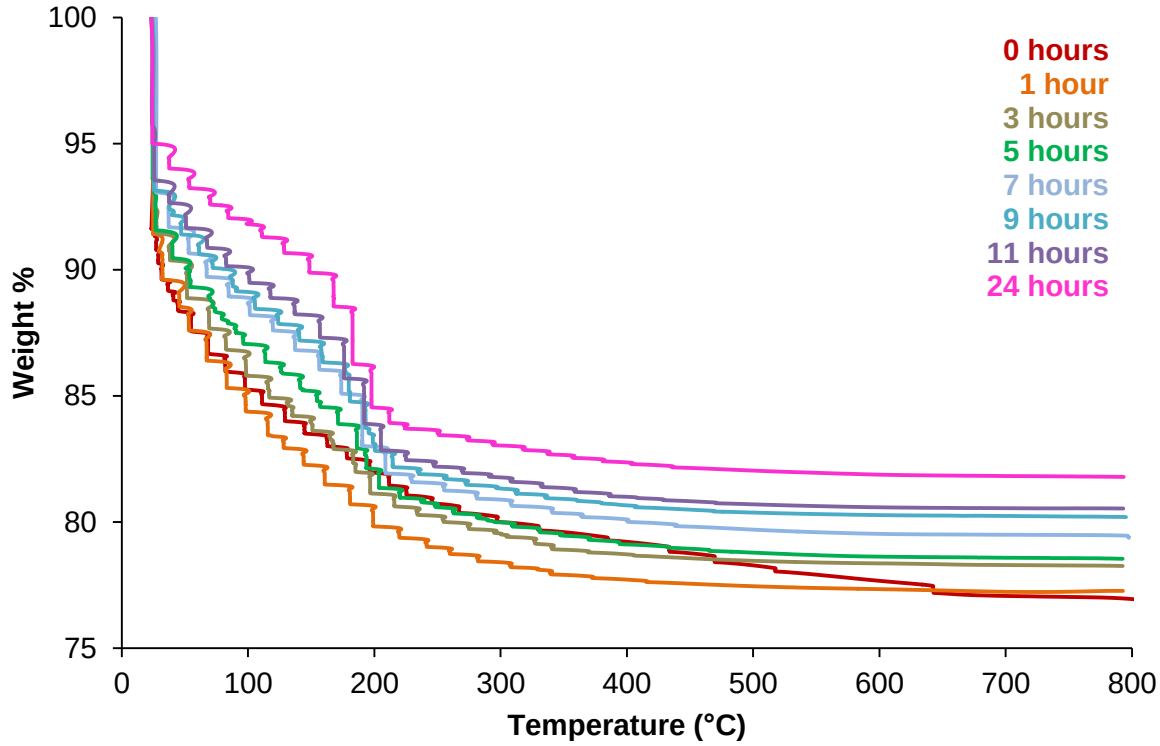

Figure 3.26: TGA weight loss profiles for goethites synthesised at 20°C.

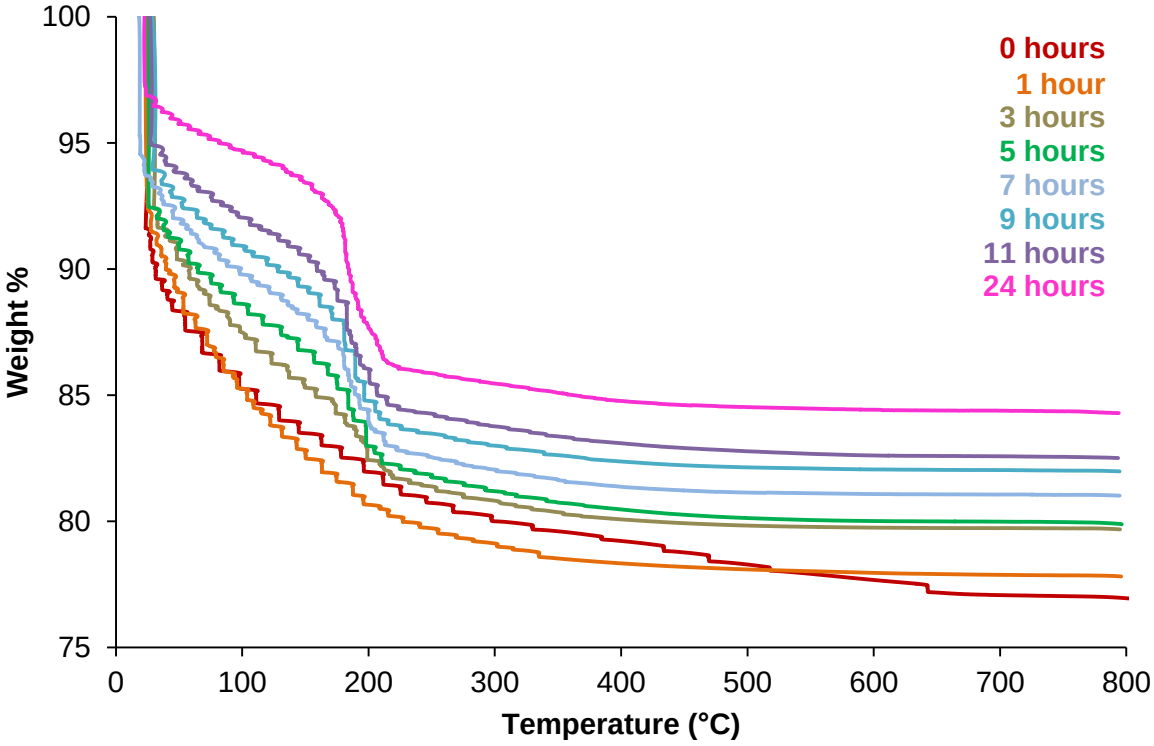

Figure 3.27: TGA weight loss profiles for goethites synthesised at 40°C.

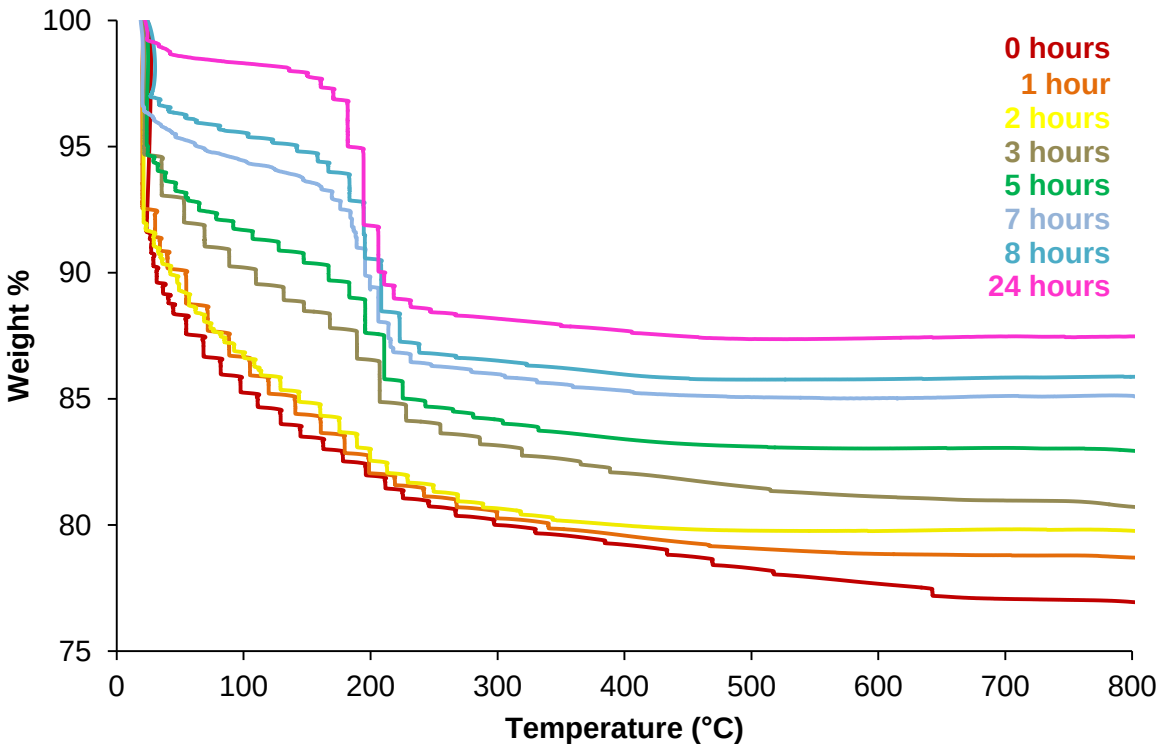

Figure 3.28: TGA weight loss profiles for goethites synthesised at 70°C.

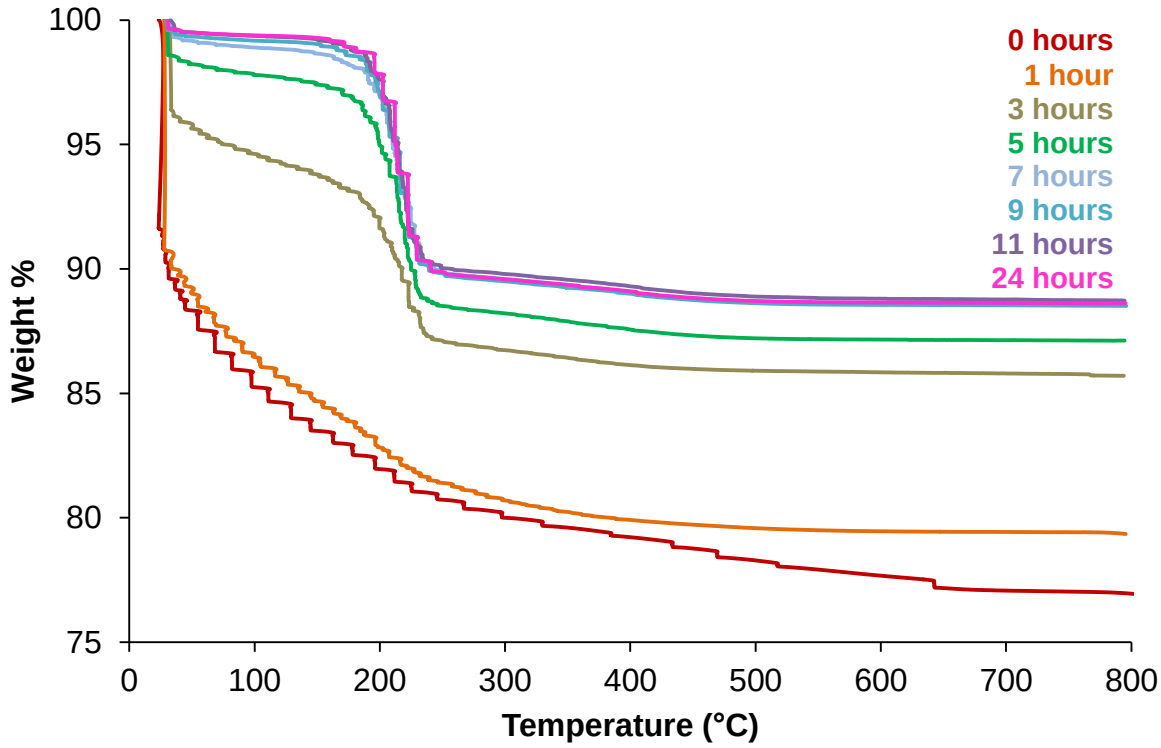

Figure 3.29: TGA weight loss profiles for goethites synthesised at 90°C.

The weight loss plots and accompanying table of weight loss measurements show that the weight loss (and therefore ferrihydrite content) is greatest at the lowest synthesis temperatures and shortest synthesis durations. As the time and/or temperature is increased the associated weight loss below 40°C decreases, as more of the sample has transformed to goethite. A higher synthesis temperature promotes the transformation of ferrihydrite to goethite, whereas at lower temperatures the transformation occurs more slowly resulting in a proportion of the sample remaining as an un-transformed ferrihydrite phase (in the time scales that the synthesis was investigated over here). At the higher synthesis temperatures the transformation seems to be occurring more rapidly – for example after 7 hours synthesis at 90°C the weight loss which occurs below 40°C is just 0.7 wt%, whereas at a 20°C synthesis temperature there is still a weight loss of 8.3 wt%, see Figure 3.30. This is supported by the work of Schwertmann *et al.* (1985), where the authors found that the time taken for goethite to form from a ferrihydrite precursor varied with temperature, ranging from 28 days at 15°C, to just 6 days at 70°C.[56]

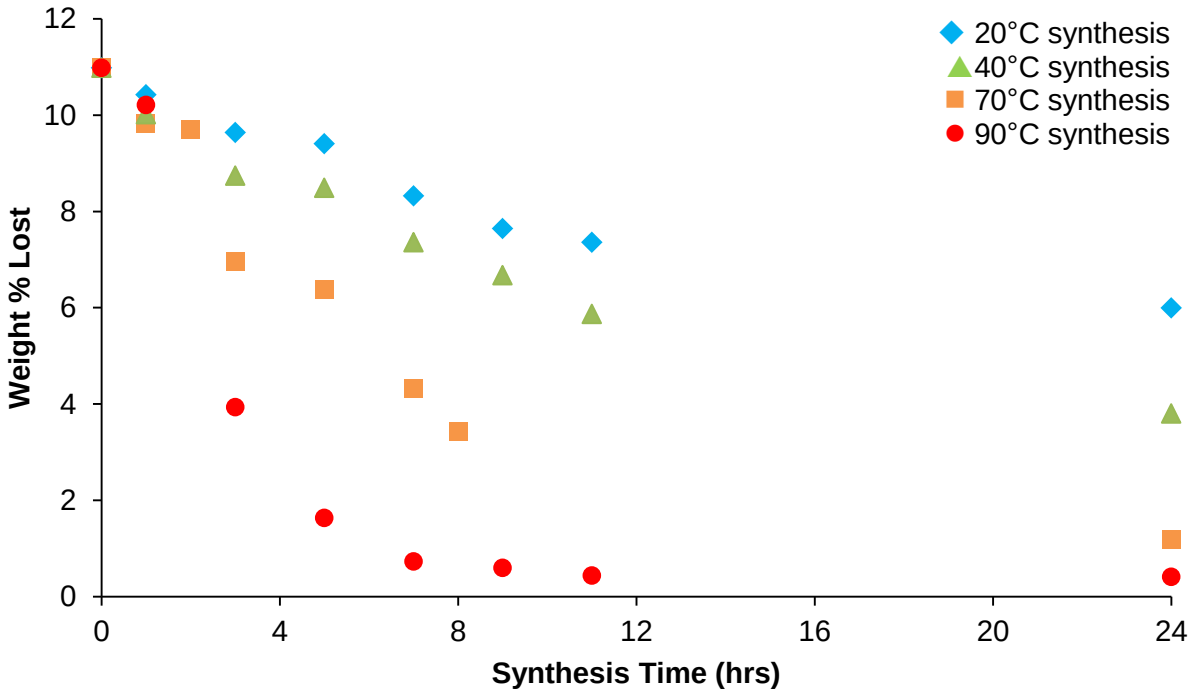

Figure 3.30: Weight % of sample lost (taken from TGA plot) below 40°C for goethites synthesised at different temperatures over 24 hours.

Using Equation 3.6 from section 3.3.3., $y = 0.1042x + 0.6475$, where y = wt% lost below 40°C and x = wt% ferrihydrite in a goethite/ferrihydrite mixture, the amount of untransformed ferrihydrite that remained in each goethite sample prepared under the various conditions could be estimated, and the values are shown in Table 3.12.

Table 3.12: Proportion of ferrihydrite in goethite samples, estimated using TGA data.

Synthesis Time (hours)	Estimates proportion of sample that is ferrihydrite (wt%)			
	20°C	40°C	70°C	90°C
0	99	99	99	99
1	94	90	88	92
2			87	
3	86	78	61	32
5	84	75	55	10
7	74	64	35	1
8			27	
9	67	58		-1
11	64	50		-2
24	51	30	5	-2

These results suggest that after 24 hours, untransformed ferrihydrite remained in all of the samples except for those prepared at 90°C (where PXRD showed that some of the sample had transformed to hematite), ranging from over 50 wt% ferrihydrite at a 20°C synthesis temperature, to ~5 wt% at 70°C, see Figure 3.31.

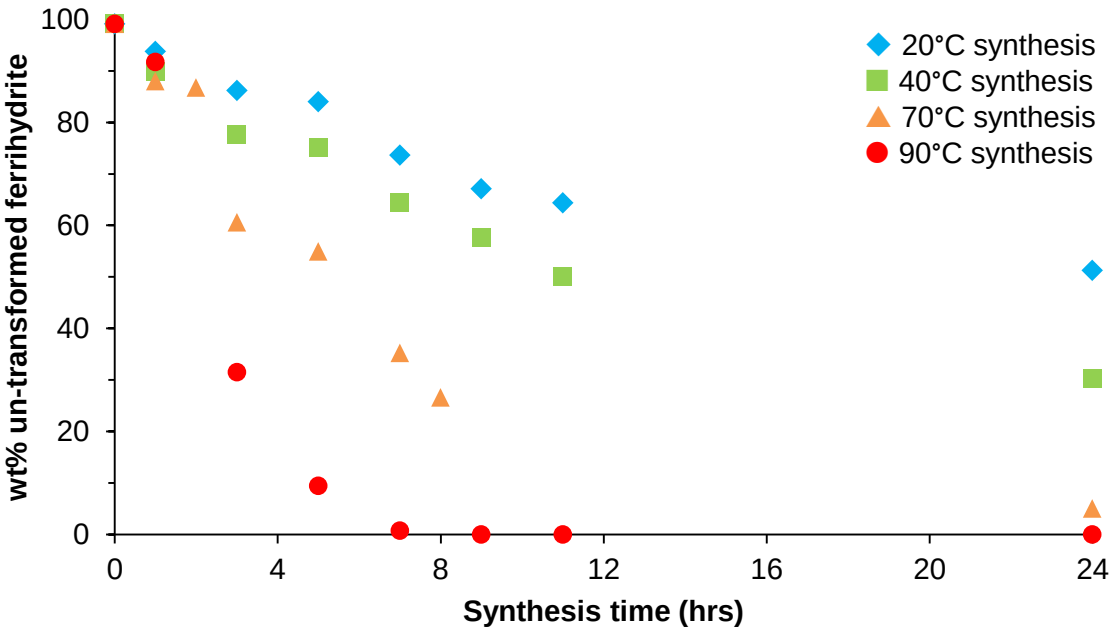

Figure 3.31: A plot of the proportion (wt%) of untransformed ferrihydrite in goethite samples after various synthesis durations, estimated using TGA. Negative estimates of ferrihydrite proportion in the 9, 11 and 24h 90°C synthesis are shown as 0 wt% in this figure.

IR Spectroscopy

The effectiveness of using IR in estimating the proportion of ferrihydrite in a mixture with goethite was questioned (section 3.3.3), due to difficulties in accurately identifying band positions when they are very broad, and differences that occur in the IR spectrum of ferrihydrite as a result of the drying conditions used. Here, IR spectra were recorded for the set of goethite samples prepared at 70°C, shown in Figure 3.32.

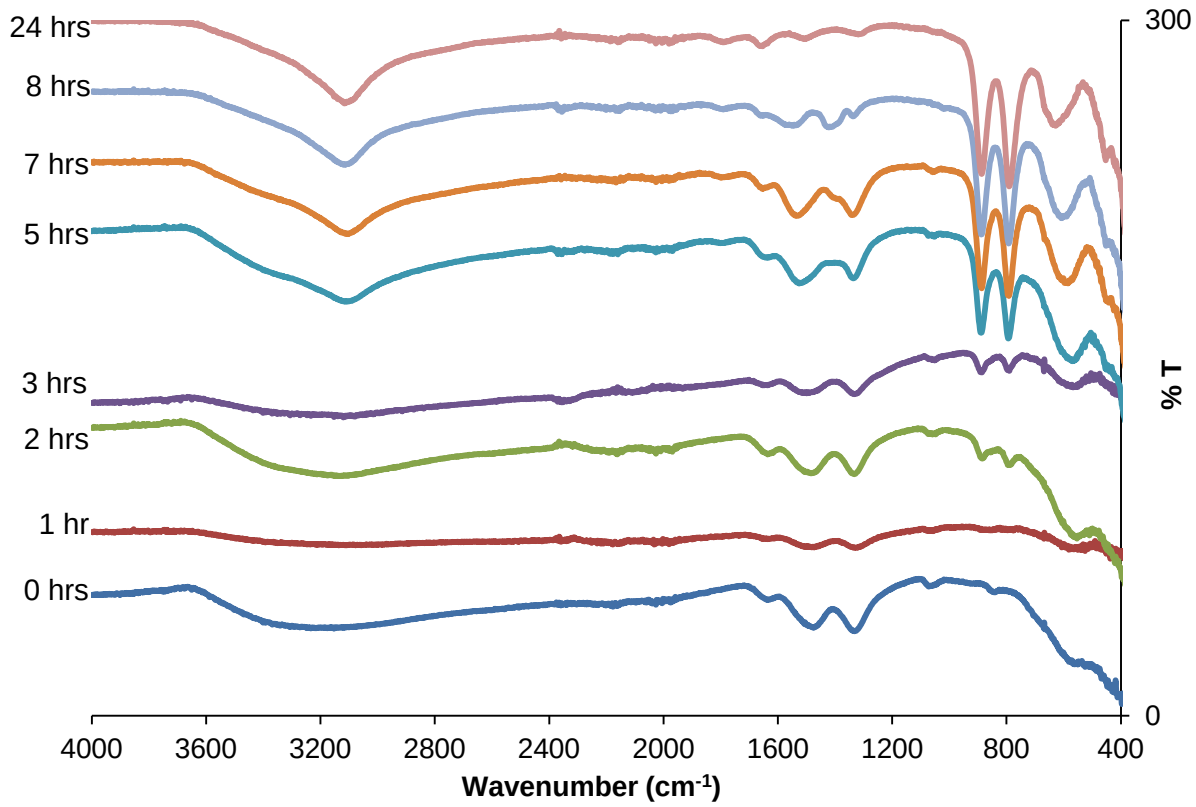

Figure 3.32: IR spectra for goethites synthesised at 70°C after different synthesis periods.

The spectra that are shown in Figure 3.32 were used to identify the exact position of the Fe-O stretch of these goethite samples (~625 cm^{-1}). This was then recorded for each of the goethites in the series, shown in Table 3.13, and by using Equation 3.7: $y = -0.6294x + 627.86$, where y = wt% ferrihydrite and x = the wavenumber of the Fe-O stretch, the amount of untransformed ferrihydrite remaining in each of the goethite samples could be estimated.

The analysis of the data shown in Table 3.13 show that the position of the Fe-O stretch shifts to a higher wavenumber as the synthesis time is increased, moving from ~550 cm^{-1} for the wholly untransformed (0h synthesis) ferrihydrite sample, to 626 cm^{-1} for the

goethite sample synthesised over 24 hours. The position of the Fe-O stretch in the 1h synthesis goethite sample could not be accurately identified.

Table 3.13: Position of the Fe-O stretch and resulting estimations of ferrihydrite proportions for a series of goethite samples synthesised at 70°C.

Synthesis Time (hrs)	Position of Fe-O stretch (cm^{-1})	Estimation of wt% ferrihydrite in sample
0	550.5	123
1	Cannot identify.	-
2	554	117
3	563.5	102
5	568	95
7	592.5	56
8	603	40
24	626	3

Examining the estimations of the ferrihydrite proportion in the samples (Table 3.13), calculated using the equation derived in section 3.3.3., it is clear that this method of quantifying the amount of ferrihydrite present is not particularly effective. The 0, 2 and 3 hour synthesis times show ferrihydrite contents that have been estimated in excess of 100 wt%, which clearly isn't possible. The main downfall of this technique is probably the difficulties (and inaccuracies) that result from identifying the Fe-O stretch band position, especially in ferrihydrite rich samples where the band is broad and poorly defined.

Raman Spectroscopy

For the PXRD, TGA and IR data described in this section so far, "calibration graphs", first created in section 3.3.3., have been used to quantify the amount of ferrihydrite present, by relating the wt% ferrihydrite in a goethite/ferrihydrite mixture to a feature of the data sets that methodically changes with the varying proportions of the two phases. In the case of Raman spectroscopy, this was not possible as the physical mixtures of goethite and ferrihydrite that were used to create these calibration graphs were too heterogeneous. As a result, distinct goethite and ferrihydrite spectra were acquired depending on the exact spot analysed. However, the goethite samples synthesised at 20°C and 70°C with the variable synthesis durations were characterised by Raman spectroscopy, shown in Figure 3.33 and Figure 3.34.

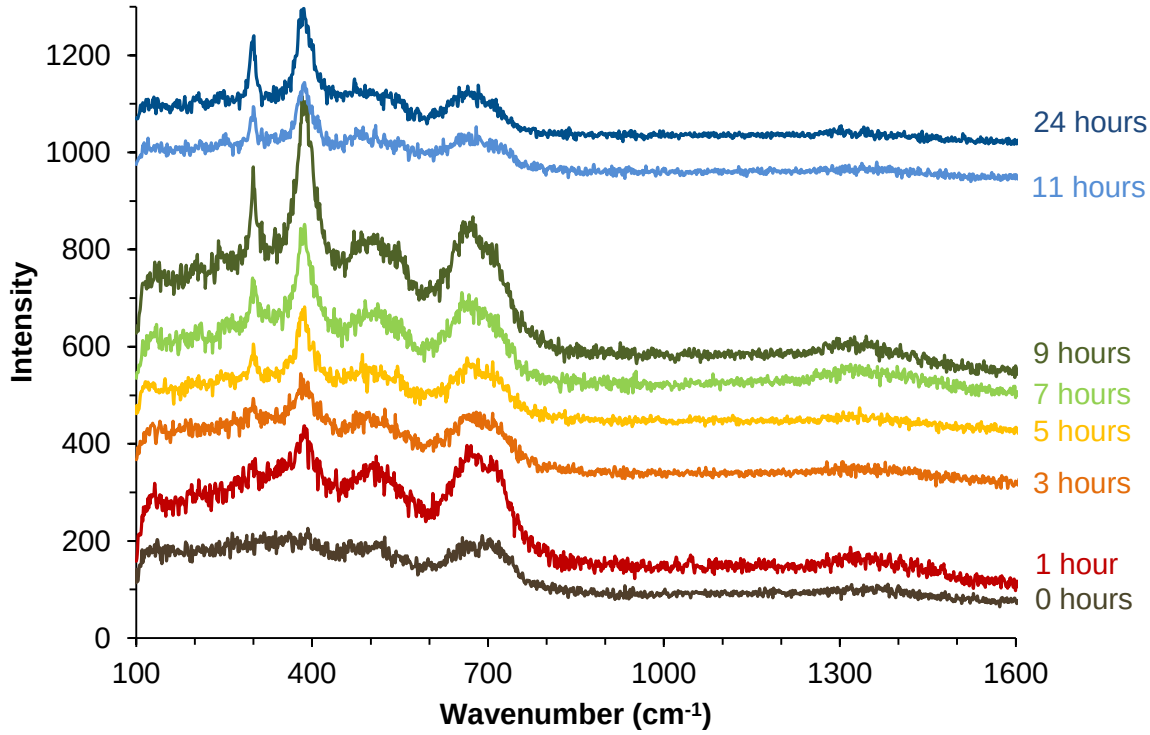

Figure 3.33: Raman spectra for goethite synthesised at 20°C.

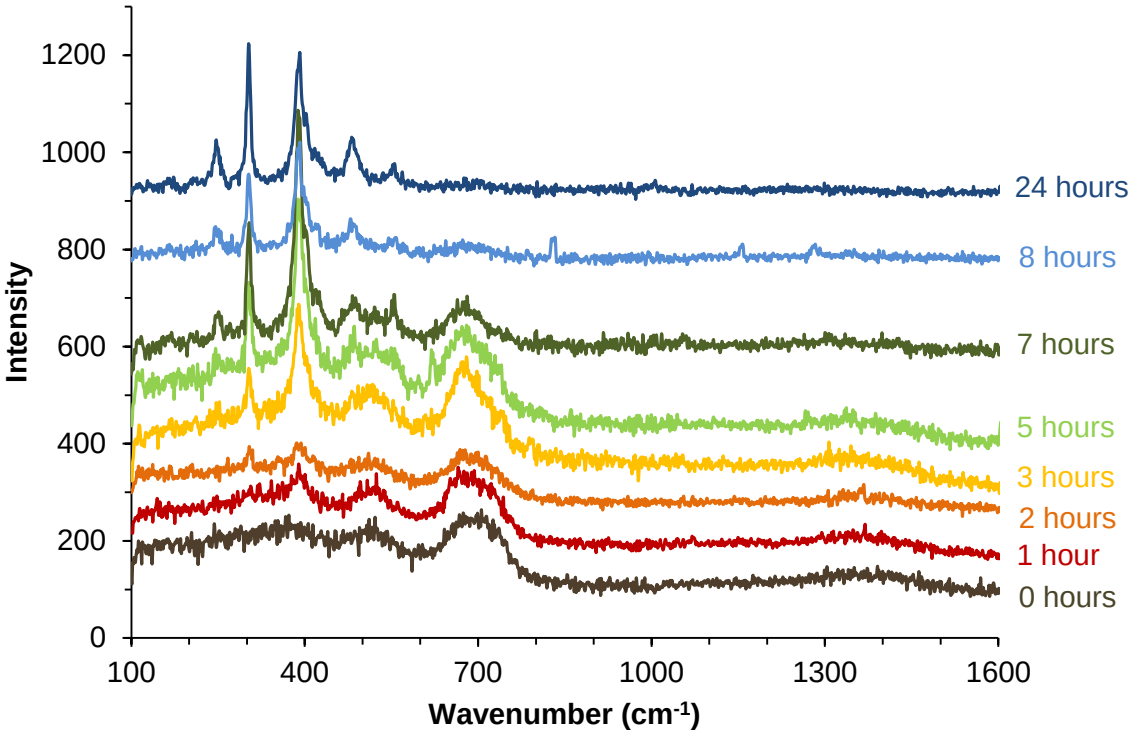

Figure 3.34: Raman spectra for goethite synthesised at 70°C.

The results obtained here suggest that goethite begins to form almost immediately at both the 20 and 70°C synthesis temperatures, with evidence of the goethite band which occurs at ~390 cm^{-1} visible in the samples after just one hour. The ferrihydrite band at ~710 cm^{-1} appears to shift to lower wavenumber (~670 cm^{-1} after 7 h) with increasing synthesis time, and in the set of samples prepared at 70°C the band is no longer present in the 24 hour synthesis sample (where the majority of ferrihydrite has transformed to goethite).

After a 24 h synthesis at 20°C, the ferrihydrite band is still visible, alongside the bands attributed to goethite, see Figure 3.35. This is as expected, as at this temperature the other characterisation techniques have suggested that in excess of 50 wt% of the sample remains as untransformed ferrihydrite.

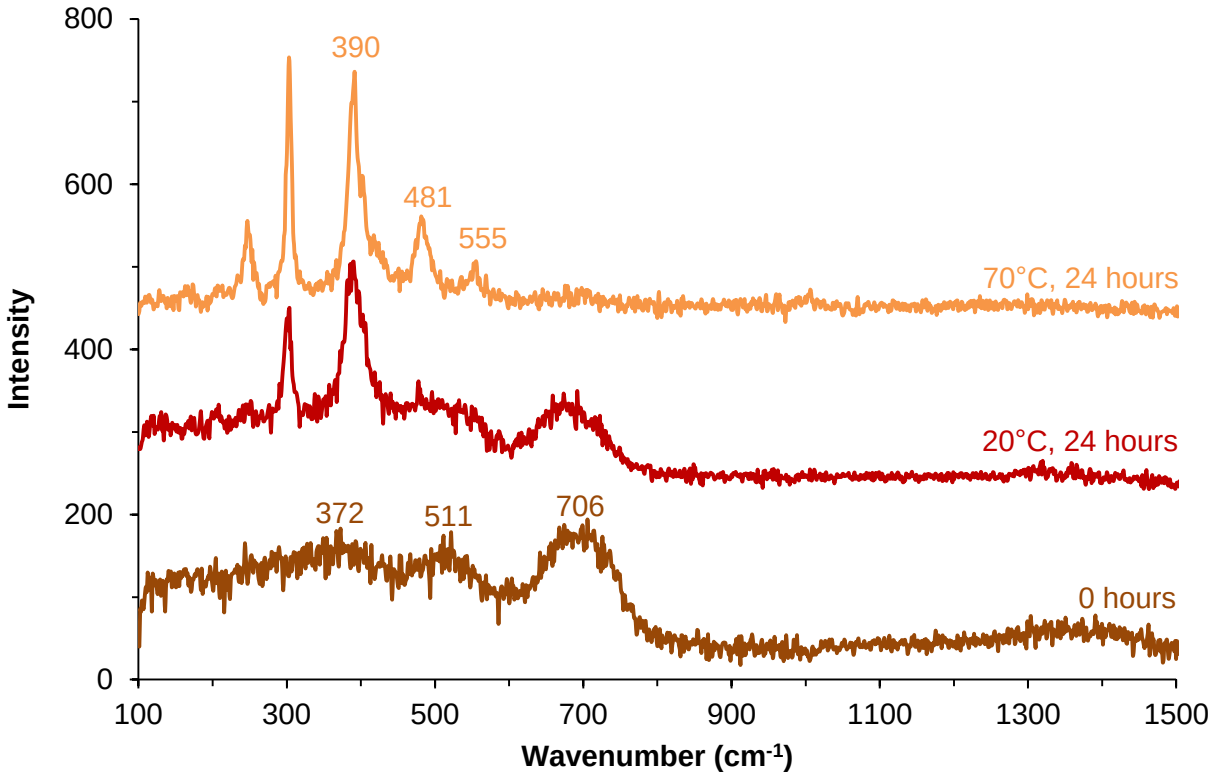

Figure 3.35: A comparison of the Raman spectra for ferrihydrite (0h), goethite at 20°C after 24 h and goethite at 70°C after 24 h.

Although we were unable to produce a calibration graph of changes that occur in the spectra with different goethite/ferrihydrite proportions, it appears that Raman spectroscopy is a technique that can be used to observe the presence of ferrihydrite in association with a goethite sample.

3.4. Summary

The formation of goethite via the transformation of a ferrihydrite precursor phase has been demonstrated and it was shown that the extent of transformation is affected by the synthesis temperature, with the transformation occurring more rapidly at higher temperatures. If the transformation is not given enough time (the exact time needed will be dependent on the synthesis temperature) then ferrihydrite will remain in the sample. It is believed that ferrihydrite could be present in natural laterite systems, impacting the apparent leachability of the materials.

Ferrihydrite is difficult to identify due to its poorly crystalline nature, especially when in a mixture with a crystalline goethite phase. Using goethite and ferrihydrite 'standards' consisting of physical mixtures of the two different phases, PXRD, TGA, IR and Raman characterisation techniques were investigated in order to find a way of both identifying the presence, and estimating the quantity, of untransformed ferrihydrite associated with a goethite sample. Calibration graphs were created for each of the characterisation techniques, relating the proportion of ferrihydrite in the standard samples to a particular property or feature of the data set.

The physical mixtures of goethite and ferrihydrite prepared here and used as standards will differ from the co-precipitated goethite/ferrihydrite mixtures that could form together in natural/synthetic systems. Optical analysis of the prepared 'standards' at 50X magnification highlighted the heterogeneity of the material at that small scale. However, both PXRD and TGA use relatively large amounts of sample for characterisation which should mean that the heterogeneity observed at small scale, resulting from the physical mixing, does not affect the bulk results obtained for each standard.

The quantities of ferrihydrite that have been estimated to be present in the different sets of goethite samples via each of the characterisation techniques are shown in Figure 3.36. It is clear that there are large differences in the amount of ferrihydrite that is predicted to be present from analysis by each of the different methods (PXRD, IR, TGA). These differences seem to be the greatest in the samples synthesised at the lower temperatures (20 and 40°C), where more of the sample remains as ferrihydrite. The level of confidence in the estimation of ferrihydrite content made by using each type of data also varies for reasons which will be discussed.

For PXRD data, the ratio of intensities between the main goethite peak and the average intensity of an area where the broad ferrihydrite reflection appears was used to relate the proportion of ferrihydrite back to the diffraction patterns. For the standard samples used

to develop this method, the data used for the calibration graph was well correlated. Repeated analysis of the same sample also demonstrated the reproducibility of the technique, with the intensities measured varying by less than 3%. In practice, trying to quantify the amount of ferrihydrite that was present in samples of goethite after various synthesis times was difficult and the results obtained were affected by the presence of other phases (e.g. hematite) in the system.

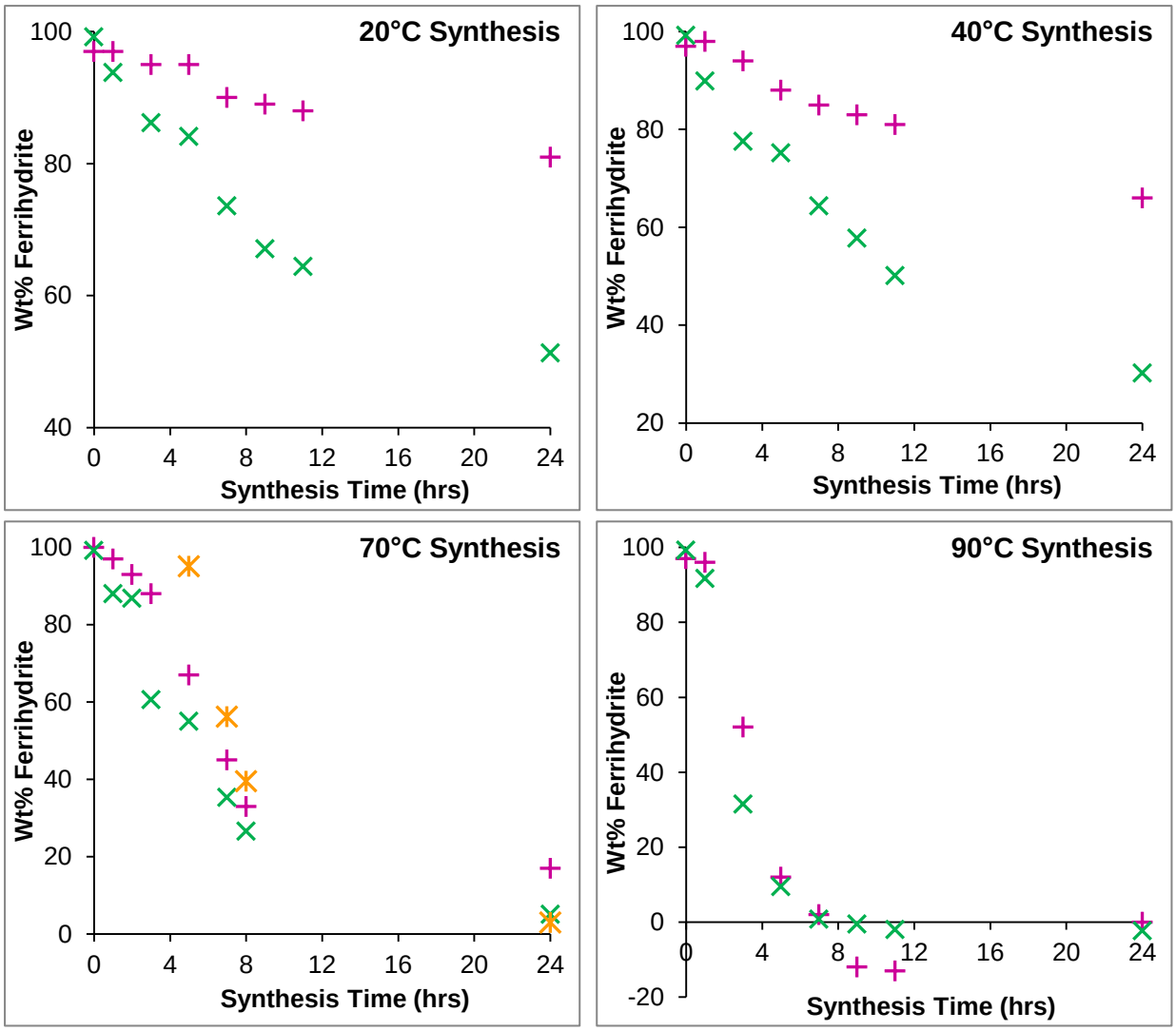

Figure 3.36: Comparison of the estimated ferrihydrite proportions of samples prepared at 20, 40, 70 and 90°C. Estimation by PXRD +, TGA X, IR ✳.

Quantifying the proportion of ferrihydrite present in a sample using data from Raman and IR spectroscopy proved to be unreliable. No calibration graph could be constructed using Raman data, due to the heterogeneous nature of the goethite/ferrihydrite standards that were created. This resulted in the observation of distinct spectra for either goethite or ferrihydrite, depending on the exact spot analysed. This could have been partly due to the

small spot size of the laser on the Raman instrument used. Using an instrument with a larger spot size would have resulted in analysis of a larger area of the sample and could have provided a better 'average' spectrum for the heterogeneous goethite/ferrihydrite mixtures. Raman spectroscopy carried out on the series of goethite samples prepared at different temperatures/durations did result in spectra that showed differences which could be attributed to the presence of ferrihydrite. It is suggested that Raman could be used for identification, but not quantification, of ferrihydrite associated with goethite samples.

Analysis of the samples using IR was slightly more effective, with a calibration graph created which related the proportion of ferrihydrite in the sample to the position of the Fe-O stretch in the spectrum of each standard. However, when this quantification method was tested with 'real' samples some of the estimations of the proportion of ferrihydrite present were far in excess of 100 wt%. It is believed that this was due to difficulties, and therefore inaccuracies, in reporting the exact position of the Fe-O stretch maxima in the ferrihydrite rich samples due to the broad, poorly defined nature of the band. IR is not proposed as a technique which could be used to identify and quantify ferrihydrite when associated with goethite samples.

Thermal analysis of the samples proved to be the most promising ferrihydrite identification and quantification technique. Using the weight loss due to surface adsorbed water for each sample to relate back to the amount of ferrihydrite that was present, a very well correlated calibration graph using the data obtained for the goethite/ferrihydrite standards was produced. Thermal analysis of the samples gave reproducible results when tested with repeat measurements, with the subsequent estimation of the ferrihydrite content shown to vary by 3 wt%. Unlike estimation using the IR and PXRD data sets, where a band position or intensity value had to be determined by eye, the feature of the TGA profile used for the quantification was the weight loss occurring below a specific temperature (40°C), so it was extremely easy to identify and report the value as there was no ambiguity. Importantly, this unique approach to ferrihydrite detection and quantification is quick and simple to carry out, using equipment which is not especially complex, so can be used as a screening method in future work to detect ferrihydrite.

3.5. References

1 U. Schwertmann, R.M. Cornell, The iron oxides: structure, properties, reactions, occurrences and uses, (Wiley, 2006).

2 U. Schwertmann, R.M. Cornell, Iron Oxides in the Laboratory – Preparation and Characterization, (Wiley, 1991).

3 P. Freyssinet, C.R.M. Butt, R.C. Morris, P. Piantone, *Society of Economic Geologists*, (2005) **100th Anniversary Volume**, 681-722.

4 MineralsUK, Nickel mineral profile. British Geological Survey. www.mineralsUK.com, last accessed August 2013.

5 S. Krehula, S.Music, S. Popovic, *Journal of Alloys and Compounds*, (2005) **403**, 368-375.

6 R. Thorne, R. Herrington, S. Roberts, *Mineralium Deposita*, (2009) **44**, 581-595.

7 S. A. Gleeson, R. J. Herrington, J. Durango, C. A. Velásquez, G. Koll, *Economic Geology*, (2004) **99**, 1197-1213.

8 J. Böhm, Z. Anorg, *Zeitschrift für Anorganische und Allgemeine Chemie*, (1925), **149**, 203.

9 J.L. Jambor, J.E. Dutrizac, *Chemical Reviews*, (1998) **98**, 2549-2585.

10 D. E. Janney, J. M. Cowley, P. R. Buseck, *Clays and Clay Minerals*, (2000) **48**, 111-119.

11 K. Tomeoka, P. R. Buseck, *Geochimica et Cosmochimica Acta*, (1988) **52**, 1627.

12 J. L. Bishop, C. M. Pieters, R. G. Burns, *Geochimica et Cosmochimica Acta*, (1993) **57**, 4583.

13 J. L. Bishop, C. M. Pieters, R. G. Burns, J. O. Edwards, R. L. Mancinelli, H. Froeschl, *Icarus*, (1995) **117**, 101.

14 D. Fortin, G. G. Leppard, A. Tessier, *Geochimica et Cosmochimica Acta*, (1993) **57**, 4391.

15 P. G. Manning, K. R. Lum, T. Birchall, *Canadian Mineralogist*, (1983) **21**, 121.

16 T. A. Jackson, W. D. Keller, American Journal of Science, (1970) **269**, 446.

17 U. Schwertmann, E. Murad, *Clay Minerals*, (1988) **23**, 291.

18 J. M. Bigham, U. Schwertmann, L. Carlson, *Biomineralization Processes of Iron and Manganese: Modern and Ancient Environments*, (Catena Verlag, 1992).

19 T. Misawa, K. Hashimoto, S. Shimodaira, *Corrosion Science*, (1974) **14**, 131.

20 E. Murad, P. Rojil, *Clay Minerals*, (2005) **40**, 427-440.

21 U. Schwertmann, Zeitschrift für Pflanzenernährung und Bodenkunde, (1964) **105**, 194-202.

22 J.M. Combes, A. Manceau, G. Calas, J. Y. Bottero, *Geochimica et Cosmochimica Acta*, (1989) **53**, 583-594.

23 A. Nørlund-Christensen, P. Convert, M. S. Lehman, *Acta Chemica Scandinavica*, (1980) **A34**, 771-776.

24 E. Murad, U. Schwertmann, The Mössbauer, *American Mineralogist*, (1980) **65**, 1044-1049.

25 R. J. Pollard, C. M. Cardile, D. G. Lewis, L. J. Brown, *Clay Minerals*, (1992) **27**, 57-71.

26 T. Nagano, S. Nakashima, S. Nakayama, K. Osada, M. Senoo, *Clays and Clay Minerals*, (1992) **40**, 600-607.

27 A. Hamzaoui, A. Mgaidi, A. Megriche, M. El Maaoui, *Industrial & Engineering Chemical Research*, (2002) **41**, 5226-5231.

28 R.K. Vempati, R. H. Loeppert, *Clays and Clay Minerals*, (1989) **37**, 273-279.

29 A.L. Ulery, L.R. Drees, *Methods of Soil Analysis, Mineralogical Methods. Part 5*, (Soil Society of America, 2008).

30 Y. Guyodo, S. K. Banerjee, R. L. Penn, D. Burleson, T. S. Berquo, T. Seda, P. Solheid, *Physics of the Earth and Planetary Interiors*, (2006) **154**, 222-233.

31 F.M. Michel, L. Ehm, S. M. Antao, P. L. Lee, P. J. Chupas, G. Liu, D. R. Strongin, M. A. A. Schoonen, B. L. Phillips, J. B. Parise, *Science*, (2007) **316**, 1726-1729.

32 A. C. Cismasu, F. M. Michel, A. P. Tcaciuc, T. Tyliszczak, G. E. Brown Jr, *Comptes Rendus Geoscience*, (2011) **343**, 210-218.

33 F. V. Chukhrov, B. B. Zvyagin, A. I. Gorshkov, L. P. Yermilova, V. V. Balashova, International Geology Review, (1974) **16**, 1131.

34 J. D. Russell, *Clay Minerals*, (1979) **14**, 109.

35 L. Carlson, U. Schwertmann, *Geochimica et Cosmochimica Acta*, (1981) **45**, 421.

36 S. V. S. Prasad, V. Sitakara Rao, *Journal of Materials Science*, (1984) **19**, 3266-3270.

37 R. K. Kukkadapu, J.M. Zachara, J. K. Fredrickson, S. C. Smith, A. C. Dohnalkova, C. K. Russell, *American Mineralogist*, (2003) **88**, 1903-1914.

38 U. Schwertmann, E. Murad, *Clays and Clay Minerals*, (1983) **31**, 277-284.

39 J. F. Banfield, S. A. Welch, H. Zhang, T. T. Ebert, R. L. Penn, *Science*, (2000) **289**, 751-754.

40 K. Rout, M. Mohapatra, S. Anand. *Dalton Transactions,* (2012) **41**, 3302.

41 J. Cai, J. Liu, Z. Gao, A. Navrotsky, S.L. Suib, *Chemistry of Materials*, (2001) **13**, 4395-4602.

42 R. A. Eggleton, R. W. Fitzpatrick, *Clays and Clay Minerals*, (1988) **36**, 111-124.

43 V. A. Drits, B. A. Sakharov, A. L. Salyn, A. Manceau, *Clay Minerals*, (1993) **28**, 185.

44 K. M. Towe, W. F. Bradley, *Journal of Colloid and Interface Science* **,** (1967) **24**, 384.

45 C. W. Childs, N. Matsue, N. Yoshinaga, *Applied Clay Science*, 1990 **8**, 9.

46 M. Kosmulski, S. Durand-Vidal, E. Maczka, J.B. Rosenholm, *Journal of Colloid and Interface Science*, (2004) **271**, 261-269.

47 C.F. Sampson, *Acta Crystallographica*, (1969) **B25**, 1683.

48 R.L. Frost, Z. Ding, H.D. Ruan, *Journal of Thermal Analysis and Calorimetry*, (2003) **71**, 783-797.

49 A.M. Saleh, and A.A. Jones, *Clay Minerals*, (1984) **19**, 745-755.

50 W. Xu, D.B. Hausner, R. Harrington, P.L Lee, D.R Strongin, J.B. Parise, *American Mineralogist*, (2011) **96**, 513-520.

51 H. Stanjek, P. G. Weidler, *Clay Minerals*, (1992) **27**, 397-412.

52 P. Cambier, *Clay Minerals,* (1986) **21**, 191-200.

53 P. Cambier, *Clay Minerals*, (1986) **21**, 201-210.

54 G. Gast E. R. Landa, G. W. Meyer, *Clays and Clay Minerals*, (1974) **22**, 31-39.

55 G. Houben, S. Kaufhold, *Clay Minerals*, (2011) **46**, 387-395.

56 U. Schwertmann, P. Cambier, E. Murad, *Clays and Clay Minerals*, (1985) **33**, 369-378.

Chapter 4.

The Removal of Secondary Phases from Goethite

4.1. Introduction

Throughout Chapter 3, some of the factors which affect the extent to which ferrihydrite transforms to goethite were discussed, including the duration and temperature of the synthesis, and the presence of foreign cations in the system.[1, 2] The influence that these factors have on the formation of goethite means that ferrihydrite often exists in association with goethite and other iron oxide/hydroxide phases. The poorly crystalline nature of ferrihydrite makes it difficult to detect using standard characterisation techniques such as PXRD, and therefore its true abundance in many synthetic and natural systems may well be underestimated.[3] In Chapter 3 alternative characterisation techniques were explored to enable identification (and quantification) of ferrihydrite when associated with goethite samples.

In order to accurately characterise goethite, and later to investigate the nature of the relationship between goethite and foreign cations (e.g. nickel), it is important to be able both to identify the presence of, and then selectively remove any ferrihydrite that is present, whilst leaving the goethite fully intact. Furthermore, in order to investigate the degree and mechanism of foreign cation substitution into the goethite structure, it is especially important to be certain that none of the structurally incorporated metal is being removed by the washing process.

There are a range of methods discussed in the literature to selectively remove poorly crystalline iron oxides, such as ferrihydrite, as well as other co-formed amorphous secondary phases, from goethite samples. The most widely used of these is extraction with ammonium oxalate solution, as ferrihydrite is readily soluble in ammonium oxalate at pH 3, whereas goethite is much more resistant.[4, 5] Although many studies report that crystalline goethite phases will remain intact, there are those that report significant amounts of goethite to be dissolved during ammonium oxalate treatment, or that fine grained goethite may be affected.[6, 7] Any selective extraction technique which is chosen needs to be used on both natural and synthetic samples, so oxalate extraction could therefore pose a problem when used on natural goethite samples from laterite deposits which are often poorly crystalline.

Other widely utilised washing techniques use sulfuric or hydrochloric acid to remove amorphous and/or poorly crystalline material from synthetic goethites - these are summarised in Table 4.1. Whist the use of these acids may well remove secondary Fe-oxide phases (e.g. ferrihydrite), there is also the distinct possibility that the goethite itself will be affected or foreign metals incorporated into it may be leached. Carvalho *et al.* (2002) used sulfuric acid to remove amorphous phases from Ni-goethites. Analysis of

their samples by TEM showed that the smaller goethite particles were affected by this treatment.[8] Some of the acid washing techniques highlighted in Table 4.1, which are used for the removal of secondary phases, use acids that are more concentrated than those used by mining companies to actually leach targeted metals from ores. An example of this is the atmospheric heap leach project in Çaldağ, Turkey, where a 75 g/l solution of H_2SO_4 (~0.7M) is used to leach the targeted metals (Ni) from the ore.[9]

Table 4.1: Reported acid washing methods for removal of secondary phases from goethite.

Washing Solution	Conditions	Notes
0.25M H_2SO_4	Room temperature for 2h, using a solid:solution ratio of 1:100. Repeated 5 times.	Removal of amorphous material in V-substituted goethites.[10]
3M H_2SO_4	2h at 50°C.	Removal of amorphous materials in Co-substituted goethites.[11]
2M H_2SO_4	2h at 80°C.	Removal of amorphous materials in Cr-substituted goethites.[12]
0.4M HCl	30 minutes, room temperature.	Removal of unconverted ferrihydrite from goethite.[13]
2M HCl	4h treatment (temperature not specified).	Removal of non-incorporated Pb/Th or ferrihydrite in substituted goethites.[14]

Removal of amorphous and/or poorly crystalline iron oxides from soils using EDTA solutions has been the subject of previous investigation, where it was shown that EDTA can selectively extract amorphous iron oxides from soils[15,16] as well as from synthetic mixtures of amorphous iron oxides, goethite and hematite.[17] Borggaard (1992) compared the effectiveness of ammonium oxalate extraction to that of EDTA extraction on synthetic mixtures of amorphous and crystalline iron oxides and concluded that only amorphous iron oxides were dissolved by EDTA, whereas ammonium oxalate extraction also attacked the more crystalline iron oxide phases.[17,18] The author concluded that a 3 - 7 month extraction using 0.02 - 0.1M EDTA at pH 7.5 - 10.5 showed comparable results in the amount of Fe extracted to those achieved using the ammonium oxalate extraction method in 2 hours.[19] The results also showed that the amount of Fe extracted by EDTA plateaued off and remained constant after approximately 3 months, whereas Fe extracted by the oxalate treatment was shown to increase continually with extraction time until all/most of the iron oxide had dissolved.[15] By comparison with the ammonium oxalate

method, the reported time period required by the EDTA technique to complete the extraction is a clear disadvantage.

A study by McCarty *et al.* (1998) found that a 2h treatment of iron oxides with Na-EDTA, buffered to pH 8 with NH_4, dissolved significant amounts of crystalline goethite as well as ferrihydrite, although it did only dissolve ~1% of the total Fe.[20] The suitability of EDTA in removing amorphous material from crystalline iron oxides has also been dismissed by other research groups, who have stated that there 'is no sound basis for using EDTA-extraction' for estimating amorphous Fe content.[21]

The use of EDTA as a technique to remove amorphous or poorly crystalline material in current literature does not appear to be widespread. The work reported in this thesis revisits the application of an EDTA washing technique to remove ferrihydrite from synthetic goethite samples, with the focus being to ensure that the goethite itself was not being leached. After optimisation of the technique using the chemically pure synthetic goethite products, the EDTA method will subsequently be used to remove the ferrihydrite secondary phase from Ni-substituted goethites (Chapter 5). This enables the production of phase pure Ni-substituted goethites, which in turn allows the accurate characterisation of these Ni-doped goethites, and also for the partitioning of Ni between the goethite and ferrihydrite phases to be quantified.

4.2. Experimental Methods

4.2.1. Synthesis of Goethite

The synthesis procedure used to prepare the goethite samples was adapted from that of Schwertmann and Cornell (1991), and is described in detail in Chapter 2.[5] Briefly, a 10 ml solution of 1M $Fe(NO_3)_3 \cdot 9H_2O$ was prepared and added to 18 ml of 5M KOH solution. Immediately, the mixed solution was diluted to 200 ml with distilled water and then held in a polyethylene flask for 7d at either 20, 40, 70 or 90°C. After 7 days the product was filtered, washed with distilled water, and left to dry in air at room temperature. These initial goethite precipitates were characterised using PXRD, Raman, TGA and TEM to establish the extent of goethite formation and therefore the amount of ferrihydrite present.

4.2.2. Development of the EDTA Washing Technique

In order to explore the potential of using EDTA for the selective removal of ferrihydrite from the synthetic goethite samples, and to subsequently optimise this method in terms of concentration and time, a series of washing experiments were performed in which different concentrations of EDTA solution and washing durations were applied. The EDTA solutions were prepared by dissolving the appropriate amounts of Na-EDTA ($C_{10}H_{14}N_2Na_2O_8 \cdot 2H_2O$, Fisher, reagent grade) in distilled water. The concentrations of EDTA solution that were investigated were 0.01, 0.1 and 0.25M, and the washing durations were 3h, 24h, 3d, 10d and 20d.

0.4 g of synthetic goethite prepared at 20°C was placed in a polyethylene flask with 40 ml of the EDTA solution and left on a roller table for between 3h and 20d. Goethite material that had been synthesised at 20°C was chosen to ensure that complete transformation of ferrihydrite to goethite had not occurred and therefore there would be material present that should be removed. At the conclusion of the washing experiment, the goethite was filtered by gravity, rinsed with distilled water and left to dry in air at room temperature. Both the solid (goethite) and liquid (EDTA) portions were retained and characterised in order to establish exactly what had been removed and to ascertain the degree (if any) of leaching or modification to the goethite phase.

4.3. Results and Discussion

4.3.1. Optimisation of the EDTA Washing Technique

The resulting solutions from the EDTA washing experiments were collected and analysed by ICP-OES to establish their Fe contents and the concentrations of Fe measured in the EDTA solutions are plotted as a function of washing duration in Figure 4.1. For all three of the EDTA concentrations investigated here, the amount of Fe removed from the goethite into the EDTA solution increased rapidly at first before plateauing. The lowest concentration of EDTA (0.01M) appears to reach saturation at ~380 ppm Fe after about 24 hours, whereas the 0.1 and 0.25M EDTA solutions appear to perform equivalently in terms of the amount of Fe removed and the time taken before the rate of removal slows down and levels off. For these more concentrated EDTA solutions, the amount of Fe removed increased rapidly over the first ~100 hours, before plateauing after around 10 days with no major increase occurring after this time. Additionally, these two EDTA solutions removed ~2500 ppm Fe, equating to approximately 25 wt% of the goethite sample.

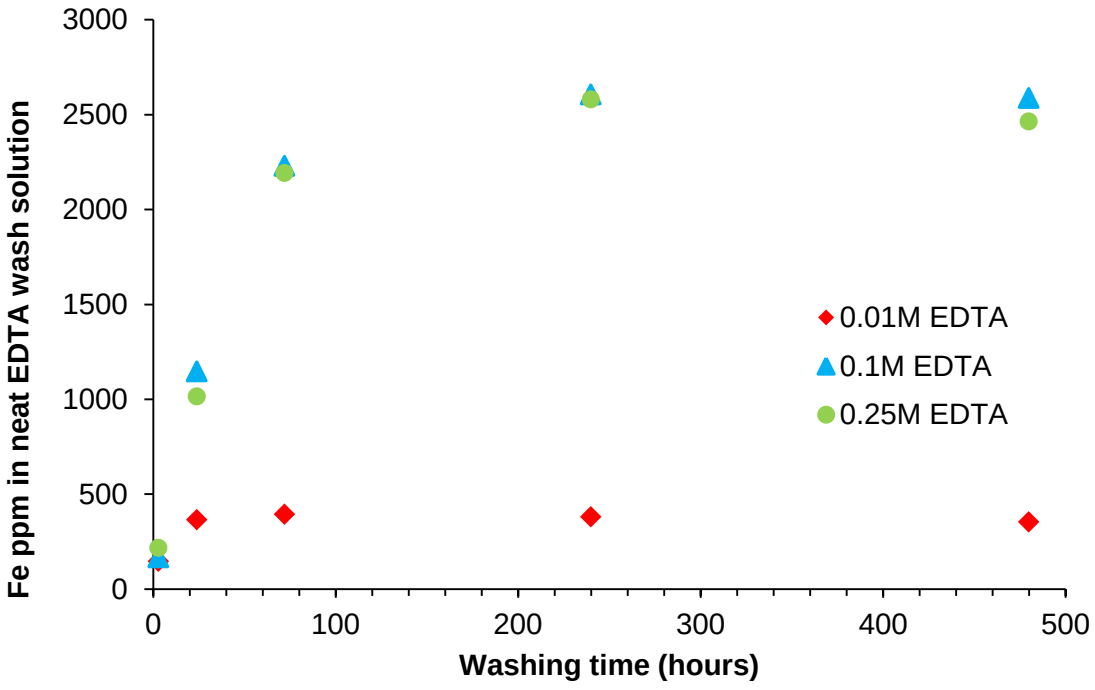

Figure 4.1: ICP-OES data comparing the amount of Fe removed from goethite by EDTA solutions of varying concentrations and washing times.

The 0.01M EDTA solution appears to be too dilute as the 0.1 and 0.25M solutions remove more Fe from the samples, highlighted by the increased Fe concentration measured in

those solutions. The concentration of Fe measured in the 0.1 and 0.25M EDTA washes mirror one another over the time period studied, indicating that all of the available iron (present as ferrihydrite) is removed from the samples using both wash concentrations. If the 0.1M EDTA wash was too dilute, it would be expected that an increased concentration of iron would be measured in the 0.25M EDTA wash. As there were no real differences in the measured Fe concentrations in the two most concentrated EDTA wash solutions, the optimum washing conditions for ferrihydrite removal from goethite were concluded to be treatment with 0.1M EDTA solution, for 10 days at 20ºC.

To ensure that the EDTA wash only removed ferrihydrite, and did not leach Fe from the goethite phase, six goethite samples were washed for 10 days in 0.1M EDTA solution. The solutions were then analysed using ICP-OES and no Fe was detected in any of the washing solutions indicating that the EDTA washing technique developed here is effective at removing ferrihydrite from mixed goethite/ferrihydrite samples, whilst leaving the goethite intact.

4.3.2. Removal of Ferrihydrite from Goethite Using EDTA

Once the optimum conditions had been established for removing the ferrihydrite (secondary phase) from the synthetic goethite samples, this selective removal process was tested on a number of goethite samples which had been synthesised at different temperatures. A range of characterisation techniques (e.g. PXRD, Raman, TGA, TEM) were then used in order to establish what effect, if any, the washing treatment had on the goethite, and the composition of the EDTA solutions themselves were investigated using ICP-OES.

Powder X-Ray Diffraction (PXRD)

When examined using Co $K_{\alpha 1}$ radiation, the PXRD pattern for 2-line ferrihydrite exhibits two broad reflections at ~40 and 70° 2θ, compared to the diffraction pattern of a crystalline goethite which features a number of clearly defined peaks (Figure 4.2).

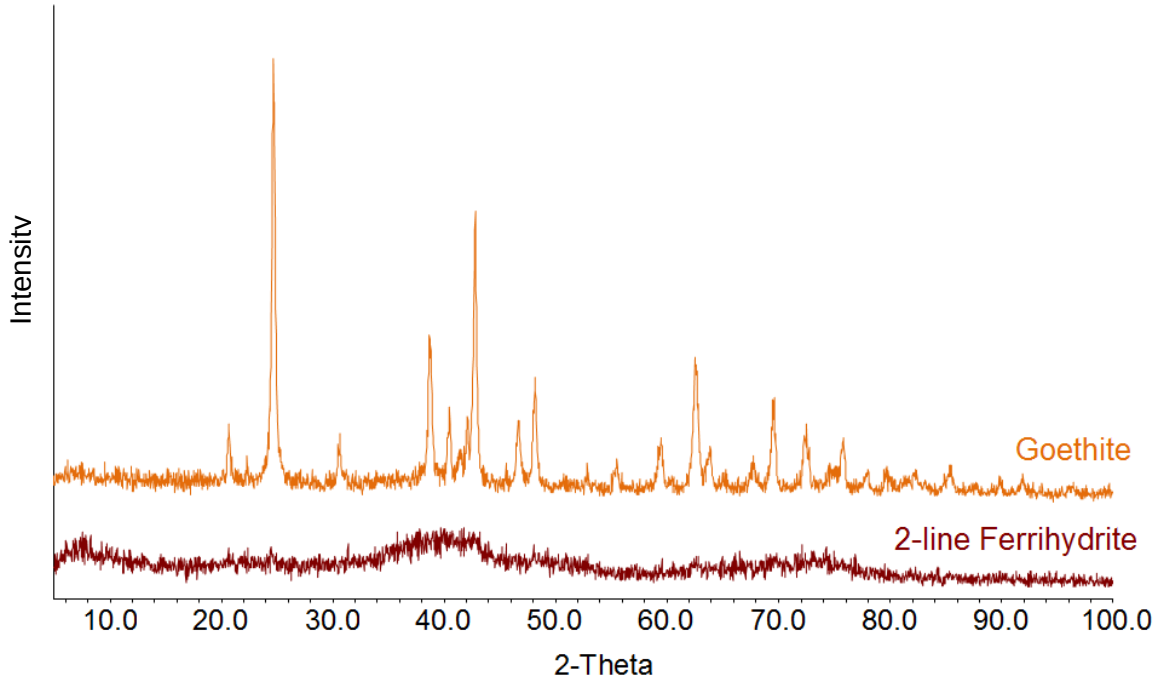

Figure 4.2: Co $K_{\alpha 1}$ PXRD patterns for goethite and 2-line ferrihydrite.

From PXRD analysis, goethite was identified as the only crystalline phase in all of the samples prepared here. The crystallinity of the unwashed goethite samples appears to increase with increasing synthesis temperature, with the low synthesis temperature goethite displaying broader, less intense peaks in the diffraction pattern than those goethite samples synthesised at the higher temperatures (Figure 4.3). In the PXRD patterns of the unwashed goethite samples there is evidence that ferrihydrite is present in the samples produced from the lower temperature syntheses (20°C and 40°C) with a distinct ferrihydrite feature visible at ~40° 2θ. At higher synthesis temperatures (70°C and 90°C) the PXRD patterns show no evidence for ferrihydrite, suggesting that the ferrihydrite to goethite transformation had progressed to completion. After the goethite samples had been washed with the EDTA solution, the presence of the broad background feature in the PXRD patterns of the 20°C and 40°C samples was no longer evident (Figure 4.4), suggesting that ferrihydrite was no longer present. Based only upon analysis of PXRD data, the ferrihydrite appears to have been entirely removed, or the quantity of ferrihydrite greatly reduced so that it is undetected, by the EDTA washing.

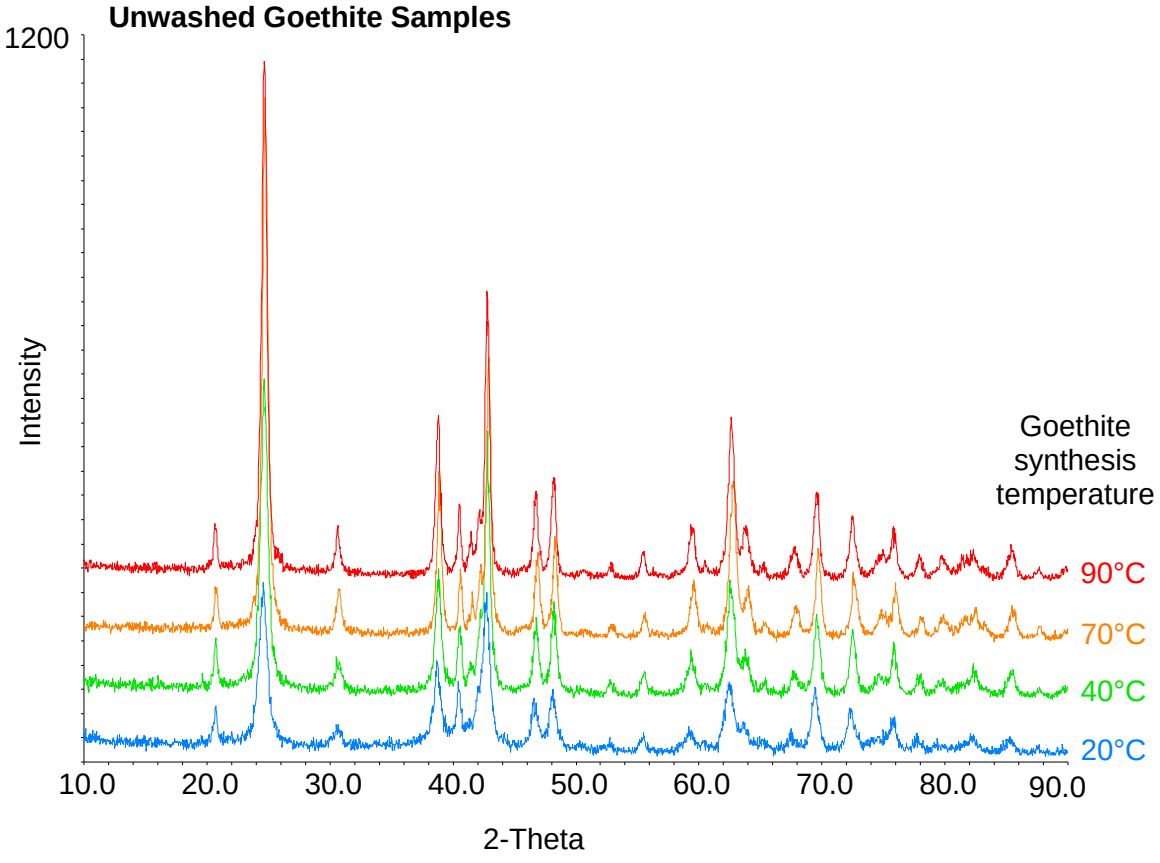

Figure 4.3: PXRD patterns of unwashed goethite samples synthesised between 20-90°C. Data collected using Co $K_{\alpha 1}$ radiation.

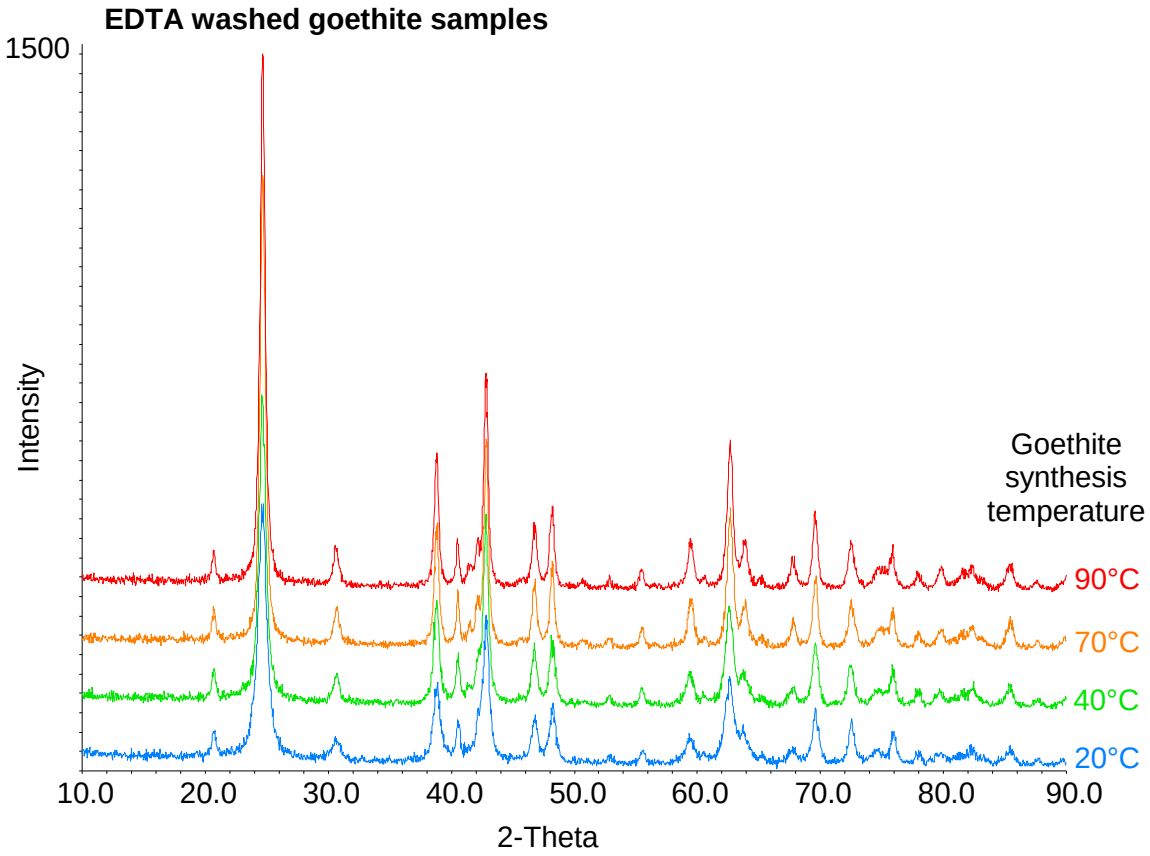

Figure 4.4: PXRD patterns of EDTA washed goethite samples synthesised between 20-90°C. Data collected using Co $K_{\alpha 1}$ radiation.

Thermo Gravimetric Analysis (TGA)

The differences observed in the weight loss profiles of physical mixtures of goethite and ferrihydrite were discussed in Chapter 3, and the results suggest that TGA could be a very useful technique in identifying the presence of ferrihydrite when in association with goethite, due to the increased weight loss which ferrihydrite exhibits at low heating temperatures (less than 40°C), see Figure 4.5. In the synthetic goethite samples studied here, the weight loss profile has been separated into three separate events, described in Table 4.2.

Table 4.2: Temperature ranges of the different weight loss regions in goethite.

Step	Temperature	Origin
1	<40°C	Loss of physically adsorbed surface water.
2	40-150°C	Loss of chemisorbed surface water.
3	>150°C	Loss of structural OH as a result of the dehydroxylation of goethite → hematite.

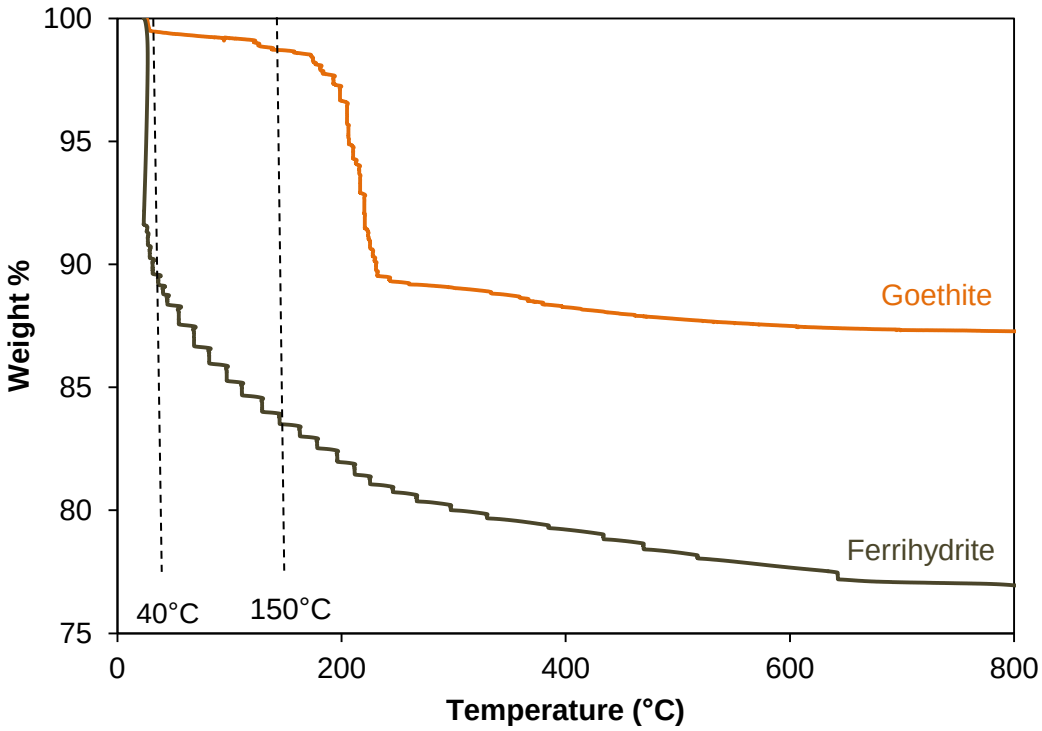

Figure 4.5: Comparison of the weight loss profiles of goethite and ferrihydrite.

Investigations into physical mixtures of goethite and ferrihydrite (Chapter 3) showed a strong linear correlation between the weight percentage of ferrihydrite mixed in with a goethite sample and the weight loss which was measured below 40°C from the TGA weight loss profile. In the case of a pure ferrihydrite sample, this can be in excess of 10 wt%, whereas in a well formed goethite it will be <1 wt% (Figure 4.5). By comparing the weight lost in the physical mixtures of goethite/ferrihydrite, with the weight losses observed in the synthetic goethite samples analysed in this study, the presence or absence of ferrihydrite, as well as an estimate of its proportion, can be inferred.

The weight loss profiles recorded for the unwashed synthetic goethite samples show systematic differences depending on the initial synthesis temperature (Figure 4.6). The weight loss measured below 40°C, due to surface adsorbed water, decreases as the synthesis temperature is increased, ranging from 6.4 wt% for the sample synthesised at 20°C, to 0.6 wt% for the sample synthesised at 90°C. After the samples had been washed with the EDTA solution, the amount by which the weight loss varied as a function of synthesis temperature was greatly reduced, ranging from 0.3-0.9 wt% (Figure 4.7). This data supports the PXRD findings and provides more evidence that the ferrihydrite secondary phase has been removed from the goethite by the EDTA washing technique.

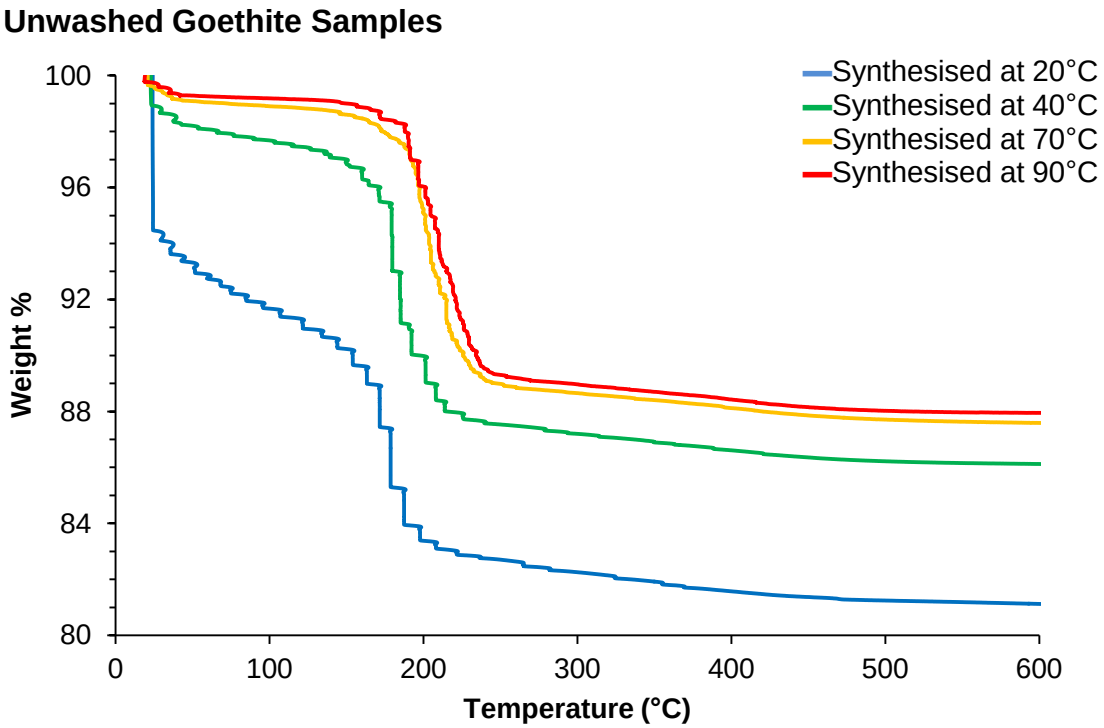

Figure 4.6: Weight loss plots for goethites prepared at 20, 40, 70 and 90°C, before EDTA treatment.

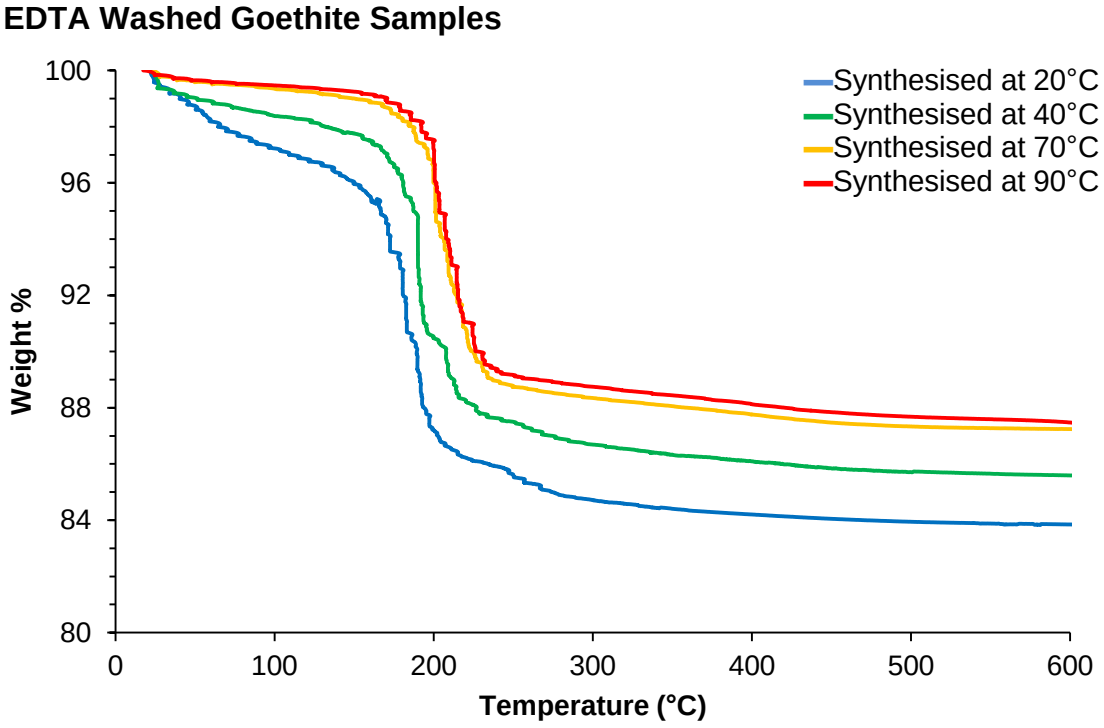

Figure 4.7: Weight loss plots for goethites prepared at 20, 40, 70 and 90°C, after EDTA treatment.

Using Equation 3.6, taken from the calibration graph created from investigations into the goethite/ferrihydrite mixtures in Chapter 3, the proportions of ferrihydrite present in the goethite samples synthesised at each of the different temperatures (20-90°C), as well as the effect of the EDTA wash, can be estimated.

Equation 3.6: Relationship between the weight loss below 40°C and the wt% ferrihydrite in a goethite/ferrihydrite mixture (y = wt% loss, x = wt% ferrihydrite).

$$y = 0.1042x + 0.6475$$

The original (unwashed) goethite samples are estimated to have ferrihydrite proportions of between 55 wt% (at a 20°C synthesis temperature) and 0 wt% (at a 90°C synthesis temperature), as shown in Table 4.3. After the samples had been washed with the EDTA solution, the weight loss occurring below 40°C for the goethite samples was between 0.3-0.9 wt%. This weight loss is believed to be a result of surface adsorbed water on the goethite itself. If the weight loss is not related to water adsorbed on the goethite sample, then using the relationship between weight loss and ferrihydrite content, the proportion of ferrihydrite present in the goethite samples, is estimated to be less than 2 wt%.

Table 4.3: Estimation of the proportion of ferrihydrite present in goethite samples synthesised at a range of temperatures before and after EDTA washing.

Goethite Synthesis Temperature	Original Goethite Samples		EDTA Washed Goethite Samples	
	Wt% lost below 40°C	Proportion of sample estimated to be ferrihydrite (wt%)	Wt% lost below 40°C	Proportion of sample estimated to be ferrihydrite (wt%)
20°C	6.4	55	0.9	2
40°C	1.7	10	0.8	2
70°C	0.9	2	0.3	-3
90°C	0.7	0	0.3	-4

While the weight loss which occurs below 40°C changes significantly between the original and EDTA washed goethite samples synthesised at lower temperatures, the weight loss recorded between 40-150°C increases with decreasing synthesis temperature in both the original and the EDTA washed samples. In this temperature region, the EDTA washing

process appears to have little effect upon the samples (see Figure 4.8 - the circles indicate the weight loss occurring from 40-150°C). A possible explanation for this is that the differences observed in this temperature region, resulting from the loss of chemisorbed water, are related to the particle size, and possibly crystallinity, of the individual goethite samples, a property influenced by the initial synthesis temperatures.

Previous work carried out by Schwertmann *et al.* (1985) on the crystallinity of un-substituted goethites showed that the amount of chemisorbed water (the authors measured it over the temperature range 80-160°C) decreased with increasing synthesis temperature and was closely related to surface area.[22] In other words, the larger the particle size, the less chemisorbed water that was present and consequently the lower the weight loss that was recorded in that temperature range.

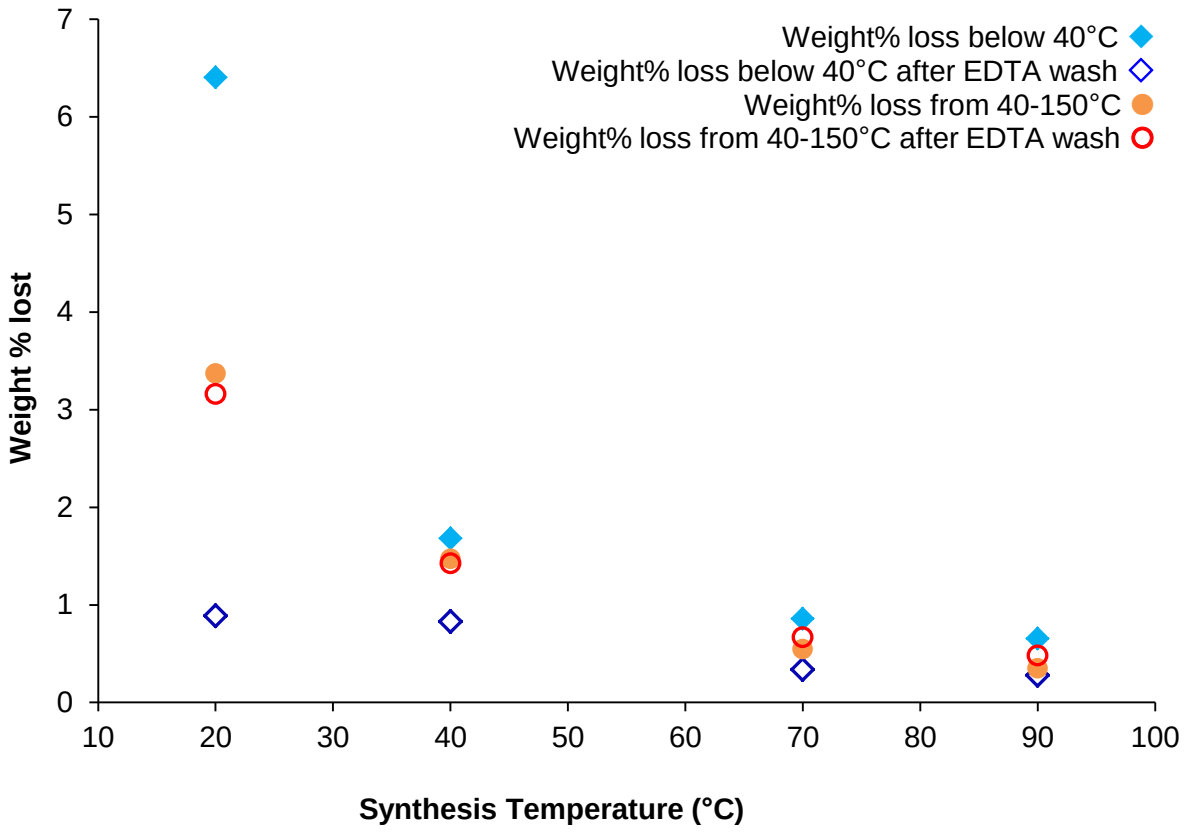

Figure 4.8: Weight losses recorded below 40°C and between 40-150°C for goethite samples before and after washing with EDTA solution.

Raman Spectroscopy

Raman spectroscopy was used to characterise the original and EDTA washed goethite samples to enable the examination of the spectra for the presence of ferrihydrite. For the synthetic goethite samples produced in this study, Raman bands have been measured at 247, 303, 390, 481 and 555 cm^{-1} (Figure 4.9), which are in good agreement with those previously reported of 243, 299, 385, 479 and 550 cm^{-1} for goethite.[23, 24, 25] The Raman spectrum reported for ferrihydrite has a relatively strong band at 710 cm^{-1} and weak bands at 370, 510 and 1340 cm^{-1}.[23, 26] The Raman spectrum recorded for the ferrihydrite synthesised in this work (Figure 4.9) shows weak bands at 372, 511 and 1373 cm^{-1}, as well as a stronger band at 706 cm^{-1}, which are in good agreement with those previously reported.[23, 26]

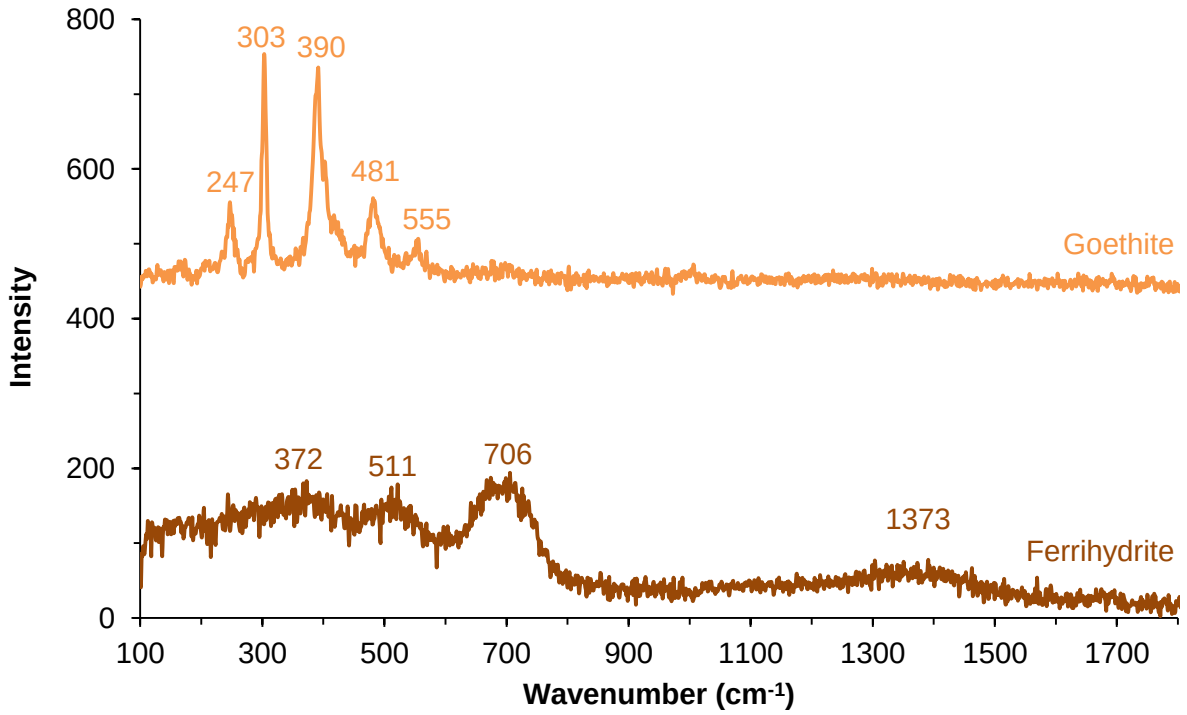

Figure 4.9: A comparison of the Raman spectra for ferrihydrite and goethite.

Das and Hendry (2011) also reported the presence of a strong band in the ferrihydrite spectrum at ~1045 cm^{-1}, however reports of this are not widespread in the literature, and all other work assigns this band to a nitrate impurity resulting from the synthesis procedure.[23, 26, 27] There is no evidence of a band at ~1045 cm^{-1} in the ferrihydrite or goethite samples shown in Figure 4.9, however the presence of this band can be observed in some of the original (non-EDTA washed) goethite samples examined later in this section (e.g. Figure 4.12) and in other Chapters of this thesis. The fact that the band is not present in any of the EDTA washed samples supports the view that it results from a

nitrate impurity, and highlights the need for thorough washing (with distilled water) of the goethite/ferrihydrite samples during the recovery process after synthesis.

The Raman spectra collected on the unwashed goethite samples shown in Figure 4.10, show the presence of the broad ferrihydrite band, as well as the bands associated with the goethite phase, most obviously in the lower temperature syntheses. The main ferrihydrite band (shown in Figure 4.9 at 706 cm^{-1}) appears to be present in the spectra of the goethite samples shown in Figure 4.10; however it is at a slightly lower wavenumber (672 cm^{-1}) than would be expected for ferrihydrite. A possible reason for this is the (part) transformation of the ferrihydrite phase to maghemite, as a result of the laser power used for the analysis being too strong. Mazetti and Thistlethwaite (2002) demonstrated the transformation of ferrihydrite to maghemite under repeated scans of a Raman laser, and Hanesch (2009) reported the appearance of a broad band in the Raman spectra between 670 - 690cm^{-1} upon heating ferrihydrite. [26, 28]

The broad band at ~670 cm^{-1} is the only additional band that can be observed in the goethite samples shown in Figure 4.10. The ferrihydrite band at 370 cm^{-1} is not very intense and is not likely to be evident when in the presence of goethite due to the intense goethite band at 384 cm^{-1}. The goethite bands that appear at 481 and 555 cm^{-1} are clearly distinguished from one another in the spectra for the goethites synthesised at higher temperatures (70°C and 90°C), but are more poorly resolved in the spectrum for goethite synthesised at 20°C. Ferrihydrite has a band at ~511 cm^{-1}, which would appear between these bands, and thus overlap with the two goethite peaks. The poorly resolved nature of these two goethite bands may therefore also be used as an indicator of the presence of ferrihydrite.

After the goethite sample had been washed with EDTA, no evidence of ferrihydrite can be observed in the Raman spectra of the goethite samples, shown in Figure 4.11, and displayed more clearly using the spectra for the goethite synthesised at 20°C in Figure 4.12. The broad band at ~670 cm^{-1} is no longer present in any of the samples, and there is much better definition between the two goethite bands at ~481 and 555 cm^{-1}.

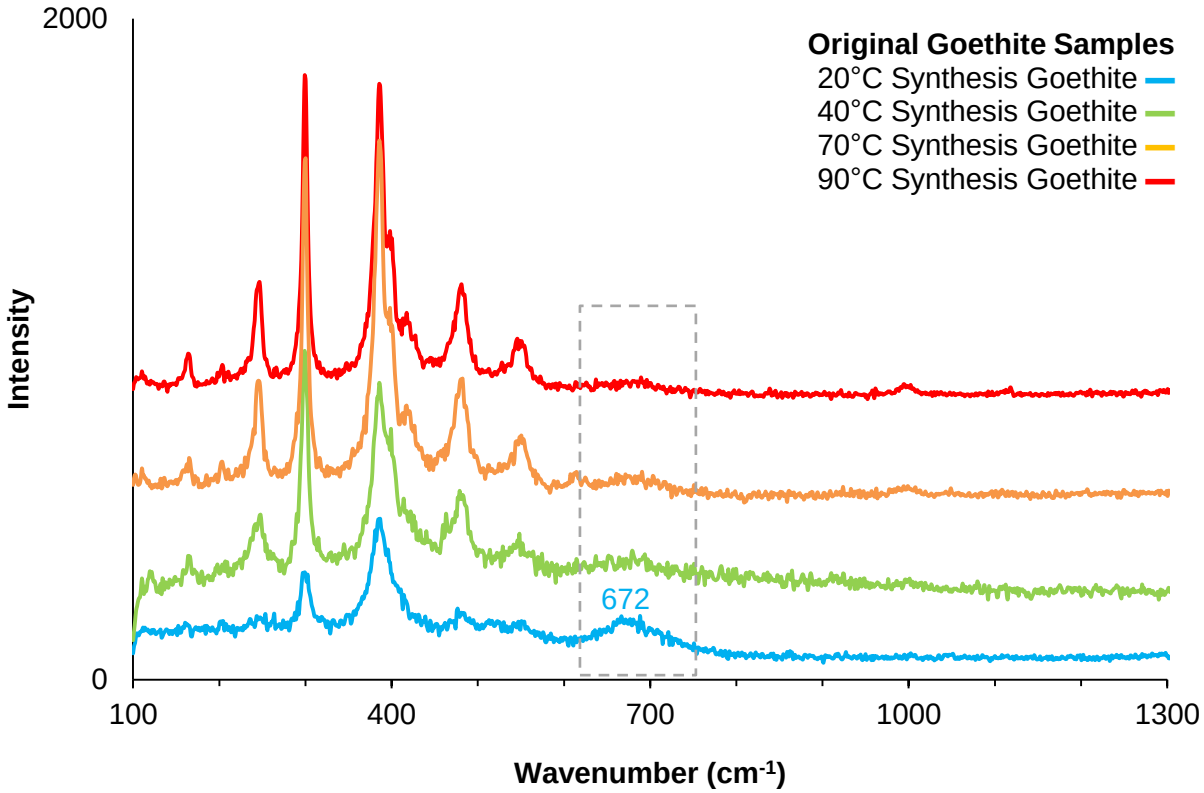

Figure 4.10: Comparison of the Raman spectra for goethite samples synthesised at different temperatures. Area where ferrihydrite band is found highlighted by grey outline.

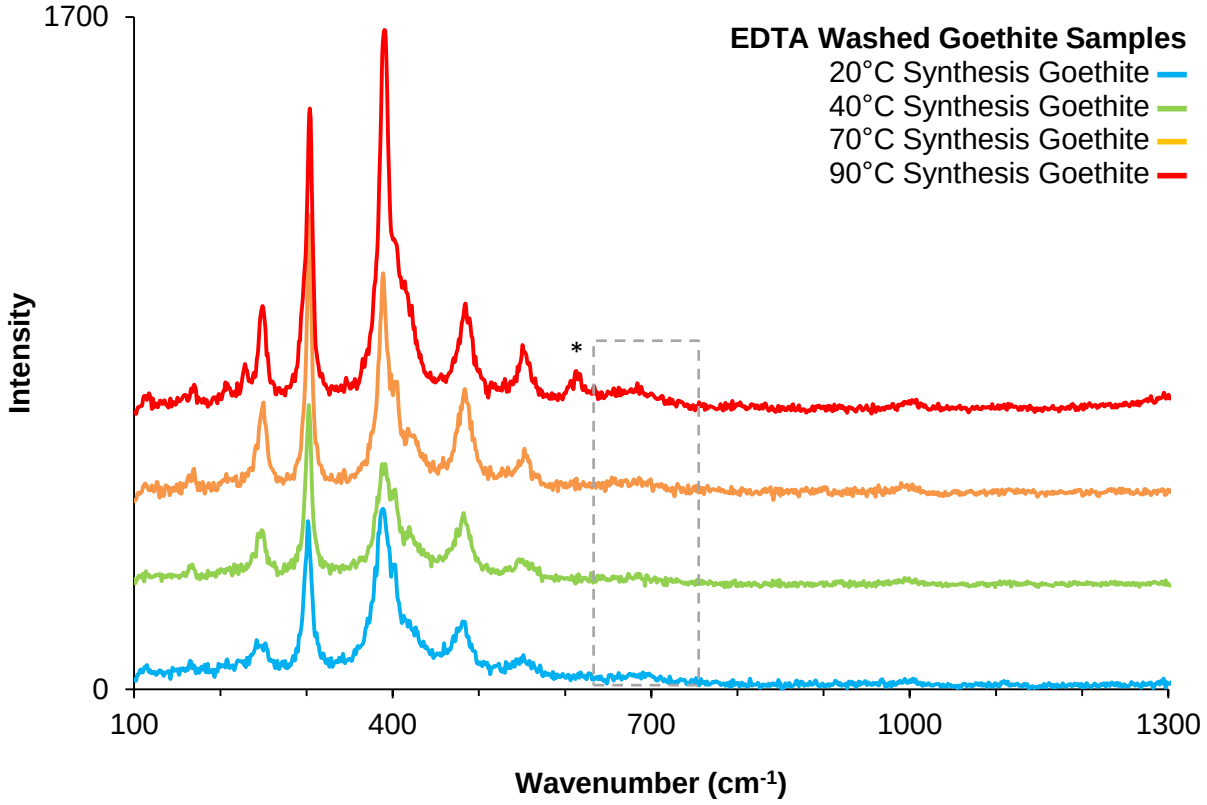

Figure 4.11: Comparison of the Raman spectra for goethite samples synthesised at different temperatures after they had been washed with EDTA. Area where ferrihydrite band is found highlighted by grey outline. * denotes hematite band.

The characterisation data collected using Raman spectroscopy provides further evidence in support of the use of the EDTA washing technique in removing a secondary ferrihydrite phase from goethite samples.

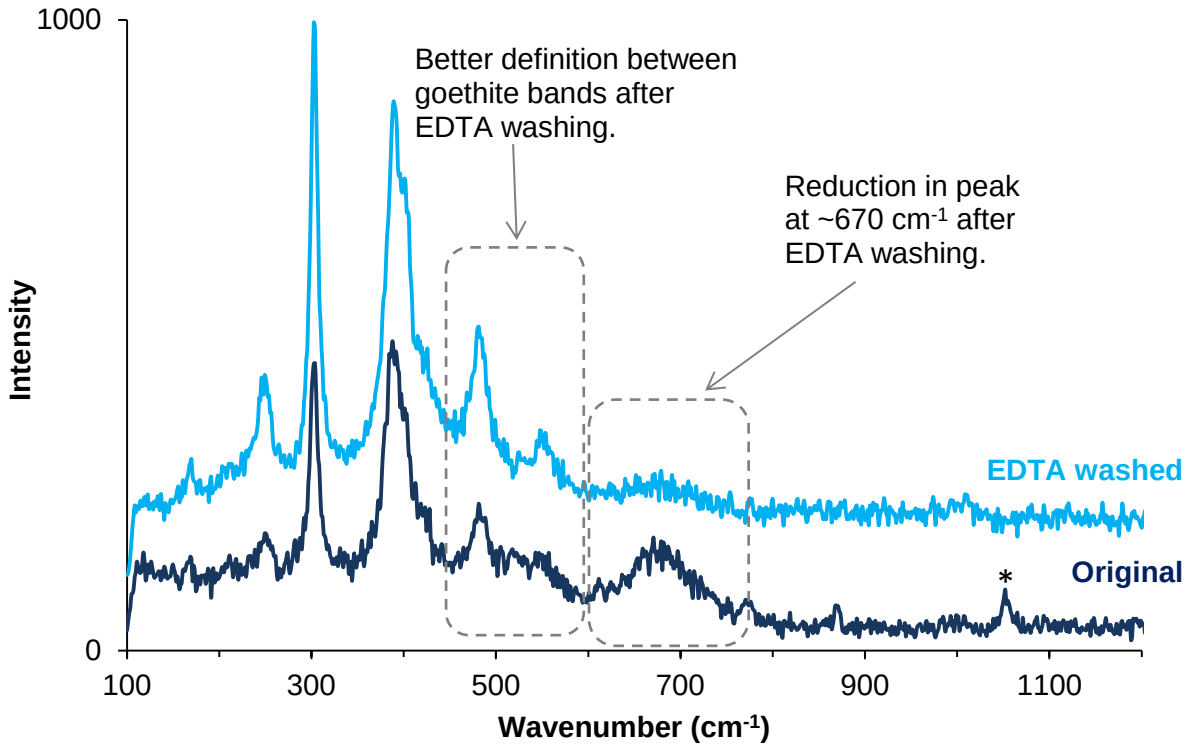

Figure 4.12: Raman spectra for a goethite synthesised at 20°C before and after EDTA washing. * denotes nitrate impurity in unwashed goethite sample.

Transmission Electron Microscopy (TEM)

TEM imaging of the goethite samples before and after the EDTA treatment was used to assess the effectiveness of the washing technique in removing the ferrihydrite phase as well as to show the extent (if any) of alteration to the goethite crystals.

The goethite produced from the 20°C synthesis, Figure 4.13, consists of poorly defined needles, certainly less well defined that those produced at the higher synthesis temperatures. There also appears to be the presence of a secondary phase, highlighted by clusters or aggregates which have a poorly defined morphology, alongside, or attached to the surface of the goethite crystals. These aggregated masses are not observed in the TEM image of the goethite sample after it had been washed with EDTA, and it is concluded that these clusters are the ferrihydrite phase. The goethite crystallites

themselves appear unaffected by the EDTA washing process as there does not appear to be any visible pitting or etching (and hence leaching) of the crystallites at the scale investigated.

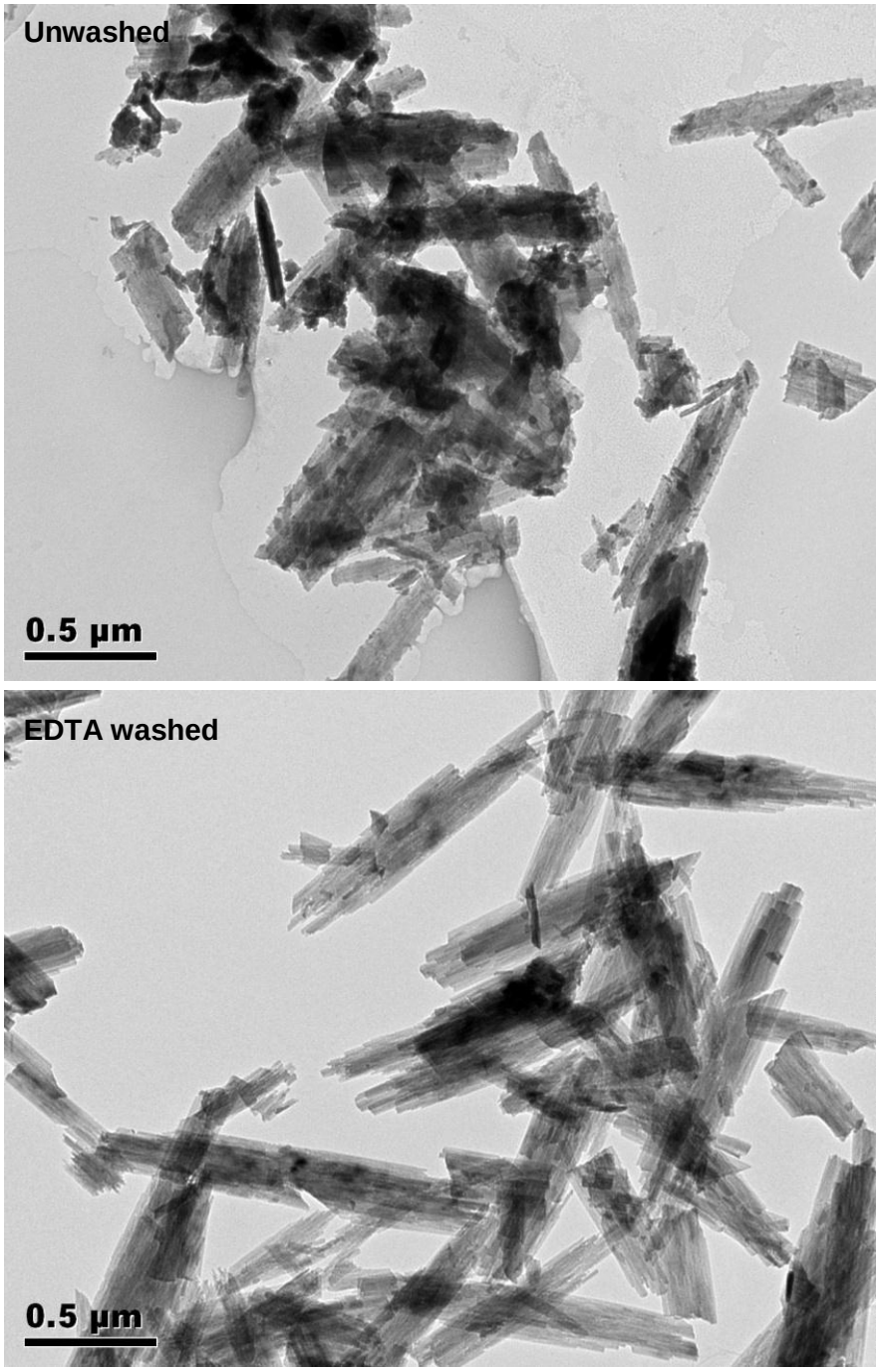

Figure 4.13: TEM images of goethites synthesised at 20°C, before and after EDTA washing.

The TEM image of the original (unwashed) goethite sample synthesised at 70°C, Figure 4.14, shows a single phase of fine needle type goethite rods. The presence of the dark coloured ferrihydrite clusters, observed in the TEM image of the 20°C synthesis goethite

sample (Figure 4.13) are not observed here. This is expected as the amount of ferrihydrite associated with a goethite sample synthesised at 70°C should be minimal. No significant differences are observed between the images of the samples before and after washing with EDTA. This suggests that no ferrihydrite was present in the samples synthesised at 70°C and again, the goethite crystals appear to remain unaffected by the EDTA washing process when imaged at the micrometre scale.

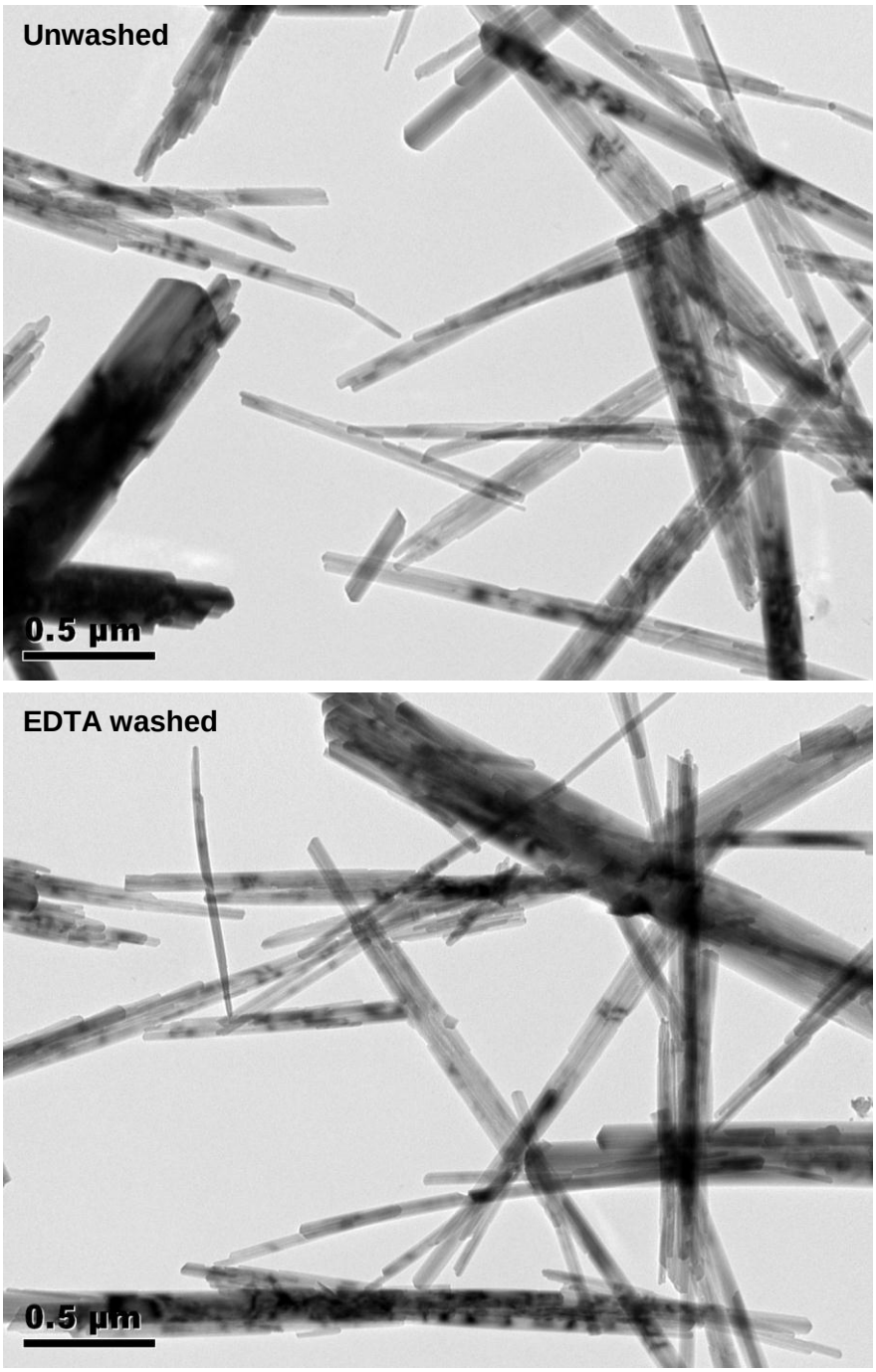

Figure 4.14: TEM images of goethites synthesised at 70°C, before and after EDTA washing.

Inductively Coupled Plasma Optical Emission Spectroscopy (ICP-OES)

The techniques utilised so far in this Chapter have demonstrated the effectiveness of the EDTA washing technique in removing the residual, untransformed, ferrihydrite from goethite samples, through characterisation of the solid phases themselves. ICP-OES was used as a way to investigate the Fe content of the EDTA solutions, after the goethite had been washed in them. If, as this work suggests, the EDTA does not react with the goethite itself, then any dissolved Fe in the EDTA solution would result directly from the dissolution of the associated ferrihydrite phase. Based upon the PXRD, TGA, Raman and TEM characterisation described earlier in this chapter, it was expected that the amount of Fe recovered in the EDTA solution would be greater in the goethite samples synthesised at lower temperatures, where ferrihydrite has been observed. Indeed, as no ferrihydrite has been observed in the goethite samples synthesised at 70°C and 90°C it was expected that no dissolved Fe would be measured in the EDTA solutions used to wash these samples. This theory is supported by the variation in the colour of the EDTA solutions after the goethite samples had been washed in them (Figure 4.15), ranging from a dark yellow for the solution used to wash the 20°C synthesis goethite, to colourless for the 70°C and 90°C samples.

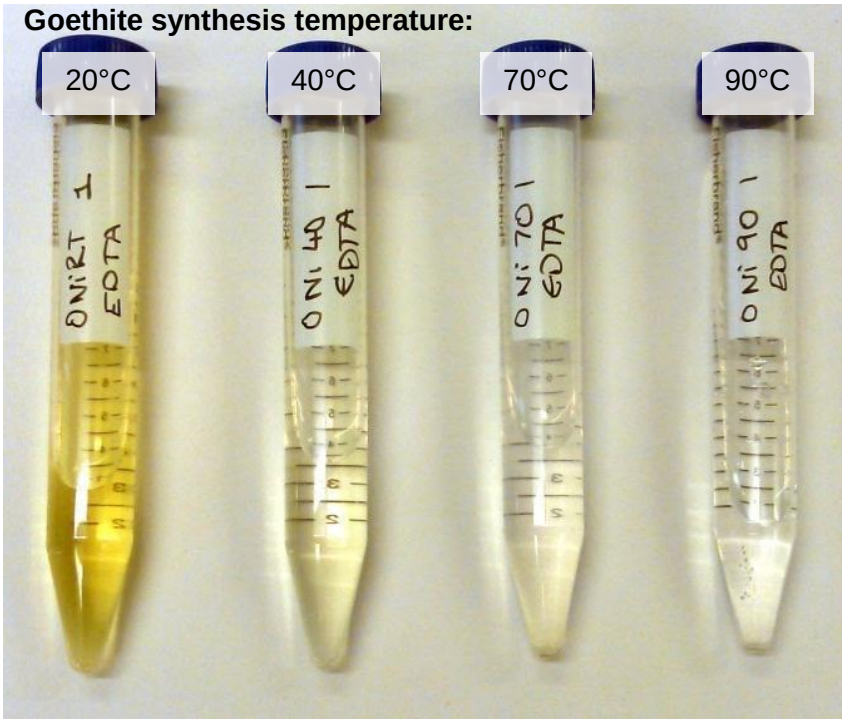

Figure 4.15: Appearance of EDTA solutions after they had been used to wash the goethite.

Using the ICP-OES data, the amount of Fe (assumed to be from the ferrihydrite phase) that had been removed from the goethite samples into the liquid EDTA solution was calculated. The data (shown in Table 4.4) supports the expectations described above, with no Fe detected in the EDTA washings of the goethite samples synthesised at 70 and 90°C, ~1 wt% of the total Fe removed from the 40°C synthesis goethite samples and ~11 wt% removed from the 20°C synthesis goethites. The goethite samples were also washed in water for comparison, and no Fe was detected in any of the washing solutions.

Table 4.4: Amount of Fe measured in EDTA solution after goethite washing.

Goethite Synthesis Temperature	Water wash	EDTA wash
	Average wt% Fe removed	Average wt% Fe removed (range)
20°C	0.0%	11.2% (9.7-13.6%)
40°C	0.0%	1.0% (0.8-1.2%)
70°C	0.0%	0.0%
90°C	0.0%	0.0%

The pH of each of the EDTA washing solutions was also recorded, shown in Table 4.5. The initial 0.1M EDTA solution had a pH of ~4.5. The pH values recorded show that the pH of the EDTA solution after the goethite had been washed in it is higher for the goethites synthesised at lower temperatures than for higher temperatures. From the ICP data (Table 4.4) it is known that the EDTA solutions from the lower temperature synthesis goethites contained the most Fe, due to the increased amounts of untransformed ferrihydrite present in association with the goethite samples.

Table 4.5: pH measurements of EDTA washing solutions.

EDTA Sample	pH Measurement		
	Replicate 1	Replicate 2	Replicate 3
0.1M EDTA Solution	4.56	4.56	4.58
EDTA solution from washing goethite synthesised at 20°C	5.98	6.03	6.17
EDTA solution from washing goethite synthesised at 40°C	5.04	5.08	5.07
EDTA solution from washing goethite synthesised at 70°C	4.7	4.69	4.69
EDTA solution from washing goethite synthesised at 90°C	4.6	4.67	4.63

The pH of the EDTA solutions was plotted against the Fe content (ppm) as measured by ICP-OES in order to examine the relationship between the two, shown in Figure 4.16. With such a small sample set it is difficult to be sure, as the 70 and 90°C synthesis goethite samples contained no ferrihydrite (and hence no Fe in the EDTA solution) at all. However, there does appear to be a trend between the pH and the Fe content, with a higher concentration of Fe corresponding to a higher pH of solution. It is therefore possible that with further investigation, the pH measurements could be used as a very quick and simple estimate of the iron content, and hence amount of ferrihydrite present.

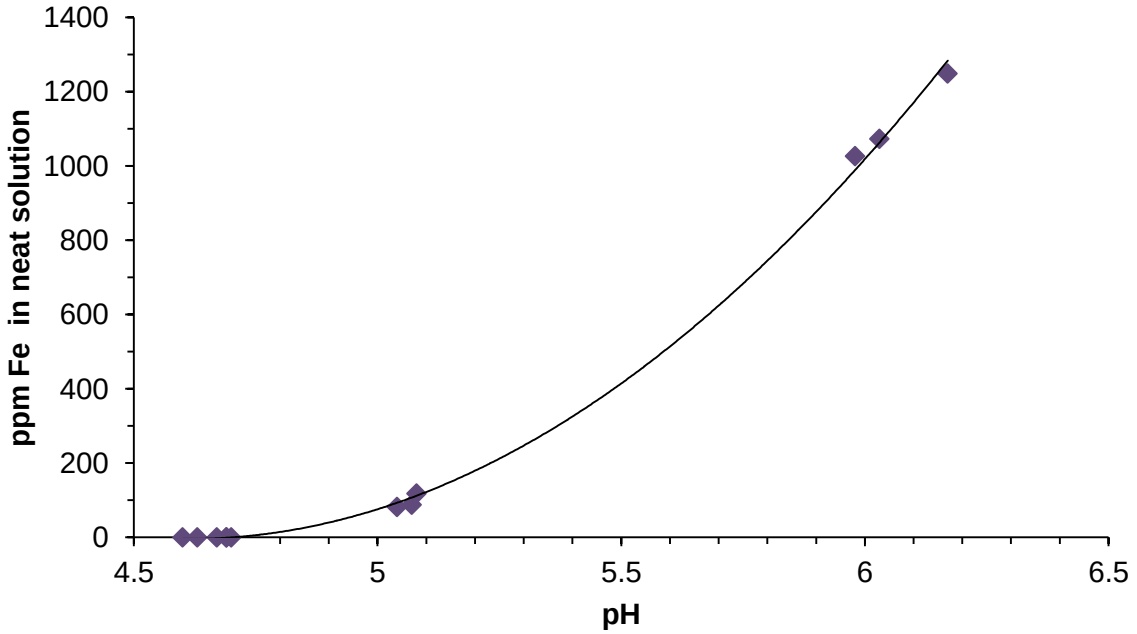

Figure 4.16: The relationship between the pH and the concentration of Fe in the EDTA washing solutions.

4.4. Summary

Although a number of techniques are discussed in the literature and are widely used in the removal of poorly crystalline or secondary phases from goethite (e.g. acid or oxalate extraction), concerns existed over the possible effects these washing techniques could have on the goethite itself. Using a variety of goethite samples synthesised at different temperatures, and hence having differing amounts of ferrihydrite associated with them (estimate of 0 – 55 wt%), a technique using EDTA to remove ferrihydrite secondary phases from goethite was developed. The multi-technique approach to characterisation, shown in earlier chapters to identify ferrihydrite in the goethite samples, demonstrated that the EDTA washing technique developed here is an effective means of removing associated ferrihydrite from goethite samples without altering the goethite itself.

The work in this chapter reaffirmed the use of the characterisation methodology in Chapter 3 (e.g. PXRD, TGA) for confirming the presence of ferrihydrite associated with goethite samples, and then demonstrated how the techniques can be used after the EDTA washing procedure to show the ferrihydrite phase has been removed. Analysis of the goethite by TEM confirmed that, at the scale investigated, the EDTA washing technique did not affect the goethite crystals themselves, which is extremely important for the investigation into Ni-substituted goethites.

The EDTA washing technique can be used as an alternative to oxalate extraction for the removal of co-formed ferrihydrite from goethite samples. Although the time taken for the EDTA wash is significantly longer than that of oxalate extraction, the EDTA technique does not require any special experimental conditions (e.g. oxalate extraction must be carried out in the dark) and it does not appear to affect the goethite itself in any way, whereas oxalate extraction can dissolve goethite, especially if poorly crystalline.

This work will now focus on the relationship between goethite and other foreign cations, particularly nickel. The characterisation methods developed so far in this project will be used to check the samples for the presence of ferrihydrite and, if found to be present, the EDTA washing technique will be used to remove it.

4.5. References

1 U. Schwertmann, E. Murad, *Clays and Clay Minerals*, (1983) **31**, 277-284.

2 A.C. Cismasu, F.M. Michel, A.P. Tcaciuc, T. Tyliszczak, G.E. Brown, *Comptes Rendus Geoscience*, (2011) **343**, 210-218.

3 E. Murad, P. Rojil, *Clay Minerals*, (2005) **40**, 427-440.

4 U. Schwertmann, *Zeitschrift für Pflanzenernährung und Bodenkunde*, (1964) **105**, 194

5 U. Schwertmann and R.M. Cornell, *Iron Oxides in the Laboratory – Preparation and Characterization,* (Wiley, 1991).

6 K.S. Brady, J.M. Bigham, W.F. Jaynes, T.J. Logan, *Clays and Clay Minerals,* (1986) **34**, 266-274.

7 G. Houben, S. Kaufhold, *Clay Minerals*, (2011) **46**, 387-385.

8 M.L.M. Carvalho-E-Silva, C.S.M. Partiti, J. Enzweiler, S. Petit, S. M. Netto, S.M.B. De Oliveira, *Hyperfine Interactions,* (2002) **142**, 559-576.

9 A. Oxley, N. Sirvanci, S. Purkiss, *Metalurgija*, (2007) **13**, 5-10.

10 N. Kaur, B. Singh, B.J. Kennedy, M. Gräfe, *Geochimica et Cosmochimica Acta,* (2009) **73**, 582-593.

11 U.G. Gasser, E. Jeanroy, C. Mustin, O. Barres, R. Nüesch, J. Berthelin, J. Herbillon, *Clay Minerals,* (1996) **31,** 465-476.

12 E.E. Sileo, A.Y. Ramos, G.E. Magaz, M.A. Blesa, *Geochimica et Cosmochimica Acta*, (2004) **68**, 3053-3063.

13 R.M. Cornell, W. Schneider, *Polyhedron*, (1989) **8**, 149-155.

14 J. Gerth, *Geochimica et Cosmochimica Acta,* (1990) **54**, 363-371.

15 O. K. Borggaard, *European Journal of Soil Science,* (1979) **30**, 727-734.

16 O. K. Borggaard, *European Journal of Soil Science,* (1981) **32**, 427-432.

17 O. K. Borggaard, *European Journal of Soil Science,* (1976) **27**, 478-486.

18 O. K. Borggaard, *Zeitschrift für Pflanzenernährung und Bodenkunde,* (1992) **155**, 431-436.

19 O. K. Borggaard, *Clay Minerals*, (1982) **17**, 365-368.

20 D.K. McCarty, J.N. Moore, W.A. Marcus, *Applied Geochemistry*, (1998) **13**, 165-176.

21 J.A. McKeague, P.A. Schuppli, *Geoderma*, (1985) **35**, 109-118.

22 U. Schwertmann, P. Cambier, E. Murad, *Clays and Clay Minerals*, (1985) **33**, 369-378.

23 S. Das, M.J. Hendry, *Chemical Geology,* (2011) **290**, 101-108.

24 M. Bouchard, D.C. Smith, *Spectrochimica Acta Part A,* (2003) **59**, 2247-2266.

25 D.L.A. De Faria, S. Venâncio Silva, M.T. de Oliveira, *Journal of Raman Spectroscopy*, (1997) **28**, 873-878.

26 L. Mazzetti, P.J. Thistlethwaite, *Journal of Raman Spectroscopy*, (2002) **33**, 104-111.

27 K. Muller, V.S.T. Ciminelli, M.S.S. Dantas, S. Willscher, *Water Research,* (2010) **44**, 5660-5672.

28 M. Hanesch, *Geophysical Journal International,* (2009) **177**, 941-948.

Chapter 5.

Incorporation of Foreign Cations into Goethite

5.1. Introduction

Naturally occurring goethite often contains a number of different metal cation impurities, such as chromium, manganese, cobalt, aluminum and most importantly for this project, nickel. [1] These foreign cations are incorporated into the goethite structure during the weathering processes which lead to its formation. In these natural samples, it is not always clear whether these minor elements are actually incorporated into the goethite structure via isomorphous substitution for the Fe^{3+} cation, or if they are occurring as part of a separate phase. [2, 3] Sometimes, these impurity elements are present in large enough amounts to warrant commercial extraction, and in order to devise the most efficient ways to extract these metals, it is fundamental to understand the crystal-chemical mechanisms by which transition metals, such as nickel, are associated with goethite [4]

There are a huge array of metal cations that have been reported to substitute for Fe^{3+} (both synthetically and/or naturally) in goethite, including Co^{3+}, Cr^{3+}, Al^{3+}, Mn^{3+}, Ni^{2+}, Ti^{4+}, Zn^{2+}, Cd^{2+}, Ga^{3+}, V^{3+}, Sc^{3+}, Pb^{4+}, Ge^{4+} and Si^{4+}. The most widely studied synthetic substituents into goethite are listed in more detail in Table 5.1. [2, 5]

Table 5.1: Reported maximum substitution levels (mol mol^{-1}) of cations which have been synthetically substituted into goethite. Ionic radii shown for 6-fold coordination. [6]

Cation	Ionic Radius (Å)	Maximum Reported Substitution (mol mol^{-1})
Fe^{3+}	0. 645 (high spin)	-
Al^{3+}	0.535	0.33 [7, 8]
Cr^{3+}	0.615	0.08 [2], 0.10 [9], 0.12 [10]
V^{3+}	0.64	0.06 [11], 0.13 [12]
Mn^{3+}	0.645 (high spin)	0.15 [2, 13, 14], 0.34 [15]
Co^{3+}	0.545 (low spin)	0.10 [16]
Ni^{2+}	0.690	0.055 [2]
Ga^{3+}	0.620	0.10 [17]

Although many of the cations that are reported to substitute into goethite are trivalent; divalent (e.g. Ni^{2+}, Zn^{2+}) and tetravalent (e.g. Si^{4+}, Pb^{4+}) cations are also able to substitute for Fe^{3+} into the structure. The charge on the substituting cation strongly influences the degree of substitution of Fe^{3+} that can be achieved. Substitution by divalent and tetravalent cations results in problems with charge balance and it has been suggested that

an uptake or release of protons could occur in order to retain charge neutrality.[18] The size of the substituting cations' ionic radii (e.g. a lot larger or smaller) will also influence the tendency of such cations to replace Fe^{3+} in the structure.[19]

Goethite has the diaspore-type structure, and there are a number of other natural and synthetic metal-oxide-hydroxides which adopt this and are therefore isostructural with goethite (Table 5.2). Of these, the naturally occurring mineral phases are diaspore (α-AlOOH), groutite (α-MnOOH), montroseite (VOOH) and bracewellite (α-CrOOH), and the synthetic phases CoOOH, ScOOH and GaOOH. The existence of these isostructural M-OOH equivalents suggests there is a possibility for solid solutions to be formed between goethite and these diaspore-type phases via isomorphous substitution for Fe^{3+} by the other cations (Al^{3+}, Mn^{3+}, V^{3+}, Cr^{3+}, Co^{3+}, Sc^{3+}, Ga^{3+}). The goethite structure itself is not modified as a result of substitution by these cations, but the unit cell dimensions do change, reflecting the differences in the sizes of the respective ionic radii.

Table 5.2: Unit cell dimensions of phases with the diaspore-type structure. Ionic radii shown are for the M(III) cation with 6-fold coordination.[6]

Phase	Unit Cell Parameters				Ionic Radius of Metal Cation (Å)
	a **(Å)**	***b*** **(Å)**	***c*** **(Å)**	**Volume (Å^3)**	
Goethite [20] α-FeOOH	4.602	9.952	3.021	138.225	0.645
Diaspore [21] α-AlOOH	4.4031	9.4252	2.8452	118.08	0.535
Groutite [22] α-MnOOH	4.560	10.700	2.870	140.03	0.645
Bracewellite [23] α-CrOOH	4.492	9.860	2.974	131.72	0.615
Montroseite [24] VOOH	4.54	9.97	3.03	137.15	0.640
CoOOH [25]	4.353	9.402	2.84	116.232	0.545
ScOOH [26]	4.755	10.301	3.209	157.18	0.745
GaOOH [27]	4.5171	9.7907	2.9732	131.49	0.620

A linear relationship exists between the volume of the M-OOH unit cell and the ionic radius of the M(III) cation (shown in Figure 5.1), a relationship which can be summarised by the Vegard rule.[28] Vegard's rule says that the lattice parameters between two end members of a solid solution series will change linearly with composition. Observing the data plotted in Figure 5.1, the relationship between the cell volume and the ionic radii for each of the M-OOH phases can be observed, with the cell volume increasing linearly with

the size of the M(III) cation. Some of the unit cell dimensions deviate very slightly from the Vegard line, thought to be as a result of structural imperfections caused by the incorporation of extra OH into the goethite structure in order to balance any cation deficit.[29]

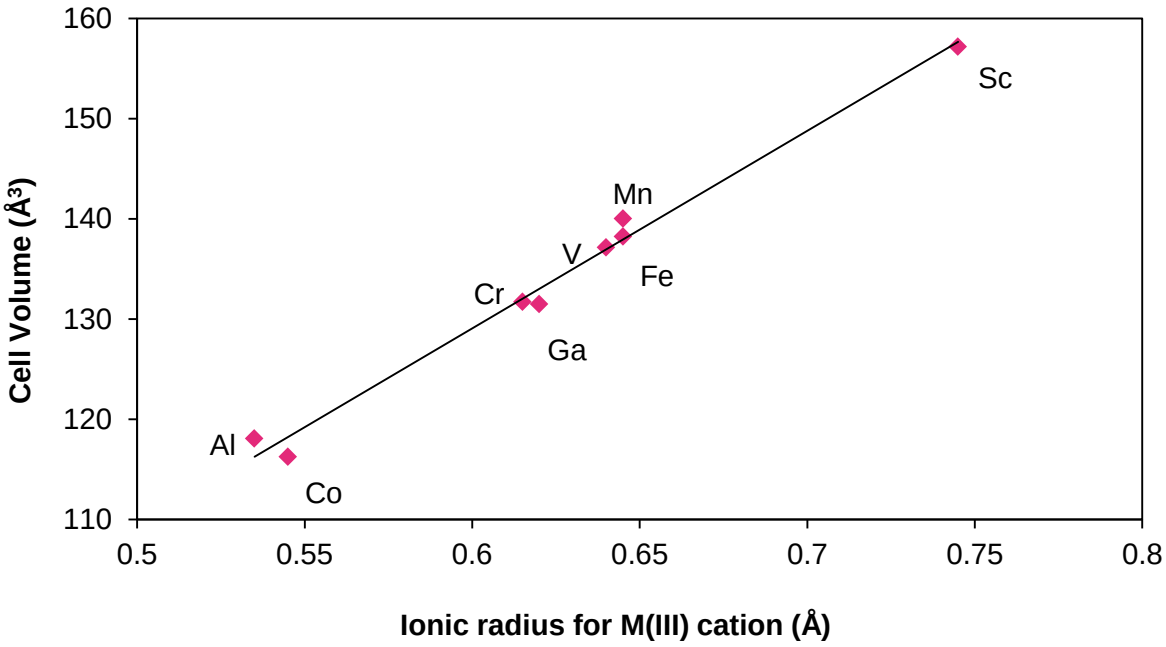

Figure 5.1: Relationship between the unit cell volume and the ionic radii of iso-structural goethite equivalents. Data adapted from Table 5.2.

The likelihood of substitution, and therefore full solid solution formation, depends on the similarity of the ionic radii and the valency of the cations.[30] Isomorphous substitution of Fe^{3+} by other cations has been observed in natural mineral samples, and investigated in the laboratory. However, as far as is known, all of these solid solutions show broad miscibility gaps, thought to be as a result of structural strain as the level of substitution increases.[31] Determining whether trace elements occur in solid solution with goethite, or separately as discrete phases, is extremely important in improving our understanding of the best ways to extract these metals.[32]

5.1.1. The Transformation of Ferrihydrite to Goethite in the Presence of Foreign Ions.

The goethite samples investigated in this work are synthesised via the transformation of a ferrihydrite precursor phase (see Chapter 2). Some factors that affect the transformation of ferrihydrite to goethite, such as synthesis time and temperature, have already been discussed in Chapter 3, but the presence of foreign metal cations has also been shown to stabilise ferrihydrite and inhibit the recrystallisation to goethite.[33, 34] In order to ascertain the precise nature of the residence of Ni that is associated with goethite (discussed later in this chapter), it is vital to understand the effect that including Ni in the synthetic procedure may have on the end products.

Giovanoli and Cornell (1992) showed that the presence of divalent transition elements (Co, Ni, Cu, Zn) can stabilise ferrihydrite, although the subsequent crystallisation products formed from the ferrihydrite precursor are dependent on the concentration of foreign cations in the system as well as the pH.[33] Evidence from this study suggests that, with the exception of Mn, the presence of a foreign metal cation stabilises ferrihydrite and prevents its transformation to goethite. To be able to understand why this is, the kinetics and mechanism of the recrystallisation process needs to be considered.

The transformation of ferrihydrite to goethite involves dissolution of the ferrihydrite phase, followed by re-precipitation. Studies carried out in alkaline environments showed that in systems that contain up to 10 mol% M^{2+} (M= Mn, Co, Ni, Cu, Zn) co-precipitated with ferrihydrite, all of the cations considered impeded the transformation process, with the exception of Mn^{2+}. Impedance of this process was greatest with increasing concentrations of foreign cation present, but the effects were observed even with small quantities (~2 mol%). It was also observed that in the case of Mn and Cu, recrystallisation of the M-ferrihydrite was congruent, whereas in the case of Co, Ni and Zn, these elements were released more slowly from the M-ferrihydrite co-precipitate. This means that in a M-ferrihydrite (where M = Co, Ni, Zn), the M is released more slowly than the iron, therefore nucleation and growth of goethite is completed before all of the M-containing ferrihydrite has crystallised.[33]

Unlike goethite and hematite, where it has been shown that partial solid solutions can be formed with a variety of metal cations, evidence for solid solution formation in ferrihydrite is lacking. It is unlikely that this is because solid solutions with ferrihydrite are not possible, but the complexities of analysing the poorly crystalline material (both with and without secondary cations present) makes characterisation problematic.[35, 36] Because of the

difficulties in concluding that isomorphous substitution has occurred in ferrihydrite, the relationship between foreign ions and ferrihydrite is often described as adsorption.[34]

As well as modifying the transformation process, the incorporation of foreign ions can dramatically modify the properties of ferrihydrite. For example, the addition of Si to ferrihydrite not only impedes its dissolution behaviour, but also drastically increases the temperature at which conversion to hematite occurs.[34]

The impact that foreign ions have on the behaviour of ferrihydrite is of interest in this study because ferrihydrite is so prevalent in soils and natural systems. It is believed that ferrihydrite could also be present alongside goethite in the lateritic ore system, stabilised against transformation by the large number of foreign cations present.

5.1.2. Incorporation of Foreign Cations Into the Goethite Structure

The incorporation of aluminum into goethite is probably the most widely studied example of cationic substitution in this system, and was first reported in natural samples in 1941.[37] Synthetic goethites have been shown to incorporate up to 33 mol% of aluminum, and natural samples have been found which contain up to 36 mol%. [38, 39] Even though the ionic radius of Al^{3+} is ~17% smaller than that of Fe^{3+}, 0.535 Å and 0.645 Å respectively, up to a third of the iron in goethite can be replaced by aluminum. Although the 33 mol% upper limit of Al-for-Fe substitution appears to be widely agreed, reports of as much as 47 mol% Al substitution exist for goethites prepared from sulfate solutions.[40] It is possible that the miscibility gap observed in the goethite – diaspore solid solution at ~33 mol% Al could merely represent the solubility limit of Al-goethite in alkaline media.[41]

Schwertmann *et al.* (1989) synthesised goethites containing up to 10 mol% Cr from both Fe(III) and Fe(II) systems. The structural incorporation of Cr was demonstrated by a linear decrease in the unit cell parameters *a*, *b* and *c* and a corresponding decrease in the cell volume as the level of Cr incorporation increased.[9] This decrease in the size of the unit cell is expected as Cr^{3+} has a slightly smaller ionic radius than Fe^{3+} (0.615 and 0.645 Å respectively). The crystal size and morphology of the goethite particles produced also changed with increasing substitution, as observed by TEM and PXRD. IR analysis observed a shift in the out-of-plane OH bending vibration, increasing from 793 to 800 cm^{-1}, reflecting a shortening of the M-OH bond length.[9]

Sileo *et al.* (2004) synthesised substituted goethites containing up to 12 mol% Cr, and their research also supports the findings described previously of a reduction in the size of the unit cell as the Cr content of a substituted goethite increased. [42] The authors found

that at low levels of Cr-for-Fe substitution the *b* parameter decreased as predicted by Vegard's rule, but at higher levels of substitution (4-12 mol%) it deviated from the line and stayed relatively constant. The opposite effect was observed with the *a* parameter, with small changes in the unit cell dimension at low levels of substitution and larger changes, approaching the predicted value, occurring as the level of substitution increased. The *c* parameter decreased in line with Vegard's rule at all substitution levels (0-12 mol%). Further characterisation by EXAFS (extended X-ray absorption fine structure) suggested that the changes observed in the unit cell by refinement of the PXRD data are a result of differences in the coordination polyhedra around Cr and Fe, not as an effect of the smaller size of the Cr(III) cation compared to Fe(III). This study also observed a change in the crystal size for the Cr substituted goethites, showing that in all cases the particles of substituted goethites were smaller than those of non-substituted goethite.

Cobalt incorporation into goethite has been shown to reach levels of up to 10 mol%, and the unit cell parameters of the resulting Co-substituted goethite phases decreased in line with Vegard's rule with increasing substitution.[16] This is as expected as the ionic radius of Co^{3+} is smaller than that of Fe^{3+}, at 0.545 and 0.645 Å respectively.

Manganese has been reported to substitute for iron in the goethite structure at levels of up to 15 mol%.[13] Furthermore, it has been suggested that when a Mn^{2+} starting solution was used to synthesise Mn-goethite, the Mn^{2+} cations were oxidized to Mn^{3+} to substitute for Fe^{3+} in the goethite structure. The substitution of Fe^{3+} by Mn^{3+} was confirmed by PXRD measurements where, with increasing manganese substitution, the unit cell size approached that of the Mn-containing, iso-structural equivalent of goethite, groutite (α-MnOOH). Although Fe^{3+} and Mn^{3+} have extremely similar ionic radii, both 0.645 Å to 3 s.f., Mn^{3+} does not fit into the goethite structure as easily as Fe^{3+} because of the Jahn-Teller effect. [43] Mn^{3+} has four d electrons which gives it a tetragonally distorted coordination sphere, with four short equatorial Mn-O bonds and two elongated axial Mn-O bonds. This effect was observed in the unit cell parameters of the Mn-substituted goethite samples, with the *a* parameter increasing and the *b* parameter decreasing with increasing substitution.[14, 44]

EXAFS spectra on Mn-substituted goethite samples showed that the local environment around Fe remained goethite-like at up to 47 mol% Mn-for-Fe substitution, but that the environment around Mn is goethite-like at only up to 13 mol% substitution. Above this level the local structure is groutite-like, suggesting the formation of groutite-like clusters in the host goethite structure which remain undetected by PXRD. Scheinost *et al.* (2001)

suggest that the driving force behind the cluster formation is the incompatibility between the increasingly distorted $Mn(O,OH)_6$ octahedra and the $Fe(O, OH)_6$ octahedra. [45]

Vanadium is often found in natural environments alongside iron, and an iso-structural goethite equivalent, montroseite (VOOH) exists, but few studies have been carried out to determine the extent of substitution that can be achieved by V in goethite. Schwertmann *et al.* (1994) synthesised V-goethite with V^{3+} for Fe^{3+} substitution of up to 6 mol%. Because of the similar ionic radii of the V^{3+} and Fe^{3+} cations (0.64 and 0.645 Å respectively), measurement of the unit cell parameters showed no significant difference with increasing levels of substitution.[11]

An alternative study by Kaur *et al.* (2009) used a low temperature synthesis method to achieve V^{3+} substitution in goethite of up to 13.3 mol%.[12] Rietveld refinement of the PXRD data for these samples showed that with increasing V^{3+} substitution there was a slight decrease in the size of the *a* parameter and a slight increase in the *b* and *c* parameters; the net effect being that the unit cell volume remained essentially unchanged. The authors suggested that despite the similarities in the ionic radii and valence states of V^{3+} and Fe^{3+}, greater levels of substitution were not occurring because of the relative ease with which V^{3+} would oxidize to V^{4+} or V^{5+}. The greater differences in the ionic radii of the 4+ and 5+ cations, as well as the difference in valency, possibly limit the levels of incorporation that can be achieved. The study also found that for vanadium substituted goethites, temperature played an important role in the extent of subsistitution that could be achieved. A lower synthesis temperature preserved the trivalent vanadium species, which is the most similar to Fe^{3+}, and therefore most likely to substitute into the goethite structure.[12]

The association between nickel and goethite is well recognised, although the nature of this relationship (e.g. whether the Ni is structurally incorporated or present as a separate phase) is sometimes unclear. The substitution of nickel into goethite is slightly different to the cations described previously, as Ni is believed to substitute into goethite as a divalent cation, rather than the trivalent variant. Naturally occurring Ni-goethite phases generally contain no more than 4% Ni-for-Fe substitution and have poor crystallinity. The exact amount of nickel present depends on the individual laterite deposits that they originate from, and naturally occurring samples also regularly contain significant amounts of other cations, such as aluminum, chromium and cobalt, alongside nickel.[46] Synthetic goethite has been reported to be prepared with up to 5.5 mol% Ni-for-Fe substitution, and studies have shown that the resulting product is single phase, i.e. the substituted nickel was in solid solution with the iron in the goethite. At increasing nickel concentrations (<10%)

PXRD, TEM and IR analysis revealed that separate amorphous, $Ni(OH)_2$ and $NiFe_2O_4$ phases were present.[4, 47, 48]

There are three different mechanisms which have been suggested to explain the way in which nickel is associated with goethite; isomorphous substitution of Ni-for-Fe into the goethite structure, association with an amorphous or poorly crystalline goethite phase or weakly adsorbed to the crystalline goethite surface. [5, 32, 46] Leaching experiments performed on natural goethite samples showed that the quantity of nickel adsorbed onto the mineral surface was minimal, and may be related to the surface area.[3, 49] Further studies on the incorporation of small amounts of Cr, Mn and Ni into the goethite structure using EXAFS found no evidence to suggest that separate phases were forming as a result of the presence of foreign cations, suggesting that isomorphous substitution for Fe^{3+} by Cr^{3+} (up to 8 mol%), Mn^{3+} (up to 15 mol%) and Ni^{2+} (up to 5.5 mol%) does occur. [2, 13] The analysis also showed that the coordination environment of the iron was changing with composition. The authors suggest this was likely to be responsible for limiting the amount of foreign cation that could be accommodated in the structure.

Unlike cobalt and managanese substituted goethite, where the divalent Mn or Co cation in solution has been shown to oxidise to the trivalent form before substitution into the goethite structure, research suggests that the nickel present in goethite is divalent. It is quite unlikely that nickel is substituting into the goethite structure as Ni^{3+} - as minerals containing trivalent Ni are quite uncommon.[50] Jamborite ($(Ni^{2+}Ni^{3+}CoFe^{2+}Fe^{3+})(OH)_2(OH, S, H_2O)$), [51] polydymite ($Ni^{2+}Ni_2^{3+}S_4$), [52] tyrrellite ($Cu(Co^{3+}Ni^{3+})_2Se_4$) [53] and violarite ($Fe^{2+}Ni_2^{3+}S_4$) [54] are all reported to contain trivalent nickel.

In order to retain charge neutrality when substituting divalent Ni^{2+} for trivalent Fe^{3+} in goethite, it has been suggested that the incorporation of nickel into the structure is accompanied by hydroxylation. This involves the replacement of O^{2-} by OH^-, resulting in the conversion of $FeO_3(OH)_3$ octahedra to $NiO_2(OH)_4$. [2, 5] This theory of charge balance by incorporation of additional OH^- is supported by thermal analysis of synthetic Ni-goethite samples carried out by Carvalho-E-Silva *et al.* (2002).[46] The authors found strong linear correlation between the amount of nickel and the weight loss which occurred in the Ni-substituted goethite samples. Conversely, in Co-substituted goethite samples (where the substituting cation is trivalent) there was no such correlation. Structurally, the incorporation of Ni^{2+} into goethite opens up the structure by breaking the H-bonds located at the vacant double chains, resulting in distortion of the framework. It is likely that this deformation is responsible for the relatively low upper limit of nickel incorporation that can be achieved in the goethite structure, considering the similarities in size of the atomic radii

and compared to the greater substitution levels which can be achieved by other elements.[5]

In this chapter, substitution of a range of metal cations (Mn^{3+}, Cr^{3+}, Al^{3+}, Co^{3+}) into the goethite structure will be briefly investigated, in order to observe the phases that form across a wide range of foreign metal cation addition levels. Later, a more in depth investigation into how Ni substitution into goethite affects its formation will be discussed, with an aim to investigate the exact nature of the association between Ni and goethite.

5.2. Experimental Methods

In the first part of this chapter, a number of M-substituted goethite samples, ideal formula $Fe_{1-x}M_xOOH$ (where M=Cr, Al, Co, Mn, Ni), are briefly investigated in order to examine both the effect that substituting cations have on the goethite structure itself, and also the different phases that form (and the substitution levels that this happens at) across the full range of substitution levels between the two end members.

The synthesis methods used to prepare these M-substituted goethite samples are summarised in Table 5.3, and full details are given in Chapter 2.1.2. As has been discussed previously, the samples are described using their target compositions, which may not be the same as their actual compositions. This is to enable the samples to be distinguished from one another and discussed in a coherent way throughout this thesis. Where the actual elemental composition is known, this will be stated where relevant.

Table 5.3: Summary of synthesis procedures to prepare M-substituted goethite samples.

Target Phase	Synthesis Procedure		
$Fe_{1-x}Cr_xOOH$	$Fe(NO_3)_3 \cdot 9H_2O + Cr(NO_3)_3 \cdot 9H_2O$	+ KOH	7d, 70°C
$Fe_{1-x}Al_xOOH$	$Fe(NO_3)_3 \cdot 9H_2O + Al(NO_3)_3 \cdot 9H_2O$	+ KOH	14d, 70°C
$Fe_{1-x}Co_xOOH$	$Fe(NO_3)_3 \cdot 9H_2O + Co(NO_3)_2 \cdot 6H_2O$	+ KOH	7d, 70°C
$Fe_{1-x}Mn_xOOH$	$Fe(NO_3)_3 \cdot 9H_2O + Mn(NO_3)_2 \cdot 4H_2O$	+ NaOH	20d, 60°C
$Fe_{1-x}Ni_xOOH$	$Fe(NO_3)_3 \cdot 9H_2O + Ni(NO_3)_2 \cdot 6H_2O$	+ KOH	7d, 70°C

The main focus of this research is on Ni residence in goethite, so a greater amount of investigation was carried out on this group of samples. As well as the standard synthesis method to prepare $Fe_{1-x}Ni_xOOH$ samples shown in Table 5.3, the Fe-Ni series of samples was also prepared via the Fe(II) precursor synthesis method ($FeCl_2 \cdot 4H_2O + NiCl_2 \cdot 4H_2O + NaHCO_3$, 48h, 20°C), described in Chapter 2. Furthermore, the effect of altering the synthesis temperature and/or time on the Ni-substituted goethite samples is discussed later in this Chapter. Sections 5.4 and 5.5 focus solely on Ni residence in goethite, including an assessment of the effectiveness of the EDTA washing technique described in Chapter 4 on these Ni-goethite phases.

5.3. Substitution of Foreign Cations into Goethite - $Fe_{1-x}M_xOOH$

5.3.1. Chromium Substitution ($Fe_{1-x}Cr_xOOH$)

The Cr-substituted goethite samples were characterised by PXRD to enable the identification of the phases that had formed in the solid solution series as the amount of Cr-for-Fe substitution increased, and to measure the variation in the size of the unit cell as a function of the level of substitution. Visually, increasing levels of Cr incorporation had an effect on the colours of the different Fe-Cr series of samples, becoming a darker brown colour with increasing Cr substitution. The pure Fe goethite was a yellow/ochre colour and the Cr-rich (non-goethite) phases were a dark green/black colour, shown in Figure 5.2.

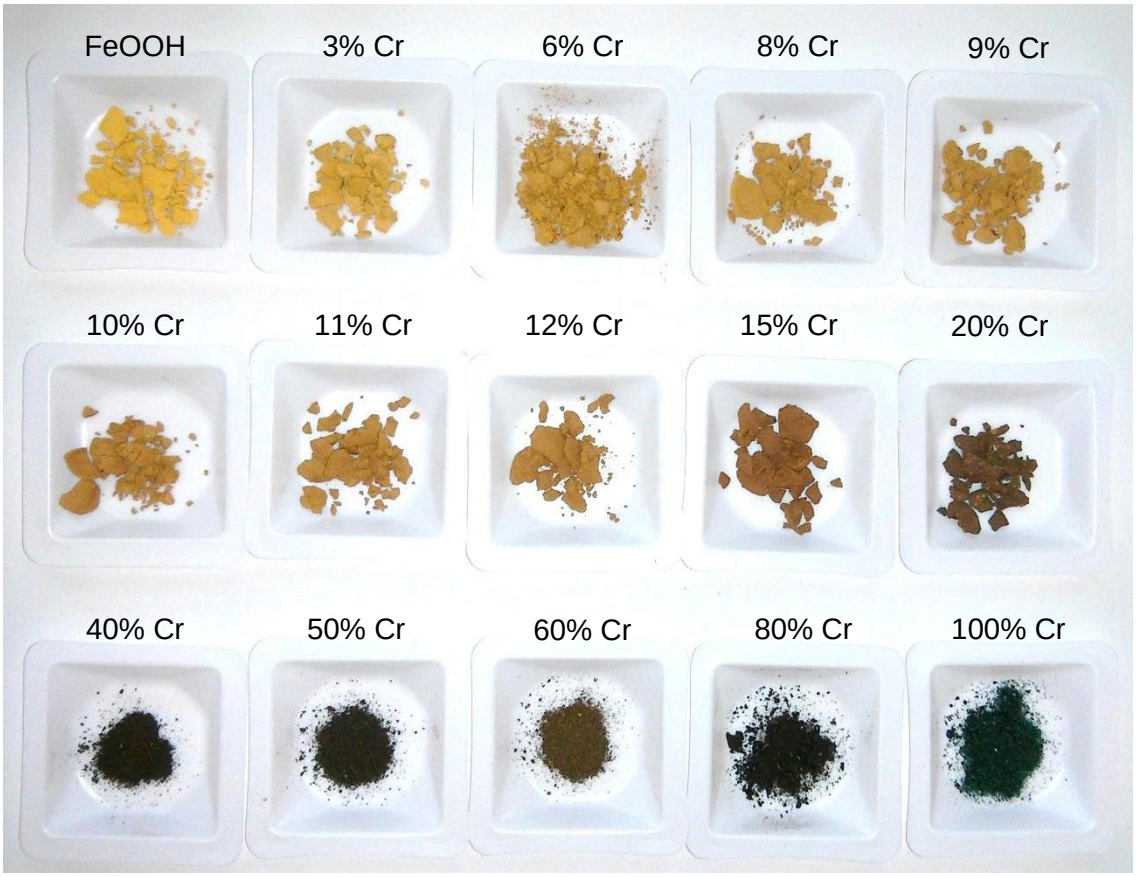

Figure 5.2: Appearance of the synthetic products in the Fe-Cr goethite solid solution series. Samples labelled by target mol% Cr.

The phases identified in the samples from analysis of the PXRD data (Figure 5.3) are shown in Table 5.4. The only identifiable phase in the samples containing between 0-20 mol% Cr was goethite and the 60% Cr-goethite samples also showed reflections which

could be attributed to goethite. The PXRD patterns for the 100, 80, 50 and 40 mol% Cr samples showed no clear diffraction peaks suggesting that the sample was either very poorly crystalline or that the particle size was extremely small. Phases with these properties are often described as being amorphous to PXRD.

Table 5.4: Phases identified by PXRD in Fe-Cr goethite solid solution series. G = goethite, A = amorphous.

Desired product: $Fe_{1-x}Cr_xOOH$															
Target value of x	0.0	0.03	0.06	0.08	0.09	0.10	0.11	0.12	0.15	0.20	0.40	0.50	0.60	0.80	1.0
Phases Identified	G	G	G	G	G	G	G	G	G	G	A	A	A G	A	A

Singh *et al.* (2004) reported the synthesis of goethite with up to 8 mol% Cr-for-Fe substitution, prepared in a similar way to the samples produced here.[2] From the PXRD data alone, the Cr-goethite samples synthesised in this work appear to be single-phase goethite for the samples with a target x value of between 0-0.2 (up to 20 mol% Cr-for-Fe substitution). There are no observable shifts in any of the goethite peak positions on the diffraction patterns as the Cr content increases. The identification of only single phase goethite with up to 20 mol% Cr-for-Fe substitution, however, does not provide conclusive evidence that this much Cr has substituted into the goethite structure, as a separate phase that has not been identified by the PXRD technique is likely to be present, and further characterisation would be needed to confirm this.

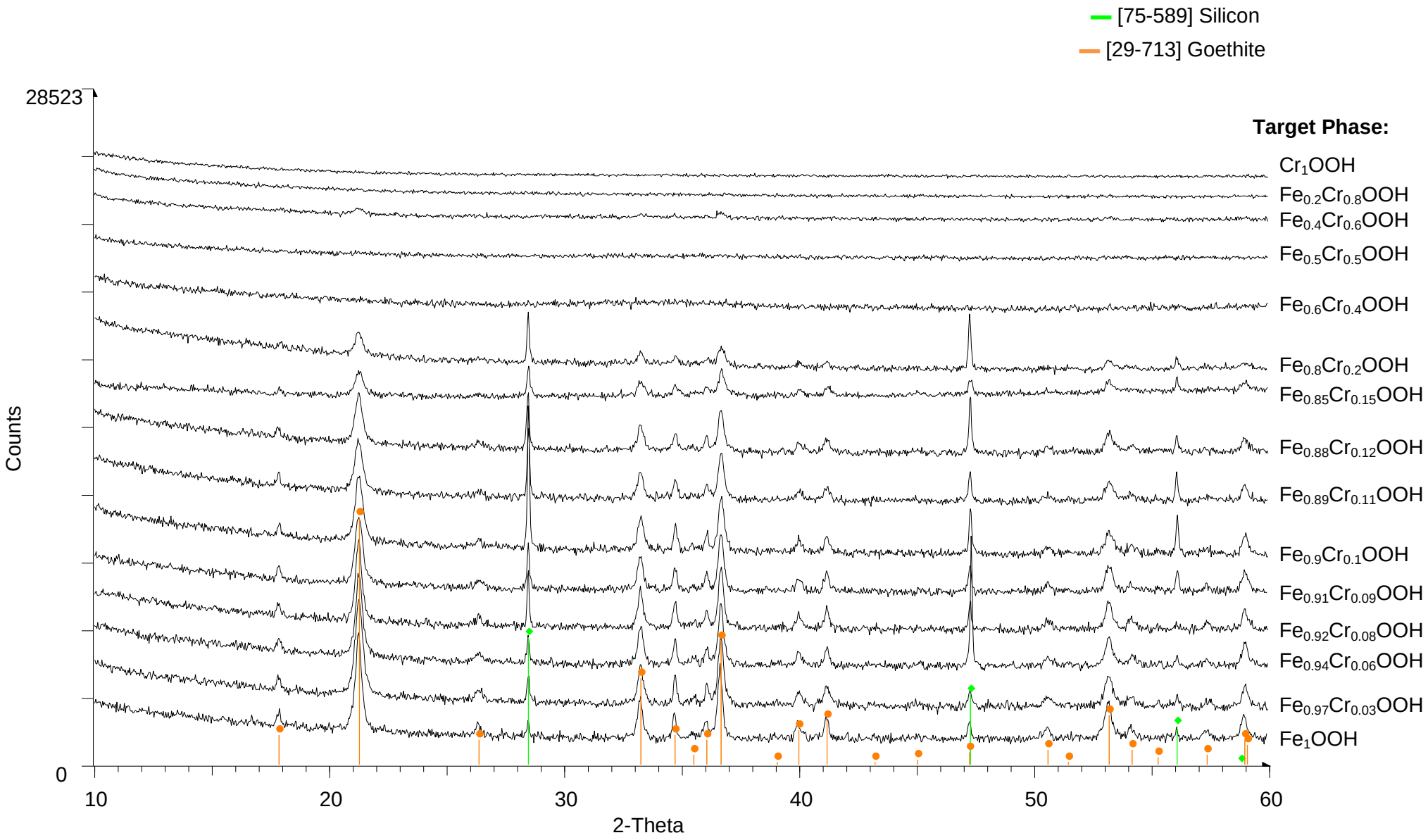

Figure 5.3: PXRD patterns collected on Cr-substituted goethites ($Fe_{1-x}Cr_xOOH$), using Cu $K_{\alpha 1}$ radiation. Target composition of phases shown on right hand side of PXRD pattern. Samples with $x \leq 0.2$ have Si added as an internal standard.

Trivalent chromium has an ionic radius of 0.615 Å, slightly smaller than that of Fe^{3+} (0.645 Å).[6] As discussed earlier in this Chapter, the smaller size of the Cr^{3+} cation when compared to the Fe^{3+} cation suggests that with increasing substitution of Fe-by-Cr in the goethite structure, the unit cell should decrease in size towards that of the isostructural Cr equivalent of goethite, bracewellite (α-CrOOH). Using the PXRD data shown in Figure 5.3, the unit cell parameters were refined for the Cr-substituted goethite samples, $Fe_{1-x}Cr_xOOH$, where x = 0-0.2 (the samples where goethite was identified), shown in Table 5.5, to enable any changes in the size of the unit cell of the goethite to be established.

Table 5.5: Unit cell parameters for Cr-substituted goethite samples, $Fe_{1-x}Cr_xOOH$, (esds shown in parentheses).

Target Product	Identified Product	*a* (Å)	*b* (Å)	*c* (Å)	*Volume* (Å^3)
Literature Goethite [4]		4.602 (3)	9.952 (4)	3.021 (2)	138.3 (1)
Fe_1Cr_0OOH	Goethite	4.612 (2)	9.957 (3)	3.023 (1)	138.8 (1)
$Fe_{0.97}Cr_{0.03}OOH$	Goethite	4.610 (3)	9.958 (4)	3.020 (2)	138.6 (1)
$Fe_{0.94}Cr_{0.06}OOH$	Goethite	4.611 (2)	9.955 (3)	3.023 (1)	138.8 (1)
$Fe_{0.92}Cr_{0.08}OOH$	Goethite	4.611 (2)	9.959 (3)	3.020 (2)	138.7 (1)
$Fe_{0.91}Cr_{0.09}OOH$	Goethite	4.614 (2)	9.959 (3)	3.019 (2)	138.7 (1)
$Fe_{0.9}Cr_{0.1}OOH$	Goethite	4.612 (2)	9.951 (4)	3.022 (2)	138.7 (1)
$Fe_{0.89}Cr_{0.11}OOH$	Goethite	4.612 (3)	9.963 (3)	3.016 (2)	138.6 (1)
$Fe_{0.88}Cr_{0.12}OOH$	Goethite	4.604 (2)	9.959 (3)	3.022 (1)	138.6 (1)
$Fe_{0.85}Cr_{0.15}OOH$	Goethite	4.609 (5)	9.957 (8)	3.020 (4)	138.6 (1)
$Fe_{0.80}Cr_{0.20}OOH$	Goethite	4.609 (5)	9.950 (5)	3.018 (3)	138.4 (1)
Literature Bracewellite [5]		4.492	9.860	2.974	131.7

An investigation by Sileo *et al.* (2004) found that with increasing incorporation of Cr into goethite, the unit cell parameters decreased in size with up to 12 mol% Cr-for-Fe substitution. The decrease in the *c* parameter approximately followed that which would be predicted by Vegard's law.[42]

When the unit cell parameters calculated for the Cr-goethite phases synthesised in this work are plotted against the molar proportion of Cr, the general trend for the unit cell edges *a*, *b* and *c*, and consequently the *cell volume,* is for their size to decrease as the Cr

content increases, shown in Figure 5.4. However, there is a large amount of scatter on the data and the difference across the whole range of each parameter is very small, with total decreases of *a* = 0.009, *b* = 0.013, *c* = 0.007 Å and *volume* = 0.41 Å^3. Whilst the degree of scatter on the data for the unit cell edges is relatively large, when these parameters are combined to give the cell volume the total decrease in the unit cell size is greater than the estimated error on the values.

From PXRD data alone, the levels of Cr substitution into goethite that appear to have been achieved are far greater, at 20 mol%, than those widely reported in the literature (8-12 mol%). PXRD only assists in the identification of crystalline phases, therefore it is likely that the excess Cr is present as part of a separate phase which was not possible to detect using this technique.

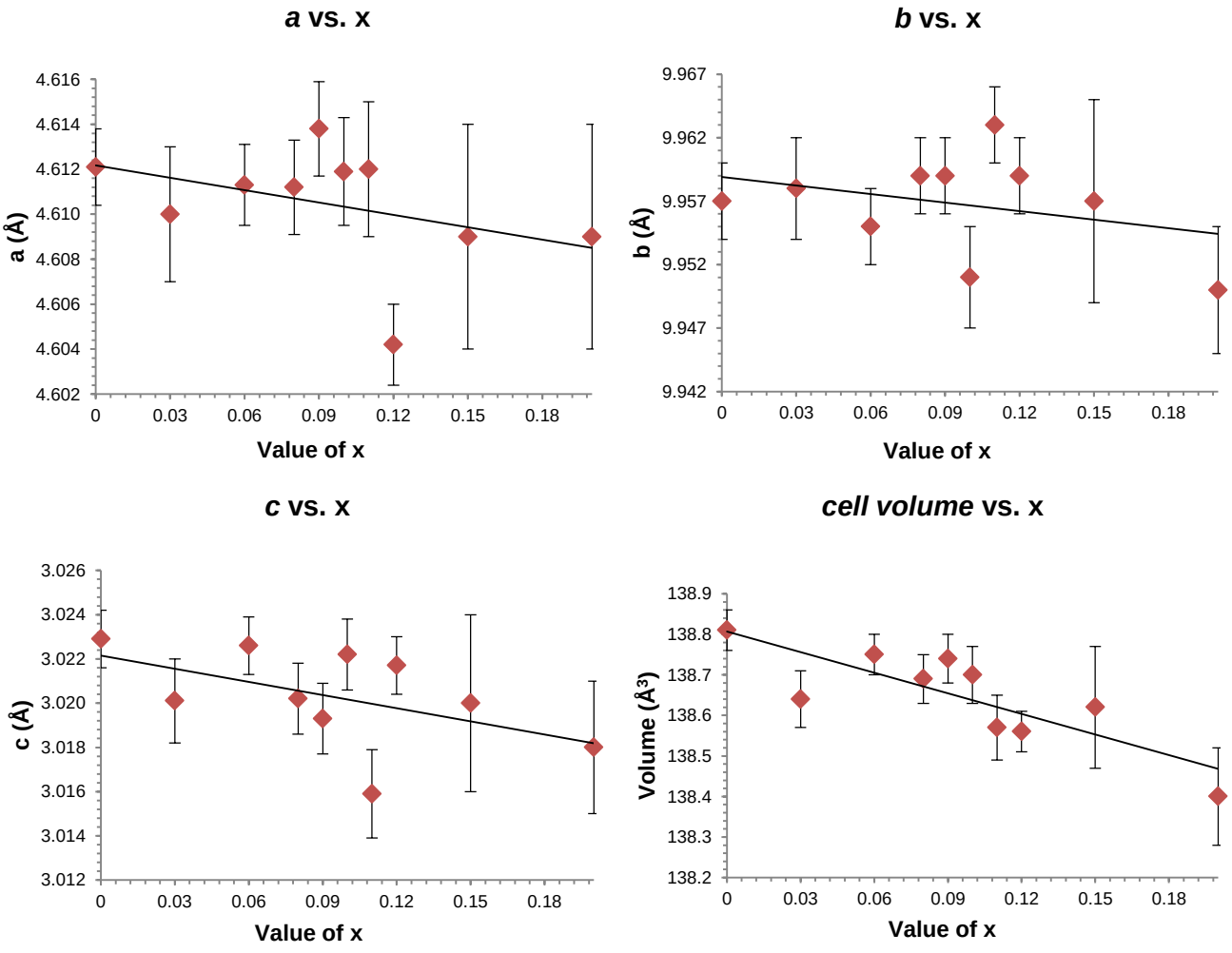

Figure 5.4: Plot of the unit cell parameters for $Fe_{1-x}Cr_xOOH$ samples vs. the target value of x.

5.3.2. Aluminium Substitution ($Fe_{1-x}Al_xOOH$)

Aluminium substituted goethite samples were prepared with up to 27% Al-for-Fe substitution. As the amount of Al incorporated into the goethite samples increased, the colour changed from the typical yellow for a well crystallised goethite, through to brick red (Figure 5.5).

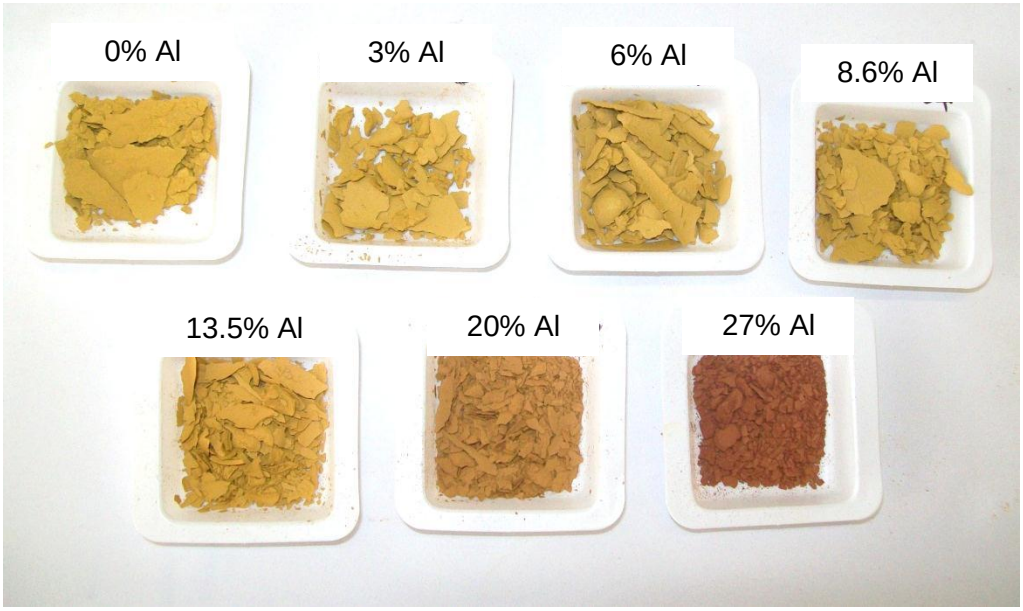

Figure 5.5: Appearance of the synthetic products in the Fe-Al goethite solid solution series. Sample labelled by target mol% Al.

The phases identified by PXRD (Figure 5.6) for the goethite samples prepared are shown in Table 5.6. From the PXRD data, goethite is the only phase which can be identified in the $Fe_{1-x}Al_xOOH$ samples with $x \geq 0.135$ (13.5 mol% Al). At higher levels of Al substitution, the PXRD pattern shows traces of hematite to be present in the samples; this is supported by the red colour which was observed in some of the powders. There is no evidence to suggest a non-goethite, Al-rich phase present in the samples.

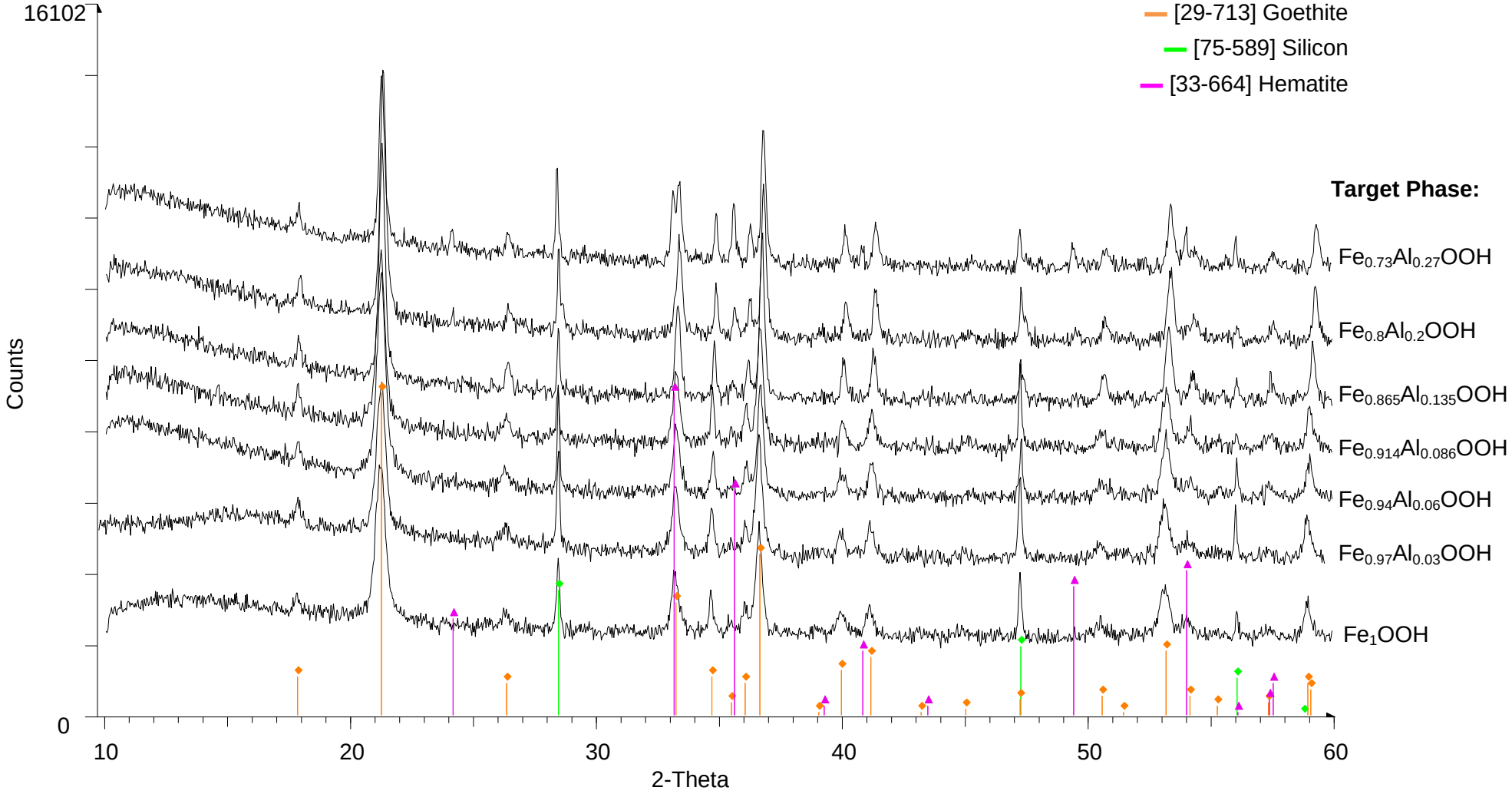

Figure 5.6: PXRD patterns collected on Al-substituted goethites, using Cu $K_{\alpha 1}$ radiation. All samples have Si added as an internal standard.

Table 5.6: Phases identified by PXRD in Al-substituted goethite samples. G=goethite, H=hematite.

Desired product: $Fe_{1-x}Al_xOOH$							
Target value of x	0	0.03	0.06	0.086	0.135	0.2	0.27
Phases identified	G	G	G	G	G	G, H	G, H

The synthesis method used to prepare the Al-goethites, taken from Schwertmann and Cornell (1991), only allowed up to a maximum of 27% Al-for-Fe substitution in goethite.[29] In order to investigate the upper limit of substitution, and to enable comparisons with research conducted by other groups, the synthesis would ideally be repeated, as it is well documented that substitution levels of greater than 27 mol% can be obtained.[7, 8] The formation of a secondary hematite phase in association with Al-goethites could have resulted from the synthesis temperature rising above 70°C.

When examining the diffraction patterns visually, a clear shift to higher 2θ value can be seen in the positions of many of the reflections with increasing Al-for-Fe substitution in the goethite structure (Figure 5.7). This suggests that the smaller Al^{3+} cation is substituting for Fe^{3+} into the goethite structure and it would be expected that the unit cell parameters would show a decrease in size as the amount of Al incorporated was increased.

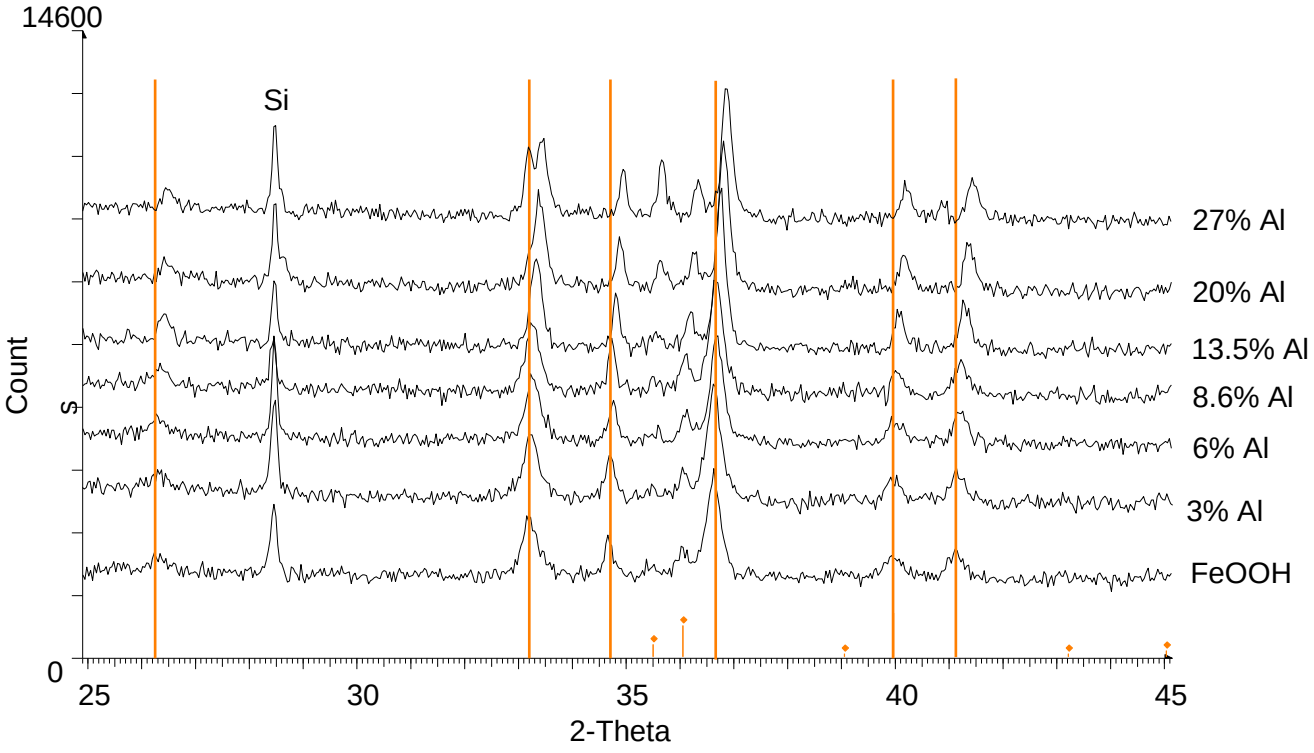

Figure 5.7: PXRD patterns of Al-goethites, $Fe_{1-x}Al_xOOH$, collected using Cu $K_{\alpha 1}$ radiation, showing the shift in peak positions as the extent of Al substitution increases. Si added as an internal standard.

The refined unit cell parameters for each Al-substituted goethite sample are presented in Table 5.7. As suggested by the observed shift in peak position (Figure 5.7), there is a clear decrease in the size of each of the unit cell parameters with increasing Al-for-Fe substitution, towards that of the isostructural aluminium equivalent of goethite – diaspore. This decrease in size of the unit cell as the Al content increases is as expected, as the ionic radius of the Al^{3+} cation is 0.545 Å, 17% smaller than that of Fe^{3+}.

Table 5.7: Unit cell parameters for Al substituted goethite samples, $Fe_{1-x}Al_xOOH$, (esds shown in parentheses).

Target Product	Identified Product	*a* (Å)	*b* (Å)	*c* (Å)	*Volume* (Å^3)
Goethite [4]		4.602 (3)	9.952 (4)	3.021 (2)	138.3 (1)
Fe_1OOH	Goethite	4.616 (3)	9.963 (5)	3.019 (2)	138.8 (1)
$Fe_{0.97}Al_{0.03}OOH$	Goethite	4.616 (2)	9.958 (3)	3.020 (2)	138.8 (1)
$Fe_{0.94}Al_{0.06}OOH$	Goethite	4.610 (4)	9.947 (8)	3.016 (3)	138.3 (1)
$Fe_{0.914}Al_{0.086}OOH$	Goethite	4.610 (2)	9.939 (3)	3.019 (1)	138.3 (1)
$Fe_{0.865}Al_{0.135}OOH$	Goethite	4.603 (2)	9.926 (3)	3.014 (1)	137.7 (1)
$Fe_{0.8}Al_{0.2}OOH$	Goethite, Hematite	4.604 (2)	9.907 (4)	3.008 (2)	137.2 (1)
$Fe_{0.73}Al_{0.27}OOH$	Goethite, Hematite	4.600 (3)	9.892 (4)	3.005 (2)	136.7 (1)
Diaspore [8]		4.403 (2)	9.4252 (5)	2.8452 (1)	118.1 (1)

When each of the unit cell parameters, *a*, *b, c* and cell volume, are plotted against the level of Al substitution in the goethite samples (Figure 5.8), the data shows strong linear correlation. Although the relationship between the amount of Al incorporated into the goethite samples and the unit cell parameters appears to be strong, the size of the unit cells deviate from what would be predicted if Vegard's Law was obeyed between the goethite and diaspore end members, see Figure 5.9. This observation has been made elsewhere, and Fey and Dixon (1981) concluded that the deviation in unit cell size away from that which was expected was caused by the highly hydrated nature of these Al-goethite samples. This results in an expansion of the unit cell, in direct contrast to the reduction in the size of the unit cell as a result of the Al-for-Fe substitution.[41]

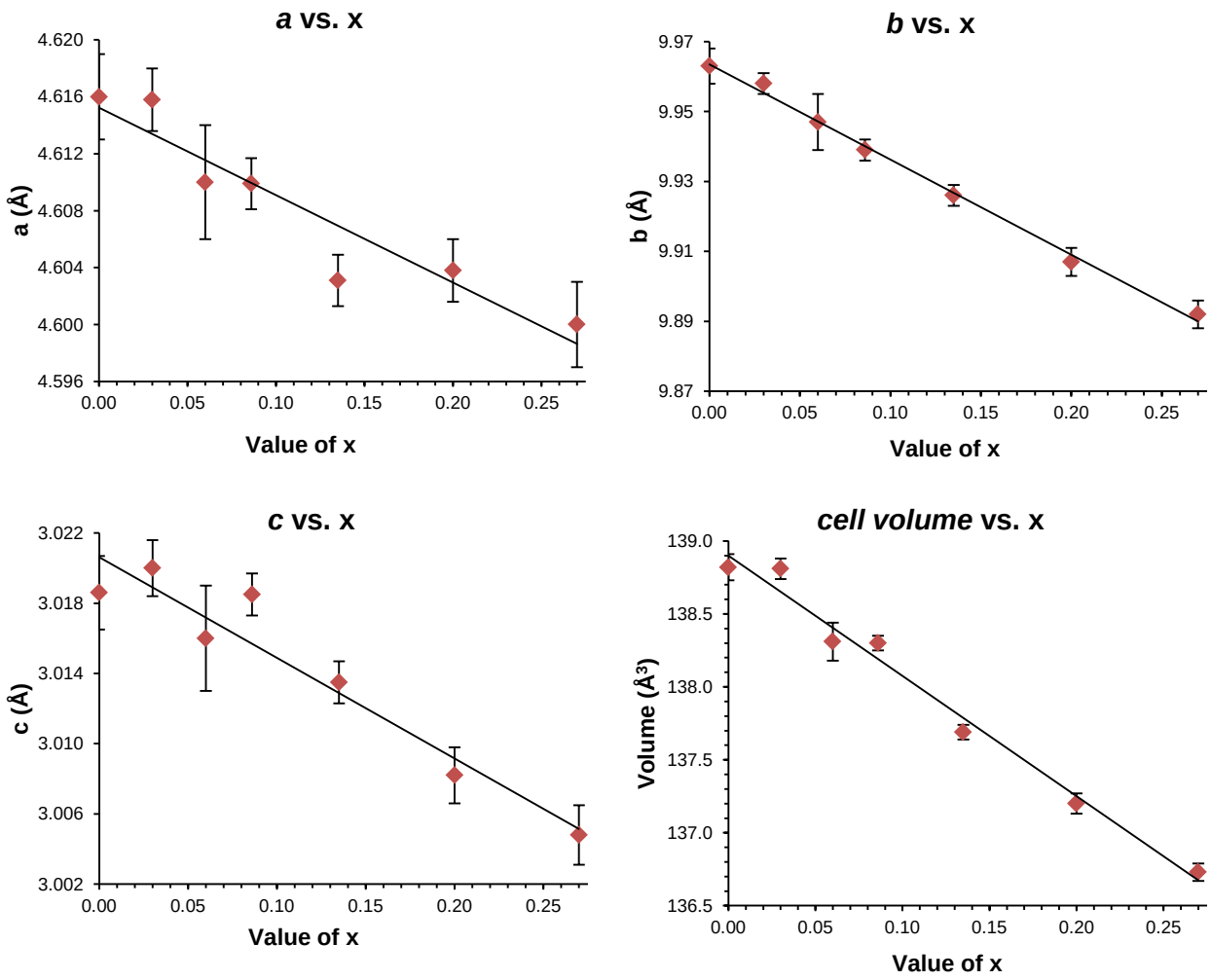

Figure 5.8: Plot of the unit cell parameters for $Fe_{1-x}Al_xOOH$ samples vs. the target value of x.

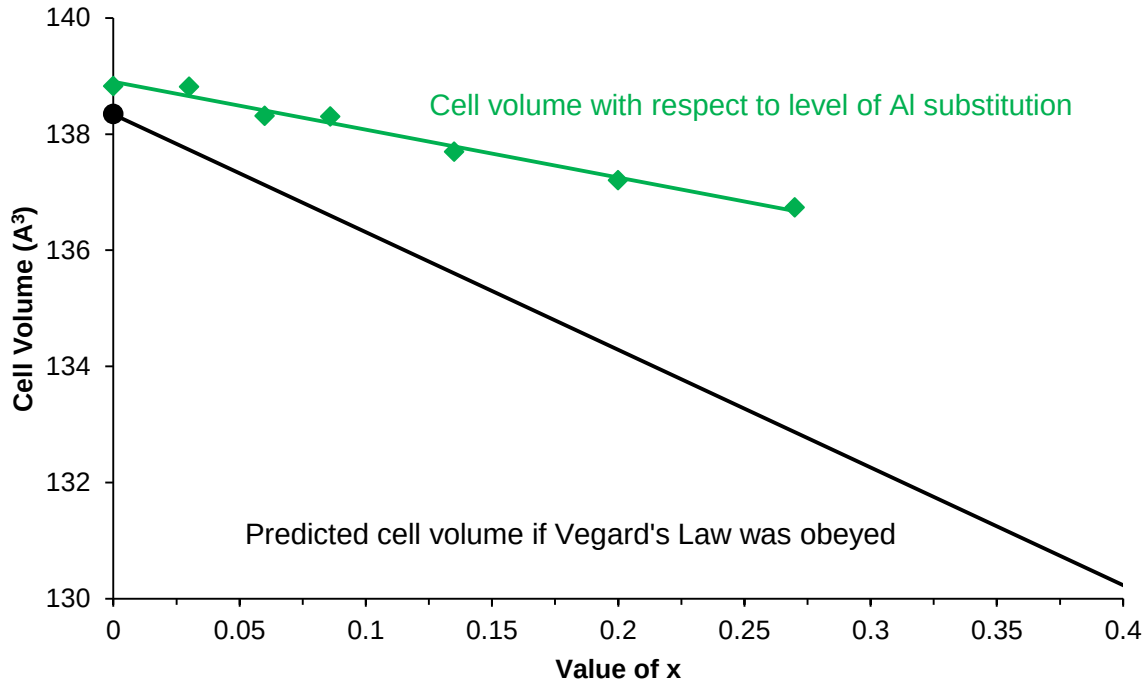

Figure 5.9: Comparison between actual cell volume and predicted cell volume for Al substituted goethites.

5.3.3. Cobalt Substitution ($Fe_{1-x}Co_xOOH$)

The cobalt substituted goethite samples were collected and analysed by PXRD. As with all of the M-substituted goethite samples that have been discussed previously, the colour of the product changes, even with small amounts of cobalt dopant as shown in Figure 5.10.

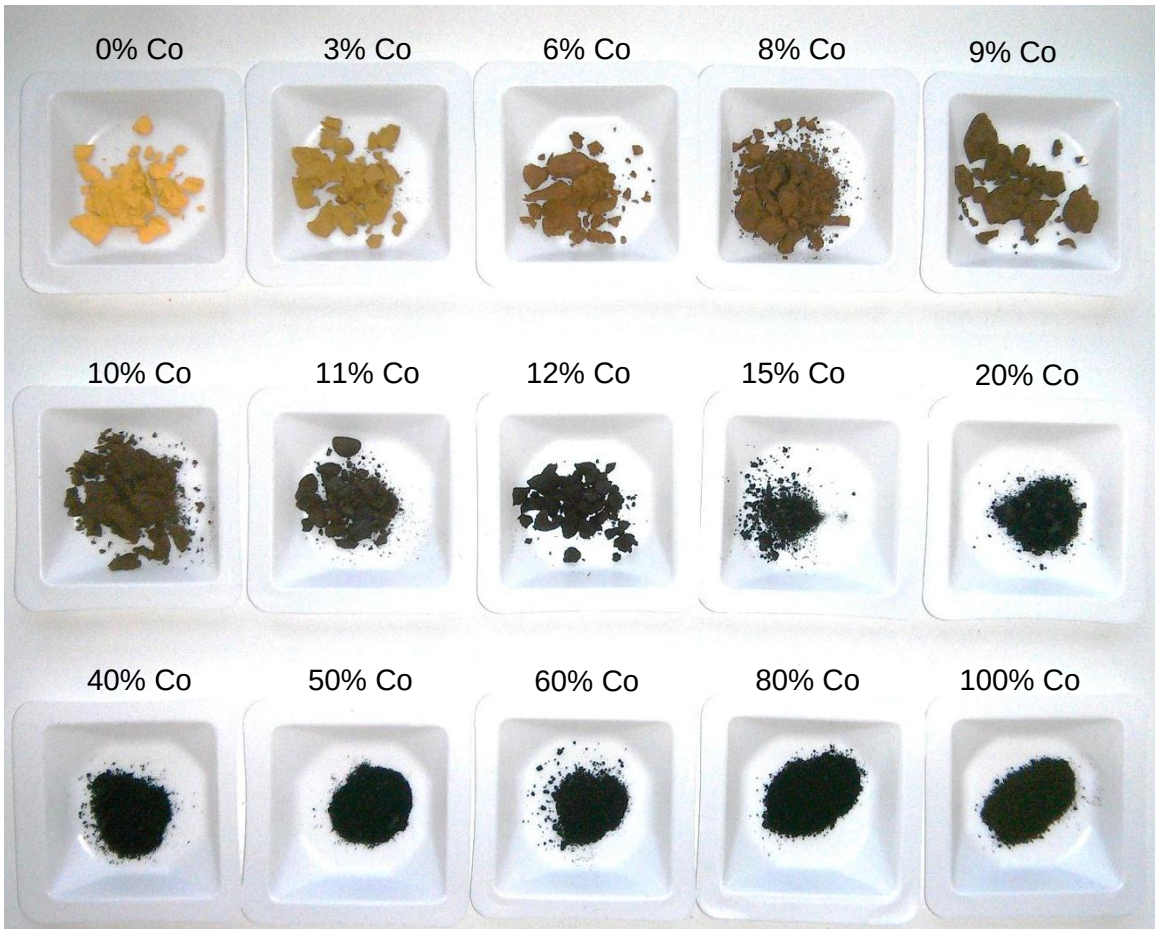

Figure 5.10: Appearance of the synthetic products in the Fe-Co goethite solid solution series. Sample labelled by target mol% Co.

The PXRD patterns collected on the Co-Fe goethite solid solution series (Figure 5.11) were used to identify the phases present, listed in Table 5.8. The only phase which could be identified with between 0-12 mol% Co was goethite, and visual observation of the peak positions in the PXRD pattern (Figure 5.12) show a gradual shift to higher 2θ position of the reflections in the pattern as the amount of Co increases.

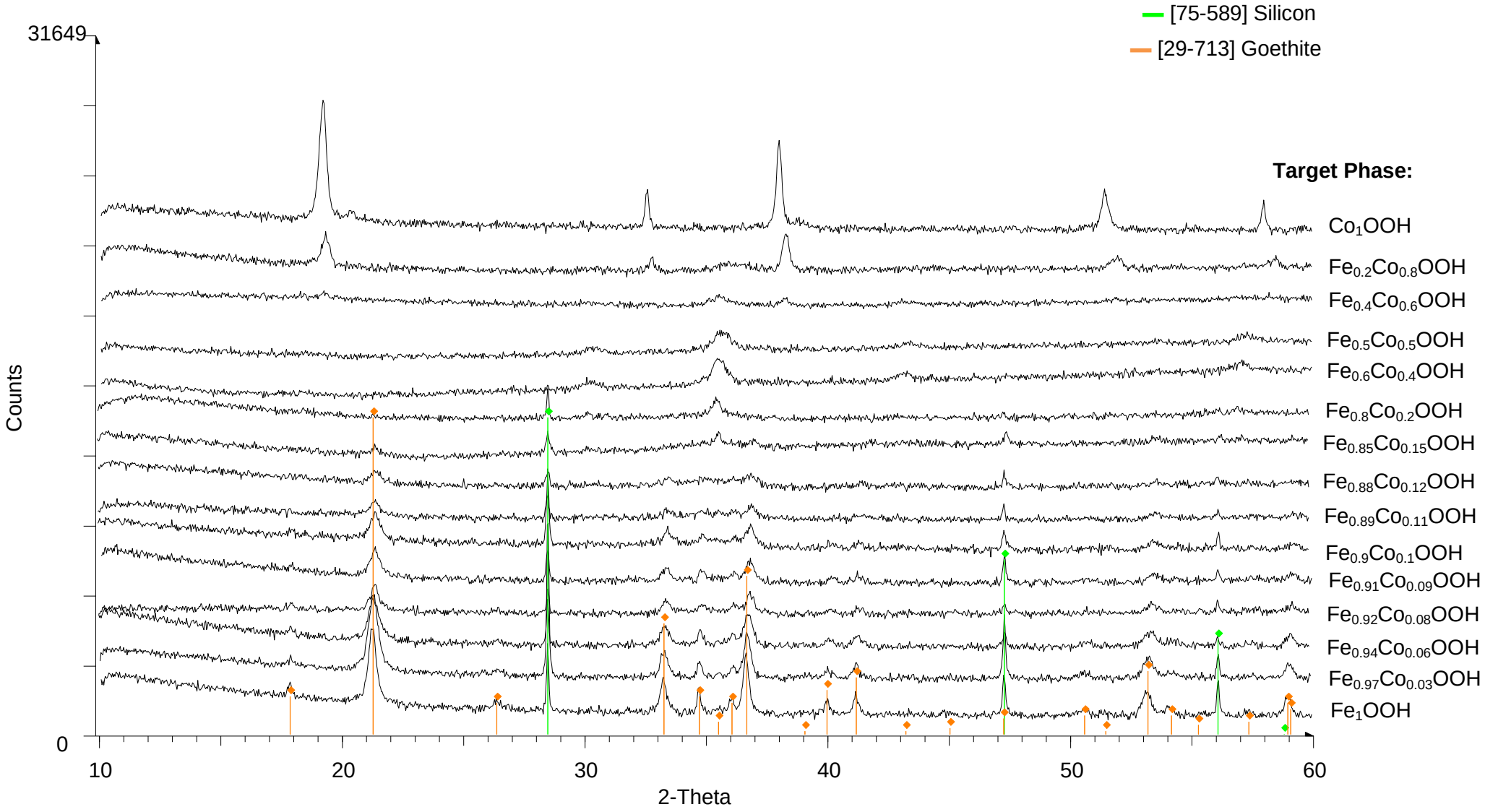

Figure 5.11: PXRD patterns collected on Co-substituted goethites, using Cu $K_{\alpha 1}$ radiation. Samples with x ≤ 0.2 have Si added as an internal standard.

Table 5.8: Phases identified by PXRD in Fe-Co goethite solid solution series. G=goethite, I=cobalt iron oxide, C=cobalt hydroxide, H=heterogenite.

Desired product: $Fe_{1-x}Co_xOOH$															
Target value of x	0	0.03	0.06	0.08	0.09	0.10	0.11	0.12	0.15	0.20	0.40	0.50	0.60	0.80	1
Phases identified	G	G	G	G	G	G	G	G	G I	I	I	I	I C	C	C H

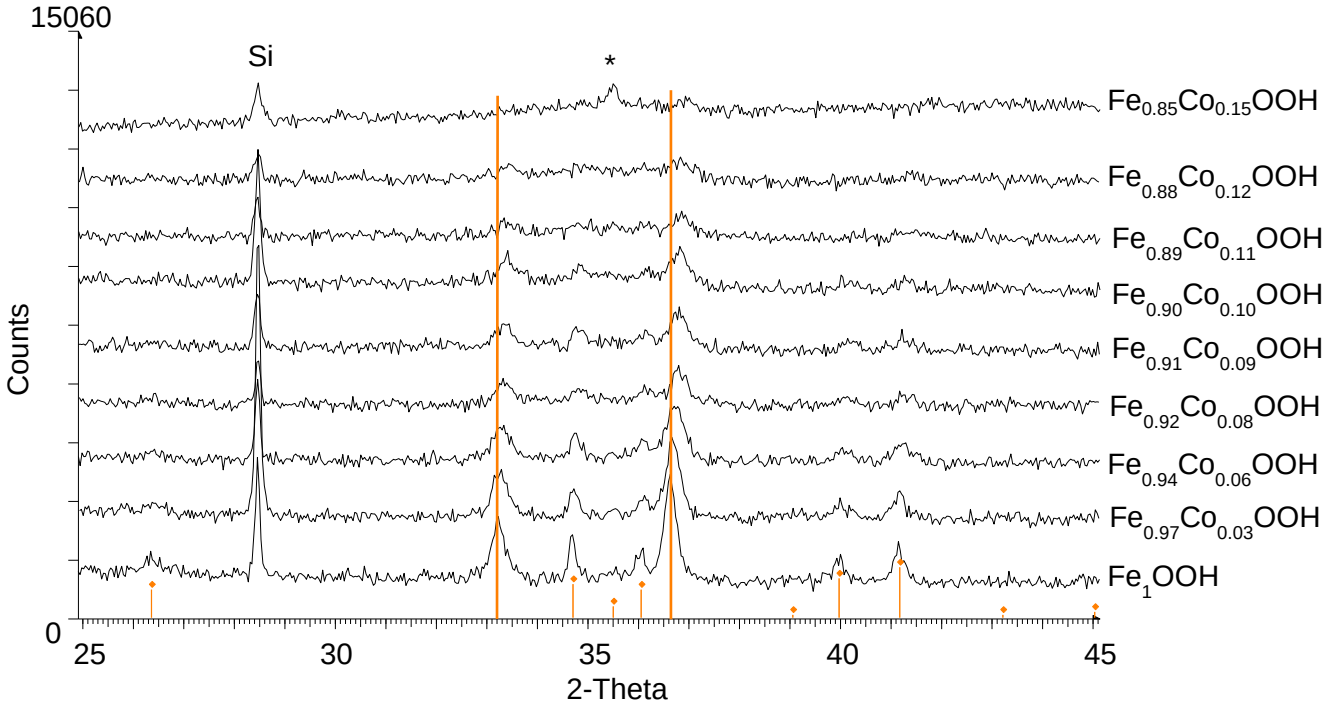

Figure 5.12: PXRD patterns of Co-goethites showing the shift in goethite peak positions as the amount of Co in the goethite sample increases. Data collected using Cu $K_{\alpha 1}$ radiation, Si added as an internal standard. * denotes $CoFe_2O_4$ reflection.

When the proportion of cobalt added to the synthesis reached 15 mol%, mixed phases of goethite and cobalt iron oxide ($CoFe_2O_4$) were identified from examination of the PXRD patterns. When the proportion of cobalt reached 20%, no trace of goethite was observed and the only phase identified was $CoFe_2O_4$.

The maximum reported level of substitution of Co-for-Fe in goethite is 10%.[16] The identification of single phase goethite (from PXRD analysis) prepared in this work with up to 12 mol% Co, could suggest that higher levels of substitution are possible. However, it is also conceivable that a separate phase is present in the 12% Co goethite sample, but

that it is either poorly crystalline (e.g. ferrihydrite) or in too small a quantity to be identified by the PXRD technique.

The diffraction patterns of the phases formed when greater than 15 mol% Co was attempted to be substituted into the goethite structure are shown in Figure 5.13. These syntheses did not produce a goethite product. Between 20-50% Co, the only crystalline phase that could be identified was cobalt iron oxide, and at 60% Co, a mixture of cobalt iron oxide ($CoFe_2O_4$) and cobalt hydroxide, $Co(OH)_2$, is observed. At 80% Co the only crystalline phase identified is cobalt hydroxide, suggesting that the 20% iron which was added to the synthesis is either incorporated into the cobalt hydroxide structure and/or present as a poorly crystalline secondary phase which has not been identified. Finally the cobalt end member synthesis produced a mixture of cobalt hydroxide and a very small amount of heterogenite, a rhombohedral polymorph of CoOOH.

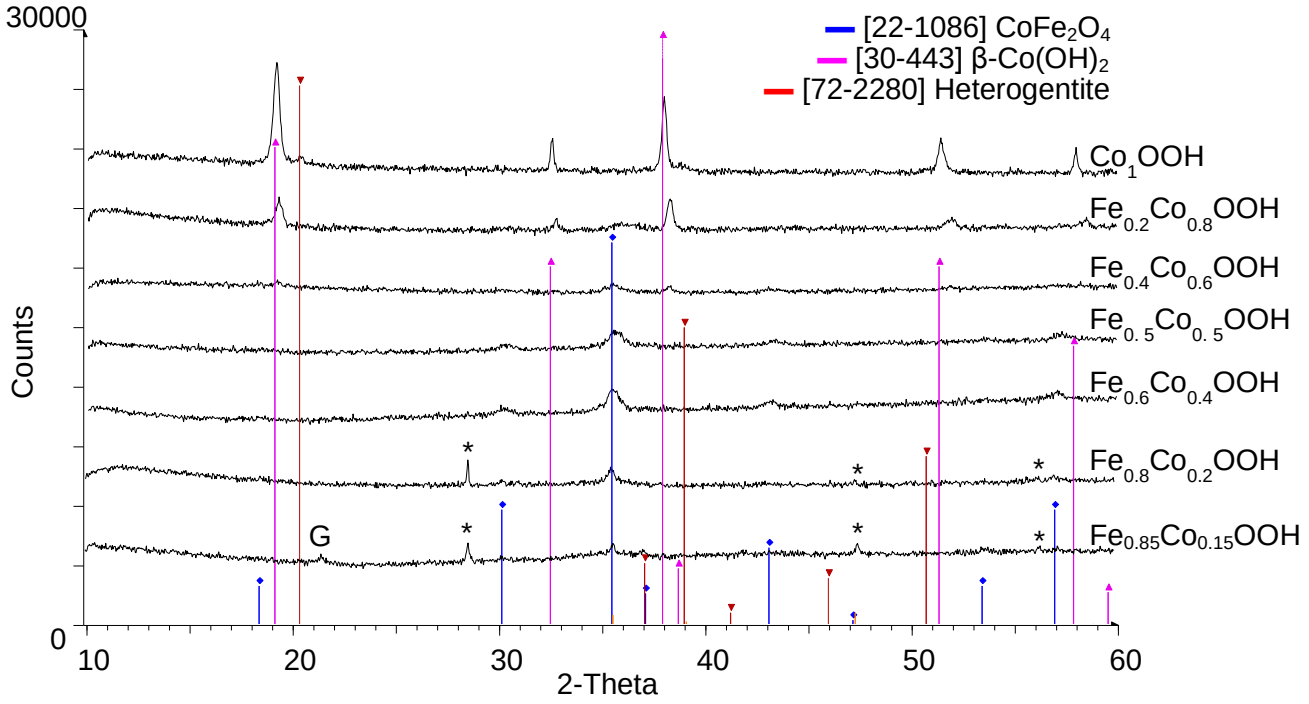

Figure 5.13: PXRD patterns of Co substituted 'goethites', ideally $Fe_{1-x}Co_xOOH$, where x= 0.15-1. Data collected using Cu $K_{\alpha 1}$ radiation, Si added as an internal standard in 15 and 20 mol% Co samples (denoted by *). Goethite reflection present in 15 mol% Co sample (G).

Using the PXRD data, the unit cell parameters were refined for the Co-substituted goethite phases with up to 12 mol% Co, and these are shown in Table 5.9.

Table 5.9: Unit cell parameters for Co substituted goethites, (esd's shown in parentheses).

Target Product	Identified Product	*a* (Å)	*b* (Å)	*c* (Å)	*Volume* (Å^3)
Goethite [4]		4.602 (3)	9.952 (4)	3.021 (2)	138.3 (1)
Fe_1OOH	Goethite	4.613 (3)	9.958 (4)	3.020 (2)	138.7 (1)
$Fe_{0.97}Co_{0.03}OOH$	Goethite	4.610 (3)	9.948 (4)	3.021 (2)	138.5 (1)
$Fe_{0.94}Co_{0.06}OOH$	Goethite	4.597 (4)	9.951 (4)	3.020 (2)	138.1 (1)
$Fe_{0.92}Co_{0.08}OOH$	Goethite	4.605 (4)	9.946 (3)	3.008 (3)	137.8 (1)
$Fe_{0.91}Co_{0.09}OOH$	Goethite	4.596 (5)	9.935 (11)	3.017 (5)	137.7 (2)
$Fe_{0.9}Co_{0.1}OOH$	Goethite	4.595 (7)	9.932 (8)	3.013 (4)	137.5 (2)
$Fe_{0.89}Co_{0.11}OOH$	Goethite	4.579 (11)	9.931 (19)	3.012 (6)	137.0 (3)
$Fe_{0.88}Co_{0.12}OOH$	Goethite	4.566 (9)	9.932 (11)	3.013 (5)	136.6 (3)
CoOOH [25]		4.353	9.402	2.840	116.2

The starting material used in the synthesis of the Co-substituted goethites was Co^{2+}, which has an ionic radius of 0.75 Å, much larger than that of Fe^{3+} (0.645 Å).[6] If the divalent Co cation was substituting into the goethite structure an increase in the size of the unit cell would, therefore, be expected. However, the clear and systematic decrease which is observed in the size of the unit cell parameters of the Co-substituted goethite samples (shown in Figure 5.14) indicates that although the starting material was Co^{2+}, cobalt is incorporated into the goethite structure in the trivalent form, Co^{3+}, as this cation has an ionic radius of 0.545 Å, smaller than that of Fe^{3+} (0.645 Å). The results obtained in this work with respect to the unit cell changes arising from Co incorporation into goethite agree with the findings of earlier authors, e.g. Gasser *et al.* (1996) and Alvarez *et al.* (2008).[16, 55] Chemically it is also a lot more likely that cobalt would enter the structure as the trivalent cation. Co^{2+} is easily oxidised to Co^{3+}, which is a d^6 ion, and in the low spin state has a full t_2g orbital, making it very stable. Co^{2+} is a d^7 ion, and has a preference for forming tetrahedral complexes as the crystal field stabilisation energy is large.

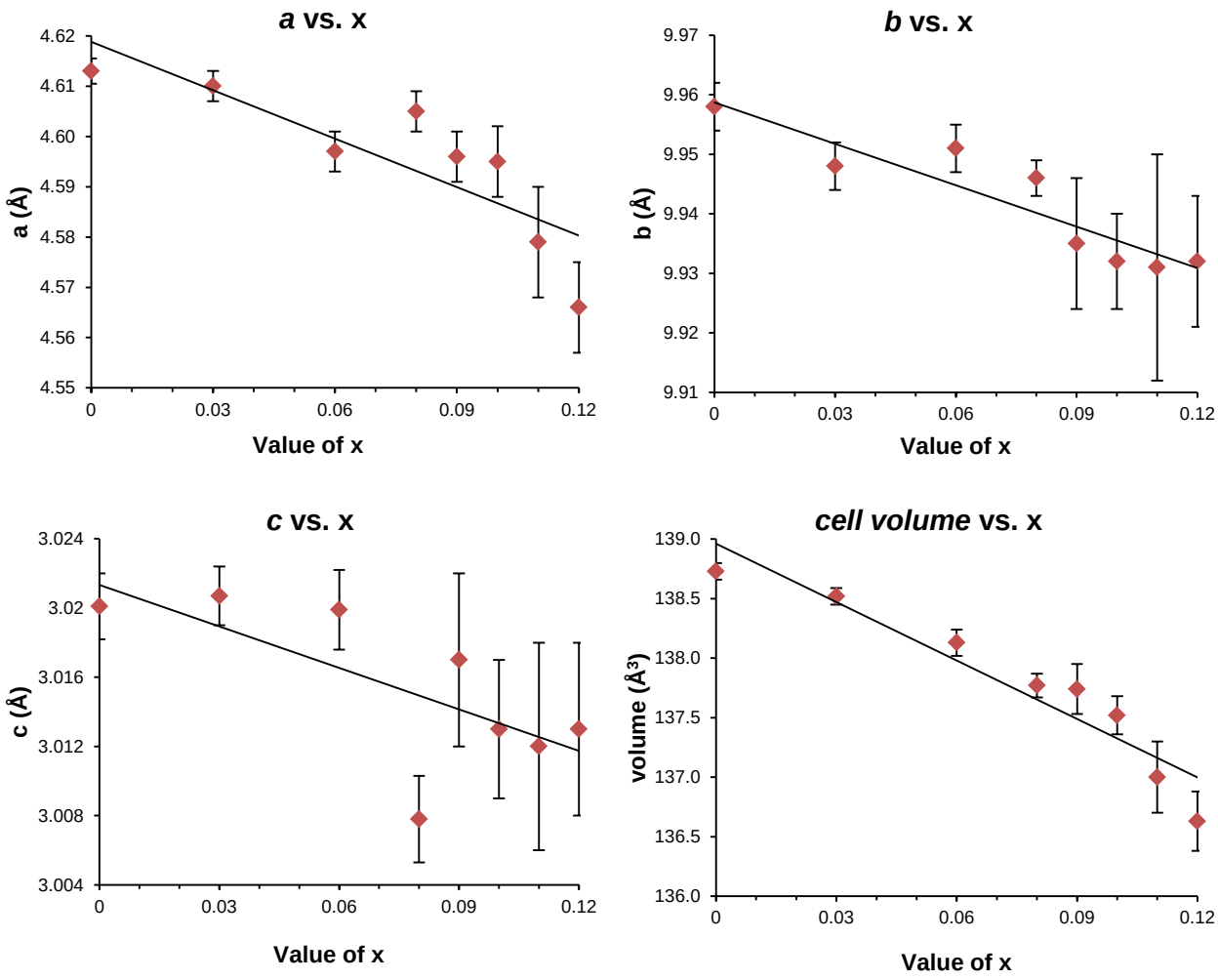

Figure 5.14: Plot of the unit cell parameters for $Fe_{1-x}Co_xOOH$ samples vs. the target value of x.

As the proportion of Co in the goethite samples increases, the errors and scatter on the data also increase. Although with up to 12 mol% Co substitution the only phase identified is goethite, the diffraction patterns, Figure 5.12, do appear to show that the samples become less crystalline with the addition of increasing amounts of cobalt, highlighted by the broader, less intense peaks that are observed. A result of these changes in the diffraction patterns is that refinement of the unit cell parameters for the samples become more complex, due to the precise position of the reflections being difficult to identify when the peaks are broad, and the fact that some reflections are not observed at all. A consequence of these factors is that the errors in the refinement of the unit cell parameters increase.

5.3.4. Manganese Substitution ($Fe_{1-x}Mn_xOOH$)

Manganese substituted goethites were prepared as described in Chapter 2 and from observation of the colours of the samples alone (shown in Figure 5.15) it is clear that even the addition of small amounts of dopant have a significant impact on the resulting product. The un-substituted goethite sample was an ochre/yellow colour, changing through beige and brown as the Mn content was increased.

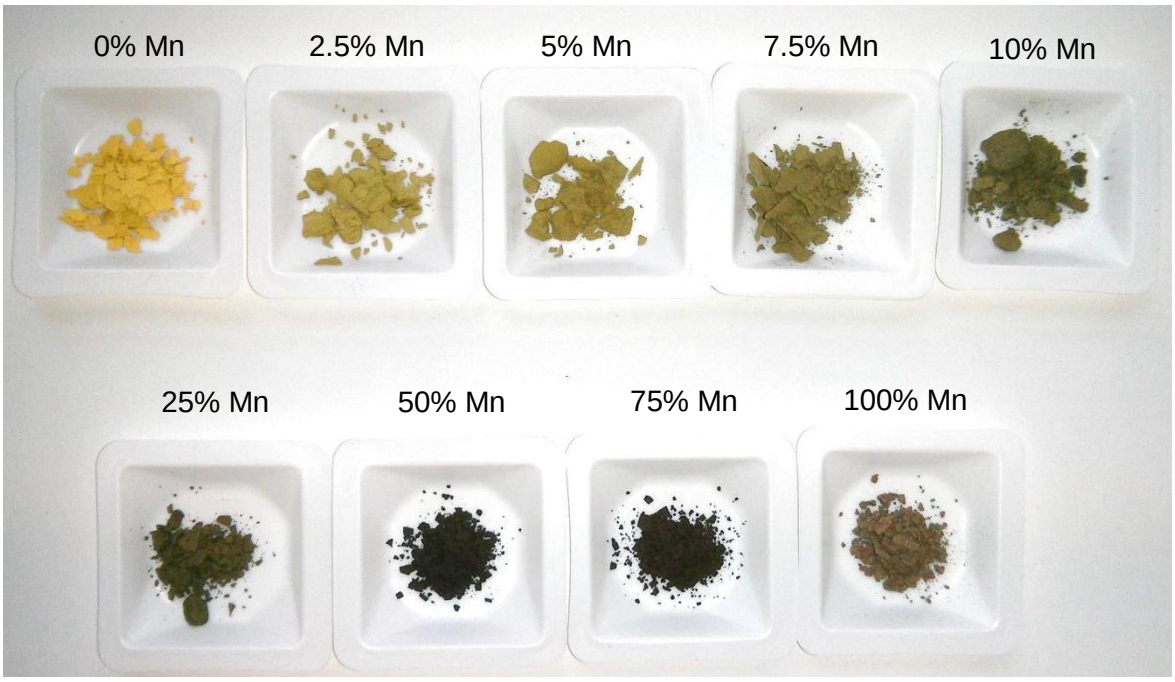

Figure 5.15: Appearance of the synthetic products in the Fe-Mn goethite solid solution series. Sample labelled by target mol% Mn.

The solid samples that were produced were analysed using PXRD (Figure 5.16) to identify the phases that were present in the solid solution series and these are listed in Table 5.10. In preparations with up to 10 mol% Mn, goethite was the only crystalline phase that could be identified. As the proportion of manganese in the synthesis was increased to 25%, a mixture of jacobsite ($MnFe_2O_4$) and goethite was identified. At 75% Mn, hausmannite (Mn_3O_4) was identified alongside jacobsite, and the end member manganese phase was identified as hausmannite. The end member Mn sample also contained potassium manganese oxide hydrate, an impurity phase resulting from the KOH used in the synthesis procedure.

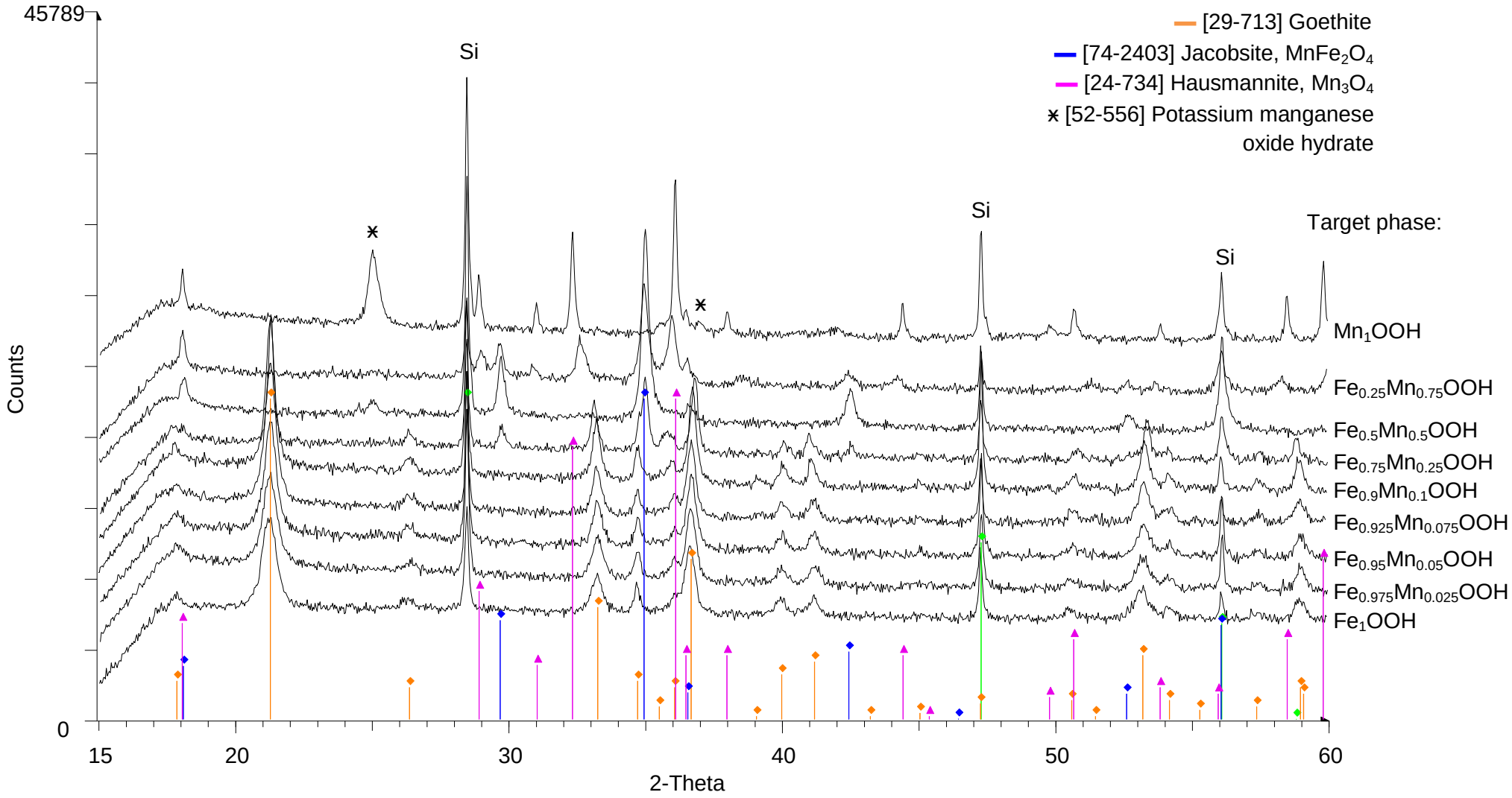

Figure 5.16: PXRD patterns collected on Mn-substituted goethites, using Cu $K_{\alpha 1}$ radiation. Samples have Si added as an internal standard.

Table 5.10: Phases identified by PXRD in Fe-Mn goethite solid solution series. G=goethite, J=jacobsite ($MnFe_2O_4$), H=hausmannite (Mn_3O_4), K=potassium manganese oxide hydrate.

Desired product: $Fe_{1-x}Mn_xOOH$									
Target value of x	0	0.025	0.05	0.075	0.1	0.25	0.5	0.75	1
Phases identified	G	G	G	G	G	G, J	J	J, H	H, K

The maximum reported Mn-for-Fe substitution in goethite is 15%.[2, 14, 45] With the large Mn increments used in this study, it is difficult to accurately confirm the extent of Mn substitution into the goethite structure that may have been achieved. The identification of single phase goethite at 10% Mn, and mixed phase goethite at 25% Mn, suggests that the limit would be somewhere between these two values, which is in agreement with the previously reported substitution levels. Visual observation of the PXRD patterns for the Mn-substituted goethites with 0-10 mol% Mn substitution showed no evidence of shifts in the peak positions, as was observed in the case of Al and Co substituted goethite phases.

Using the PXRD data (Figure 5.16), the unit cell parameters of each phase were refined and are shown in Table 5.11. For the goethite-type phases, with increasing incorporation of Mn into the goethite structure, the unit cell parameters *a* and *c* decrease, whilst there is an increase in the *b* parameter (shown in Figure 5.17).

For the samples that were a mixture of phases, the reflections belonging to each phase were selected and refined based on each structure type individually. For the samples with a Mn content of 25-75 mol%, the peaks were refined based on the jacobsite unit cell. As the proportion of Mn increased, the unit cell parameters also increased, approaching those reported for jacobsite.[56] The 100% Mn sample was refined based on the structure of hausmannite and the unit cell parameters are in good agreement with those reported (Table 5.11).[57]

Table 5.11: Unit cell parameters for Mn substituted goethites, $Fe_{1-x}Mn_xOOH$, as well as other Mn/Fe oxide phases formed in the syntheses (esd's shown in parentheses).

Target Product	Phases Identified	*a* (Å)	*b* (Å)	*c* (Å)	*Cell volume* (Å^3)
Goethite [4]		4.602 (3)	9.952 (4)	3.021 (2)	138.3 (1)
Fe_1OOH	Goethite	4.613 (4)	9.953 (5)	3.025 (3)	138.9 (1)
$Fe_{0.975}Mn_{0.025}OOH$	Goethite	4.607 (2)	9.958 (4)	3.024 (2)	138.7 (1)
$Fe_{0.95}Mn_{0.05}OOH$	Goethite	4.606 (3)	9.958 (4)	3.019 (2)	138.4 (1)
$Fe_{0.925}Mn_{0.075}OOH$	Goethite	4.602 (2)	9.961 (3)	3.020 (1)	138.5 (1)
$Fe_{0.90}Mn_{0.10}OOH$	Goethite	4.599 (2)	9.984 (4)	3.014 (1)	138.4 (1)
$Fe_{0.75}Mn_{0.25}OOH$	Goethite	4.586 (2)	10.019 (4)	3.007 (2)	138.2 (1)
Jacobsite, $MnFe_2O_4$ [56]		8.511			616.5 (1)
$Fe_{0.75}Mn_{0.25}OOH$	Jacobsite	8.491 (5)			612.2 (1)
$Fe_{0.50}Mn_{0.50}OOH$	Jacobsite	8.501 (1)			614.3 (2)
$Fe_{0.25}Mn_{0.75}OOH$	Jacobsite	8.510 (2)			616.2 (2)
Hausmannite, Mn_3O_4 [57]		5.762		9.470	314.4
$Fe_{0.25}Mn_{0.75}OOH$	Hausmannite	5.785 (2)		9.363 (1)	313.4 (4)
Mn_1OOH	Hausmannite	5.763 (1)		9.466 (1)	314.4 (1)

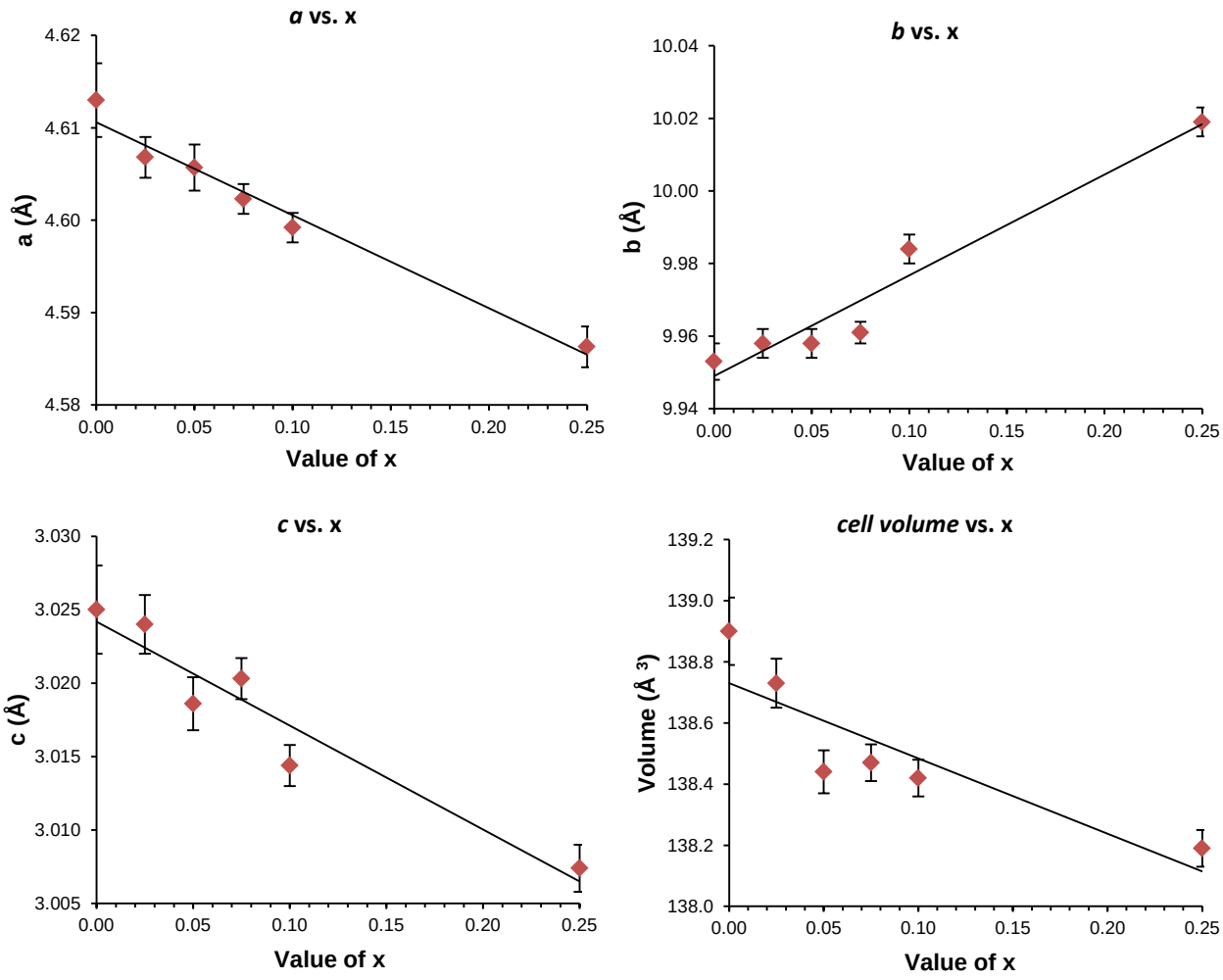

Figure 5.17: Plot of the unit cell parameters for $Fe_{1-x}Mn_xOOH$ samples vs. the target value of x.

Since Mn^{3+} has an ionic radius of 0.645 Å, the same as that of Fe^{3+}, as well as the fact that an isostructural manganese equivalent of goethite exists (groutite, α-MnOOH), it may be expected that a complete solid solution between the Fe and Mn end members could exist. However, from the results obtained here, and previous published work, this is not the case.[13] The incomplete solid solution is thought to result from the Jahn Teller effect. Although Mn^{3+} and Fe^{3+} have the same ionic radii, the electronic configuration of Mn^{3+}, a d^4 ion, results in manganese having a tetragonally distorted coordination sphere, meaning it cannot fit as easily into the goethite structure as Fe^{3+} does. This distortion is reflected in the size of the unit cell parameters, with the *b* parameter increasing whilst the *a* and *c* parameters decrease, highlighted in Figure 5.17.

A pictorial representation of the effect this distortion has on the bond lengths in the goethite structure is shown in Figure 5.18. In the undistorted goethite structure, Figure 5.18a, the Fe-O1 bond lengths are 1.96 and 1.95 Å, and the Fe-O2 bond lengths are 2.09 Å. As Mn^{3+} is Jahn-Teller active when occupying an octahedral site, there will be an increase in the size of the axial Mn-O bonds. In the goethite structure, to accommodate this distortion and therefore allow the incorporation, there must be a shift in the O1 and O2 atom positions. A representation of this shift is shown in Figure 5.18b; here the axial Fe-O1 and Fe-O2 bond lengths increase (from 1.95 and 2.09 Å, to 2.11 and 2.25 Å respectively) which results in a decrease of the equatorial Fe-O1 and Fe-O2 bond lengths (from 1.96 and 2.09 Å, to 1.91 and 2.02 Å respectively). This lengthening of the axial and shortening of the equatorial bonds is responsible for the increase in size observed for the *b* parameter of the unit cell and the decrease in *a* and *c.*

a) Undistorted goethite structure

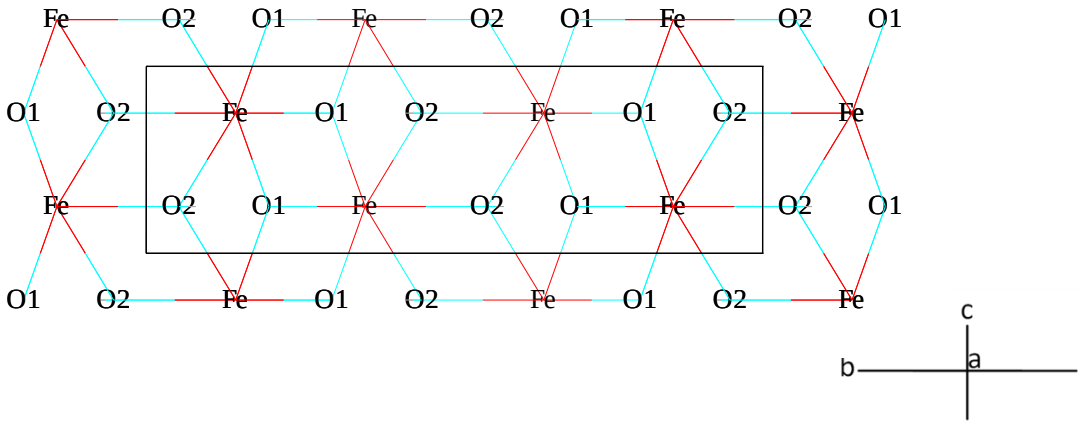

b) Structural distortions within the goethite structure as a result of Mn incoorporation

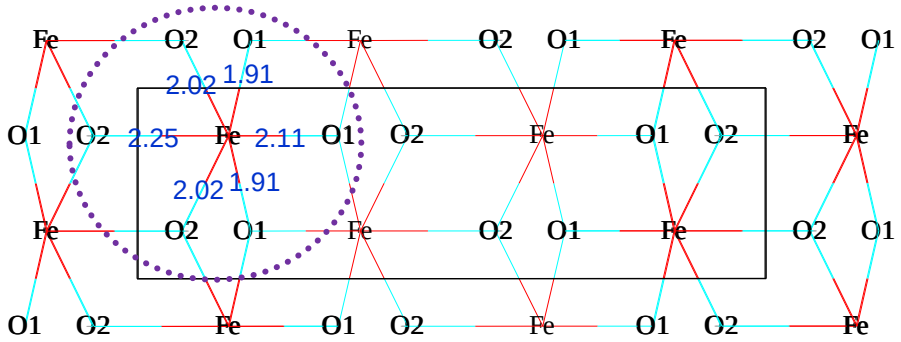

Figure 5.18: The effect of Mn substitution on the crystal structure of goethite.

The unit cell changes for goethite that were observed with increasing manganese substitution suggest that manganese is entering the goethite structure as Mn^{3+}. This conclusion is supported by the findings of previous work which showed that regardless of the oxidation state of the starting Mn material (2+ or 4+), the majority of the manganese ends up as Mn^{3+}, allowing a level of isomorphous substitution of Fe by Mn in goethite.[45]

5.3.5. Nickel Substitution ($Fe_{1-x}Ni_xOOH$)

The main focus of this work was to understand the association between Ni and goethite. An improved understanding of the residence of Ni in goethite rich systems, for example establishing if Ni is totally incorporated into the goethite structure, or if some/all remains associated with a separate phase, is vital in order to better understand the behaviour of Ni in laterite systems. Ni substituted goethites were prepared from both the Fe(II) and Fe(III) synthesis methods described in Chapter 2. Furthermore, the effect of temperature on the formation of Ni-substituted goethites prepared via each method was also investigated. Large incremental substitutions were made in all of the synthesis methods (where x_{Ni} = 0, 0.2, 0.4, 0.5, 0.6, 0.8 and 1) to investigate the phases that form across the whole range of Ni addition levels and then smaller ranges, where x_{Ni} = 0-0.1, were synthesised for the Fe(II) at room temperature and Fe(III) at 70°C methods in order to look specifically at nickel substitution into, and association with, goethite.

From examining the appearance of the full range (x=0-1) of solids prepared via the Fe(III) synthesis method at 70°C, the colour changes from yellow/ochre for the un-substituted goethite, through to a darker brown as the Ni content increases, and then finally a bright green for the Ni-rich end member, see Figure 5.19.

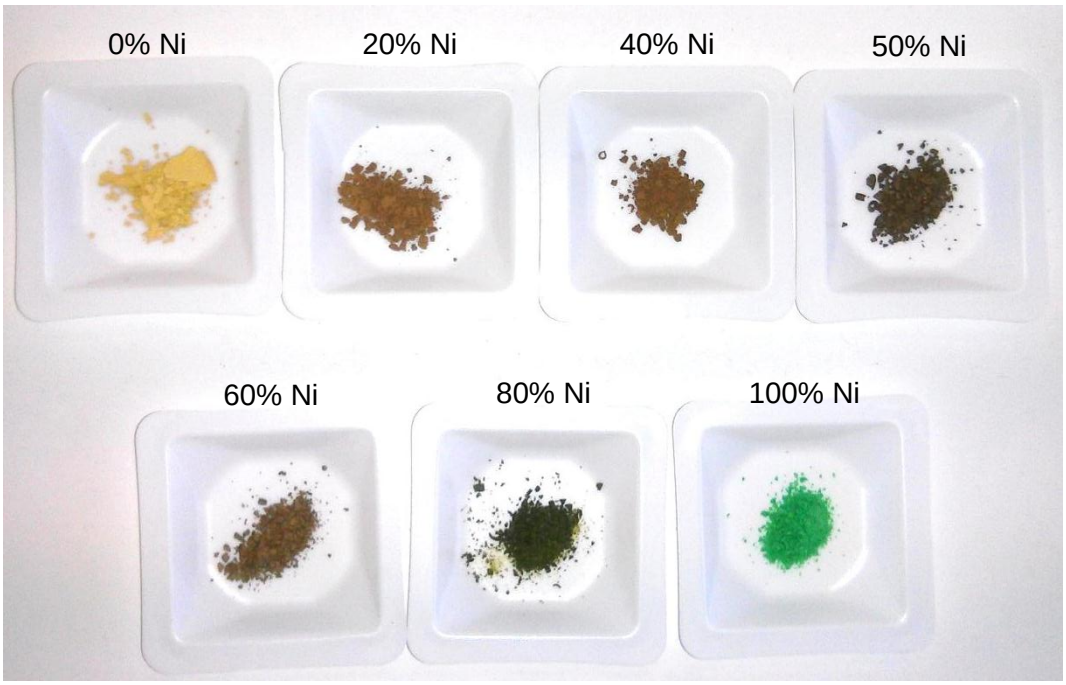

Figure 5.19: Appearance of the synthetic products in the Fe-Ni goethite solid solution series, prepared from Fe(III) at 70°C. Samples labelled by target mol% Ni.

PXRD data were collected for all of the nickel substituted goethite samples prepared via the different synthesis methods and the phases identified are presented in Table 5.12 (0-100 mol% Ni) and Table 5.13 (0-10 mol% Ni).

Table 5.12: Phases identified by PXRD in the Ni substituted goethites, desired product $Fe_{1-x}Ni_xOOH$, where x = 0-1. G=goethite, J=jamborite, F=siderite ($Fe(CO)_3$), M=magnetite, O=iron hydroxide ($Fe(OH)_3$), C=iron nickel carbonate hydroxide hydrate, T=theophrastite, A=amorphous.

Synthesis Method		Target value of x: (desired product $Fe_{1-x}Ni_xOOH$)							Figure
		0	0.2	0.4	0.5	0.6	0.8	1	
Fe^{3+} method	20°C	G	G	G	G, J	G, J	J, T	T	Figure 5.23
	70°C	G	G	G, J	G, J	G, J	J, T	T	Figure 5.24
Fe^{2+} method	20°C	G, F	G,J	G, J	J	J	J	A	Figure 5.20
	70°C	G, F, M	G, M, O	G, M, O, J, C	J, G, M	J, G	J	T	Figure 5.23

Table 5.13: Phases identified by PXRD in the Ni substituted goethites, desired product $Fe_{1-x}Ni_xOOH$, where x = 0-0.1. G=goethite, L=lepidocrocite, F=siderite ($Fe(CO)_3$), M=magnetite.

Synthesis Method	Target value of x: (desired product $Fe_{1-x}Ni_xOOH$)									Figure
	0	0.01	0.02	0.03	0.04	0.05	0.06	0.08	0.1	
Fe^{3+} method 70°C	G	G	G	G	G	G	G	G	G	Figure 5.25
Fe^{2+} method 20°C	G, F, L	G	G, L	G, M	G, L	G, L	G		G	Figure 5.22

Examining the PXRD patterns for the full series (0-100 mol% Ni) of samples synthesised from an Fe(II) precursor at 20°C, Figure 5.20, the Fe-goethite end member is identified as goethite, with traces of siderite ($Fe(CO)_3$) present. The identification of siderite in the sample possibly results from the presence of dissolved carbonate in the water used for the synthesis. The samples containing 20-40 mol% Ni have been identified as a mixture of goethite and jamborite, and between 50-80 mol% Ni, jamborite was the only phase identified. The reflections attributed to the presence of jamborite are shifted from their expected positions – thought to be a consequence of iron incorporation in the jamborite structure. No crystalline phases could be identified in the pure nickel end member.

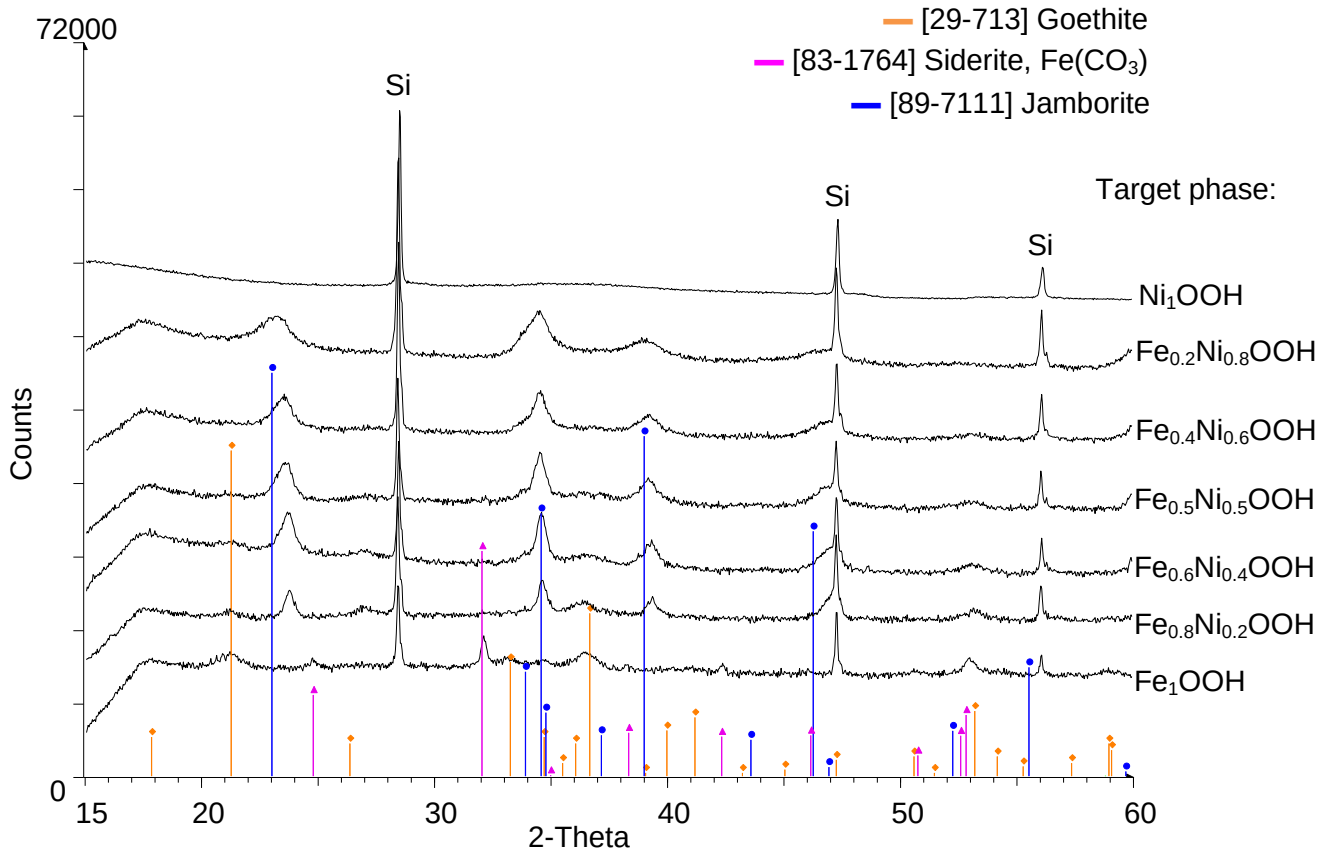

Figure 5.20: PXRD patterns collected on Ni-substituted goethite samples with 0-100 mol% Ni, prepared from an Fe(II) precursor at 20°C. Data collected using Cu $K_{\alpha 1}$ radiation, Si added as an internal standard.

Examination of the PXRD patterns for the 0-10 mol% Ni substituted goethites prepared from Fe(II) at 20°C (Figure 5.21), identifies the presence of goethite at all substitution levels. In addition to goethite, siderite was identified in the Fe end member phase and magnetite was identified in the 3% Ni sample. Lepidocrocite was identified in the 0, 2, 4 and 5 mol% Ni samples.

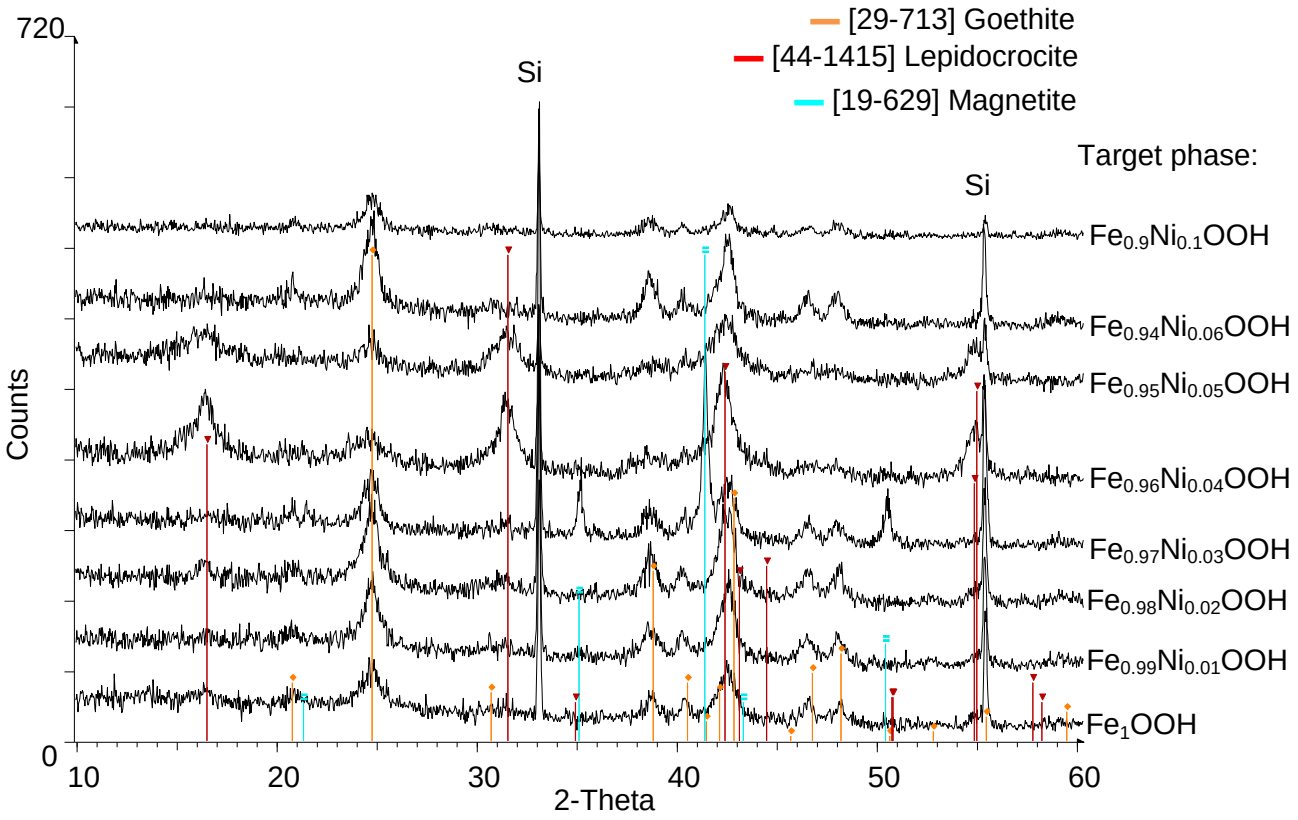

Figure 5.21: PXRD patterns collected on Ni-substituted goethite samples with 0-10 mol% Ni, prepared from an Fe(II) precursor at 20°C. Data collected with Co $K_{\alpha 1}$ radiation, Si added as an internal standard.

The effect of raising the synthesis temperature to 70°C on the phases formed in the full (0-100% Ni) range of products formed via the Fe(II) method was investigated, and characterisation of the products by PXRD (Figure 5.22) showed that these samples contained many more impurity phases than those made at 20°C. As was found in the products from the 20°C synthesis (Figure 5.20) goethite was identified in all samples containing up to and including 60% Ni. However, in the samples containing 0, 20 and 40% Ni, the impurity phases magnetite, siderite and lepidocrocite were also present. Jamborite was identified in the samples from the synthesis that contained 40-80% Ni, and the only phase that was identified in the 100% Ni sample was a very poorly crystalline theophrastite.

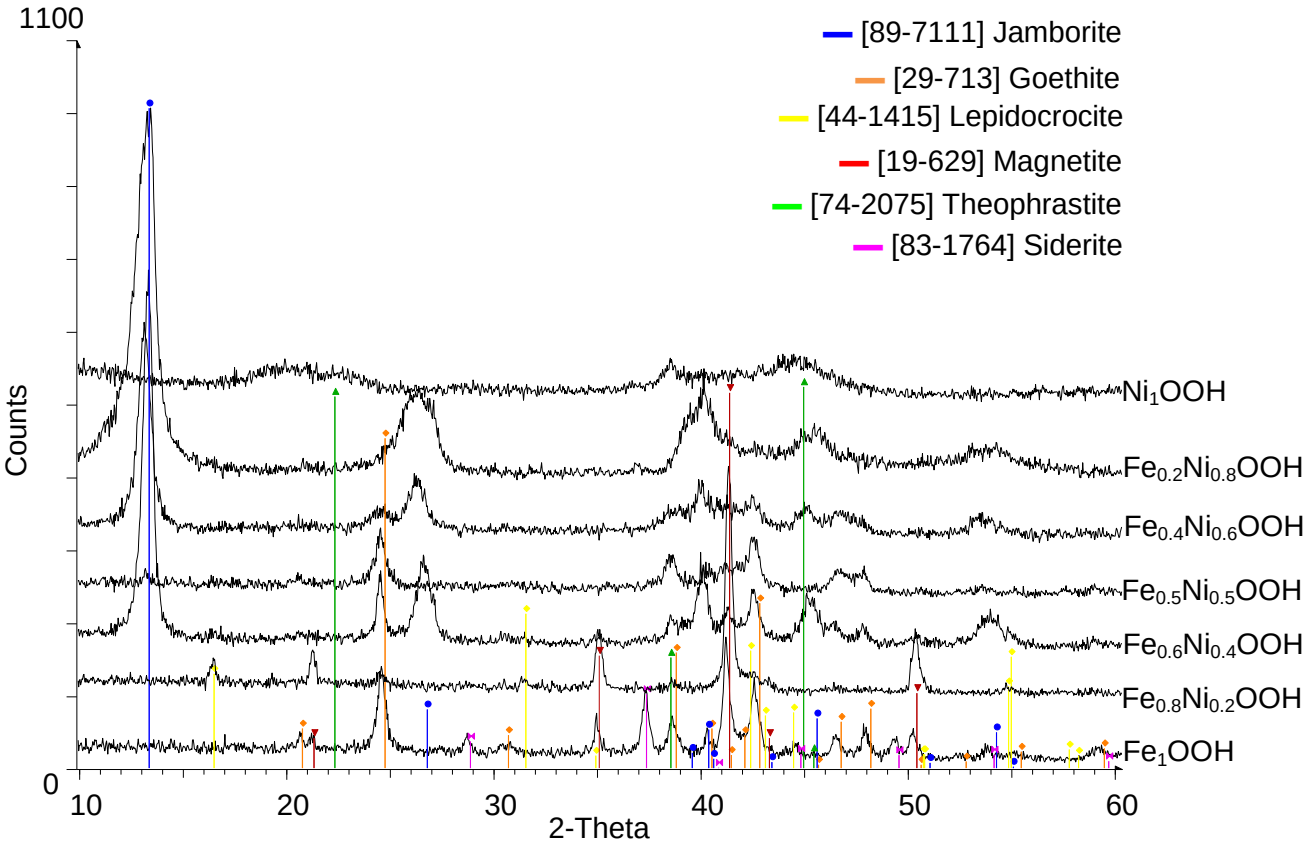

Figure 5.22: PXRD patterns for collected for nickel substituted goethites prepared from Fe(II) at 70°C, data collected using Co $K_{\alpha 1}$ radiation.

The PXRD patterns collected for the Ni-goethites prepared via the Fe(III) precursor method contain far fewer impurity phases than those identified in the Fe(II) synthesis Ni-goethite samples. The Fe(III) synthesis method was carried out at 20°C to ascertain if this resulted in any differences in the phases formed when compared to the standard 70°C synthesis temperature. In the samples resulting from the 20°C synthesis (Figure 5.23) goethite was the only phase which could be identified in samples up to and including 40 mol% Ni. Upon addition of 50 and 60% Ni to the synthesis, both goethite and jamborite were identified in the products, and at 80% Ni the phases identified were jamborite and theophrastite. The 100% nickel sample was identified as being theophrastite.

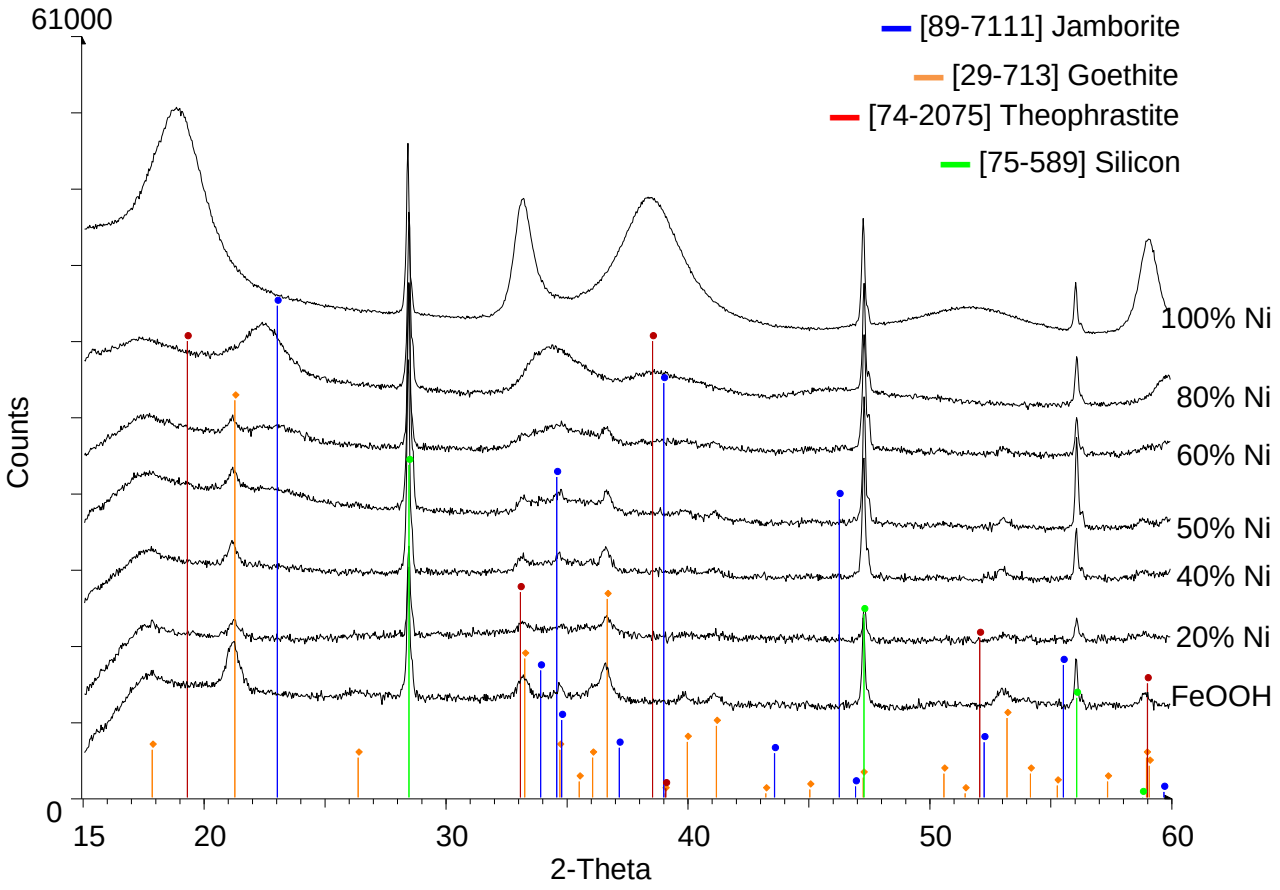

Figure 5.23: PXRD patterns recorded for nickel substituted goethites, ideally $Fe_{1-x}Ni_xOOH$, prepared from Fe(III) at 20°C, data collected using Cu $K_{\alpha 1}$ radiation with Si added as an internal standard.

The phases identified in the products of the 20°C Fe(III) synthesis procedure are very similar to those obtained via the 70°C synthesis, shown in Figure 5.24. The only difference that was observed was the identification of jamborite at lower levels of Ni addition in the 70°C synthesis, being present at 40 mol% Ni rather than at 50% Ni in the 20°C synthesis. This could be down to individual sample variation and data collection, or alternatively the increased temperature could have favoured the formation of jamborite. It can be noted again here that the jamborite peaks are slightly shifted from their expected positions, which again is probably due to different amounts of iron being incorporated in the jamborite structure.

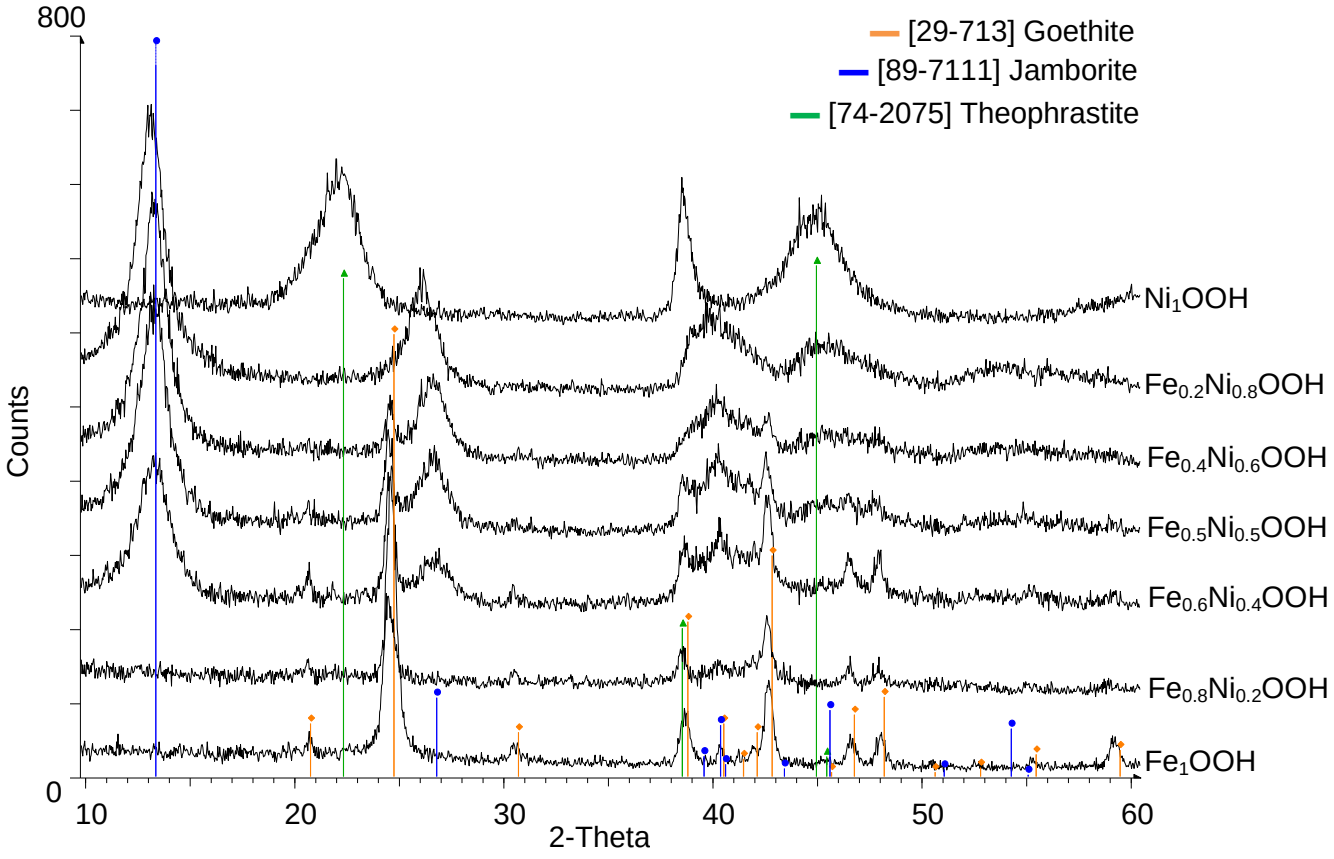

Figure 5.24: PXRD patterns collected for nickel substituted goethites, ideally $Fe_{1-x}Ni_xOOH$, prepared from Fe(III) at 70°C, data collected using Co $K_{\alpha1}$ radiation.

A set of samples with smaller increments of Ni addition (0-10 mol%) were also synthesised at 70°C and the PXRD patterns are shown in Figure 5.25. Goethite is the only crystalline phase identified in the samples at all Ni dopant levels and no shifts in the peak positions with increasing nickel content are observed.

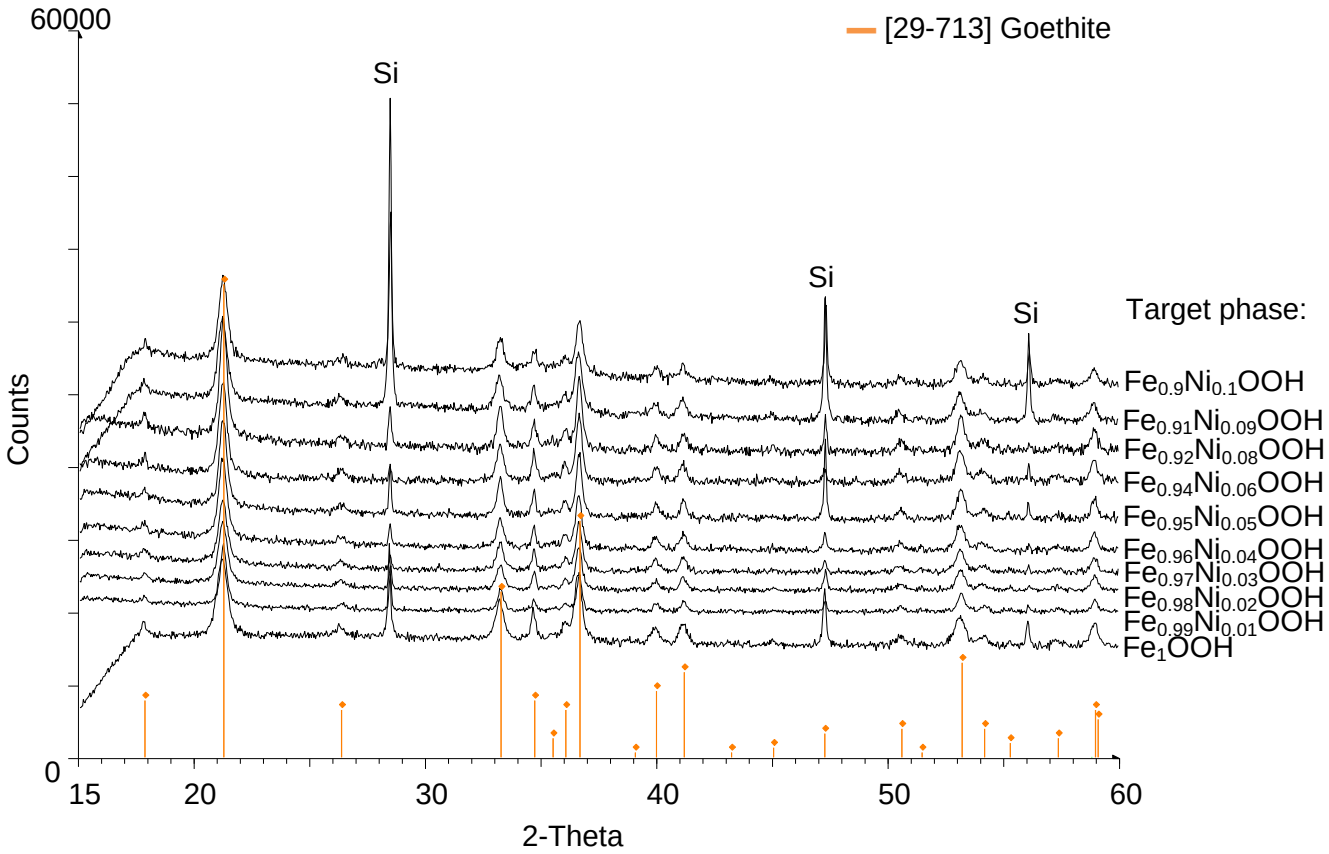

Figure 5.25: PXRD patterns collected for nickel substituted goethites, ideally $Fe_{1-x}Ni_xOOH$, where x=0-0.1, prepared from an Fe(III) precursor at 70°C, data collected using Cu $K_{\alpha 1}$ radiation. Si added as an internal standard.

The maximum reported substitution level of Ni in synthetic goethites is 5.5 mol%, with the presence of separate phases appearing at greater substitution levels.[2] It is therefore highly unlikely that a minimum of 20 mol% Ni (indicated by the 70°C synthesis, Figure 5.24) or 40 mol% Ni (20°C synthesis, Figure 5.23) has been substituted into the goethite structure, despite the fact that no other crystalline phases were observed in the PXRD patterns of these samples. It is believed that the excess Ni is residing in a poorly crystalline secondary phase (e.g. ferrihydrite), not identified by the PXRD technique.

In the set of Ni substituted goethite samples prepared by Krehula *et al.* (2005) a gradual broadening of the PXRD reflections with increasing Ni substitution was observed.[4] The FWHM (full width at half maximum) was measured for each reflection in PXRD patterns of

the series of nickel substituted goethite samples synthesised from Fe(III) at 70°C (Figure 5.25), but no systematic broadening was observed in the data for the samples prepared in this study.

From analysis of the phases formed via the synthesis pathways that were investigated here, differences do seem to be occurring in the way in which nickel incorporates into/associates with goethite, depending on the synthesis method used. In all cases goethite was formed initially (at lower levels of Ni addition), however, the point at which a separate nickel phase (jamborite) was identified was found to vary between 20-50% nickel added, depending on the synthesis route used. For example, in the Fe(III) method at room temperature, a jamborite-type phase is not detected until addition of 50 mol% Ni, however, it is unlikely that half of the iron has actually been replace by nickel in the goethite structure. It is probable that there is a separate phase present (e.g. ferrihydrite) which is accommodating the nickel, which is either amorphous or not detected under the PXRD conditions used.

Goethite was identified as a phase in the synthesised samples with the addition of up to 60 mol% Ni, however, it was not always the dominant phase at the higher levels of Ni addition, with jamborite also being identified. At 80% Ni substitution, the samples all contained jamborite, and those synthesised via the Fe(III) method also contained theophrastite. The pure nickel end member samples were identified as theophrastite, except for that formed via the Fe(II) synthesis pathway at 20°C, where the resulting Ni end member was amorphous to PXRD.

The unit cell parameters were refined for each of the nickel substituted goethite samples prepared via the Fe(III) synthesis method at 70°C (Figure 5.25), and these are shown in Table 5.14. There was no observable shift in the position of the reflections in the PXRD patterns as was observed for the goethite samples with incorporated Al or Co. The ionic radius of the Ni^{2+} cation is 0.690 Å, slightly larger than that of Fe^{3+} (0.645 Å), and the largest of all of the dopants investigated in this research. A plot of unit cell parameter vs. substitution level is presented in Figure 5.26, however, there appears to be very little correlation between the *a, b* and *c* unit cell parameters and the extent of substitution (particularly when the size of the error on each point is taken into account). A general trend of increasing cell volume with increasing Ni is observed, from 138.3 $Å^3$ for the unsubstituted goethite, to 139.2 $Å^3$ for the goethite prepared with 20% Ni.

Table 5.14: Unit cell parameters for Ni substituted goethites prepared from Fe(III) at 70°C, (esds shown in parentheses).

Desired Composition	Identified Product	*a* (Å)	*b* (Å)	*c* (Å)	*Volume* (Å^3)
Goethite [4]		4.602 (3)	9.952 (4)	3.021 (2)	138.3 (1)
Fe_1OOH	Goethite	4.609 (3)	9.955 (3)	3.025 (2)	138.8 (1)
$Fe_{0.99}Ni_{0.01}OOH$	Goethite	4.609 (2)	9.957 (4)	3.023 (2)	138.7 (1)
$Fe_{0.98}Ni_{0.02}OOH$	Goethite	4.621 (2)	9.963 (2)	3.021 (1)	139.1 (1)
$Fe_{0.97}Ni_{0.03}OOH$	Goethite	4.613 (2)	9.957 (2)	3.023 (1)	138.9 (1)
$Fe_{0.96}Ni_{0.04}OOH$	Goethite	4.620 (3)	9.964 (4)	3.022 (2)	139.1 (1)
$Fe_{0.95}Ni_{0.05}OOH$	Goethite	4.611 (2)	9.959 (4)	3.023 (2)	138.8 (1)
$Fe_{0.945}Ni_{0.055}OOH$	Goethite	4.615 (1)	9.967 (2)	3.023 (1)	139.1 (1)
$Fe_{0.94}Ni_{0.06}OOH$	Goethite	4.614 (3)	9.959 (4)	3.022 (2)	138.9 (1)
$Fe_{0.92}Ni_{0.08}OOH$	Goethite	4.614 (2)	9.959 (3)	3.024 (1)	139.0 (1)
$Fe_{0.90}Ni_{0.10}OOH$	Goethite	4.620 (2)	9.964 (3)	3.025 (2)	139.3 (1)
$Fe_{0.85}Ni_{0.15}OOH$	Goethite	4.615 (4)	9.965 (6)	3.026 (3)	139.2 (1)
$Fe_{0.80}Ni_{0.20}OOH$	Goethite	4.620 (4)	9.963 (6)	3.024 (2)	139.2 (1)

Wells *et al.* (2006) studied Ni substituted goethite and reported that there was no difference in the *a* and *c* parameters of goethite with increasing nickel incorporation but they did find that the *b* parameter increased in the samples containing up to 5 mol% nickel; an observation consistent with the incorporation of a slightly larger cation.[10] Manceau *et al.* (2000) and Carvalho de Silva *et al.* (2003) also observed an increase in the *b* parameter with substitution of up to 6 mol% Ni.[1, 5] With the quality of the data used to carry out the lattice parameter refinements in this work, it is difficult to conclude if systematic changes in the size of the unit cell are occurring in the Ni substituted goethites. It could be concluded that the size of the *b* parameter is increasing with the addition of Ni in the samples prepared here, however the absolute changes in the sizes of the unit cell parameters are extremely small (e.g. the *b* parameter changes by just 0.011 Å across the range) and the estimated errors are quite large.

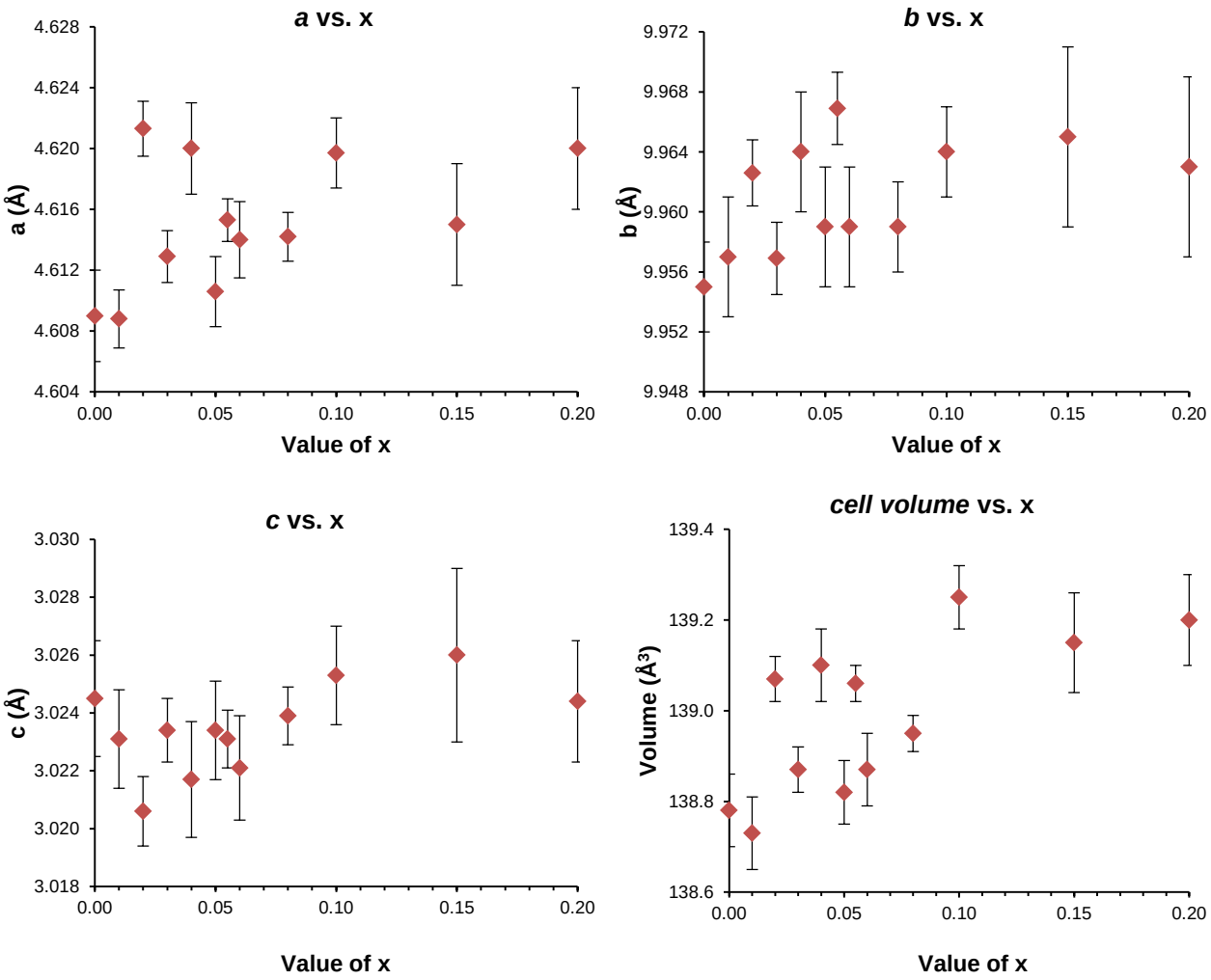

Figure 5.26: Plot of the unit cell parameter vs. target value of x for Ni substituted goethites.

The synthetic work discussed in this section appears to show far higher levels of Ni incorporation into goethite than have been previously reported. The preliminary characterisation work has failed to identify the presence of any other phases in the samples which could be hosting the excess nickel that cannot be incorporated into the goethite structure. It is believed that ferrihydrite is present in the samples alongside goethite, and that the additional Ni that cannot be accommodated in the goethite structure is associated with the ferrihydrite phase.

This chapter will now focus on a more in depth investigation into the association between nickel, goethite and ferrihydrite, using the methods developed in Chapter 3 to try to identify co-formed ferrihydrite when goethite is prepared. Furthermore, a number of techniques will be utilised in order to try to establish how much Ni is incorporated into the goethite structure, and how much (if any) is associated with a ferrihydrite phase.

5.4. The Use of the EDTA Washing Solution to Remove Co-Formed Ferrihydrite from Ni Goethite Samples

5.4.1. Introduction

In Chapter 4 the development and subsequent use of an EDTA washing solution was discussed and the technique was shown to successfully remove ferrihydrite when in a mixture of phases with goethite, whilst leaving the goethite itself intact. In section 5.3.5., initial characterisation work into Ni substituted goethites was presented, with apparently single phase goethite observed (from PXRD) with far higher levels of Ni incorporation than have been reported elsewhere. This observation, together with the knowledge that Ni stabilises ferrihydrite, preventing its transformation to goethite, indicates that untransformed ferrihydrite probably remains in the samples and is hosting the excess nickel.

In order to progress this work and ascertain the precise nature of the nickel association with goethite, the efficiency of the EDTA washing technique needed to be tested on Ni containing goethites to ensure that only the Ni contained in the ferrihydrite phase was removed and that the Ni incorporated into the goethite structure was not leached out. The successful use of the EDTA wash on the Ni-rich goethite samples would allow the way in which nickel is distributed across the two phases to be evaluated.

Ni goethites with the target formula $Fe_{0.91}Ni_{0.09}OOH$ (referred to in this work as “9% Ni goethite”) were synthesised at 20°C and 70°C and were then washed in 0.1M EDTA solution for 10 days. The addition of 9 mol% nickel was chosen as this is a higher amount of nickel than that which should be incorporated into the structure of goethite,[2] so the excess nickel should stabilise the ferrihydrite phase (which will then be removed using the EDTA). After the washing period, both the solid and the resulting EDTA solution were collected and retained. A portion of the EDTA washed goethite solid was then taken and the washing procedure repeated to observe if any more Fe/Ni was removed. Again both the solid “twice-washed” goethite and the EDTA washing solution were retained.

5.4.2. Results and Discussion

Figure 5.27 shows the appearance of the washing solutions; the filtrates from the once washed 9% Ni goethite samples are strongly coloured (more so in the case of the 20°C synthesis goethite), suggesting a large amount of Fe/Ni has been removed via the washing process. The twice-washed filtrates appeared colourless, indicating that no visually detectable Fe/Ni was removed from the goethite samples during the repeated washing.

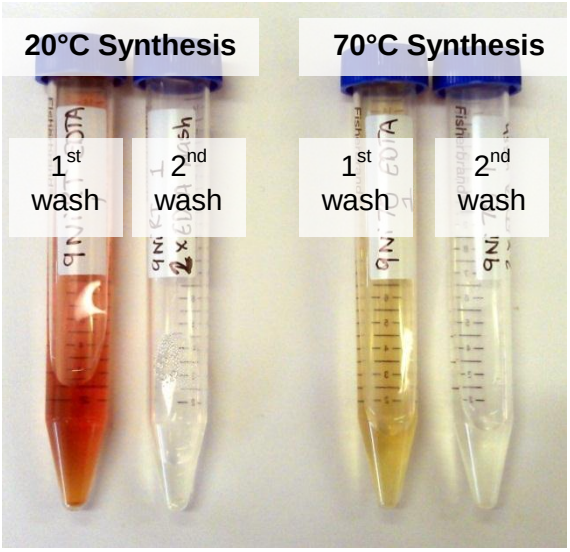

Figure 5.27: Comparison of EDTA washing solutions for 20°C and 70°C goethites after an initial and repeated wash.

ICP-OES analysis of the composition of the EDTA washing solutions (Table 5.15) showed that the initial EDTA wash removed both nickel and iron from the goethite samples, indicating that at least some of the nickel resides in the secondary ferrihydrite phase (and is therefore not all incorporated into the goethite structure). Analysing the results more closely, for the Ni goethite prepared at 20°C, over 20 wt% of the sample has been removed by the EDTA washing technique, 17 wt% from Fe and 3.7 wt% from Ni. The sample synthesised at 70°C loses less Fe in the EDTA wash, but slightly more Ni than that prepared at the lower temperature. These results follow those that would be expected. The goethite synthesised at the lower temperature would not have time to fully transform from ferrihydrite to goethite, so it would be expected that more Fe would be removed from this sample than from that of the 70°C synthesis.

The ICP results from the second EDTA wash of the goethite (Table 5.15) show that less than 0.2 wt% of the total sample was removed during the repeat wash, indicating that the ferrihydrite is fully removed from the sample during the first wash, and that subsequent

washes do not cause nickel to be leached from the goethite itself. Consequently, the EDTA technique is confirmed to be suitable for use in removing secondary ferrihydrite phases from Ni-substituted goethites, without leaching the structurally incorporated Ni from the goethite.

Table 5.15: Composition of EDTA washes of Ni-substituted goethite.

Target Sample Composition	Composition of original goethite solid (wt%)		Composition of EDTA solution after first wash (wt% of Fe/Ni from original goethite)		Composition of EDTA solution after second wash (wt% of Fe/Ni from original goethite)	
	Fe	Ni	Fe	Ni	Fe	Ni
$Fe_{0.91}Ni_{0.09}OOH$ Prepared at 20°C	63.1	5.8	17.3	3.7	0.19	0.06
$Fe_{0.91}Ni_{0.09}OOH$ Prepared at 70°C	73.0	6.6	11.9	4.1	0.0	0.02
Theoretical*	57.0	5.9				
**Assuming composition of sample is entirely $Fe_{0.91}Ni_{0.09}OOH$*						

Characterisation of the Ni-goethites by PXRD before and after they had been washed with the EDTA solution shows that in the 20°C goethite synthesis, a higher background profile is present around 40° 2θ in the unwashed sample, indicating the presence of ferrihydrite (Figure 5.28). The PXRD pattern also suggests that the goethite phase is not as well crystalline, with weak, broad peaks in the diffraction pattern. In contrast, after the sample had been washed in the EDTA solution, the broad background 'bump' around 40° 2θ attributed to ferrihydrite is no longer present, and the reflections for goethite are sharper and more intense.

Although more subtle, the same observations can be made about the PXRD patterns of the 9% Ni goethite sample prepared at 70°C (Figure 5.29). Again, there is a definite 'bump' in the background profile around 40° 2θ in the unwashed sample, which is no longer present after the EDTA washing. The differences between the diffraction patterns of the washed and unwashed 70°C sample are less obvious than those observed in the equivalent patterns from the samples prepared at 20°C. This suggests that the synthesis temperature has a greater impact on the amount of untransformed ferrihydrite remaining in the sample than the presence of Ni in the synthesis.

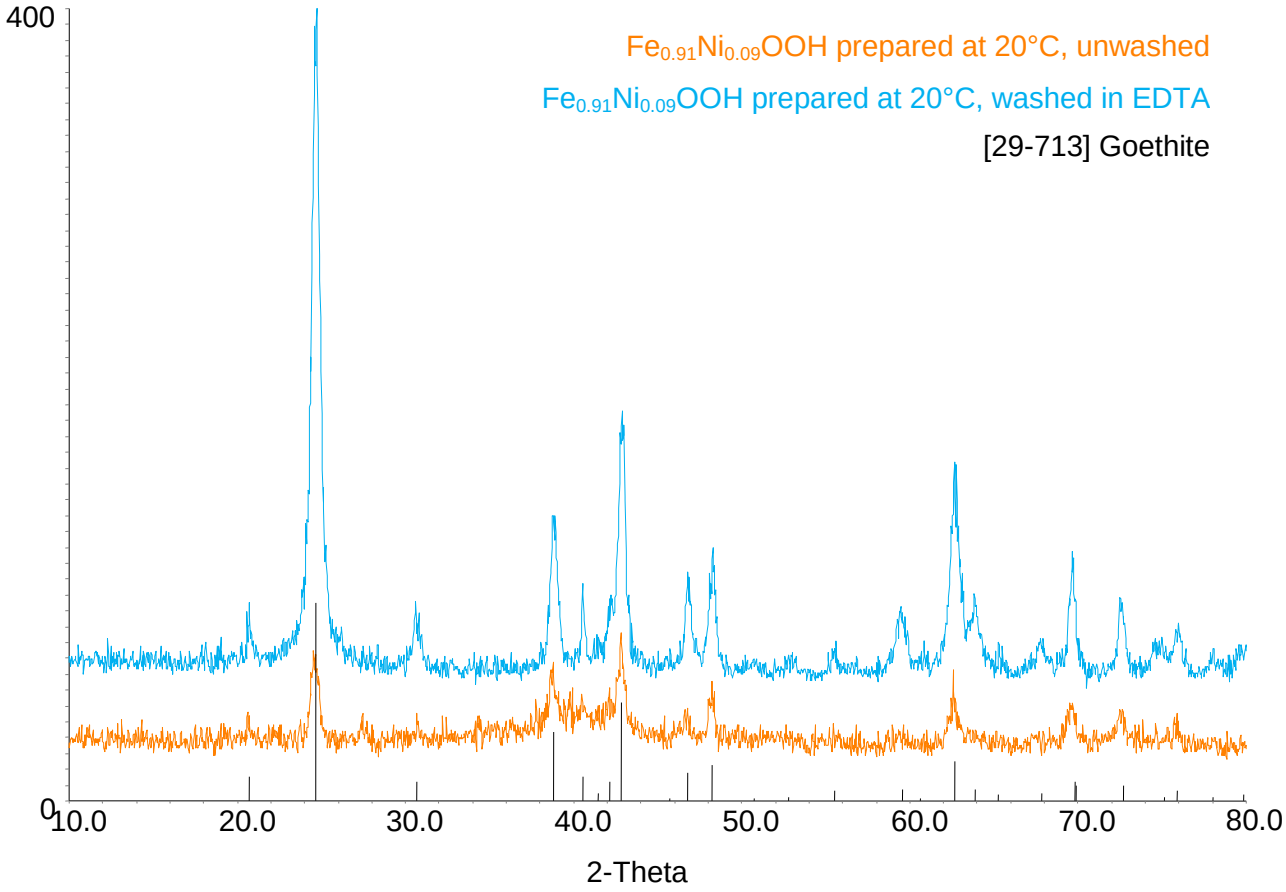

Figure 5.28: PXRD patterns showing the effect of EDTA washing on removing ferrihydrite from Ni-goethite prepared at 20°C. Data collected using Co $K_{\alpha 1}$ radiation.

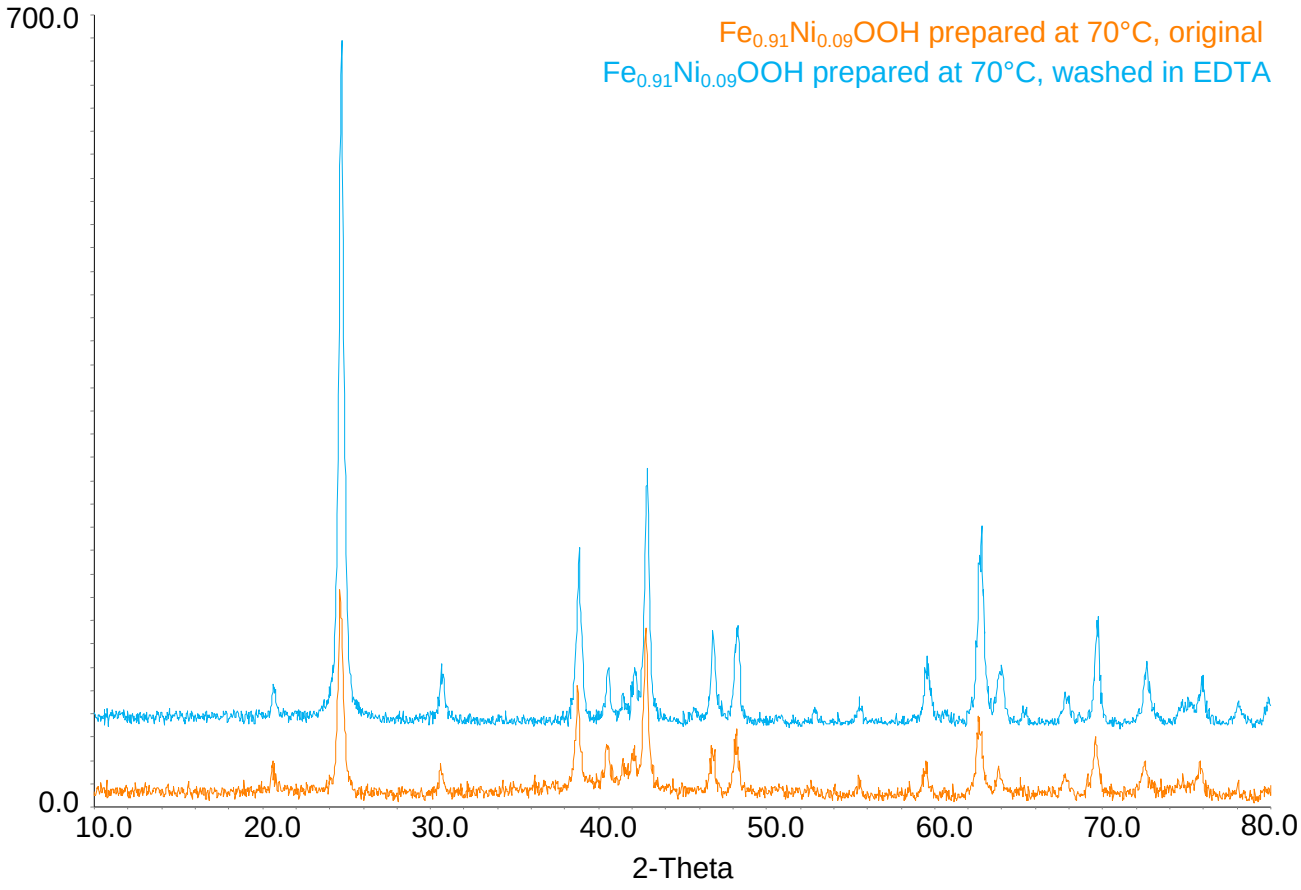

Figure 5.29: PXRD patterns showing the effect of EDTA washing on removing ferrihydrite from Ni-goethite prepared at 70°C. Data collected using Co $K_{\alpha 1}$ radiation.

Analysis of the goethite samples by TGA showed that after the EDTA washing, the weight loss which was occurring below 40°C (associated with the presence of ferrihydrite in the samples) was greatly reduced, from ~6.9 to ~1.2 wt% for the Ni-goethite synthesised at 20°C (Figure 5.30), and from 4.1 to 0.3 wt% for the sample synthesised at 70°C (Figure 5.31). The second (repeat) EDTA wash made very little difference to the weight loss profiles. This supports the evidence from the ICP-OES analysis of the washing solutions that the ferrihydrite is fully removed from the goethite in the first wash and further washes do not affect the goethite.

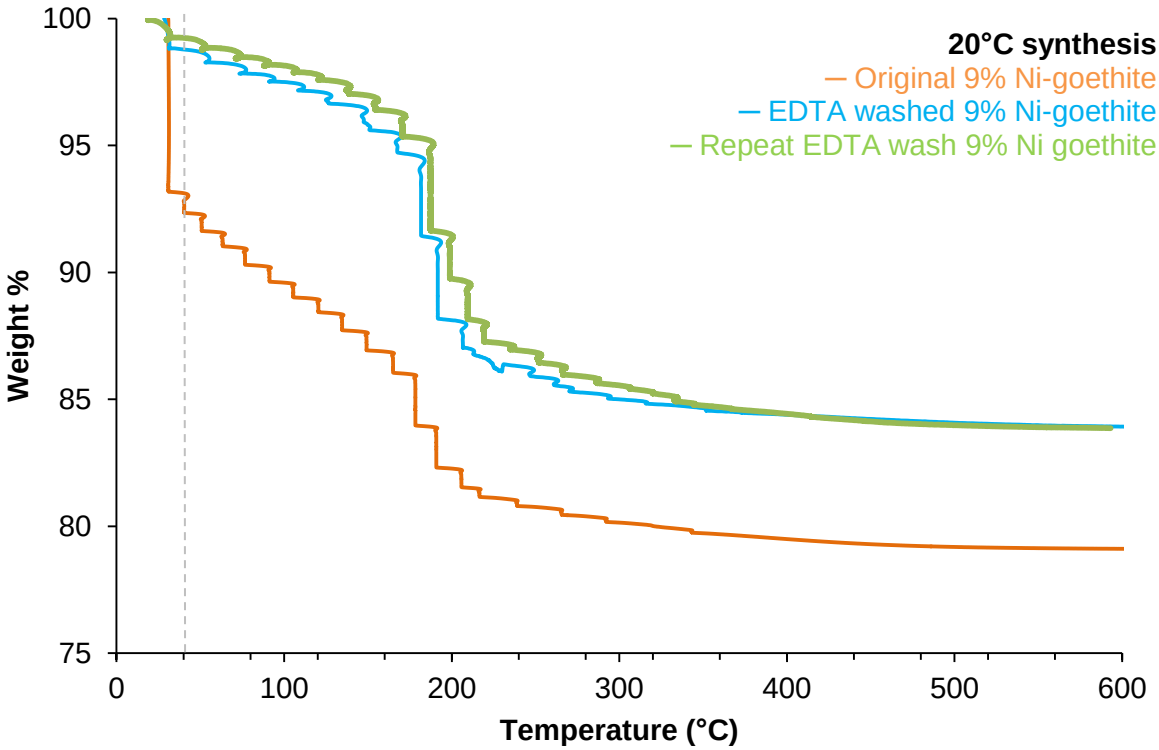

Figure 5.30: TGA weight loss profiles of unwashed 9%Ni goethite prepared at 20°C and after repeated washes with the EDTA solution. Dashed line is at 40°C.

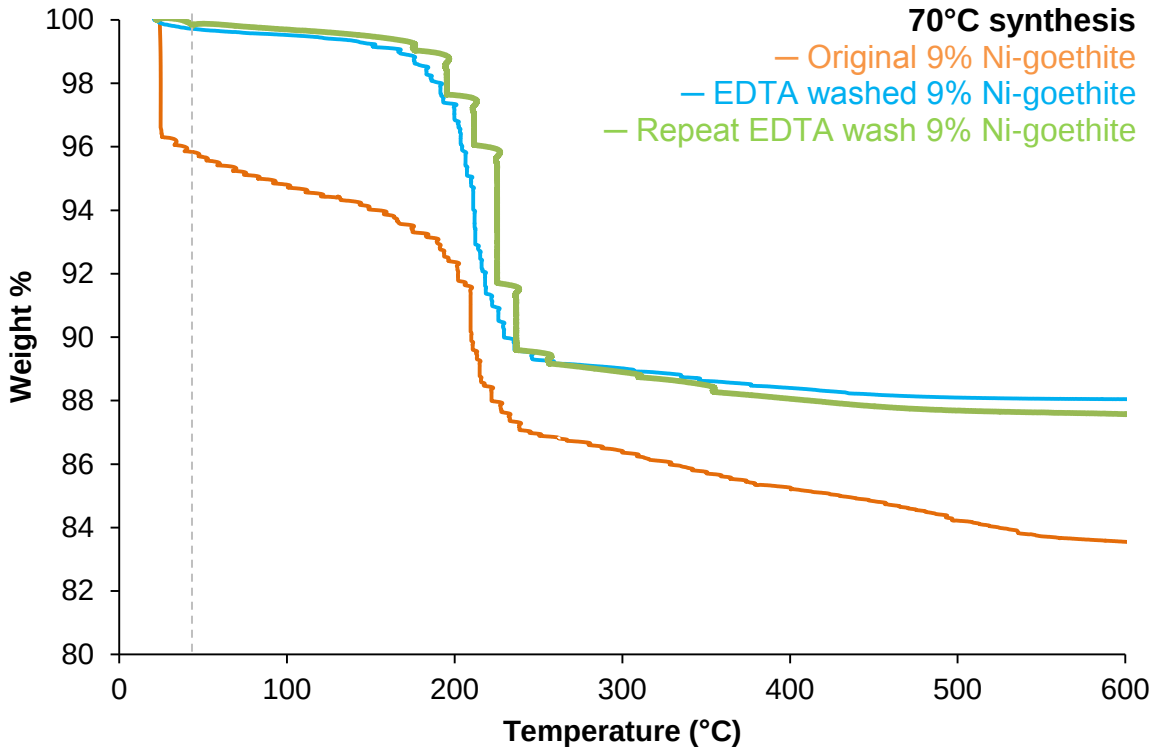

Figure 5.31: : TGA weight loss profiles of unwashed 9%Ni goethite prepared at 70°C and after repeated washes with the EDTA solution. Dashed line is at 40°C.

The Ni-goethite samples that were synthesised were imaged using TEM to establish the effect on the appearance of the particles that could be observed as a result of both adding Ni into the goethite system, and then any changes that occur as a result of the EDTA wash. As found in the observations of the TEM images of the Ni-free goethite samples (Chapter 4), the unwashed 9% Ni goethite prepared at 20°C consisted of a mixture of goethite rods and dark 'clumpy' aggregates of crystallites, the ferrihydrite phase, dispersed amongst those rods (Figure 5.32a). After the goethite had been washed using the EDTA solution, the dark clumpy aggregates were removed, leaving behind the goethite rods (Figure 5.32b).

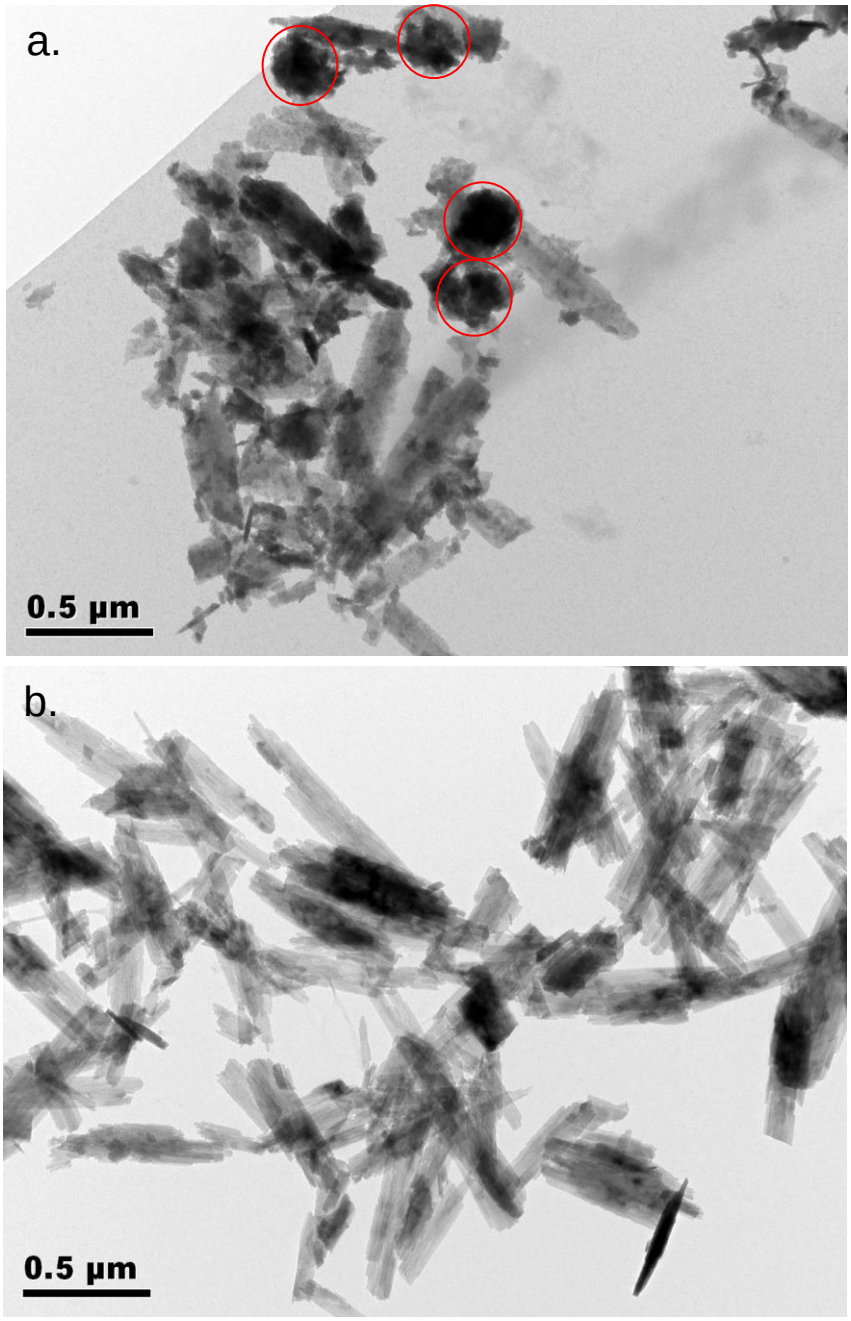

Figure 5.32: TEM images of 9% Ni-goethite particles, synthesised at 20°C, before and after EDTA treatment. Red circles highlight the ferrihydrite clusters.

5.4.3. Summary

Characterisation of the Ni-goethite samples prepared here prior to and after EDTA treatment has shown that the EDTA washing technique appears to be effective in removing a ferrihydrite secondary phase from a mixture with goethite, whilst leaving the goethite and any Ni incorporated into the structure intact. The ICP-OES results demonstrated how both iron and nickel were removed in the first EDTA wash, supporting the theory that excess nickel resides in the ferrihydrite phase. Repeated washes with the EDTA solution were shown to remove no more iron or nickel from the goethite, indicating that the EDTA technique only removes the ferrihydrite phase and has no effect on the goethite itself. Thermal analysis of the samples demonstrated both that the EDTA wash removed the ferrihydrite from the goethite, and that once this had been removed (after the first wash) no further changes to the goethite itself occurred.

Although surface adsorption of nickel is not believed to account for its residence in naturally occurring goethite from laterite deposits,[49, 58] it is possible in the synthetic samples prepared for this research that some nickel may be adsorbed to the surface of the goethite, rather than being incorporated into the goethite structure or associated with the co-formed ferrihydrite phase. Investigating the extent (if any) of surface adsorbed nickel on synthetic goethite has not been investigated as part of this research. Instead, the focus is on how much nickel is structurally incorporated into goethite vs. how much nickel resides elsewhere (e.g. in ferrihydrite). If any nickel is sorbed to the goethite surface, it will be removed by the EDTA wash (pH ~4.5) and measured as if it were associated with the ferrihydrite phase. Further investigation is needed in order to determine the extent of nickel adsorption to mineral surfaces in the synthetic systems studied here.

From this investigation, it can be concluded that the EDTA wash can be used to remove ferrihydrite from Ni-goethites, as it does not leach nickel that is incorporated in the goethite structure, or modify the goethite itself in any way.

5.5. Characterisation and EDTA Washing of Ni-Substituted Goethites

5.5.1. Introduction

In part 5.3 of this thesis, the incorporation of a number of different metal cations into the goethite structure was broadly investigated. This section focuses solely on Ni incorporation into goethite and the associated ferrihydrite phase that may be stabilised as a result of the addition of nickel to the system. The effect of temperature on the incorporation and products that form will also be discussed. The proportion of untransformed ferrihydrite remaining in the Ni-goethite samples will be estimated using the techniques devised in Chapter 3. Finally, the EDTA washing technique will be used to remove secondary ferrihydrite phases from the Ni-goethite samples, allowing the way in which Ni partitions itself between goethite and ferrihydrite to be established.

As in previous sections, the samples are described using their target compositions, based on the actual amount of nickel initially added to the synthesis. This allows the samples to be distinguished from one another and discussed in a coherent way throughout the text. Table 5.16, below, details the target level, as well as the measured Ni incorporation level both before and after EDTA washing of the samples discussed in this part of the work.

Table 5.16: Target vs. measured nickel incorporation levels for the samples discussed in section 5.5.

Target Ni Incorporation Level (mol %)	Average Measured Ni Incorporation Level	
	Original Goethite (mol %)	EDTA Washed Goethite (mol %)
0	0	0
1	0.89	0.40
2	1.82	0.89
3	2.67	1.13
4	3.34	1.26
5	4.38	1.30
6	5.25	1.52
8	7.27	1.68
9	7.71	1.38

5.5.2. Experimental Methods

Ni-goethites were prepared with between 0-9 mol% Ni (ideally $Fe_{1-x}Ni_xOOH$, where x = 0-0.09) at 20, 70 and 90°C (methodology discussed in Chapter 2), and the products formed, as well as any effect resulting from the EDTA washing (see Chapter 4 for details), were investigated using a number of different techniques including PXRD, TGA, Raman and ICP-OES.

5.5.3. Results and Discussion

Powder X-Ray Diffraction (PXRD)

Initial characterisation by PXRD of the samples prepared with increasing levels of Ni addition (0-9%) suggested that all of the samples, regardless of synthesis temperature or Ni content, were goethite, with no evidence of the presence of other crystalline phases (see Figures 5.33-5.35) It is unrealistic to believe that goethite really is the only phase present, since the amount of Ni that was attempted to be incorporated into the goethite structure was much higher than the maximum (5.5 mol%) reported previously.[2] The presence of a secondary phase, believed to be ferrihydrite from the preliminary work discussed in previous chapters, is suspected to be accommodating the excess Ni.

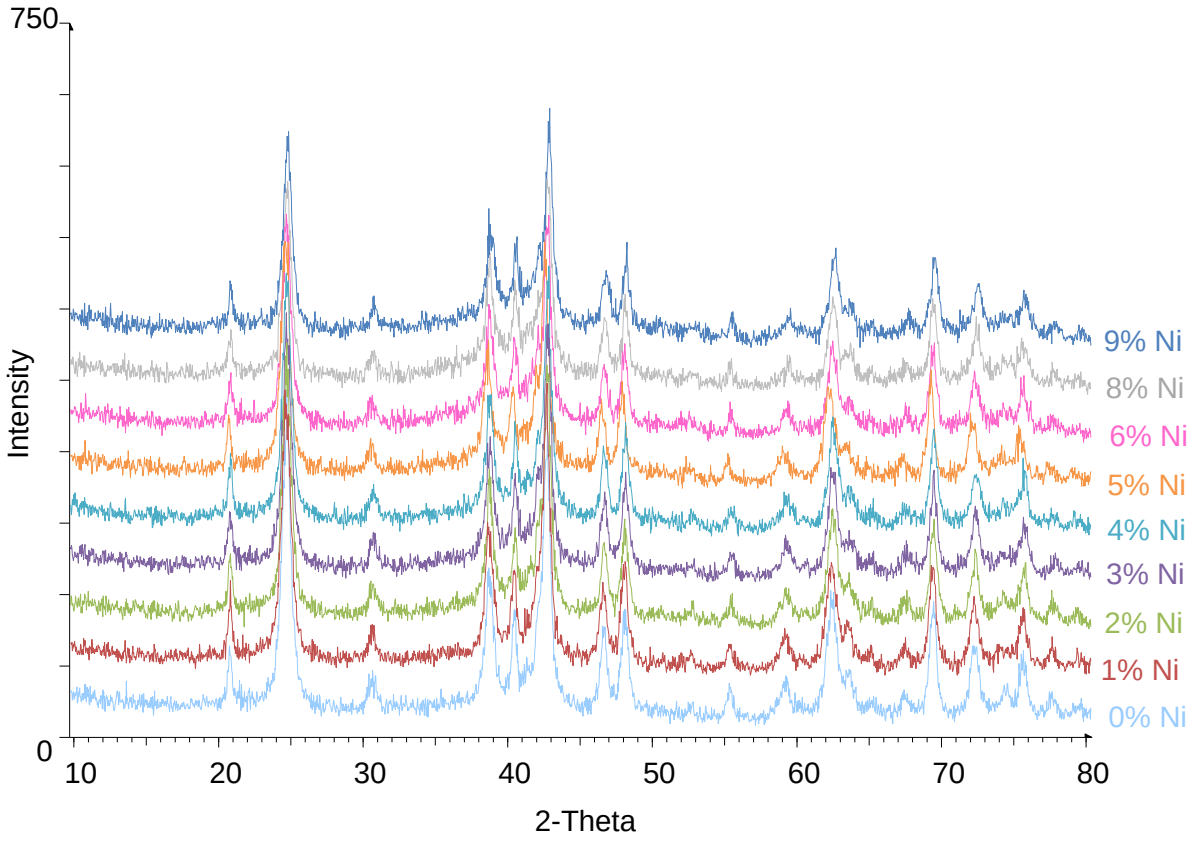

Figure 5.33: PXRD patterns of Ni-substituted goethite prepared at 20°C, data collected using Co $K_{\alpha 1}$ radiation. Samples labelled by target Ni incorporation level in goethite.

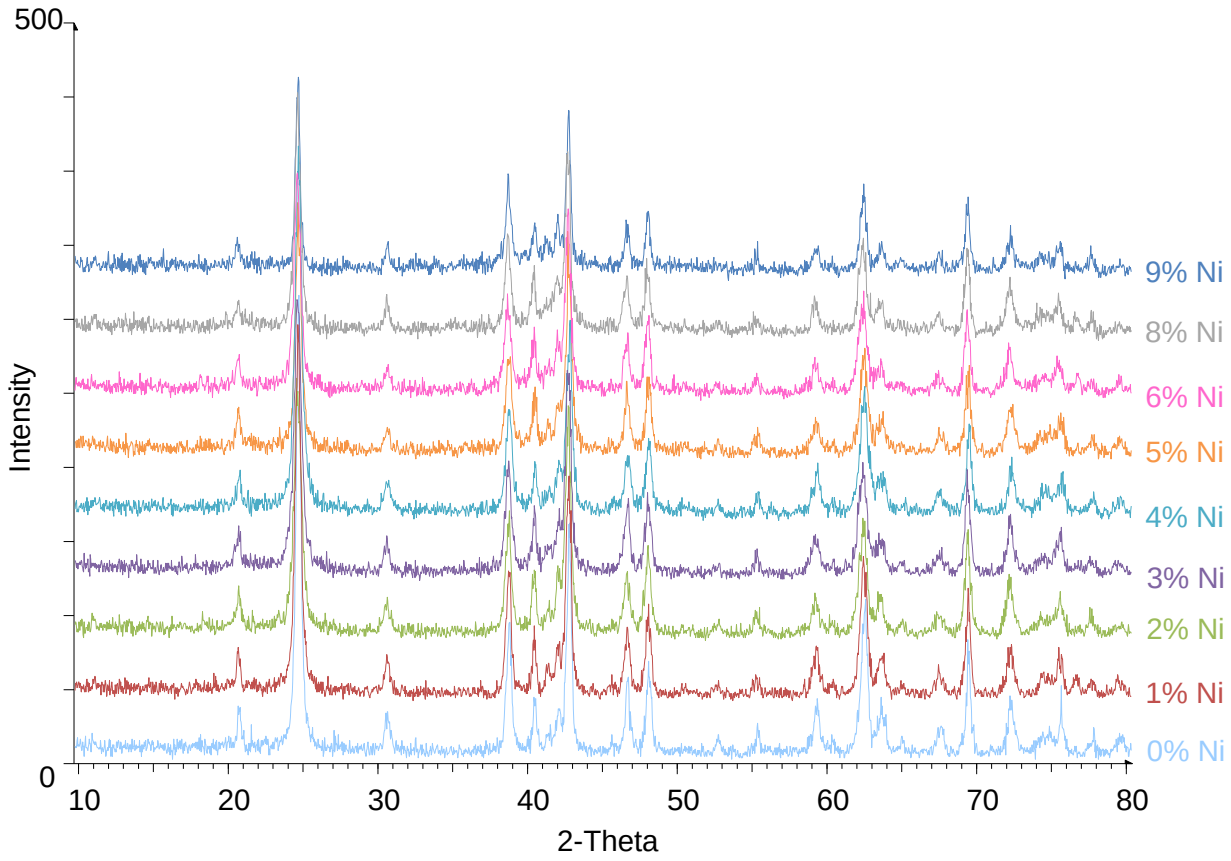

Figure 5.34: PXRD patterns of Ni-substituted goethite prepared at 70°C, data collected using Co $K_{\alpha 1}$ radiation. Samples labelled by target Ni incorporation level in goethite.

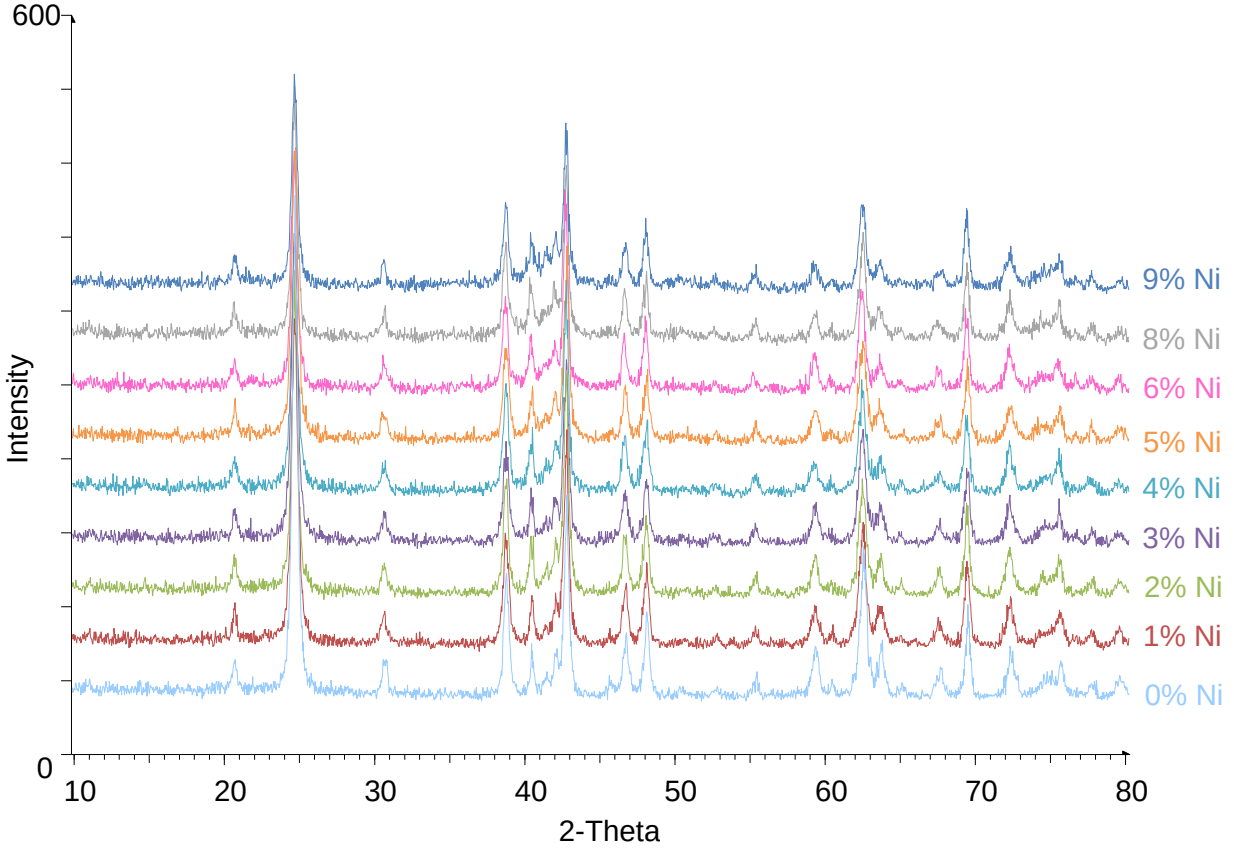

Figure 5.35: PXRD patterns of Ni-substituted goethite prepared at 90°C, data collected using Co $K_{\alpha 1}$ radiation. Samples labelled by target Ni incorporation level in goethite.

As was discussed in Chapter 3, detecting the presence of ferrihydrite when mixed with crystalline goethite is problematic, due to its near amorphous nature. However, this work has previously demonstrated how ferrihydrite can be identified by the observation of a slightly increased background profile in the ~40° 2θ region of PXRD patterns, and a method was developed to estimate the proportion present.

Using Equation 3.4, (methodology discussed in Chapter 3), the proportion of ferrihydrite present in the goethite samples as the amount of nickel was increased was estimated from the PXRD data presented in Figures 5.33-5.35, and these estimations are shown in Table 5.17.

Equation 3.4: The relationship between intensity ratios from PXRD patterns and the proportion of ferrihydrite present in a goethite/ferrihydrite mixture.

$$y = 0.0022x^2 - 0.5293x + 31.568$$

Where y=the ratio between intensities and x=wt% ferrihydrite

Table 5.17: Estimation of the ferrihydrite content of Ni-substituted goethite samples using PXRD data.

Target Mol % Ni in Goethite	Estimated ferrihydrite content (wt%)		
	20°C synthesis	70°C synthesis	90°C synthesis
0	65	6	0
1	70	15	17
2	71	39	17
3	72	40	28
4	72	29	39
5	76	49	30
6	77	52	44
8	80	50	48
9	79	59	52

Regardless of the synthesis temperature used to prepare the goethite samples, the proportion of ferrihydrite present increases with increasing Ni content. Looking at the quantities of ferrihydrite that are estimated to be present in the samples, it is clear that increased nickel addition results in an increase in the amount of stabilised ferrihydrite in the sample, from 65-80 wt% at 20°C, 6-59 wt% at 70°C, and 0-52 wt% at 90°C, see Figure 5.36. However, in the time period that the synthesis was studied over, the synthesis temperature appears to play a more important role in the remaining ferrihydrite proportion, with the sample prepared at 20°C estimated to contain 65 wt% ferrihydrite in

the Ni-free sample, compared to the sample prepared at 70°C containing just 6 wt% ferrihydrite.

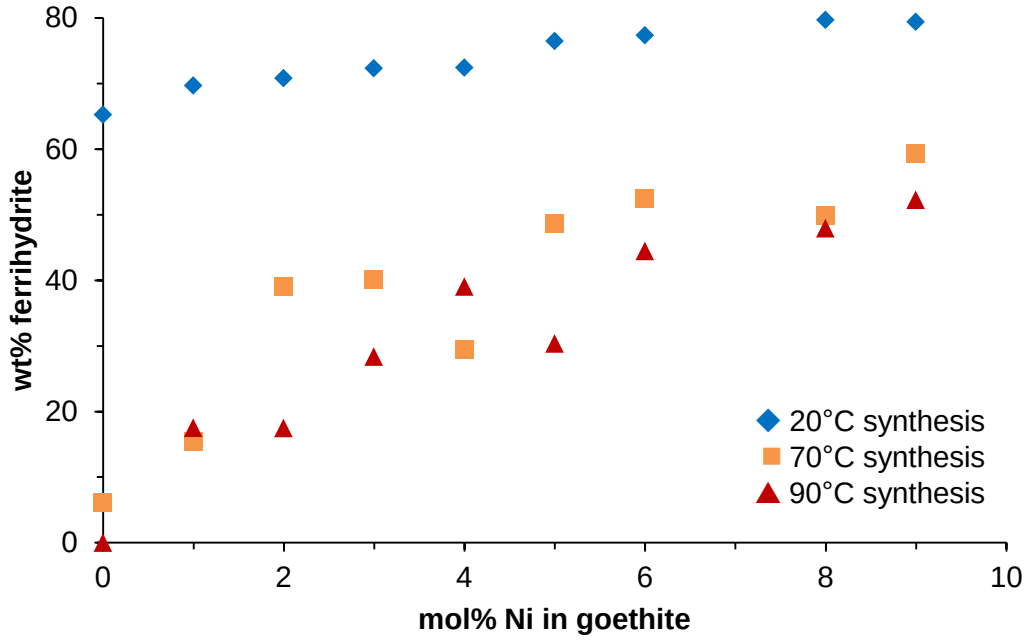

Figure 5.36: Proportion of ferrihydrite estimated from PXRD data in Ni-substituted goethites.

Although characterisation of the Ni-goethite samples by PXRD confirms the presence of a ferrihydrite phase alongside the goethite, and demonstrates that the proportion of ferrihydrite in the sample increases with increased Ni, the exact residence of the Ni remains unclear. Further characterisation work was needed in order to confirm that ferrihydrite was hosting the excess Ni, as well as providing a more thorough assessment of the way in which Ni partitions itself between goethite and ferrihydrite. In order to do this, the two phases needed to be separated. In part 5.4, the effectiveness of the EDTA washing technique for use with Ni-substituted goethites was investigated and proved to be succesful in removing ferrihydrite whilst leaving the goethite intact. Washing the Ni-goethites in the EDTA solution allows the separation of the two phases. The ferrihydrite and any Ni associated with it, ends up in the washing solution whilst the Ni-goethite remains as a solid phase, allowing charactersaion of both parts independently.

The Ni-goethite samples prepared at the three different temperature ranges (20, 70 and 90°C) were washed in the 0.1M EDTA solution, described in detail in Chapter 4. The resulting solutions and the washed goethite solid were retained for analysis.

Previous work described in this thesis, as well as by others (e.g. Schwertmann *et al.* (1985)) has shown that the synthesis temperature affects the extent of transformation from ferrihydrite to goethite; lower temperatures resulting in a slower transformation (one that is not complete after 7 days).[59] It is also known that foreign cations can stabilise ferrihydrite, preventing it transforming to the more stable goethite phase.[34] As a result of this, it might be expected that at lower temperatures and higher Ni contents, more of the Ni-goethite sample would remain as ferrihydrite than is the case in those samples which were prepared at higher temperatures and/or contained less Ni.

Visual observation of the washing solutions (Figure 5.37) supports the theory described above. All of the washing solutions resulting from the 20°C synthesis are a dark yellow colour, even in the Ni-free goethite sample, indicating that ferrihydrite was present with the goethite regardless of the amount of Ni that was added. The colour of the washing solutions does appear to intensify as the Ni content of the synthesis increases, suggesting that more ferrihydrite is present in the Ni-rich goethite samples than the Ni-poor. The Ni-goethite samples prepared at higher temperatures (70 and 90°C) resulted in washing solutions which for the 0% Ni sample were colourless, indicating that there was no ferrihydrite present. The colour of the solutions then intensified, gradually becoming more yellow as the Ni content of the goethite samples increased, again suggesting an increase in the proportion of ferrihydrite associated with the samples. Basic observation of the EDTA washing solutions alone clearly indicates an increase in dissolved Fe/Ni at both higher Ni contents and lower synthesis temperatures. This suggests that ferrihydrite is being stabilised by the Ni added to the synthesis procedure, as the proportion of ferrihydrite which appears to be present increases with Ni content.

The appearance of the solid samples is also affected by the EDTA wash, with the colour of the unwashed samples changing from a yellow for the pure goethite, and becoming more brown as the Ni content increases – an observation supported by previous work and indicating that ferrihydrite (dark brown in colour) is present.[60]

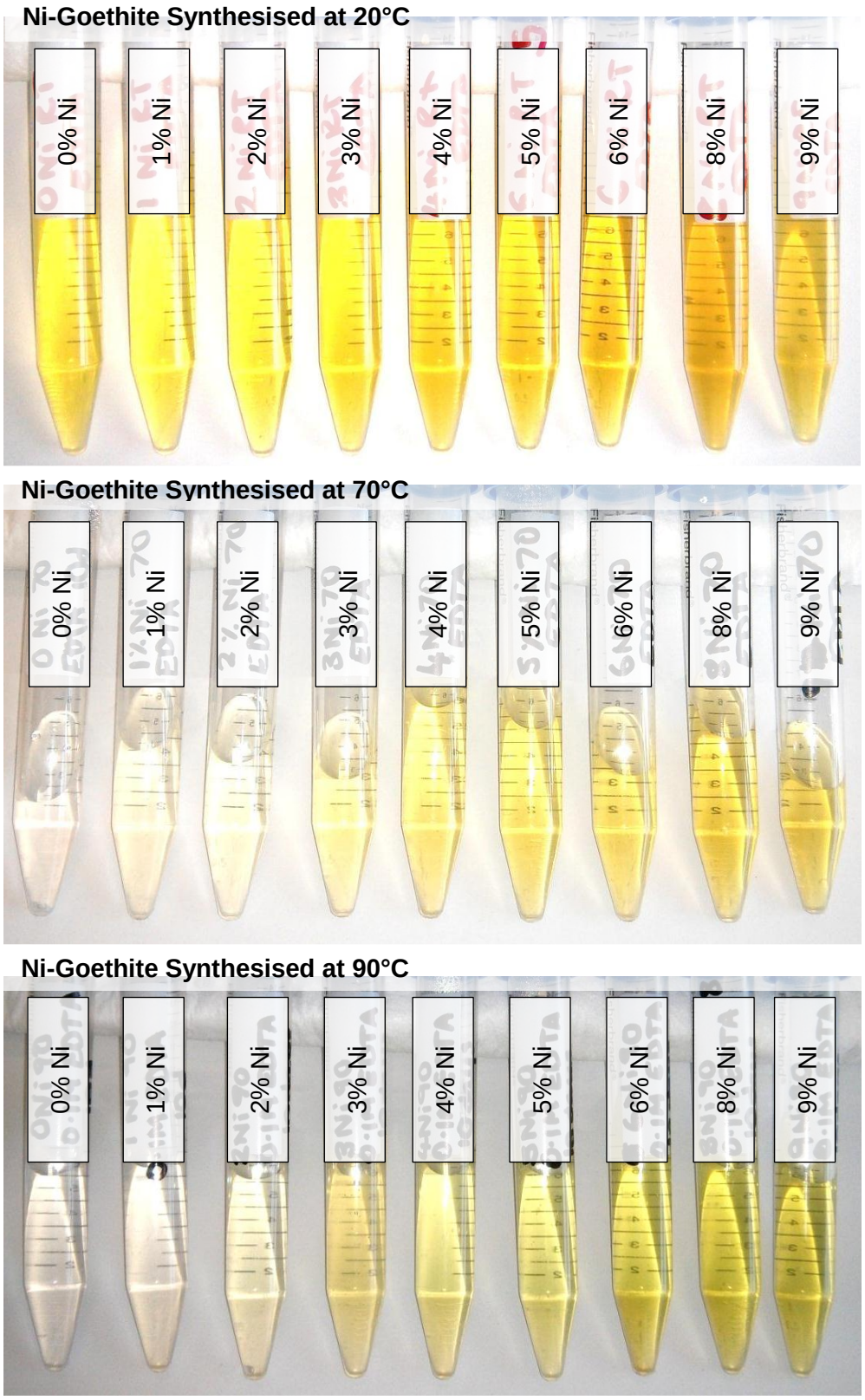

Figure 5.37: Appearance of the EDTA washing solutions of Ni-containing goethites prepared at different synthesis temperatures.

After the solid Ni-goethite samples had been washed with EDTA, they were again characterised by PXRD, shown in Figures 5.38-5.40. As with the unwashed samples, the only crystalline phase which could be identified at all synthesis temperatures and Ni concentrations was goethite. In comparison to the PXRD patterns of the unwashed samples shown previously, no visible difference in the background profiles, indicating the presence of ferrihydrite, was observed as the Ni content increased. The reflections do appear to be sharper in the EDTA washed samples, and the background much flatter in the 30-50° 2θ region when compared to the original, unwashed Ni-goethite samples.

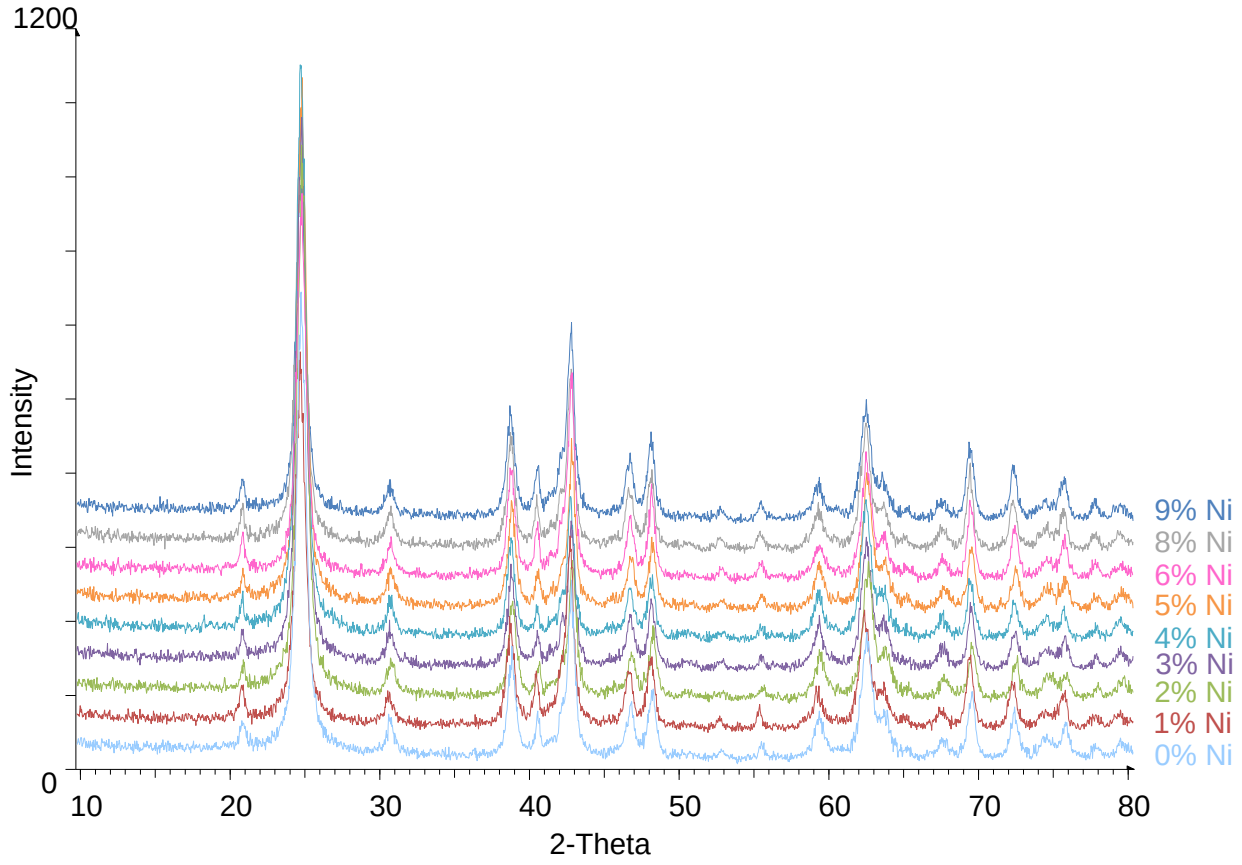

Figure 5.38: PXRD patterns of Ni-goethite samples synthesised at 20°C, after EDTA washing. Data collected using Co $K_{\alpha 1}$ radiation. Samples labelled by target Ni incorporation level in goethite.

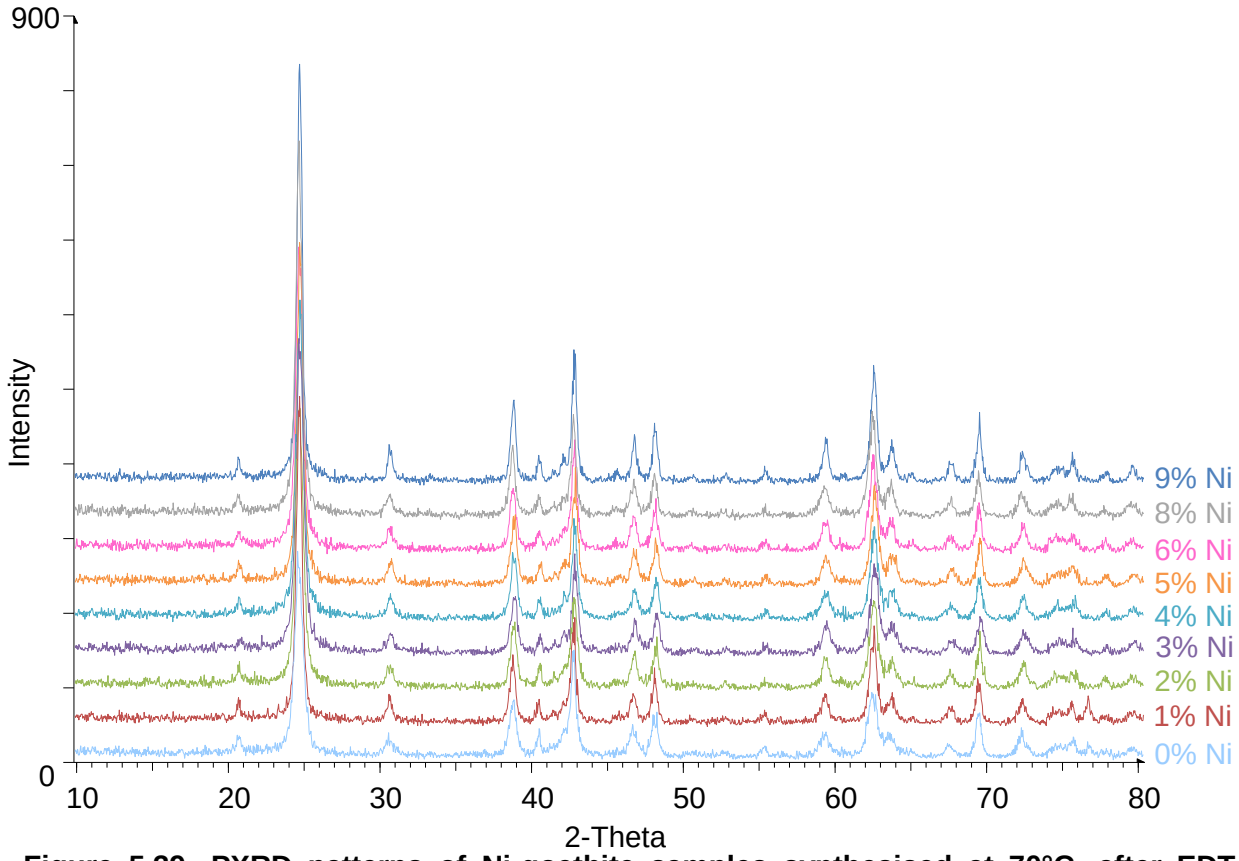

Figure 5.39: PXRD patterns of Ni-goethite samples synthesised at 70°C, after EDTA washing. Data collected using Co $K_{\alpha 1}$ radiation. Samples labelled by target Ni incorporation level in goethite.

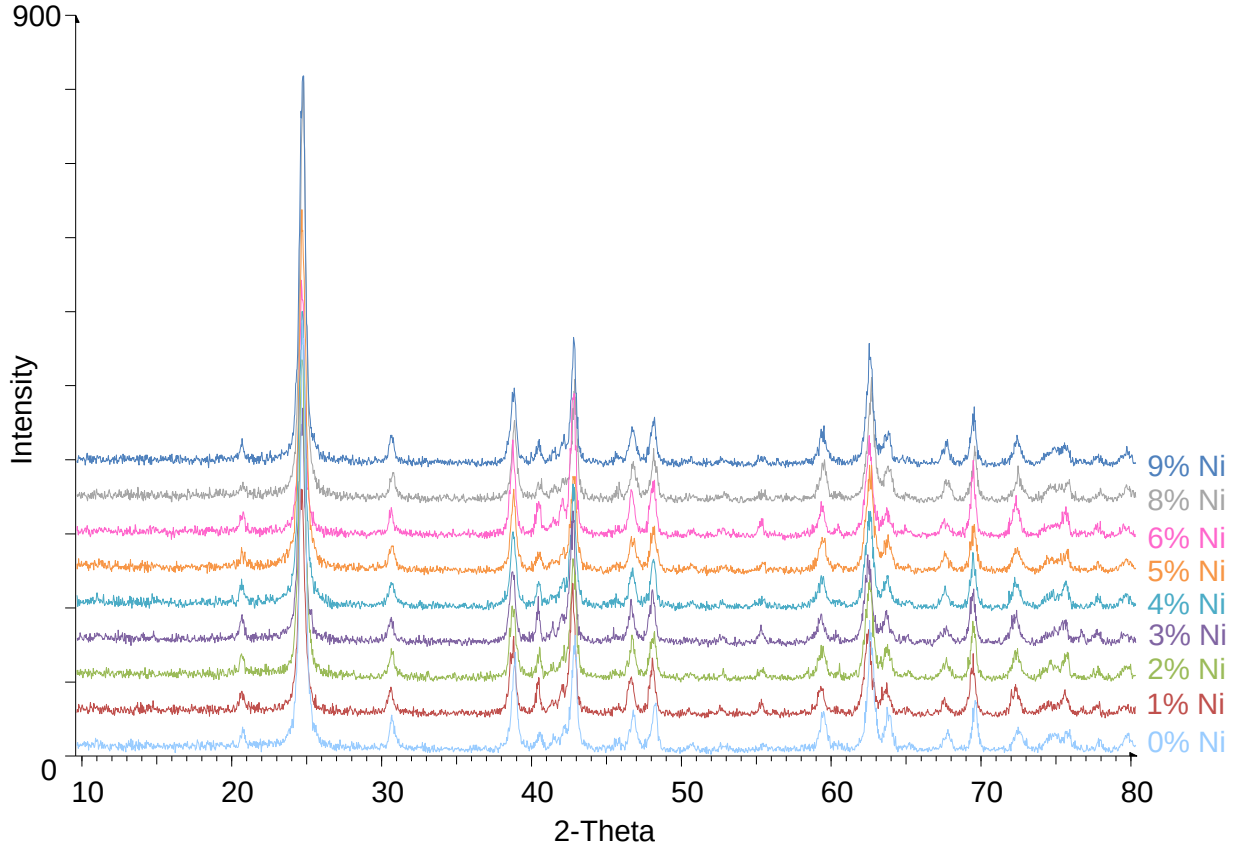

Figure 5.40: PXRD patterns of Ni-goethite samples synthesised at 90°C, after EDTA washing. Data collected using Co $K_{\alpha 1}$ radiation. Samples labelled by target Ni incorporation level in goethite.

An example of a Ni-goethite diffraction pattern before and after EDTA washing and compared to 2-line ferrihydrite is shown in Figure 5.41. The diffraction pattern for an unwashed Ni-free goethite sample prepared at 70°C (Figure 5.41a) has a flat background profile between 30-50° 2θ, unlike that of ferrihydrite (shown in the same figure), supporting the view that the sample is pure goethite. As previously reported (Chapter 3), the transformation of a Ni-free goethite should be complete at 70°C over the synthesis period used (7 days), so no ferrihydrite should remain. This, however, is not the case when Ni is added to the synthesis procedure. The diffraction pattern of the unwashed 9 mol% Ni-goethite sample prepared at 70°C (Figure 5.41b) has a raised background profile between 30-50° 2θ which overlaps with that of the ferrihydrite phase and therefore indicates that ferrihydrite is present alongside the goethite phase. The PXRD pattern of the 9 mol% Ni-goethite sample after it had been washed with EDTA is shown in Figure 5.41c. The background profile no longer follows that of the ferrihydrite diffraction pattern and is flat, confirming that even at elevated temperatures, ferrihydrite remains in the Ni-rich goethite samples and that this is removed with the EDTA wash.

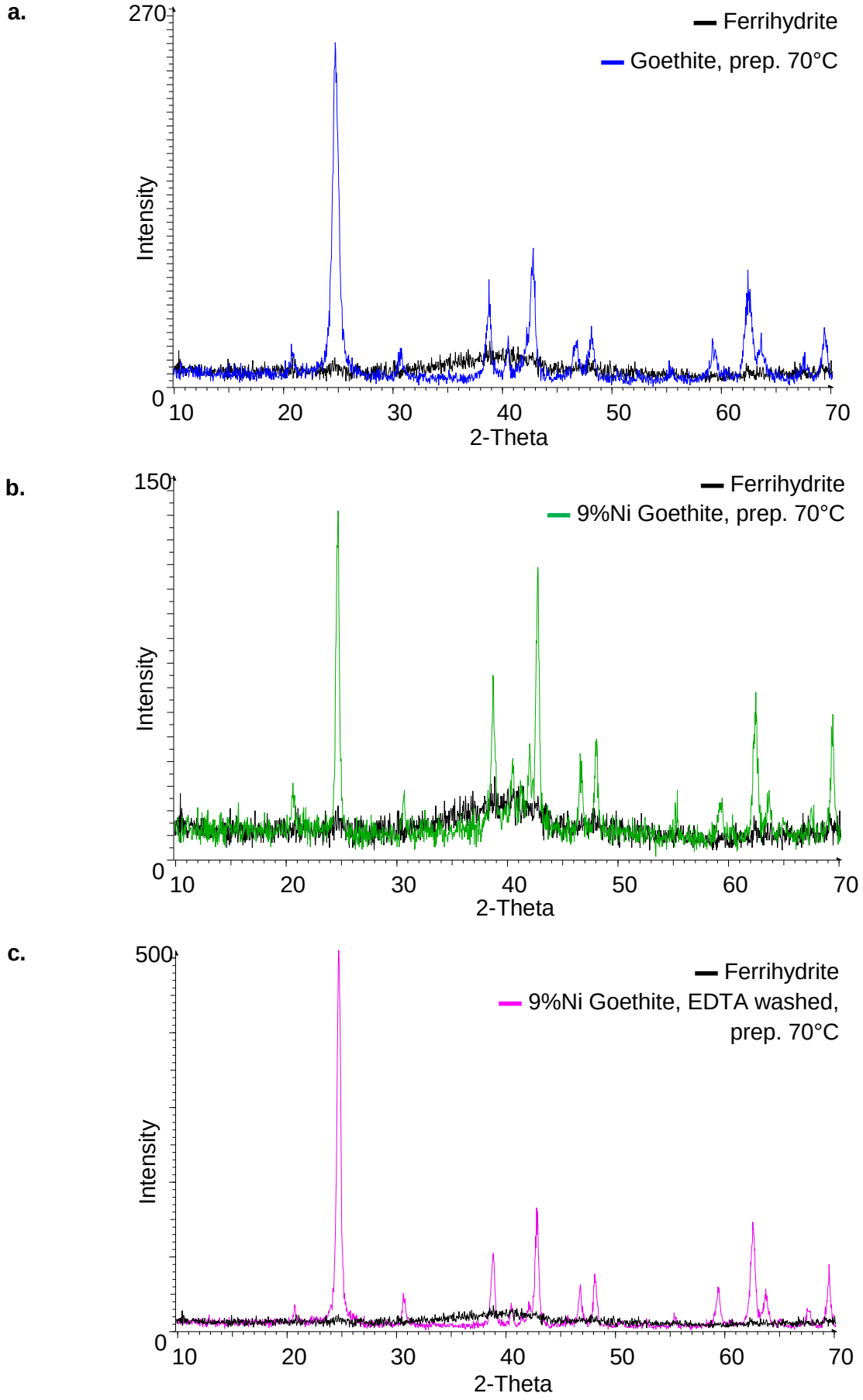

Figure 5.41: PXRD patterns showing evidence of ferrihydrite presence in Ni-goethite samples and the effect of EDTA washing on removing this. Data collected using Co $K_{\alpha 1}$ radiation. a. ferrihydrite and goethite, b. ferrihydrite and Ni-goethite, c. ferrihydrite and EDTA washed Ni-goethite.

The lattice parameters were refined for the Ni-substituted goethite samples prepared at 70°C (see Table 5.18) to look for evidence of structural incorporation of nickel into the goethite. Previous work by Wells *et al.* (2006) reported that although the *a* and *c* parameters of goethite remained unchanged with increasing nickel incorporation, the *b* parameter increased in the samples containing up to 5 mol% nickel.[10] Manceau *et al.* (2000) and Carvalho de Silva *et al.* (2003) also observed an increase in the *b* parameter with substitution of up to 6 mol% Ni, an observation consistent with the incorporation of a slightly larger cation.[1, 5]

Table 5.18: Unit cell parameters for Ni-substituted goethites prepared at 70°C.

Goethite prepared at 70°C	*a* (Å)	*b* (Å)	*c* (Å)	Cell Volume (Å^3)
Unwashed Samples				
0% Ni	4.614 (2)	9.977 (3)	3.028 (1)	139.4 (1)
1% Ni	4.619 (3)	9.980 (6)	3.030(1)	139.7 (1)
2% Ni	4.628 (3)	9.975 (5)	3.031 (1)	140.0 (1)
3% Ni	4.631 (3)	9.971 (5)	3.029 (1)	139.9 (1)
4% Ni	4.629 (2)	9.961 (5)	3.025 (1)	139.5 (1)
5% Ni	4.619 (2)	9.982 (6)	3.028 (2)	139.6 (9)
6% Ni	4.620 (3)	9.960 (7)	3.029 (2)	139.9 (1)
8% Ni	4.634 (4)	10.002 (7)	3.028 (2)	140.3 (1)
9% Ni	4.616 (3)	9.984 (7)	3.029 (2)	139.6 (1)
EDTA washed Samples				
0% Ni	4.634 (4)	9.957 (5)	3.028 (2)	139.7 (1)
1% Ni	4.608 (3)	9.978 (6)	3.027 (1)	139.2 (1)
2% Ni	4.616 (3)	9.953 (6)	3.025 (1)	139.0 (1)
3% Ni	4.611 (3)	9.964 (5)	3.022 (1)	138.8 (1)
4% Ni	4.617 (3)	9.953 (6)	3.023 (1)	138.9 (1)
5% Ni	4.608 (3)	9.967 (8)	3.024 (2)	138.9 (1)
6% Ni	4.601 (3)	9.967 (5)	3.024 (2)	139.0 (1)
8% Ni	4.617 (2)	9.971 (7)	3.028 (2)	139.4 (1)
9% Ni	4.610 (2)	9.970 (5)	3.024 (1)	139.0 (1)

Examination of the plotted unit cell parameters for the unwashed Ni-goethite samples (Figure 5.42) shows that the *a* parameter increases in size, up to 3 mol% Ni before decreasing again. The *b* parameter decreases in size with up to 4 mol% Ni, before increasing at higher levels of Ni addition. The *c* parameter remains relatively constant throughout. The increase in *a* parameter has not been noted elsewhere, with previous research reporting that the *a* parameter does not change with incorporation of Ni into goethite.[10] The apparent decreasing size of the *b* parameter observed in this work is in direct contrast to that which has been reported in the literature previously of an increase in the *b* parameter with increasing levels of Ni.[1, 5] It is important to note that the actual amounts of change in the size of the unit cell size are very small, with a range in the size of the *a* parameter across the whole series of ~0.02 Å, the *b* parameter ~0.04 Å and the *c* parameter ~0.006 Å.

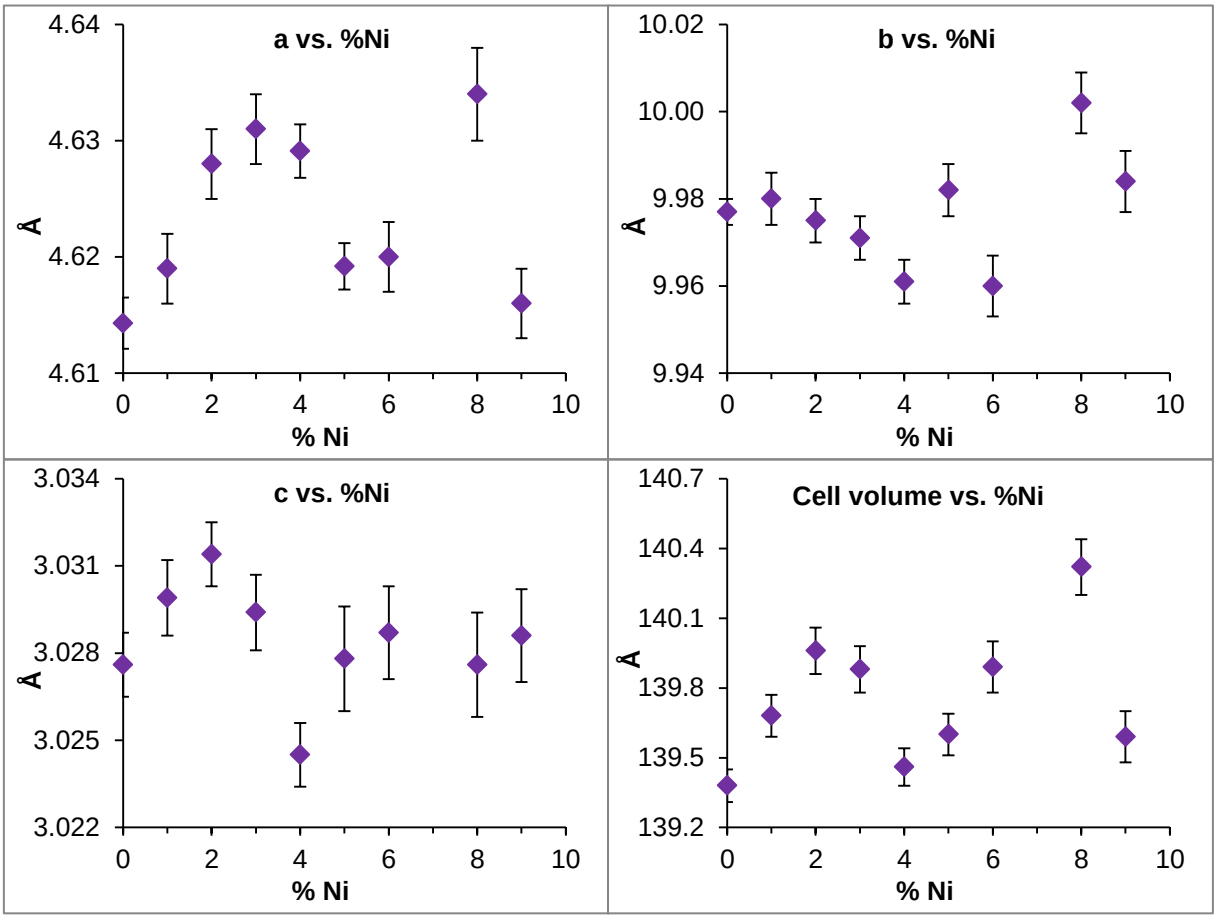

Figure 5.42: The relationship between the unit cell parameters and the % Ni in synthetic goethite samples.

The refined unit cell parameters for the Ni-goethites after they had been washed in EDTA solution are shown in Figure 5.43.

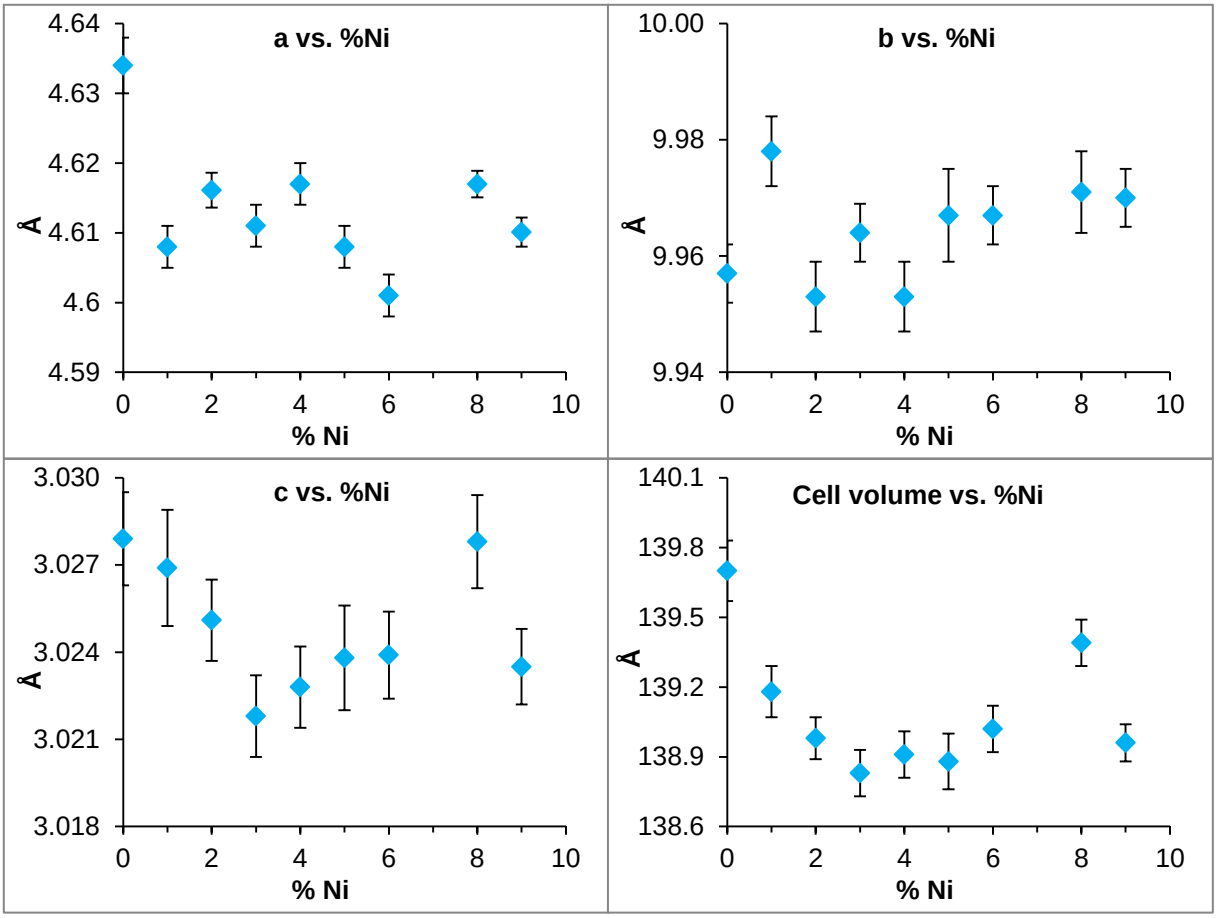

Figure 5.43: The relationship between the unit cell parameters and the % Ni in synthetic goethite samples after they had been washed with EDTA.

The trends observed in the *a* and *b* parameters of the unwashed goethite samples are not observed in the size of the unit cell after EDTA washing. The *c* parameter appears to decrease in size with up to 3 mol% Ni addition, before increasing again as more Ni is added. Again, the actual changes in the size of the unit cell parameters are very small, and the errors on the values are quite large.

From the data available here, it does not appear that any meaningful information can be gathered to identify the extent of Ni incorporation into goethite. The observation made by other research groups of an increase in the size of the *b* parameter with increasing structural incorporation of goethite cannot be made here. In order to investigate this area of work further, higher quality PXRD data is required, to allow more accurate refinement of the unit cell parameters in order to monitor the very small changes that may be occurring as a result of the structural incorporation of Ni into goethite.

Thermo-Gravimetric Analysis (TGA)

TGA has proven to be an extremely useful technique in identifying ferrihydrite in goethite samples due to the different temperatures at which the two phases begin to decompose (see Chapter 3). Weight loss plots were recorded for the range of Ni-substituted goethite samples synthesised at each of the three temperatures (20, 70 and 90°C), both before and after they had been washed with EDTA. Figures 5.44-5.46 show the weight loss profiles recorded for the unwashed Ni-goethite samples prepared at 20, 70 and 90°C, respectively. In all cases, the weight loss measured below 40°C increases as the Ni content in the samples increase. For the samples prepared at 20°C, (Figure 5.44) the weight loss which occurs below 40°C ranges from ~4.5 to 7.7 wt% with increasing Ni, indicating that, as discussed previously, even the Ni-free goethite synthesised at this low temperature contains some ferrihydrite. The proportion of ferrihydrite that is present then appears to increase with further addition of Ni to the system.

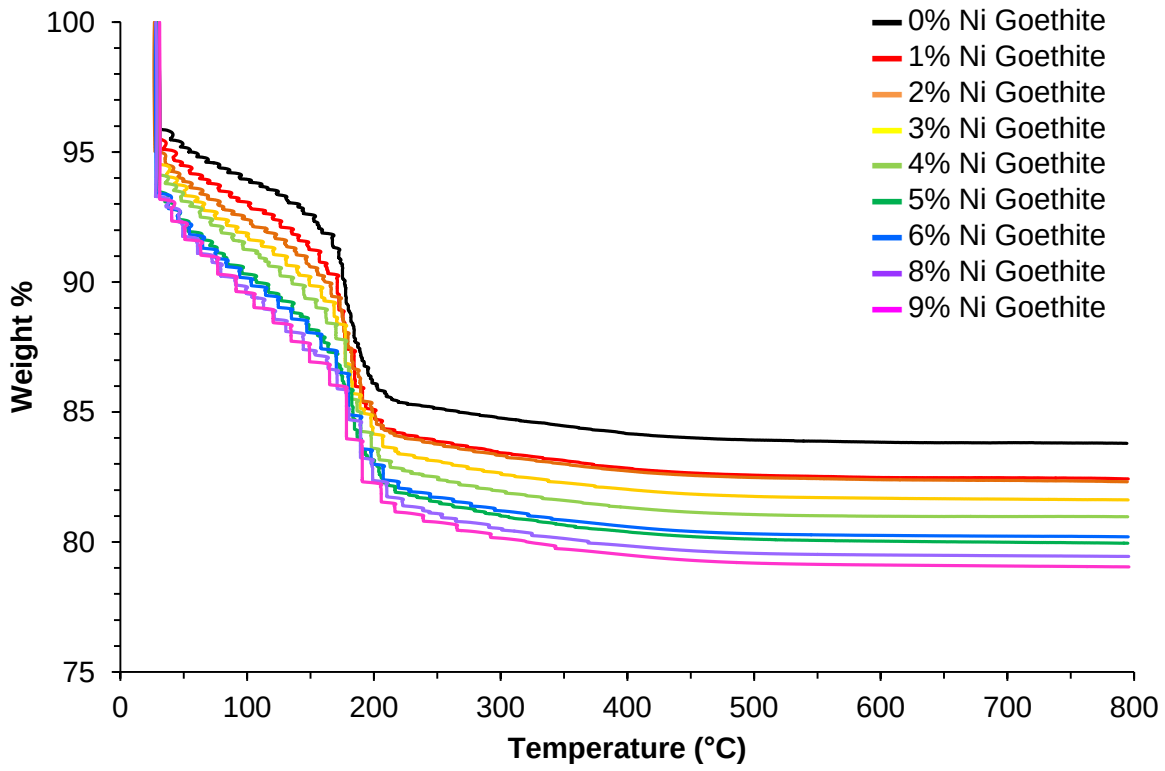

Figure 5.44: Weight loss profiles for Ni-substituted goethites synthesised at 20°C.

The Ni-goethites prepared at the higher (70 and 90°C) synthesis temperatures (Figures 5.45 and 5.46) display the same trend of increasing weight loss with increasing Ni content (in the temperature region below 40°C). However, the weight losses occurring in the samples prepared at these higher synthesis temperatures are in a lower range; 0.4 to 4 wt% (70°C synthesis) and 0.3-3 wt% (90°C synthesis) than the weight losses in the equivalent

20°C synthesis samples. This observation follows what would be expected, considering that at the higher synthesis temperatures over the 7 day synthesis period, full transformation from ferrihydrite to goethite should occur in an un-substituted goethite.

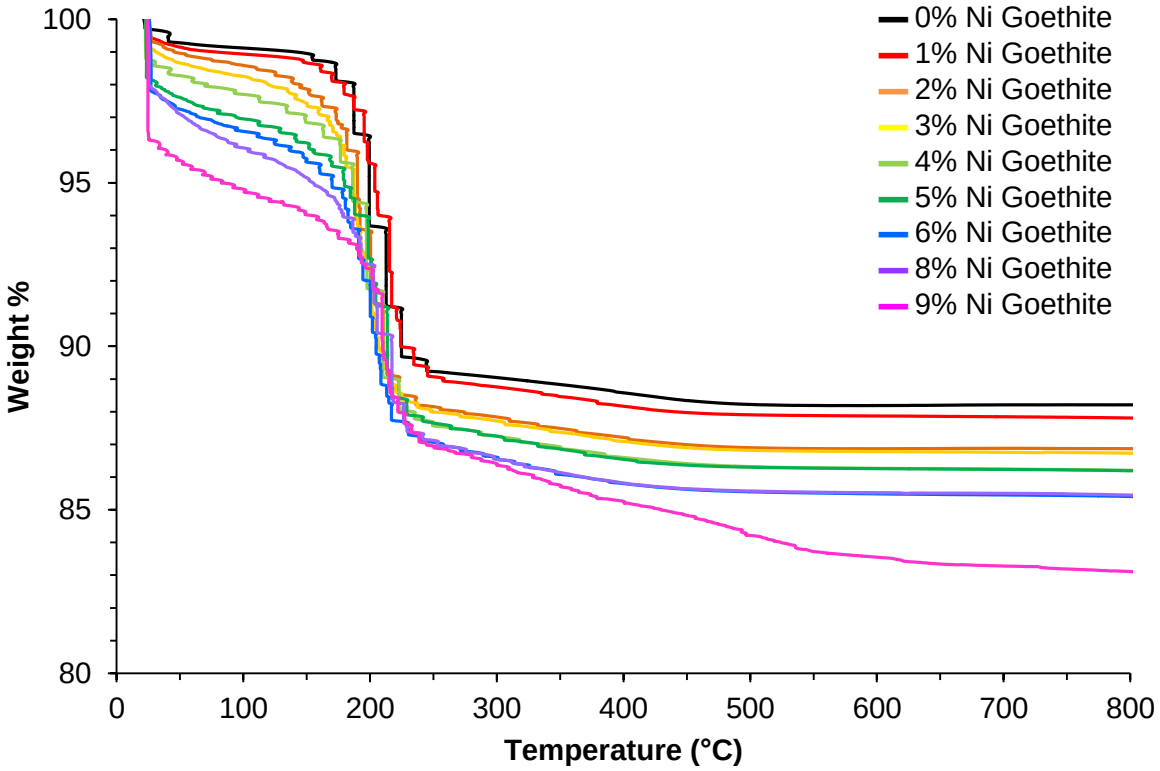

Figure 5.45: Weight loss profiles for Ni-substituted goethites synthesised at 70°C.

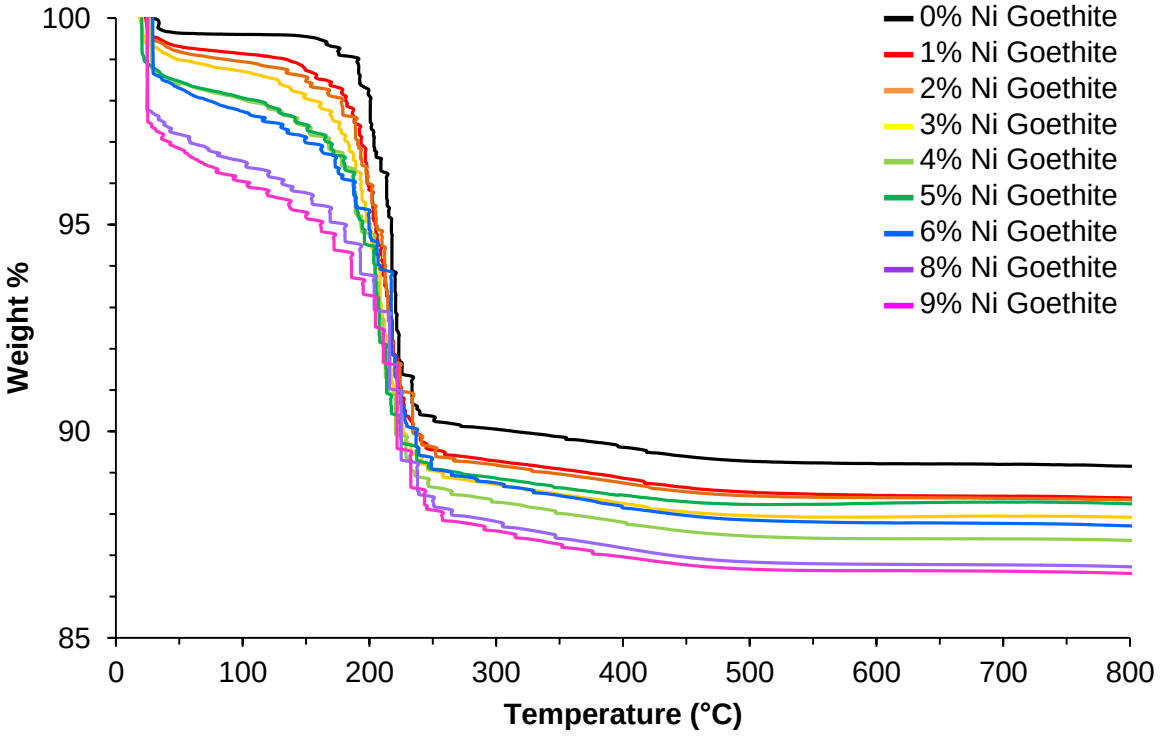

Figure 5.46: Weight loss profiles for Ni-substituted goethites synthesised at 90°C.

After washing the Ni-goethite samples in the EDTA solution, the TGA weight loss profiles were recorded again and are shown in Figures 5.47-5.49. From examination of these weight loss profiles, it is clear that the EDTA washing technique has been successful in removing ferrihydrite from the samples. The weight loss profiles for each set of Ni goethites look very similar – there are no apparent increases in weight loss relating to the Ni content of the samples. The weight losses recorded below 40°C have also decreased in all cases, most obviously in the samples synthesised at 20°C (Figure 5.47), where previously the weight loss ranged from 4.5 – 7.7 wt%, the washed samples have a weight loss in this region of between 1 – 1.4 wt%. The same observation can be made for the samples prepared at 70°C (Figure 5.48) and 90°C (Figure 5.49), where, in the original unwashed samples, the weight losses ranged from 0.4 – 4 wt% and 0.3 – 3 wt% respectively and after the EDTA washing treatment they range from ~0.3 – 0.7 wt% and ~0.2 – 0.5 wt%.

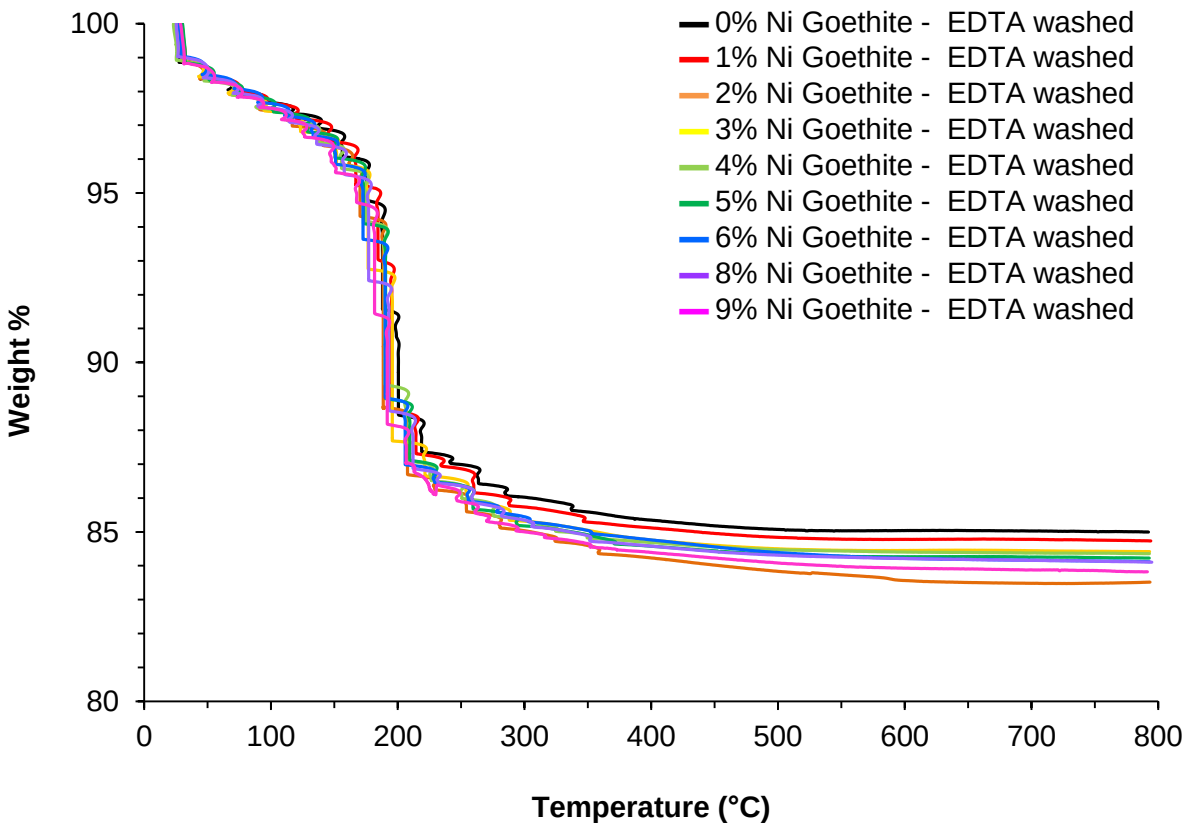

Figure 5.47: Weight loss profiles for EDTA washed Ni-substituted goethites synthesised at 20°C.

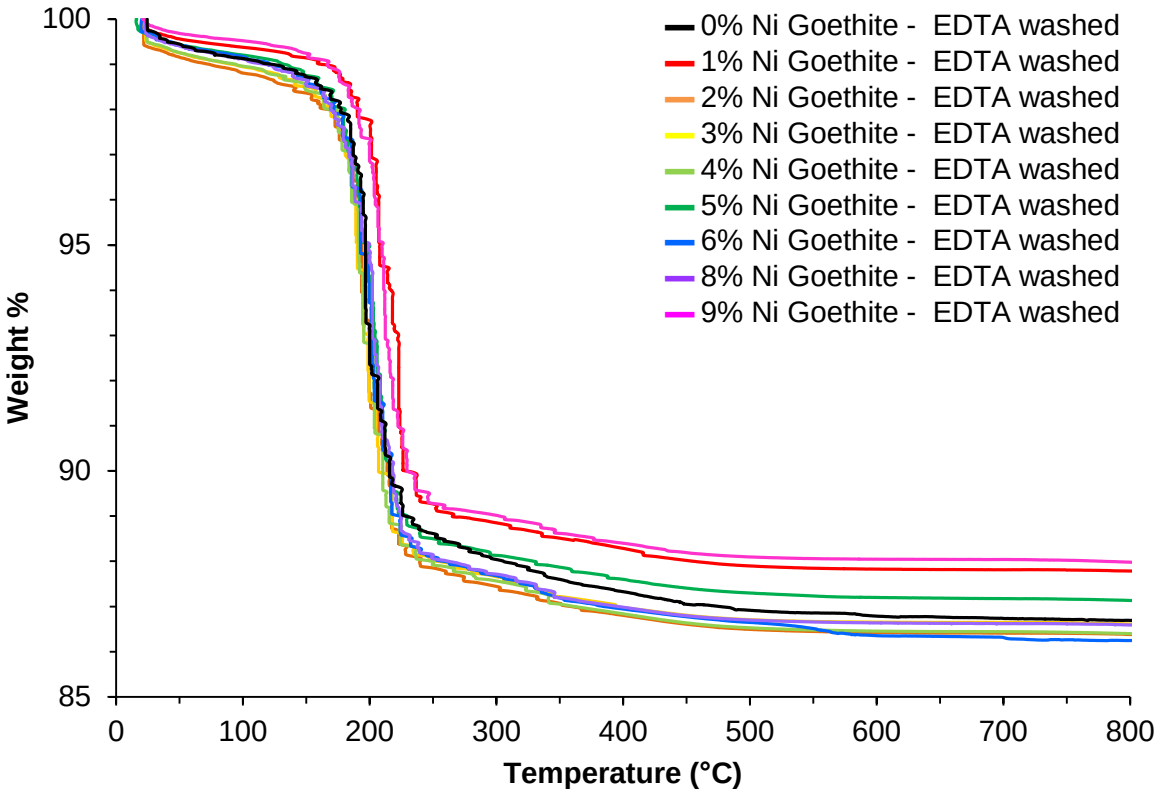

Figure 5.48: Weight loss profiles for EDTA washed Ni-substituted goethites synthesised at 70°C.

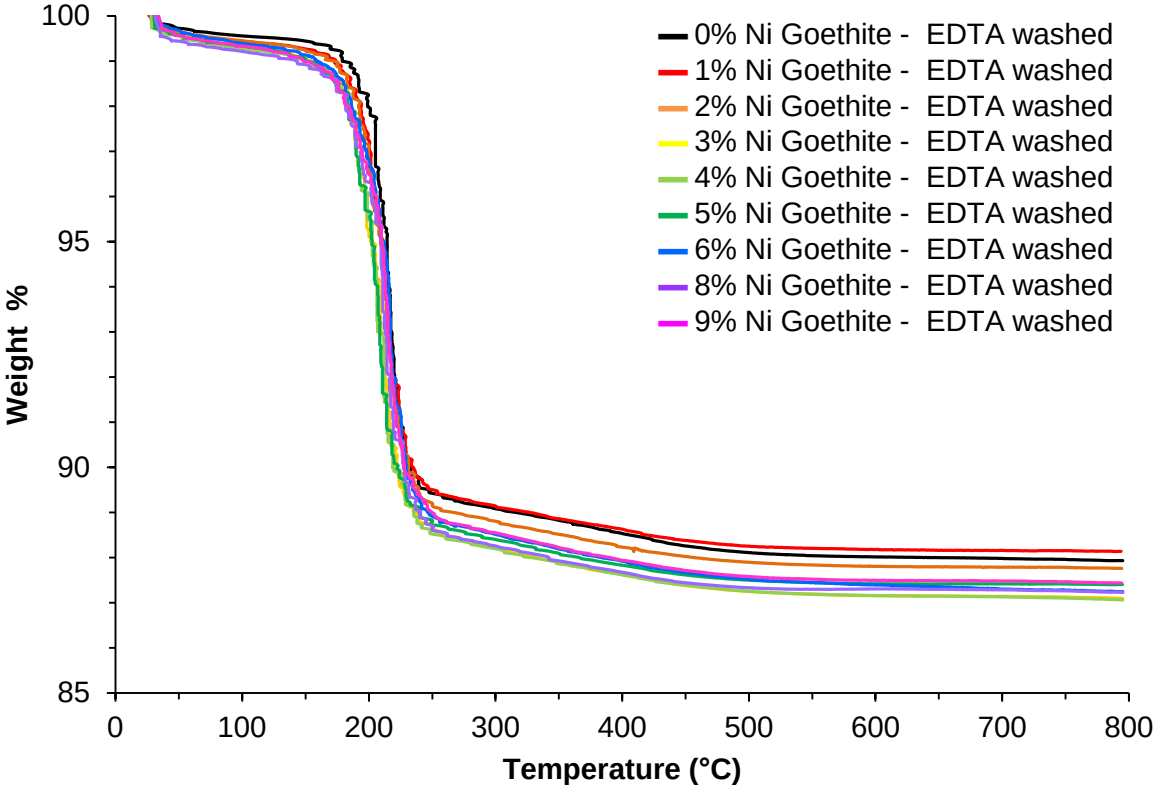

Figure 5.49: Weight loss profiles for EDTA washed Ni-substituted goethites synthesised at 90°C.

A comparison of the weight loss which occurred below 40°C for each of the Ni-goethite samples before and after the EDTA washing are shown in Table 5.19. All of the unwashed Ni-goethite samples show a strong correlation (R^2>0.92) between the target amount of Ni in the goethite sample and the weight loss below 40°C, see Figure 5.50. After the samples had been washed with EDTA, the trend of increasing weight loss below 40°C with increasing Ni content was no longer apparent, and there was virtually no correlation between the amount of Ni in the sample and the weight loss below 40°C (R^2 ~0.2), shown in Figure 5.51. These results show that in the unwashed samples, the amount of ferrihydrite present increases linearly with increasing Ni addition, highlighted by the increasing weight loss observed. After EDTA washing the weight loss below 40°C is very small, indicating an absence of ferrihydrite in the system, regardless of the amount of Ni originally added to the synthesis.

Table 5.19: Comparison of weight loss occurring below 40°C in Ni-goethite samples before and after EDTA washing.

Target %Ni in Goethite	Weight loss (wt%) occurring below 40˚C					
	20°C Synthesis		70°C Synthesis		90°C Synthesis	
	Original	EDTA washed	Original	EDTA washed	Original	EDTA washed
0	4.53	1.40	0.39	0.47	0.33	0.19
1	4.94	1.15	0.75	0.44	0.61	0.30
2	5.54	1.21	0.92	0.75	0.70	0.26
3	5.97	1.08	1.18	0.67	0.87	0.37
4	6.24	1.17	1.48	0.63	1.44	0.41
5	6.96	1.20	2.21	0.49	1.44	0.34
6	7.19	1.03	2.50	0.48	1.54	0.23
8	7.14	1.07	2.54	0.52	2.62	0.48
9	7.65	1.22	4.07	0.26	2.98	0.32

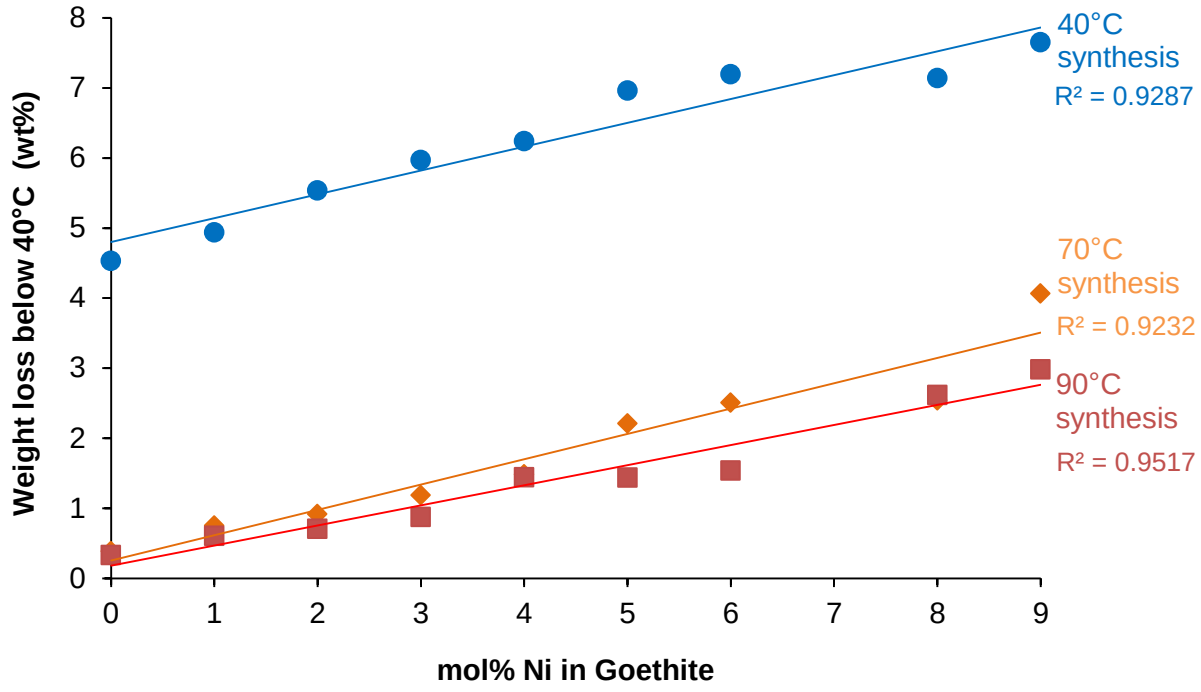

Figure 5.50: The relationship between Ni-content in goethite and weight loss occurring below 40°C.

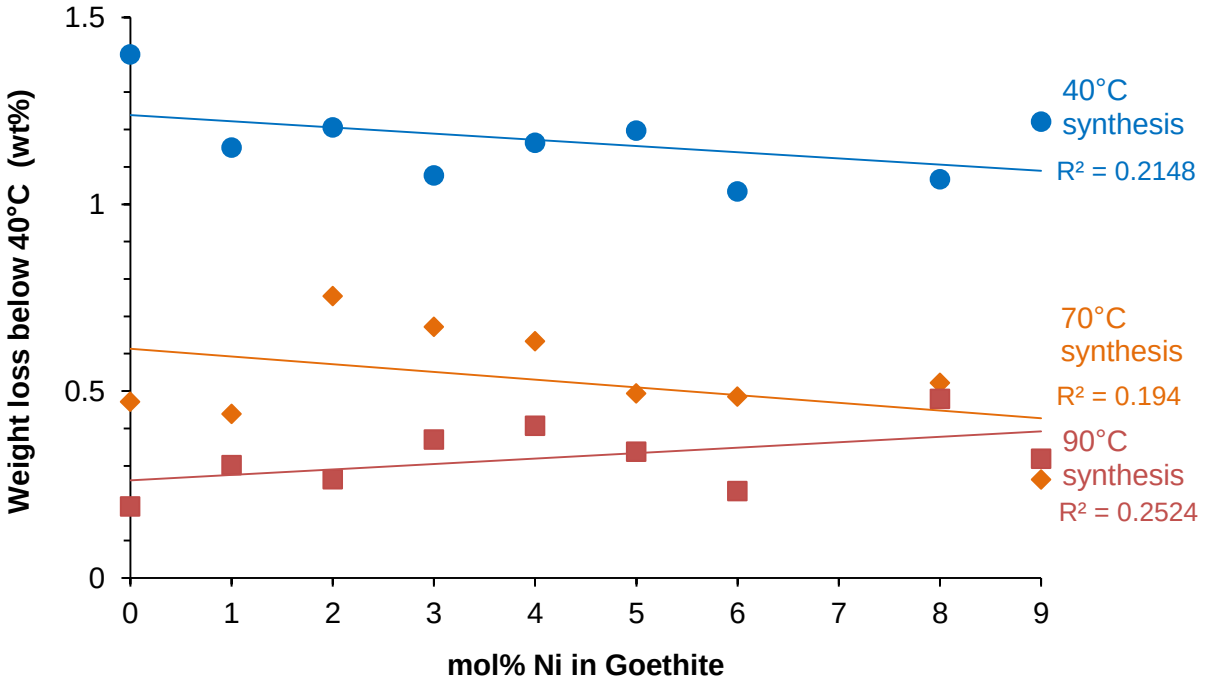

Figure 5.51: The relationship between Ni-content in goethite and weight loss occurring below 40°C after the samples had been washed with EDTA.

It was shown in Chapter 3 that the thermal analysis data for the decomposition of goethite/ferrihydrite mixtures could be used to estimate the proportions of ferrihydrite and goethite in a sample, using the relationship shown in Equation 3.6. Here, this method will be used to estimate the quantities of ferrihydrite that are stabilised, and therefore remain untransformed, in a goethite sample as a result of the addition of nickel.

Equation 3.6: The relationship between the weight loss below 40°C and the wt% ferrihydrite in a goethite/ferrihydrite mixture (y = wt% lost, x = wt% ferrihydrite).

$$y = 0.1042x + 0.6475$$

The proportion of ferrihydrite estimated to be present in each of the Ni-goethite samples by using Equation 3.6 are shown in Table 5.20.

Table 5.20: Estimates of the wt% of ferrihydrite in each of the Ni-substituted goethite samples.

% Ni substitution in goethite	Wt% of sample that is estimated to be ferrihydrite					
	20°C synthesis		70°C synthesis		90°C synthesis	
	Original	EDTA washed	Original	EDTA washed	Original	EDTA washed
0	37	7	-3	-2	-3	-4
1	41	5	1	-2	0	-3
2	47	5	3	1	1	-4
3	51	4	5	0	2	-3
4	54	5	8	0	8	-2
5	61	5	15	-1	8	-3
6	63	4	18	-2	9	-4
8	62	4	18	-1	19	-2
9	67	6	33	-4	22	-3

At a synthesis temperature of 20°C, the unwashed Ni-free goethite sample is estimated to have ~37 wt% ferrihydrite associated with it, rising to ~67 wt% for the 9% Ni goethite (Figure 5.52). After the 20°C synthesis samples had been washed in EDTA, the samples were estimated to have between ~3-7 wt% ferrihydrite associated with them. Unlike the unwashed samples, there is no longer any correlation between the estimated proportion of ferrihydrite in the sample and the Ni content (Figure 5.53). The proportions of ferrihydrite estimated to be remaining in the EDTA washed samples are higher than may be expected. As the goethite samples here were synthesised at low temperature (20°C), the particle size of the goethite will be smaller and therefore the samples are likely to have a greater

amount of surface adsorbed water associated with them than would be found with those samples prepared at a higher temperature. The methodology used for estimating the quantity of ferrihydrite in a sample was developed using goethite synthesised at 70°C, which has very little surface water adsorbed to it. It is probable that the proportions of ferrihydrite estimated to be remaining in the samples synthesised at lower temperatures after the EDTA wash are actually being overestimated, as the weight loss which is measured below 40°C results from surface adsorbed water on the goethite itself, not that resulting from a ferrihydrite phase. As has been mentioned previously, differences in the amount of adsorbed water associated with the goethite phase are not currently accounted for in the quantification method, and further work needs to be undertaken to address this.

The goethite samples synthesised at 70 and 90°C are estimated to contain no ferrihydrite in the Ni-free samples, with the proportion of ferrihydrite increasing linearly to ~33 wt% and 22 wt% respectively in the 9% Ni goethite sample (Figure 5.52).

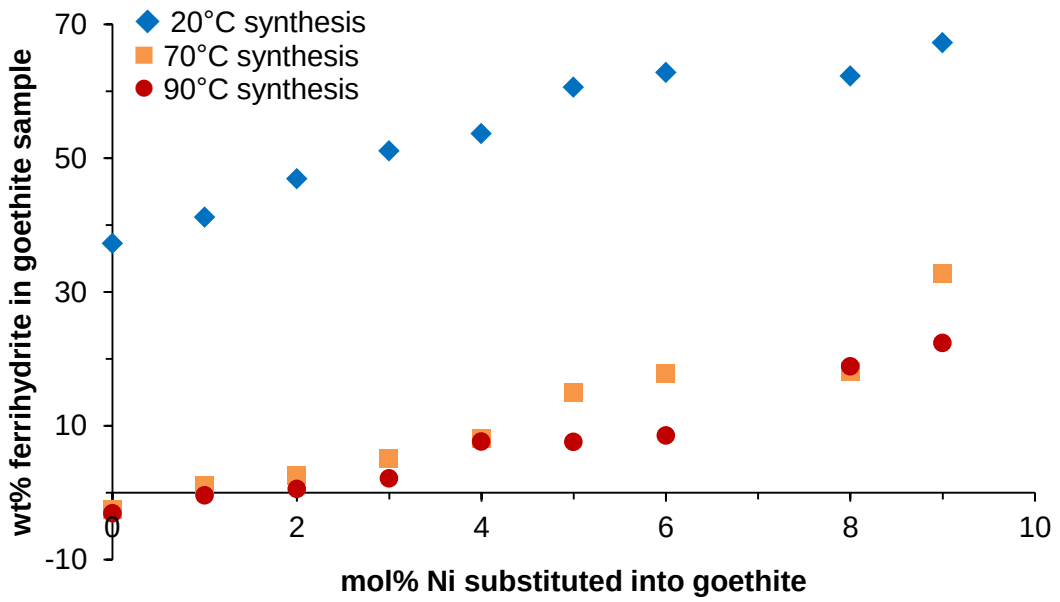

Figure 5.52: Proportions of ferrihydrite estimated to be present in Ni-substituted goethite samples.

After the EDTA washing, virtually all of the Ni-goethite samples prepared at 70 and 90°C are estimated to have no ferrihydrite associated with them, see Figure 5.53. The actual quantities of ferrihydrite estimated to be present are, for most of the samples, negative values. Clearly a negative proportion cannot be an accurate estimation of the quantity, and this, coupled with the higher than expected amounts of ferrihydrite calculated to be

present after the EDTA wash in the 20°C synthesis samples, highlights the difficulties in quantification using this technique. It is believed that these discrepancies in the calculations arise from the surface adsorbed water associated with the goethite, which can vary depending on the particle size (which is related to the synthesis temperature).

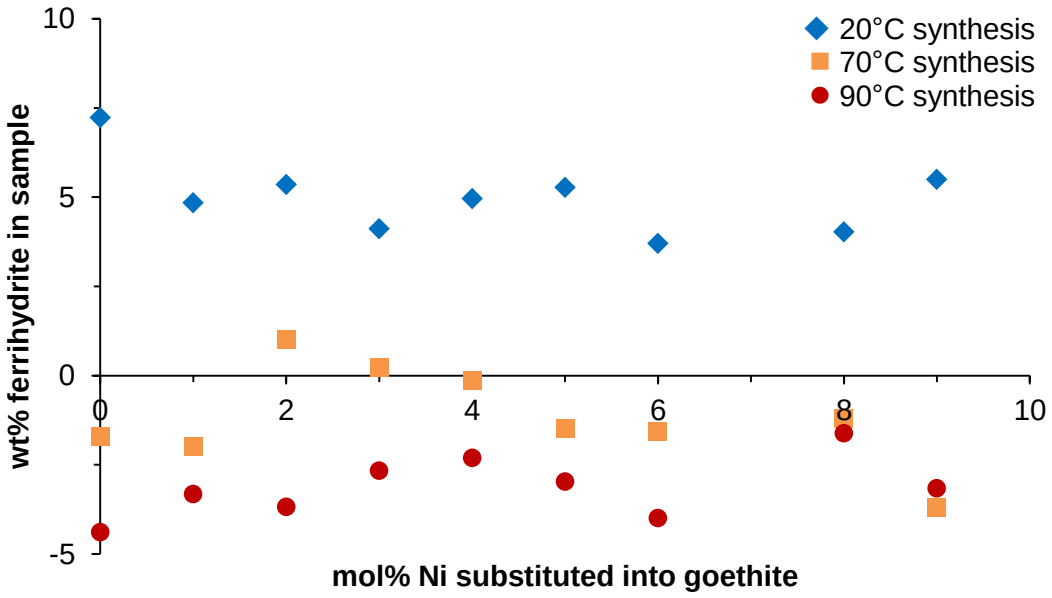

Figure 5.53: Proportions of ferrihydrite estimated to be present in Ni-substituted goethite samples after they had been washed with EDTA.

Raman

Characterisation of each set of Ni-substituted goethite samples by Raman spectroscopy also identified the presence of ferrihydrite in the samples and indicated that, as has been suggested by the other characterisation techniques, the amount of ferrihydrite present increased with increasing Ni incorporation. The spectra recorded for the Ni-goethite samples synthesised at 20°C, Figure 5.54, shows that the band around 670-690 cm^{-1}, and attributed to ferrihydrite, is present in all of the samples, and the definition between the two goethite bands at ~479 and ~550 cm^{-1} is poor, due to the overlapping ferrihydrite band at ~517 cm^{-1}. These observations support the PXRD and TGA findings, showing that at the low temperature synthesis the goethite samples contain untransformed ferrihydrite, regardless of Ni content.

The Raman spectra collected for the set of Ni-goethite samples synthesised at 70°C, shown in Figure 5.55, display clearer evidence for the presence of increasing amounts of ferrihydrite present in the samples (identified by the band at 670-690 cm^{-1}) as the amount of Ni is increased. The Ni-free goethite sample synthesised at 70°C shows no evidence of

the ferrihydrite band at ~670 cm^{-1}, and there is good definition between the goethite bands at ~479 and ~550 cm^{-1}. As the amount of Ni incorporated into the goethite is increased, the definition between the two bands decreases (as a result of the overlap with the ~517 cm^{-1} ferrihydrite band) and the band at 670-690 cm^{-1} appears and then increases in intensity with Ni addition.

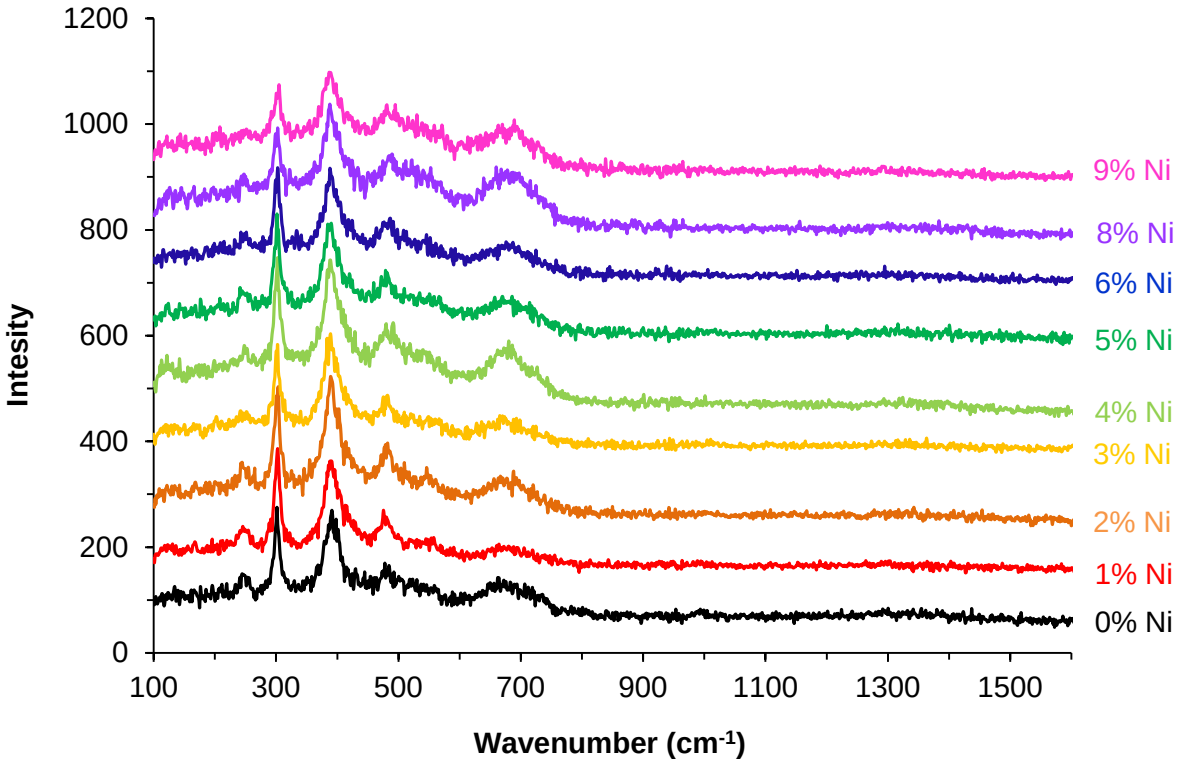

Figure 5.54: Raman spectra of Ni-substituted goethite synthesised at 20°C.

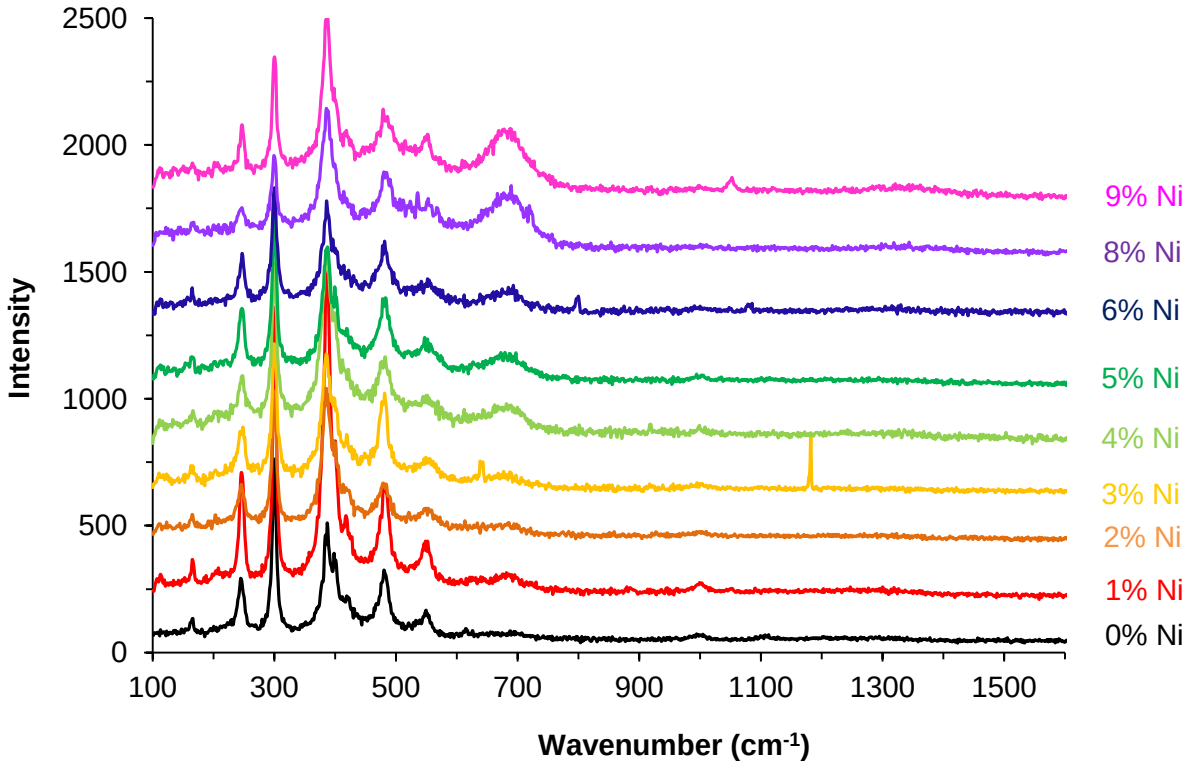

Figure 5.55: Raman spectra of Ni-substituted goethite synthesised at 70°C.

After the Ni-goethite samples had been washed with EDTA, the ferrihydrite band at ~670 cm^{-1} is no longer present, and there is clear definition between both of the goethite bands (~479 and 550 cm^{-1}) at all Ni concentrations and synthesis temperatures (see Figures 5.56 and 5.57).

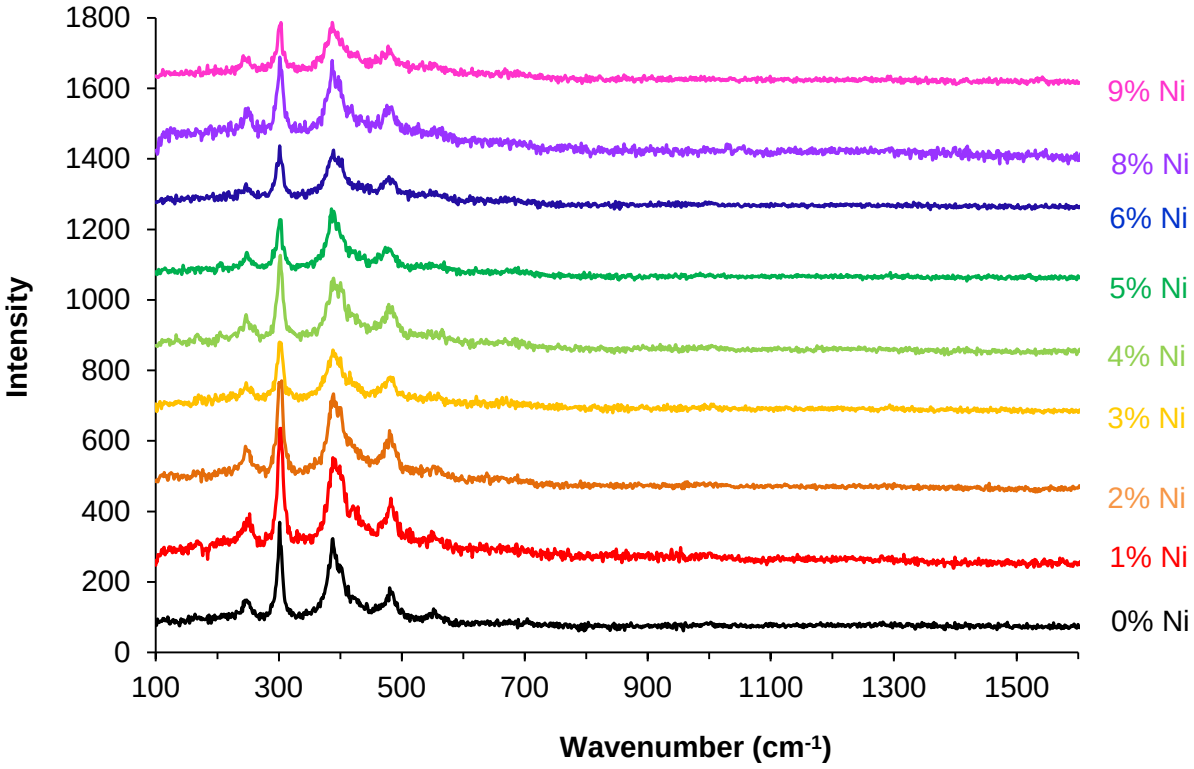

Figure 5.56: Raman spectra of Ni-substituted goethite synthesised at 20°C, after EDTA washing.

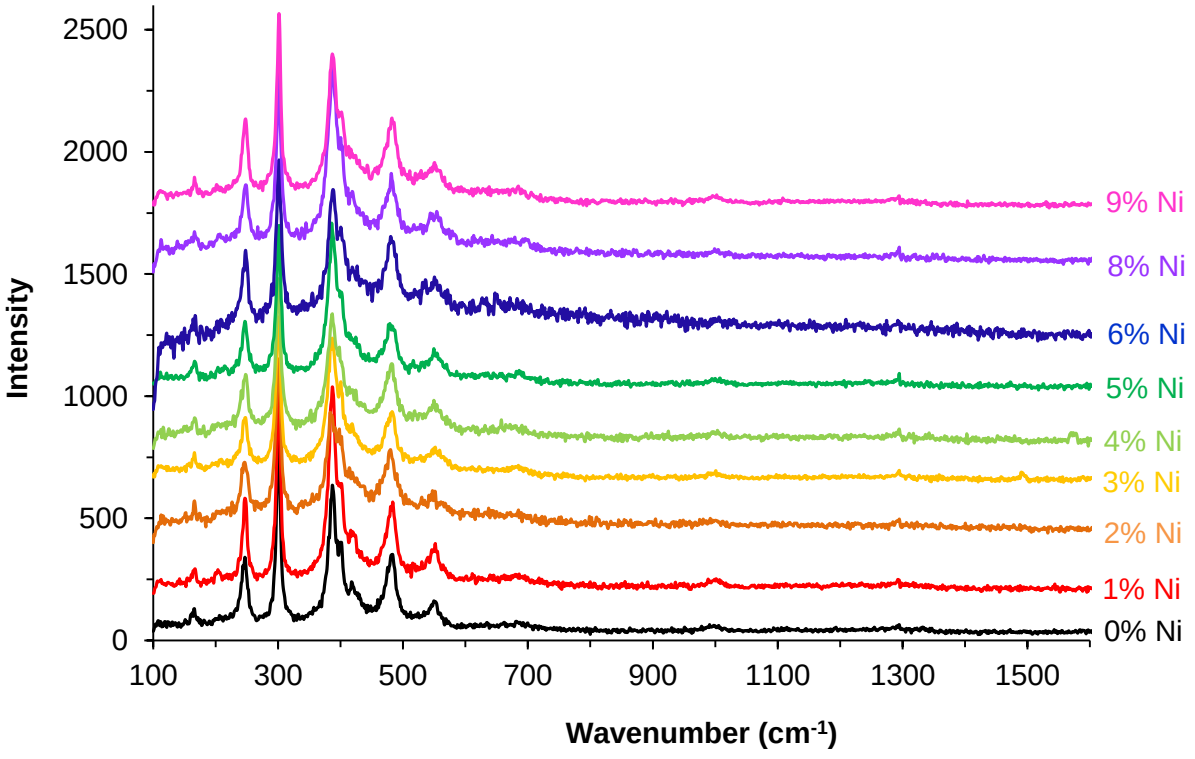

Figure 5.57: Raman spectra of Ni-substituted goethite synthesised at 70°C, after EDTA washing.

Inductively Coupled Plasma – Optical Emission Spectroscopy (ICP-OES)

The characterisation of the Ni goethite samples discussed so far has focused on identifying the presence of ferrihydrite associated with the samples, and subsequently its successful removal using the EDTA wash. The residency of the nickel, be that in goethite or ferrihydrite (or the proportions in each) is yet to be quantified. This section aims to establish the partitioning of nickel between these two phases using ICP-OES and SEM.

ICP-OES was used to determine the elemental composition of the resulting EDTA solutions after the goethite samples had been washed in them (solutions shown in Figure 5.37). The results, displayed in Table 5.21, and Figures 5.58 and 5.59, are presented as the amount of each element (in wt%) that has been removed from the solid phase, as a percentage of the expected value (based on the target composition of the system). For example, in the Ni-free goethite samples, at the 20°C synthesis temperature ~23% of the total Fe that should have been present was removed, whereas at 70°C only 0.2% was removed and at 90°C, no Fe was removed at all.

Table 5.21: Composition of EDTA washing solutions determined by ICP-OES for Ni-substituted goethite samples.

%Ni	Percentage of Fe/Ni removed (wt%)					
	20°C synthesis		70°C synthesis		90°C synthesis	
	Fe	Ni	Fe	Ni	Fe	Ni
0	22.9	0.0	0.2	0.0	0.0	0.0
1	25.2	71.5	1.6	16.6	0.3	7.7
2	29.6	42.5	2.0	21.2	2.3	25.8
3	31.7	48.2	4.9	31.8	4.8	34.2
4	33.9	51.4	8.1	42.2	8.2	42.0
5	37.0	54.7	15.3	53.3	10.8	45.8
6	40.4	58.6	15.2	53.9	17.7	60.8
8	42.9	61.3	24.2	62.7	23.2	61.9
9	41.9	59.6	29.6	64.5	27.4	65.3

For the samples synthesised at 20°C, a large amount of Fe was removed from all of the Ni goethites, increasing from ~23% of the total in the 0% Ni goethite, through to ~42% in the 9% Ni goethite. At this synthesis temperature a large proportion of the Ni is also removed, ranging from ~43% of the nickel in the 2% Ni goethite sample, to ~60% in the 9% Ni goethite sample. The ICP data for the 1% Ni goethite sample indicates that over 70 wt% of the Ni was removed from the sample. This is significantly higher than the amount of Ni that was removed from any other sample, and this single result does not fit with the trend followed by the rest of the data (Figure 5.59). It is likely that the reason for this

unexpectedly high Ni content is as a result of errors made in the preparation of the sample for ICP-OES analysis.

The same trend that is observed in the ICP-OES data for the goethites synthesised at 20°C, is also observed for the data obtained for the 70 and 90°C synthesis temperature goethites, although the amount of Fe removed starts at ~0% in the Ni free goethite, and increases to 29.6% and 27.4% respectively for the Ni-rich goethite samples. At these higher synthesis temperatures a huge amount of Ni is still removed from the 9% Ni goethite samples – 64.5% of the total Ni at a synthesis temperature of 70°C, and 65.3% at 90°C.

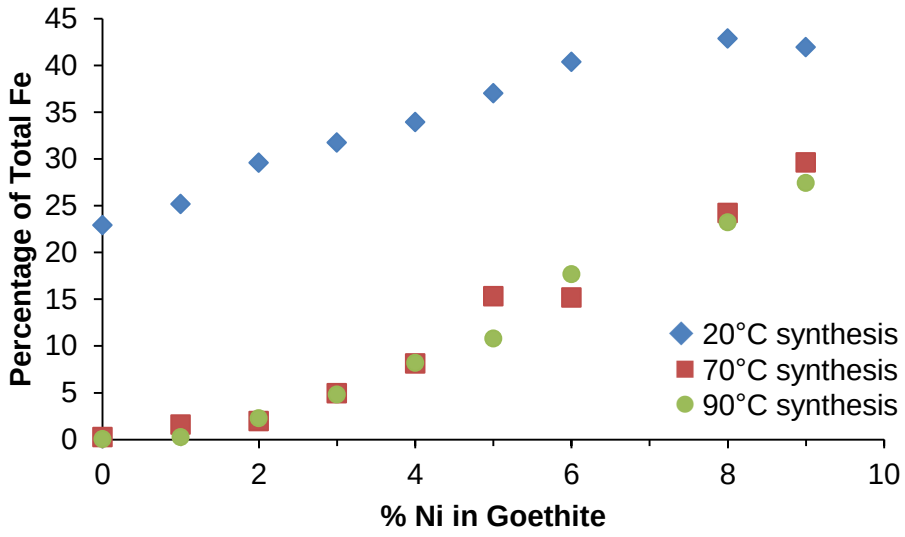

Figure 5.58: Percentage of total Fe removed from Ni-goethite samples as a result of the EDTA wash.

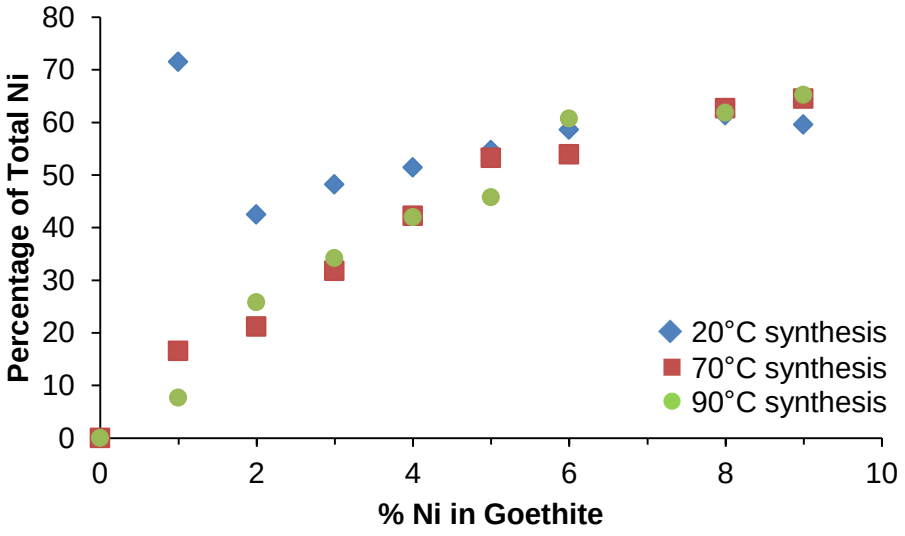

Figure 5.59: Percentage of total Ni removed from Ni-goethite samples as a result of the EDTA wash.

The results obtained using ICP-OES show that at Ni addition levels of 4% and greater, over 40% of the nickel added to the system is not incorporated into the structure of goethite.

The pH of the EDTA solutions in which the goethite had been washed was taken to monitor any changes that occurred as a result of the washing process, and these values are shown in Table 5.22. The 0.1M EDTA solution has a pH of 4.56 (prior to it being used to wash the goethite). Once the goethite samples had been washed in the EDTA solution, regardless of the synthesis temperature, the pH increased linearly with increasing nickel, see Figure 5.60.

Table 5.22: pH measurements of EDTA solutions after goethite samples had been washed in them.

Target %Ni in goethite sample	pH measurement of EDTA solution after goethite had been washed in it:		
	20°C synthesis	70°C synthesis	90°C synthesis
0	5.95	4.80	4.72
1	6.00	5.30	4.82
2	6.18	5.36	5.15
3	6.27	5.56	5.30
4	6.25	5.70	5.48
5	6.38	5.81	5.57
6	6.54	5.85	5.82
8	6.58	6.14	6.03
9	6.52	6.49	6.23

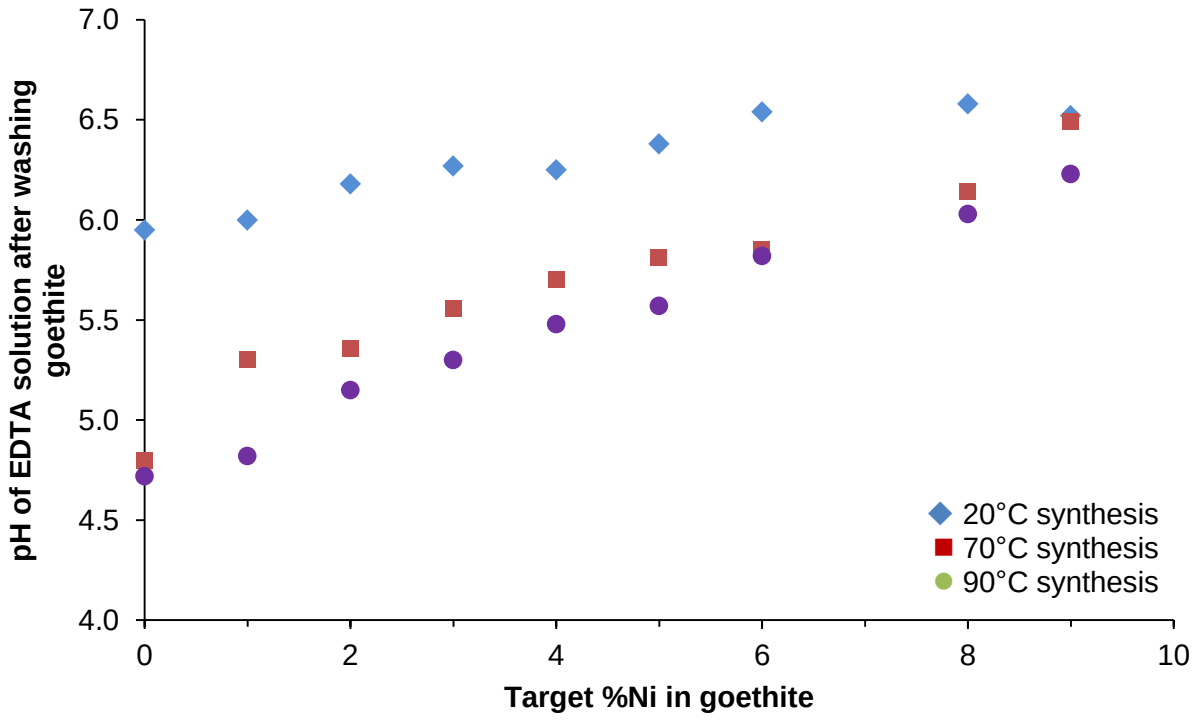

Figure 5.60: Relationship between the %Ni in goethite samples and the pH of the EDTA solution after washing.

In Chapter 3, the relationship between the pH of the EDTA solution after the goethite had been washed in it and the amount of Fe in the EDTA solution (measured by ICP-OES) was discussed, with a suggestion that pH measurements could be used as a quick and easy method to estimate the amount of Fe (from the ferrihydrite) that had been removed from the samples as a result of the EDTA wash. This system is more complex, as both Fe and Ni are being removed by the EDTA solution, however, when plotted (see Figure 5.61) a strong relationship can be seen between the total concentration of Fe+Ni in the solution and the pH. The data shows that as the concentration of Fe+Ni in the EDTA solution increases, the pH also increases – in other words the more ferrihydrite in the original solid sample (which is removed by the EDTA wash), the higher the pH of the resulting washing solution.

Although it is not possible to establish the individual concentrations of Fe and Ni using this technique, pH measurements could be used to estimate the combined concentration of the elements in solution.

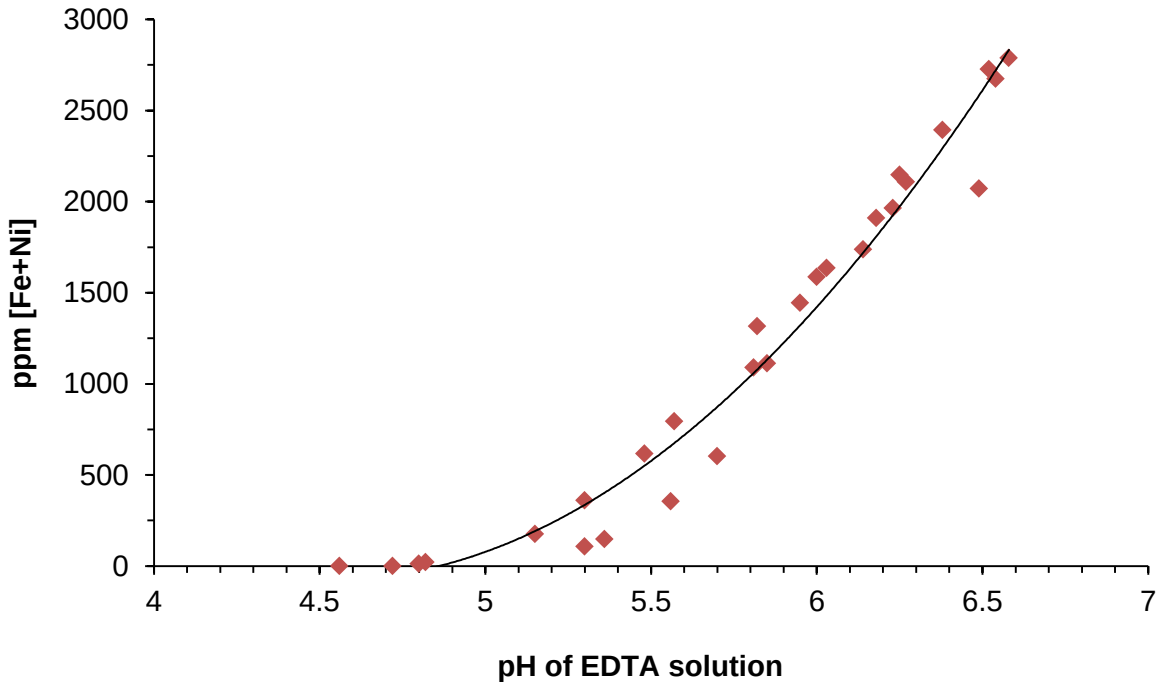

Figure 5.61: The relationship between pH of the EDTA solution and ppm of Fe+Ni that it contains.

Scanning Electron Microscopy (SEM)

All of the characterisation work carried out so far has confirmed that ferrihydrite does form as a secondary phase with Ni-goethites, with increasing amounts of ferrihydrite present in those samples which have the most Ni added to them. The EDTA washing technique has been shown to successfully remove this secondary ferrihydrite phase, as well as the Ni associated with it.

Elemental maps of the 9% Ni goethite samples obtained using FEG-SEM show the heterogeneous nature of this unwashed synthesis product, shown in Figure 5.62. The map shows both Ni-rich (green) and Ni-poor (red) areas, and it is believed that the Ni-rich areas are where there is a large amount of ferrihydrite. The ICP-OES data of the EDTA washing solutions showed that in a 9% Ni goethite sample, over 60% of the Ni that was added to the system was removed in the EDTA wash – i.e. it was part of the ferrihydrite phase. If ~60% of the Ni is present in association with ferrihydrite this would account for the Ni-rich areas being observed on the map.

After the 9% Ni goethite sample had been washed with EDTA, the elemental map (Figure 5.63) shows a homogenous sample with an even distribution of Ni and Fe throughout since there are no excessively red or green areas visible on the map. This suggests that the remaining nickel, that which isn't associated with the ferrihydrite, is incorporated into the goethite structure.

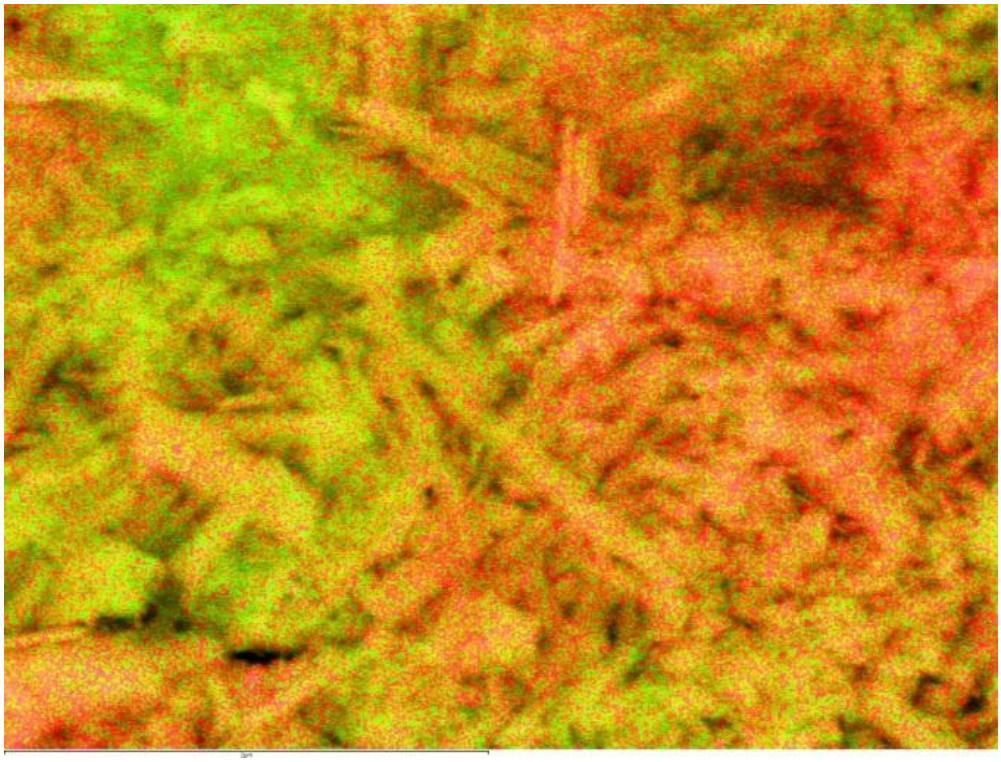

Figure 5.62: An elemental map of 9% Ni goethite, prepared at 70°C, showing the heterogeneous nature of the sample. Ni shown in green, Fe shown in red.

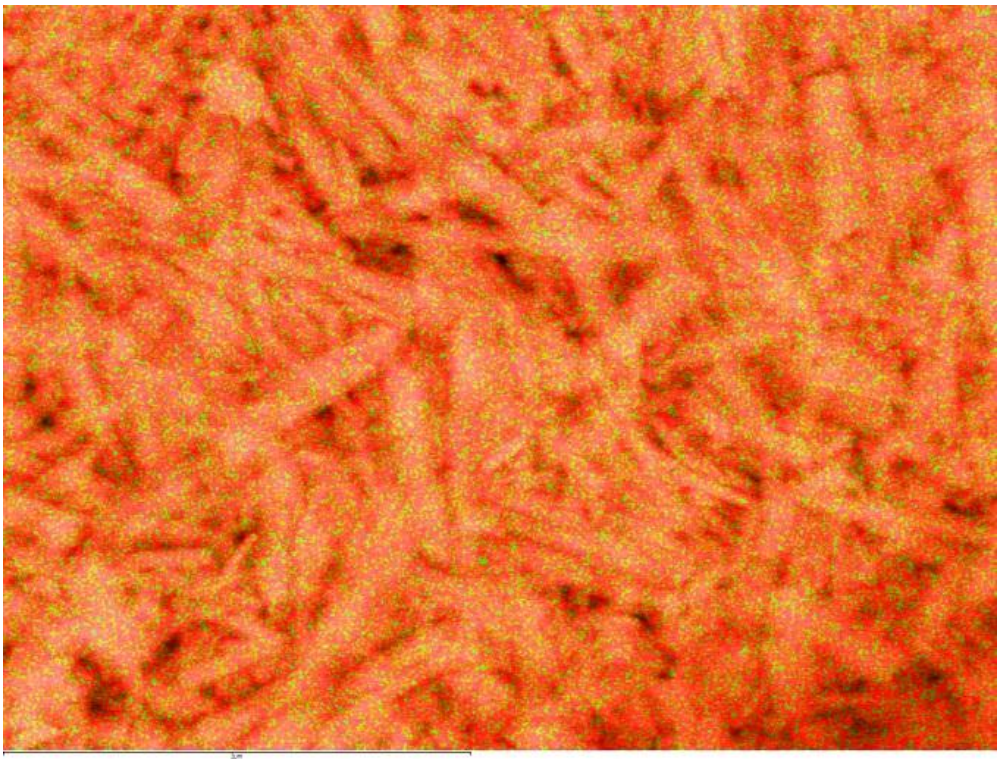

Figure 5.63: An elemental map of 9% Ni goethite, prepared at 70°C, after EDTA washing showing the homogenous nature of the sample. Ni shown in green, Fe shown in red.

SEM was then used to analyse the elemental composition of the Ni-goethite samples (synthesised at 70°C) before and after washing with EDTA, to establish the actual Ni content. A number of different area analyses were carried out on each sample in the series (example shown in Figure 5.64) and both the average Ni content and the range of Ni compositions found are shown in Table 5.23.

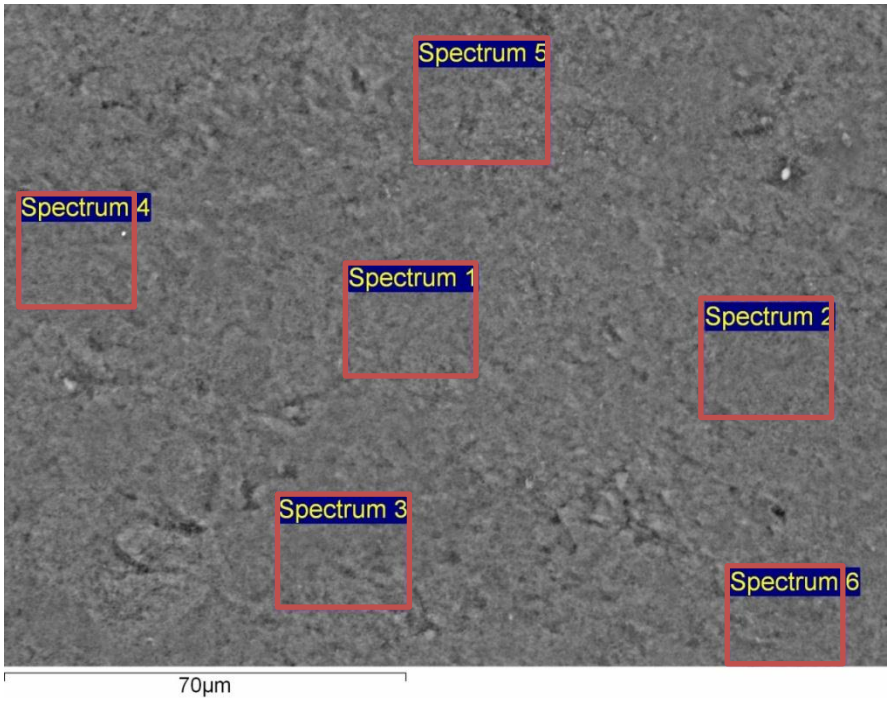

Figure 5.64: An example of how the compositional analysis of Ni-goethite samples was carried out using SEM. A number of areas were selected at different sites on the sample (areas marked in red).

Table 5.23: Amount of nickel (wt%) measured in Ni-substituted goethite samples (mol% values shown in blue).

Target Ni Level	Measured Ni Level			
Wt% Ni (mol% Ni)	Average wt% Ni (mol% Ni)		Range (wt% Ni)	
	Original Goethite	EDTA Washed Goethite	Original Goethite	EDTA Washed Goethite
0 (0)	0 (0)	0 (0)	0	0
0.66 (1)	0.59 (0.89)	0.40 (0.60)	0.41-0.76 (0.62-1.15)	0-0.6 (0-0.91)
1.32 (2)	1.20 (1.82)	0.89 (1.35)	1.06-1.42 (1.60-2.15)	0.78-1.13 (1.18-1.71)
1.98 (3)	1.76 (2.67)	1.13 (1.71)	1.47-2.03 (2.23-3.08)	1.03-1.25 (1.56-1.89)
2.64 (4)	2.20 (3.34)	1.26 (1.91)	1.54-2.71 (2.33-4,11)	1.17-1.40 (1.77-2.12)
3.30 (5)	2.89 (4.38)	1.30 (1.97)	2.55-3.49 (3.87-5.30)	1.19-1.44 (1.80-2.18)
3.96 (6)	3.46 (5.25)	1.52 (2.30)	2.92-4.4 (4.43-6.68)	1.26-1.69 (1.91-2.56)
5.27 (8)	4.79 (7.27)	1.68 (2.55)	4.28-5.2 (6.49-7.89)	1.57-1.81 (2.38-2.74)
5.93 (9)	5.08 (7.71)	1.38 (2.09)	4.17-5.78 (6.33-8.77)	1.08-1.49 (1.64-2.26)

In the unwashed set of samples, the amount of Ni measured increases as expected with the experimental Ni incorporation level (see Figure 5.65). There is quite a large spread in the data, in excess of 1 wt% in some samples, supporting the observations made on the elemental map (Figure 5.62) that the samples are heterogeneous, with both Ni-rich and Ni-poor areas.

After washing with EDTA, the average Ni content in each of the goethite samples is a maximum of ~1.6 wt% (2.5 mol%), indicating that the majority of the nickel is residing in the ferrihydrite phase which is removed by the EDTA washing process. In fact, closer inspection of the data reveals that even at very low Ni incorporation levels (e.g. 1 mol%) almost a third of the nickel is associated with the ferrihydrite phase, not incorporated into the structure of goethite, see Table 5.24. The spread of data is also much smaller in the EDTA washed samples, approximately 0.3 wt% compared with the ~1 wt% observed in the unwashed samples, again supporting the observations made from the elemental map (Figure 5.63) that the EDTA washed samples are much more homogenous than their unwashed counterparts.

Table 5.24: Proportion of nickel estimated to be associated with the ferrihydrite phase.

Target Composition		Percentage of nickel associated with ferrihydrite phase.
Mol% Ni	Wt% Ni	
0	0	N/A
1	0.66	32
2	1.32	26
3	1.98	36
4	2.64	43
5	3.30	55
6	3.96	56
8	5.27	65
9	5.93	73

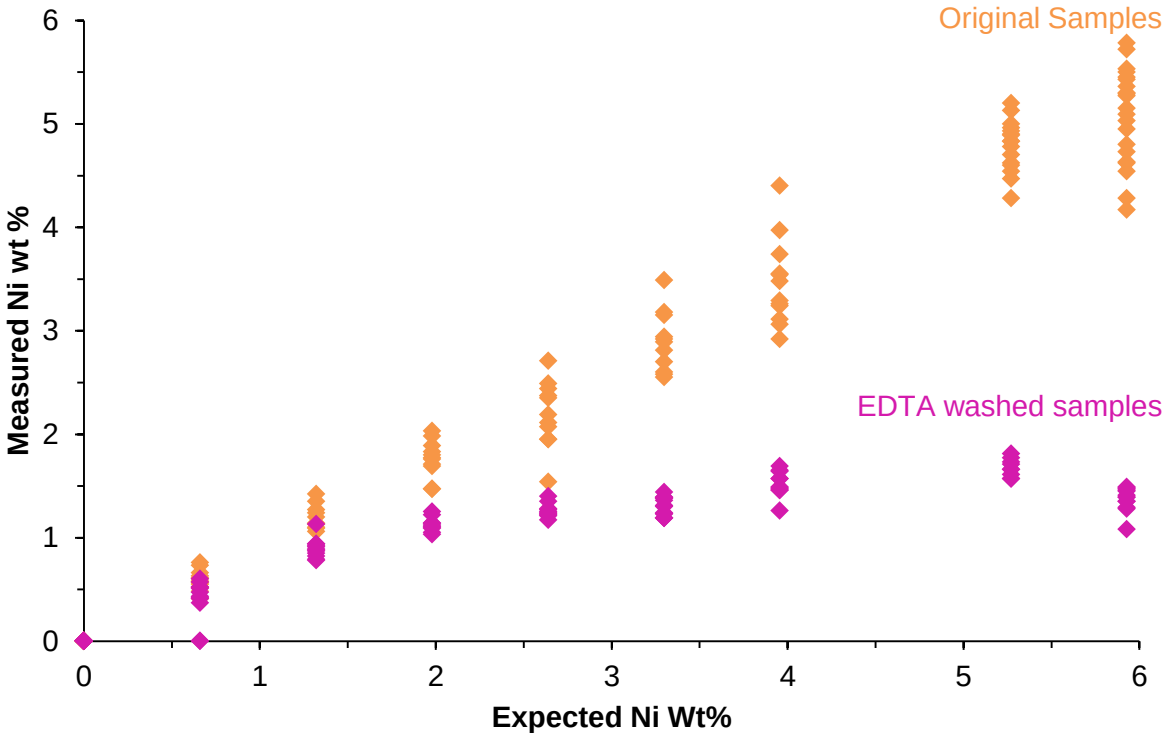

Figure 5.65: The effect of EDTA washing on the wt% Ni measured in substituted goethite samples.

5.6. Summary

Goethite has the ability to accommodate a number of different metal cations into its structure, via isomorphous substitution for Fe. In this chapter, the substitution of Cr, Al, Co, Mn and Ni into the goethite structure was examined, and the phases that form at higher levels of attempted incorporation were identified.

In most cases, the levels of substitution that appear to have been achieved in this work (from PXRD analysis) are higher than those reported elsewhere. Single phase goethite was identified with up to 20 mol% Cr, 13.5 mol% Al, 12 mol% Co and between 10-25 mol% Mn. Shifts in the peak positions with increasing incorporation levels were observed in the PXRD patterns of Al and Co substituted goethites, indicative of M-for-Fe substitution occurring in the goethite structure. Unit cell refinements of the Al, Co and Mn substituted samples showed changes in the size of the unit cell which could be explained by substitution of Fe by the foreign cation. It is believed that at least one other unidentified phase was present in the samples in all cases (accounting for the higher substitution levels that appear to be observed), which was probably poorly crystalline (e.g. ferrihydrite) and hosting the excess foreign cation.

A more in depth study was carried out on Ni incorporation and association with goethite. The addition of nickel to the synthesis system was shown to stabilise the ferrihydrite precursor from which these samples form, preventing its transformation to goethite. Using the characterisation methodology developed in Chapter 3 (e.g. TGA) there was found to be a linear relationship between the amount of nickel added to the synthesis and the amount of ferrihydrite estimated to be present in the samples. This associated ferrihydrite phase was difficult to detect using PXRD, and as was seen in the goethite samples with Al, Co, Mn and Cr incorporation, it appeared that single phase goethite had formed with far higher Ni substitution levels than had previously been reported. The increasing ferrihydrite levels in the samples as the Ni content increased were identified using Raman spectroscopy, and attempts to quantify the amount were made using PXRD and TGA. As was shown in the Ni free samples, thermal analysis proved to be the most favourable identification and quantification technique.

In order to establish the precise residence of Ni in the system, that is the amount incorporated into the structure of goethite and the amount associated with ferrihydrite, the EDTA washing technique was tested on the Ni-rich samples. The technique appeared to be effective at removing the ferrihydrite phase whilst leaving the goethite, and its incorporated Ni, intact.

ICP-OES of the EDTA washing solutions and SEM of the solid samples before and after washing indicated that Ni is mainly associated with the ferrihydrite phase. As was previously discussed, some of the nickel that is removed by the EDTA wash may be adsorbed to the surface of the goethite, rather than associated with the ferrihydrite phase. Investigations into the possibility and extent of nickel surface adsorption to goethite were not conducted as part of this research and further work would be required in order to ascertain the influence (if any) this may be having.

The amount of nickel found to be structurally incorporated into goethite prepared at 70°C was ~2.5 mol%, far lower than the 5.5 mol% maximum reported elsewhere. However, those authors used a longer ageing time and lower temperature for the synthesis than was used in this study, which could account for the differences observed.[2] Krehula *et al.* (2005) reported incorporation of 5 mol% Ni into goethite, but they carried out the synthesis at higher temperatures and pressures.[4] Carvalho et Silva *et al.* (2002) reported that they achieved maximum Ni incorporation into goethite of 3.2 mol%, via a synthesis procedure more comparable to that which was used in this work.

By demonstrating how nickel stabilises ferrihydrite, inhibiting its transformation to goethite in synthetic systems, questions arise about whether this is occurring in natural systems. The presence of nickel rich ferrihydrite phases alongside the goethite could account for the differences in leachability that have been observed in lateritic ore samples. This work will now focus on trying to find evidence of ferrihydrite in natural ore materials in order to support this theory.

5.7. References

1 A. Manceau, M.L. Schlegel, M. Musso, V.A. Sole, C. Gauthier, P.E. Petit, F. Trolard, *Geochimica et Cosmochimica Acta*, (2000) **64**, 3643-3661.

2 B. Singh, D. Sherman, R.J. Gilkes, M.A. Wells, J.F.W. Mosselmans, *Clay Minerals,* (2002) **37**, 639-649.

3 J.P. Beukes, E.W. Giesekke, W. Elliott, *Minerals Engineering,* (2000) **13**, 1573-1579.

4 S. Krehula, S.Music, S. Popovic, *Journal of Alloys and Compounds,* (2005) **403**, 368-375

5 M.L. Carvalho-E-Silva, A.Y. Ramos, H.C.N. Tolentino, J. Enzweiler, S.M. Netto, M.D.C.M. Alves, *American Mineralogist*, (2003) **88**, 876-882.

6 R.D. Shannon, C.T. Prewitt, *Acta Crystallographica* (1969) **B25**, 925-946.

7 K. Norrish, R.M. Taylor, *European Journal of Soil Science,* (1961) **12**, 294-306.

8 D.G. Schulze, *Clays and Clay Minerals*, (1984) **32**, 36-44.

9 U. Schwertmann, U. Gasser, H. Sticher, *Geochimica et Cosmochimica Acta,* (1989) **53**, 1293-1297.

10 M.A. Wells, R.W. Fitzpatrick, R.J. Gilkes, *Clay and Clay Minerals*, (2006) **54**, 176-194.

11 U. Schwertmann, G. Pfab, *Geochimica et Cosmochimica Acta,* (1994) **58**, 4349-4352.

12 N. Kaur, B. Singh, B.J. Kennedy, M. Gräfe, *Geochimica et Cosmochimica Acta,* (2009) **73**, 582-593.

13 W. Stiers, U. Schwertmann, *Geochimica et Cosmochimica Acta,* (1985) **49**, 1909-1911.

14 E.E. Sileo, M. Alvarez, E.H. Rueda, *International Journal of Inorganic Materials*, (2001) **3**, 271-279.

15 M.H. Ebinger, D.G. Schulze, *Clays and Clay Minerals,* (1989) **37**, 151-156.

16 M. Alvarez, E.E. Sileo, E.H. Rueda, *American Mineralogist*, (2008) **93**, 584-590.

17 C.A. dos Santos, A.M.C. Horbe, C.M.O. Barcellos, J.B. Marimon da Cunha, *Solid State Communications*, (2001) **118**, 449-452.

18 L.R. Bernstein, G.A. Waychunas, *Geochimica et Cosmochimica Acta,* (1987) **51**, 623-630.

19 B.S.W. Dawson, J.E. Fergusson, A.S. Campbell, E.J.B. Cutler, *Geoderma*, (1985) **35**, 127-143.

20 C.F. Sampson, *Acta Crystallographica*, (1969) **B25**, 1683.

21 J.L. Hazemann, J.F. Berar, A. Manceau, *Materials Science Forum*, (1991) **79**, 821-826.

22 L.S. Dent Glasser, L. Ingram, *Acta Crystallographica*, (1949) **2**, 104-106.

23 C. Milton, D.E. Appleman, M.H. Appleman, E.C.T. Chao, *US Geological Survey Professional Paper*, (1976) **887**, 1-29.

24 H.T. Evans, S.Block, *American Mineralogist*, (1953) **38**, 1242-1250.

25 J. Chenavas, J.C. Joubert, J. Capponi, M. Marezio, *Journal of Solid State Chemistry*, (1973) **6**, 1-15.

26 A.N. Christensen, S.J. Jensen, *Acta Chemica Scandinavica,* (1967) **21**, 121-126.

27 S.J. Li, C. Zheng, K.C. Lobring, *Z. Kristallogr.*, (2003) **218**, 11-12.

28 L.Z. Vegard, *Physics*, (1921) **5**, 17.

29 U. Schwertmann, R.M. Cornell, *Iron Oxides in the Laboratory – Preparation and Characterization,* (Wiley, 1991).

30 V.M. Goldschmidt, *Journal of the Chemical Society*, (1937) 655-673.

31 R.M. Cornell, U. Schwertmann, *The iron oxides: structure, properties, reactions, occurrences and uses,* (Wiley, 1996).

32 R.G. McDonald, B.I. Whittington, *Hydrometallurgy*, (2008) **91**, 35-55.

33 R. Giovanoli, R. M. Cornell, *Zeitschrift für Pflanzenernährung und Bodenkunde,* (1992) **155**, 455-460.

34 J. L. Jambor, J. E. Dutrizac, *Chemistry Reviews*, (1998) **98**, 2549-2585.

35 L. Charlet, A. A. Manceau, *Journal of Colloid and Interface Science*, (1992) **148**, 443.

36 J.B. Harrison, V.E. Berkheiser, *Clays and Clay Minerals,* (1982) **30**, 97.

37 C.W. Correns, W. Von Engelhardt, *Nachr. Akad. Wiss. Göttingen, Math. Phys. K.I,* (1941) **213,** 131–137.

38 B. Singh, R.J. Gilkes, *Journal of Soil Science,* (1992) **43**, 77-98.

39 U. Schwertmann, L. Carlson, *Soil Science Society of America Journal,* (1994) **58**, 256-261.

40 V.A. Bronevoi, L.N. Furmakova, *Zap. Vses. Mineral. Obshchest*, (1975) **104**, 461-466.

41 M.V. Fey, J.B. Dixon, *Clays and Clay Minerals,* (1981) **29**, 91-100.

42 E.E. Sileo, A.Y. Ramos, G.E. Magaz, M.A. Blesa, *Geochimica et Cosmochimica Acta*, (2004) **68**, 3053-3063.

43 H.A. Jahn, E. Teller, *Proceedings of the Royal Society of London. Series A, Mathematical and Physical Sciences,* (1937) **161**, 220-235.

44 M. Alvarez, E.E. Sileo, E.H. Rueda, *Chemical Geology*, (2005) **216**, 89-97.

45 A.C. Scheinost, H. Stanjek, D.G. Schulze, U. Gasser, D.L. Sparks, *American Mineralogist*, (2001) **86**, 139-146.

46 M.L.M. De Carvalho-E-Silva, C.S.M. Partiti, J. Enzweiler, S. Petit, S.M. Netto, S.M.B De Oliveira, *Hyperfine Interactions*, (2002) **142**, 559-576.

47 C. Sudakar, G.N. Subbanna, T.R.N Kutty, *Journal of Materials Science,* (2004) **39**, 4271-4286.

48 R.M. Cornell, W. Schneider, R. Giovanoli, *Journal of Chemical Technology and Biotechnology,* (2007) **53**, 73-79.

49 F. Trolard, G. Bourrie, E. Jeanroy, A.J. Herbillon, H. Martin, *Geochimica et Cosmochimica Acta*, (1995) **59**, 1285-1297.

50 W.H. Emmons, The Enrichment of Ore Deposits, Bulletin 625. *United States Geological Survey,* 1917.

51 N. Morandi, G. Dalrio, *American Mineralogist*, (1973) **58**, 835-839.

52 J.F. Riley, *Mineralogical Magazine,* (1980) **43**, 733-739.

53 N.D Sindeeva, *Mineralogy and Types of Deposits of Selenium and Tellurium*, (Interscience Publishers, 1964).

54 J.R. Craig, *The Americal Mineralogist*, (1971) **56**, 1301-1311.

55 U.G. Gasser, E. Jeanroy, C. Mustin, O. Barres, R. Nüesch, J. Berthelin, A.J. Herbillon, *Clay Minerals*, (1996) **31**, 465-476.

56 U. König, G. Chol, *Journal of Applied Crystallography,* (1968) **1**, 124.

57 National Bureau of Standards (U.S.) Monograph. 25, 10, (1972), 38.

58 Y.V. Swamy, B.B. Kar, J.K. Mohanty, *Hydrometallurgy*, (2003) **69**, 89-98.

59 U. Schwertmann, P. Cambier, E. Murad, *Clays and Clay Minerals*, (1985) **33**, 369-378

60 T. Nagano, S. Nakashima, S. Nakayama, K. Osada, M. Senoo, *Clays and Clay Minerals*, (1992) **40**, 600-607.

Chapter 6.

Characterisation of Goethite Containing Ores from Selected Laterite Deposits

6.1. Introduction

The formation of high grade nickel laterite ores is relatively poorly understood. Because of this, their characteristics, for instance leaching behaviours, are difficult to predict. This results in ores, even from the same ore body, that appear to be mineralogically/geologically similar, displaying a huge amount of variability in their leaching performance. [1, 2] Atmospheric heap leaching (described in Chapter 1) to extract Ni from limonitic laterite ores is being highlighted as a breakthrough in environmentally conscious extraction techniques, due to its small carbon footprint and low energy consumption. [3, 4] In order to improve the extraction techniques, in turn improving the economic/environmental performance, it is vital to understand the precise mineralogy of the Ni-containing phases that are present in these nickeliferous limonite ores.

The goethite materials studied in this chapter and described later, were sampled from laterite systems that were found to be extremely complex natural environments. The samples host many different mineral phases and are chemically impure. As a result of this, comparison of the results from the characterisation of natural goethites to those obtained from characterisation of their synthetic analogues may not be straightforward.

In Chapter 5, this thesis demonstrated how the inclusion of Ni into synthetic goethite samples also resulted in the stabilisation of a secondary Ni-ferrihydrite phase which was difficult to identify, in part owing to its poor crystallinity, using standard characterisation techniques (e.g. PXRD). Alternative methods to identify ferrihydrite were investigated, and thermal analysis proved to be a particularly capable technique. It is suggested that ferrihydrite may also be present in these natural ore samples, stabilised by the presence of foreign cations in the ore body, and this theory will be investigated as a possible explanation for the variability in the ease of extraction observed for Ni from different ore materials.

A number of naturally occurring goethite samples, taken from two different localities and from preliminary characterisation work, determined to be both Ni-rich and Ni-poor, were selected from the collections at the Natural History Museum.[5] These goethite samples were then characterised to try to draw comparisons with the observations that were made in Chapter 5 for the synthetic Ni-goethites, in particular, looking for evidence of ferrihydrite within these natural samples, and any correlation between that and the amount of nickel present. The use of the methodologies developed in Chapter 3 (e.g. using PXRD and TGA) to estimate the quantity of ferrihydrite present in natural samples will also be tested where possible.

6.1.1. Çaldağ Deposit

The Çaldağ nickel laterite deposit is located in the west of Turkey and is estimated to contain 33 million tons of Ni ore, with an average nickel grade of 1.14 wt%, see Figure 6.1.[6] Goethite is the main ore mineral present and the maximum concentration of Ni in the goethite at this location is reported to be 3 wt%, found near the base of the limonite zone.[7] Ten samples taken from this deposit were investigated in this study.

Figure 6.1: The location of the Çaldag mine site in Turkey. [8]

6.1.2. Cerro Matoso Deposit

The Cerro Matoso nickel deposit is located in northern Columbia (Figure 6.2) and

Figure 6.2: The location of the Cerro Matoso mine site in Columbia.[8]

combines a lateritic nickel ore deposit with a low-cost ferronickel smelter. It is the world's second largest producer of ferronickel and boasts some of the lowest operating costs.[9,10] The deposit has reserves of approximately 40 Mt, with an average grade of 2.4 wt% Ni.[1] Six samples from the Cerro Matoso nickel deposit were investigated in this study.

6.2. Experimental Methods

A number of naturally occurring goethite samples were selected (examples are shown in Figure 6.3) and ground to a fine powder by hand using a pestle and mortar. The samples labelled 'CN' were taken from the Çaldağ deposit, and those labelled 'CM' were taken from the Cerro Matoso deposit. These goethite samples were then characterised by PXRD in order to confirm or otherwise that goethite was the only phase present, and then further characterisation work was conducted using a range of other techniques (e.g. TGA, elemental analysis and EDTA washing) to enable comparison with the synthetic Ni-goethites discussed in Chapter 5.

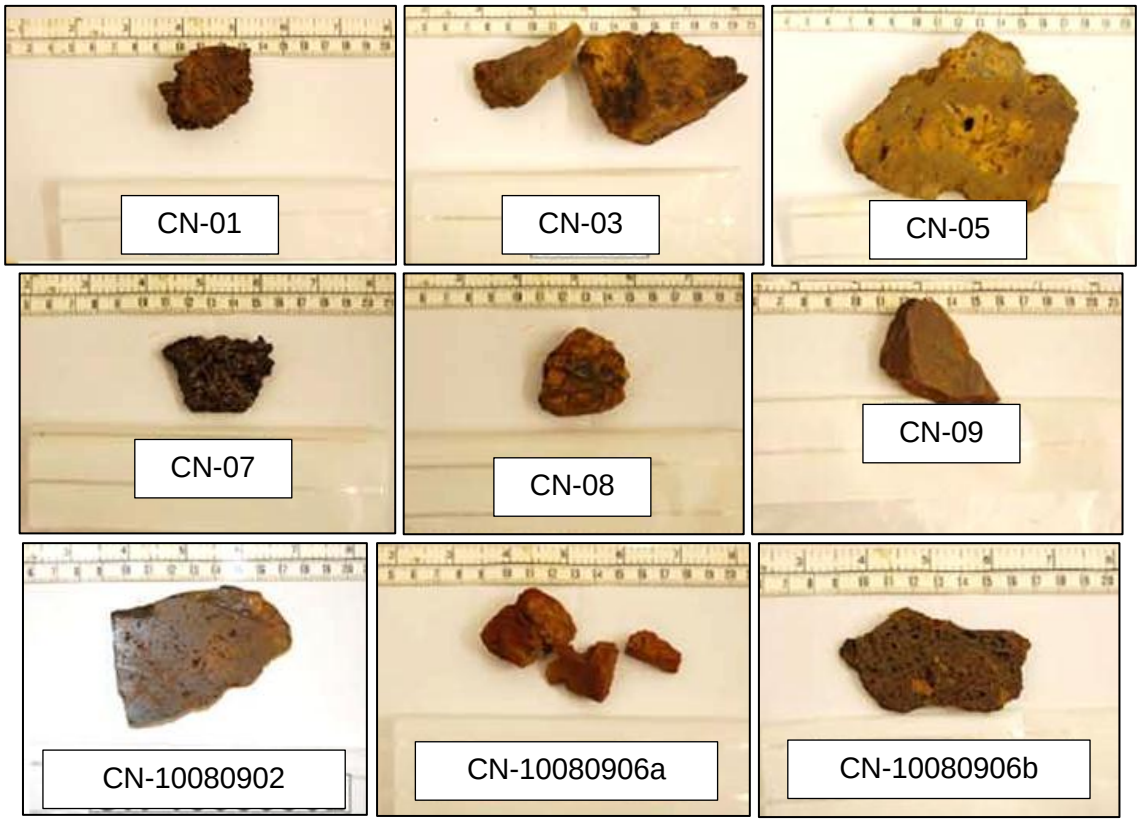

Figure 6.3: Appearance of some naturally occurring goethite samples.

6.3. Results and Discussion

6.3.1. PXRD

Initially, the natural goethite samples taken from the laterite deposit were characterised by PXRD to confirm the phases present; the results are shown in Table 6.1 and Figures 6.4-6.15. Data are presented in sets depending on the mineral phases found to be present by PXRD characterisation. Samples BM1905,46 and BM18571 are from the NHM collections and are used as standards for phase identification and quantification by PXRD. These have been included in the study as phase pure or 'ideal' samples to use for comparison with the natural laterite samples.

Table 6.1: Phases identified by PXRD in natural goethite samples.

Sample Name	Phases Identified by PXRD	Figure
BM1905, 46	Goethite	Figure 6.4
BM18571	Goethite	Figure 6.4
CM022	Goethite, $MgAl_2O_4$	Figure 6.5
CM026	Goethite, quartz, iron aluminum oxide	Figure 6.6
CM038	Goethite, maghemite, gibbsite ($Al(OH)_3$), $MgAl_2O_4$	Figure 6. 7
CM039	Goethite, $MgAl_2O_4$	Figure 6.5
CM040	Goethite, $MgAl_2O_4$, illite	Figure 6.12
CN-04	Goethite, montmorillonite	Figure 6.13
CM043	Goethite, Magnetite, Chlorite-serpentine	Figure 6.9
CN-05	Goethite, Quartz	Figure 6.8
CN-08	Goethite, maghemite	Figure 6.10
CN-03	Goethite	Figure 6.4
CN-10080906b	Goethite, Quartz, $NiFe_2O_4$	Figure 6.11
CN-10080902	Goethite	Figure 6.4
CN-01	Goethite	Figure 6.4
CN-07	Goethite, Quartz	Figure 6.8
CN-09	Goethite, Quartz, Hematite, Spinel-type phase	Figure 6.14
CN-10080906a	Goethite, Hematite, clay-type phase	Figure 6.15

Only five of the 18 samples that were characterised here consisted of monophasic goethite (as identified by PXRD analysis), the remainder containing secondary iron minerals such as magnetite, hematite and maghemite, as well as other impurity phases, for example quartz, aluminosilicate/clay phases and spinel type phases.

As the majority of the natural laterite samples were found to be multi-phase, making direct comparisons with the synthetic Ni-goethite samples requires careful consideration. The difficulties result from the presence of secondary mineral phases in association with the goethite, which will influence the data obtained through the characterisation methods used.

In previous sections (e.g. Chapter 3), ferrihydrite was identified and the quantity estimated using PXRD data collected on a set of synthetic samples. Even in the simple, two phase synthetic goethite/ferrihydrite systems, analysis of PXRD data to determine the presence of ferrihydrite was challenging, and the proportion of ferrihydrite estimated to be present often appeared unreliable. In goethite/ferrihydrite samples containing a third phase, a small amount of hematite, the proportion of ferrihydrite estimated to be present was found to be inaccurate, as the amounts were underestimated. As the natural samples in this study were mostly multi-phase, identifying and quantifying the proportion of ferrihydrite present reliably and consistently using the PXRD technique will not be possible.

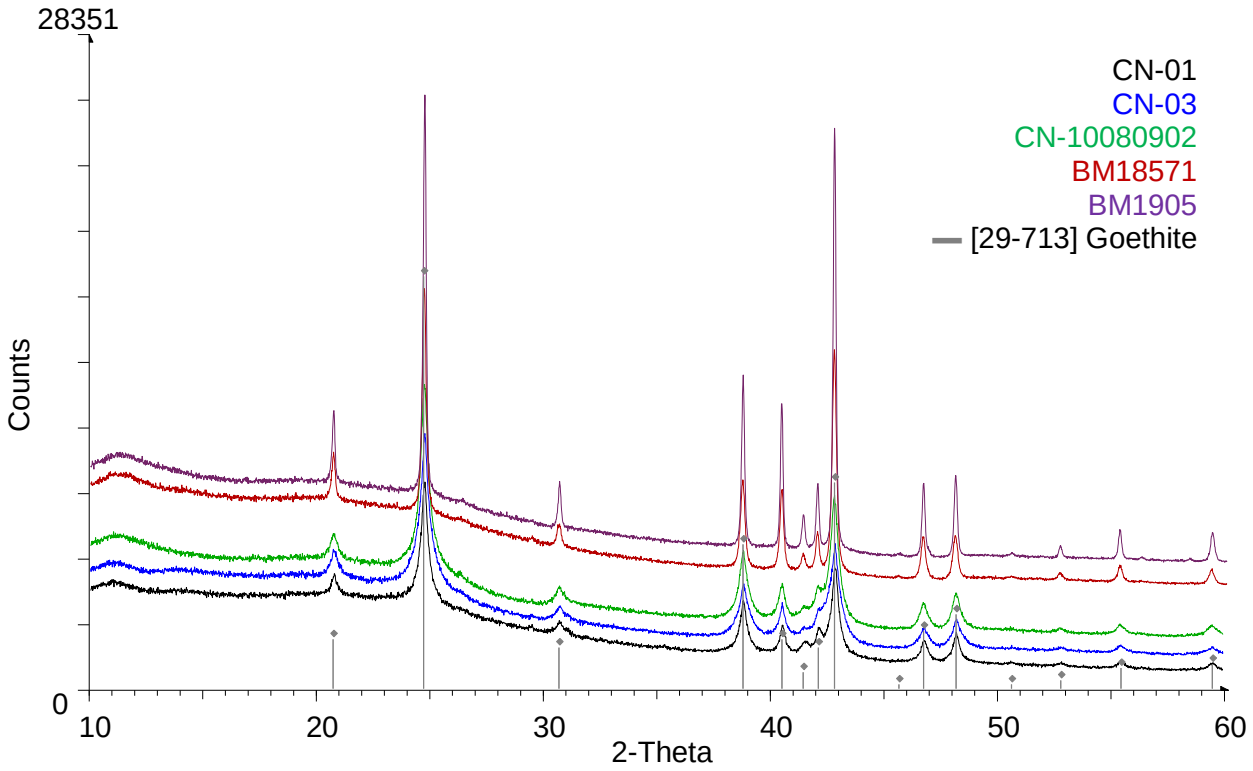

Figure 6.4: PXRD patterns collected for natural samples CN-01, CN-03, CN-10080902, BM18571 and BM1905. Data collected using Co $K_{\alpha 1}$ radiation.

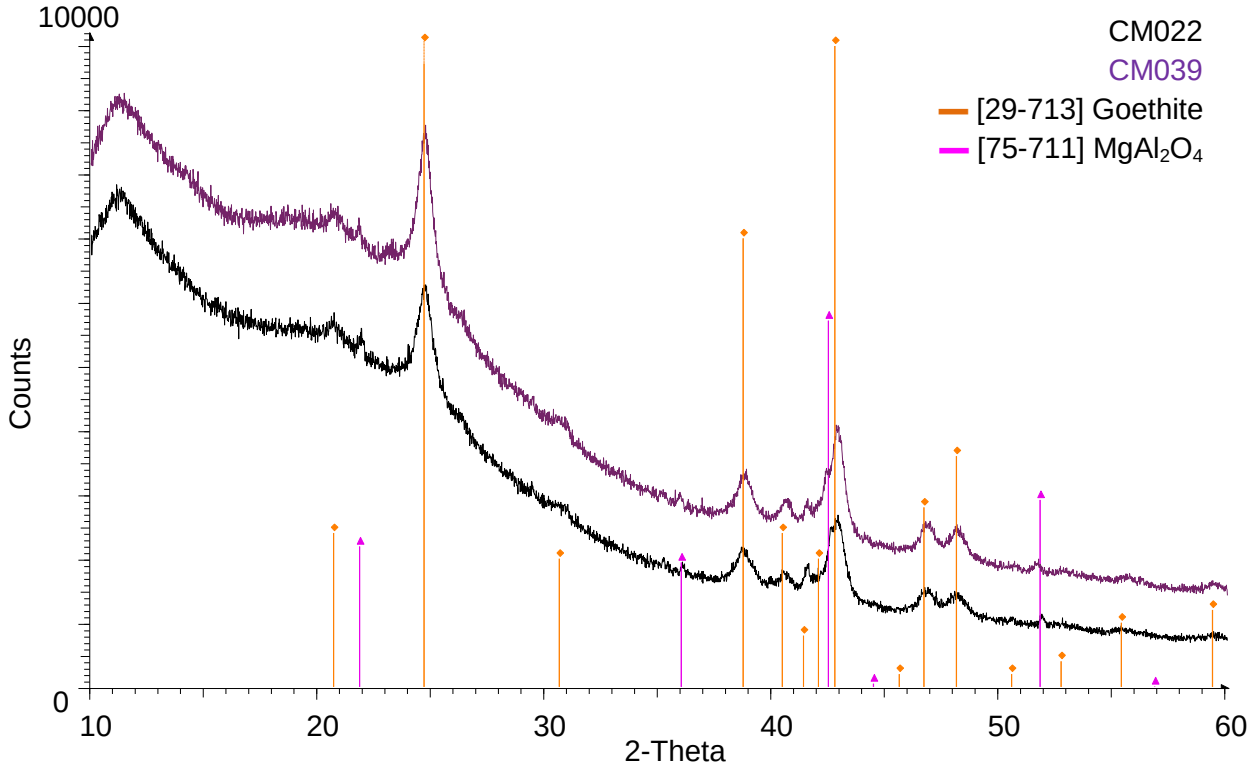

Figure 6.5: PXRD patterns collected for natural samples CM022 and CM039. Data collected using Co $K_{\alpha 1}$ radiation.

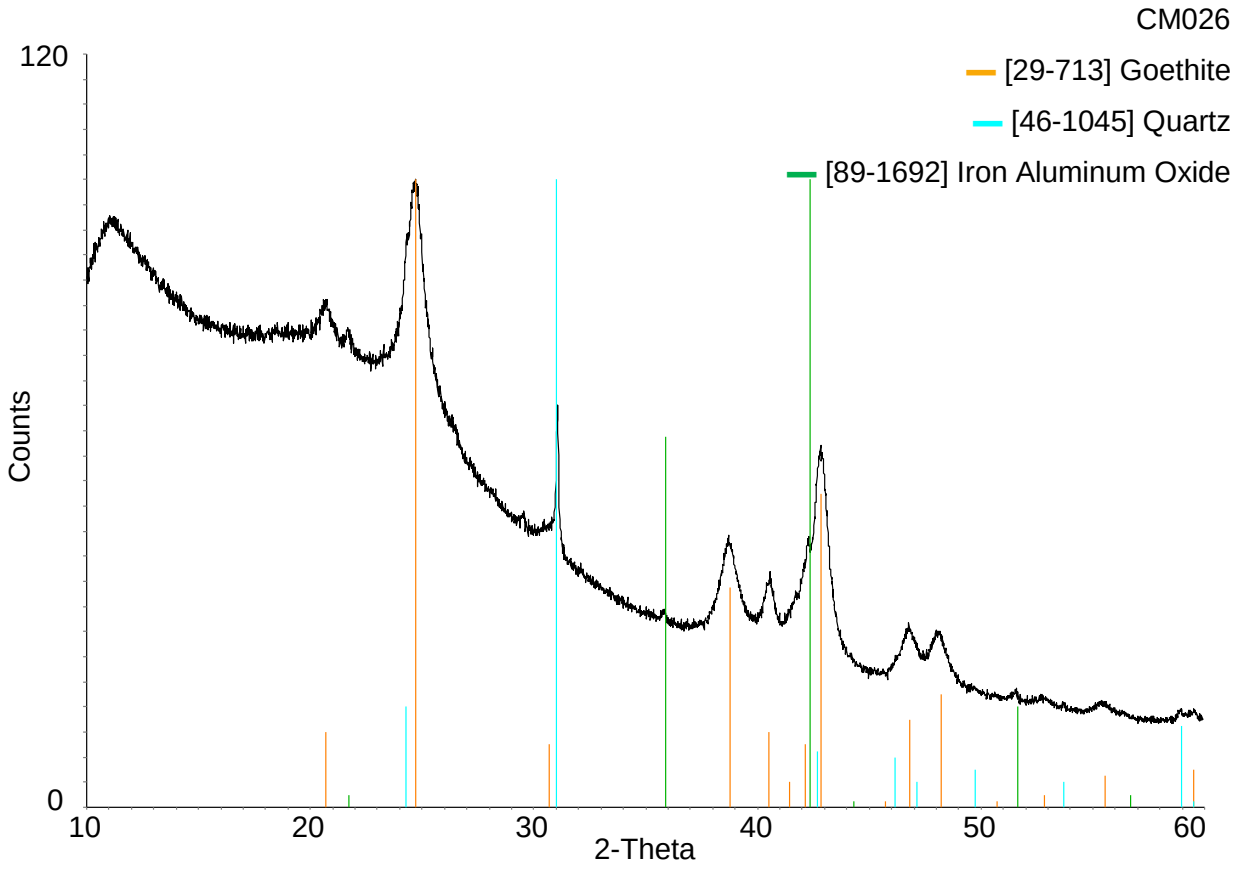

Figure 6.6: PXRD patterns collected for natural sample CM026. Data collected using Co $K_{\alpha 1}$ radiation.

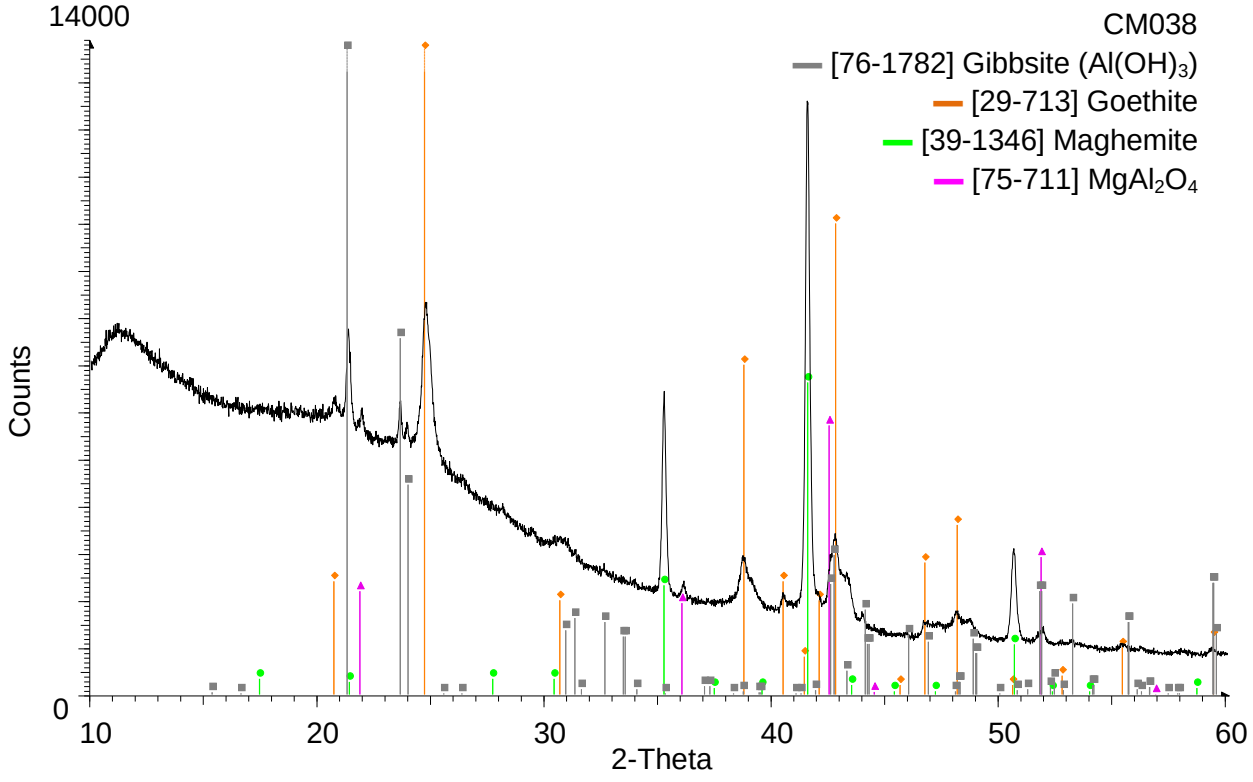

Figure 6.7: PXRD patterns collected for natural sample CM038. Data collected using Co $K_{\alpha 1}$ radiation.

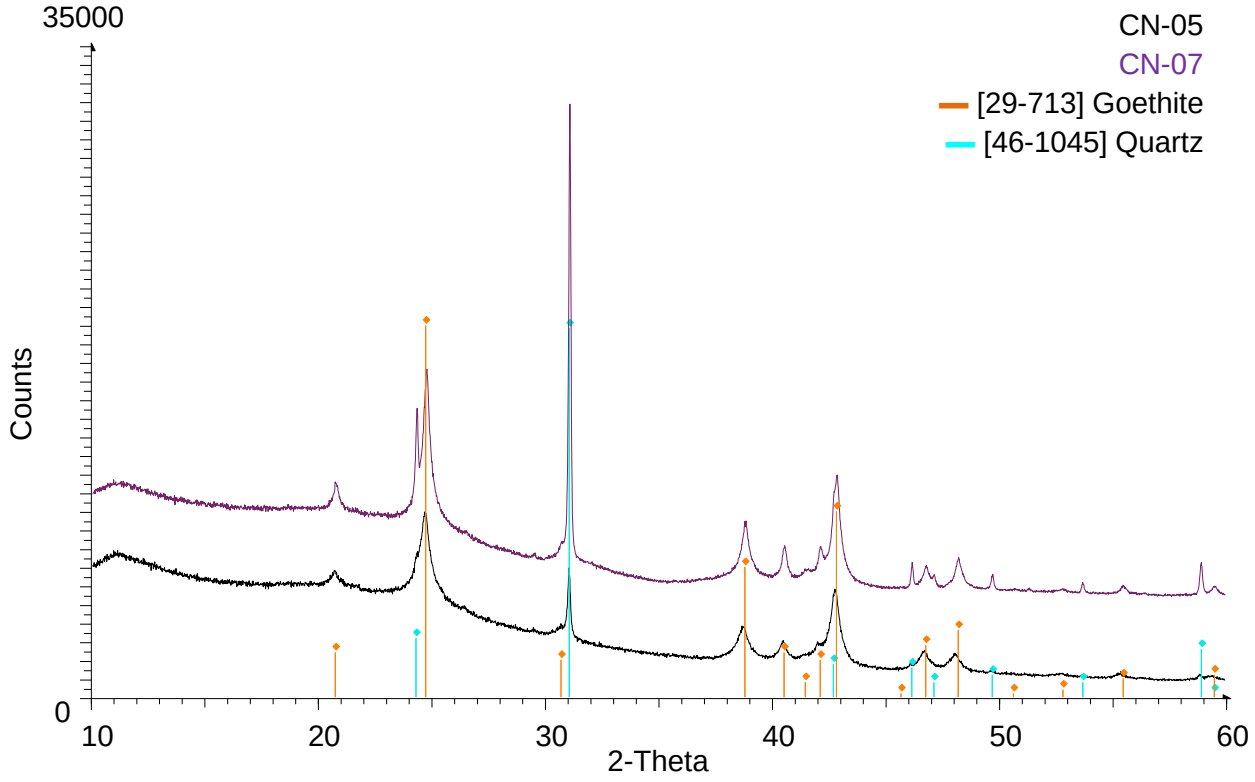

Figure 6.8: PXRD patterns collected for natural samples CN-05 and CN-07. Data collected using Co $K_{\alpha 1}$ radiation.

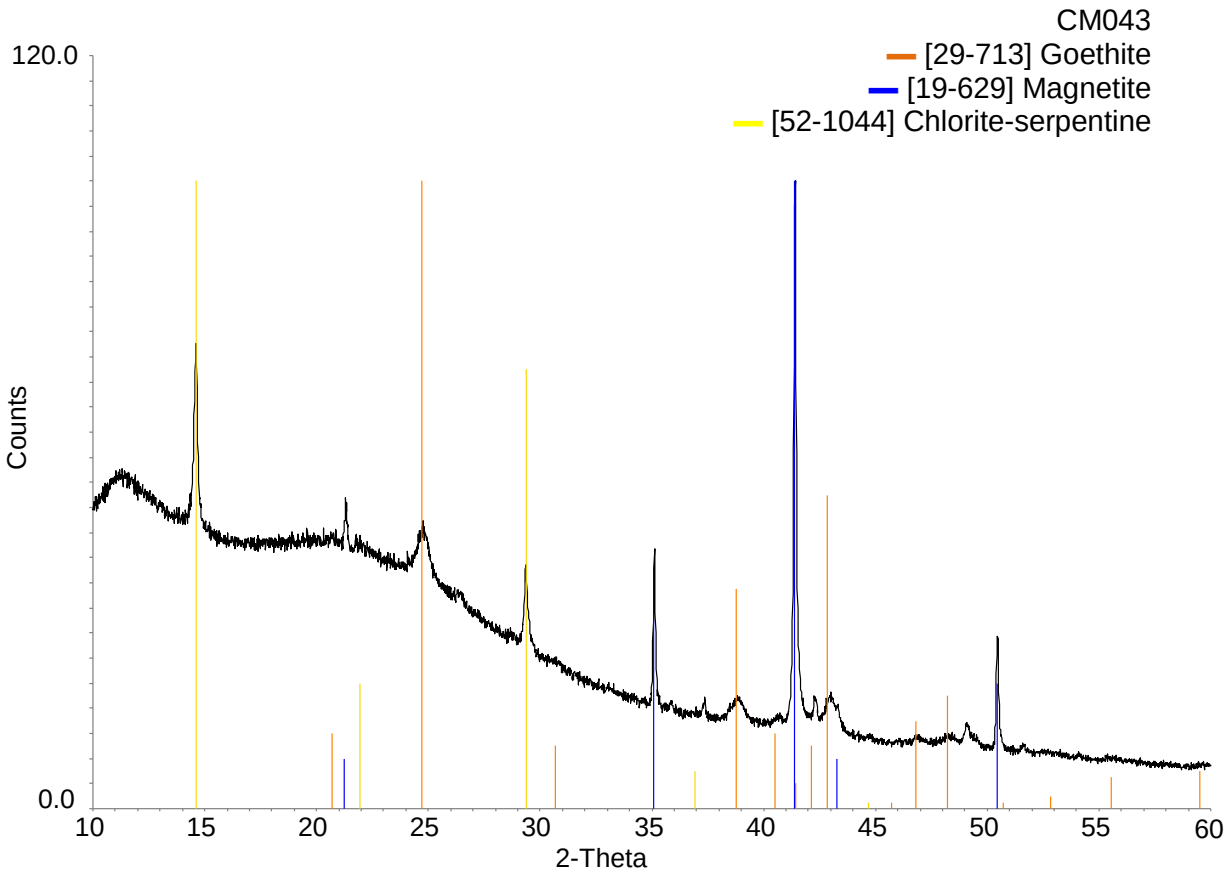

Figure 6.9: PXRD patterns collected for natural sample CM043. Data collected using Co $K_{\alpha 1}$ radiation.

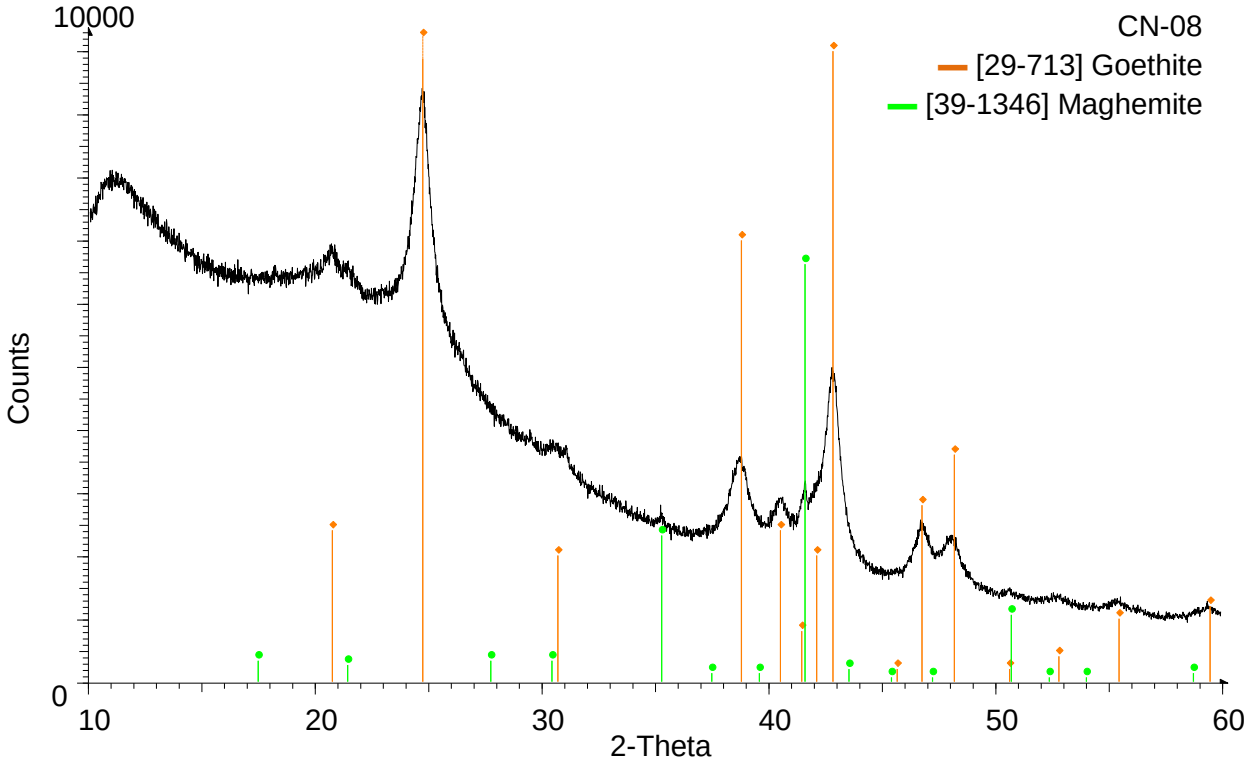

Figure 6.10: PXRD patterns collected for natural sample CN-08. Data collected using Co $K_{\alpha 1}$ radiation.

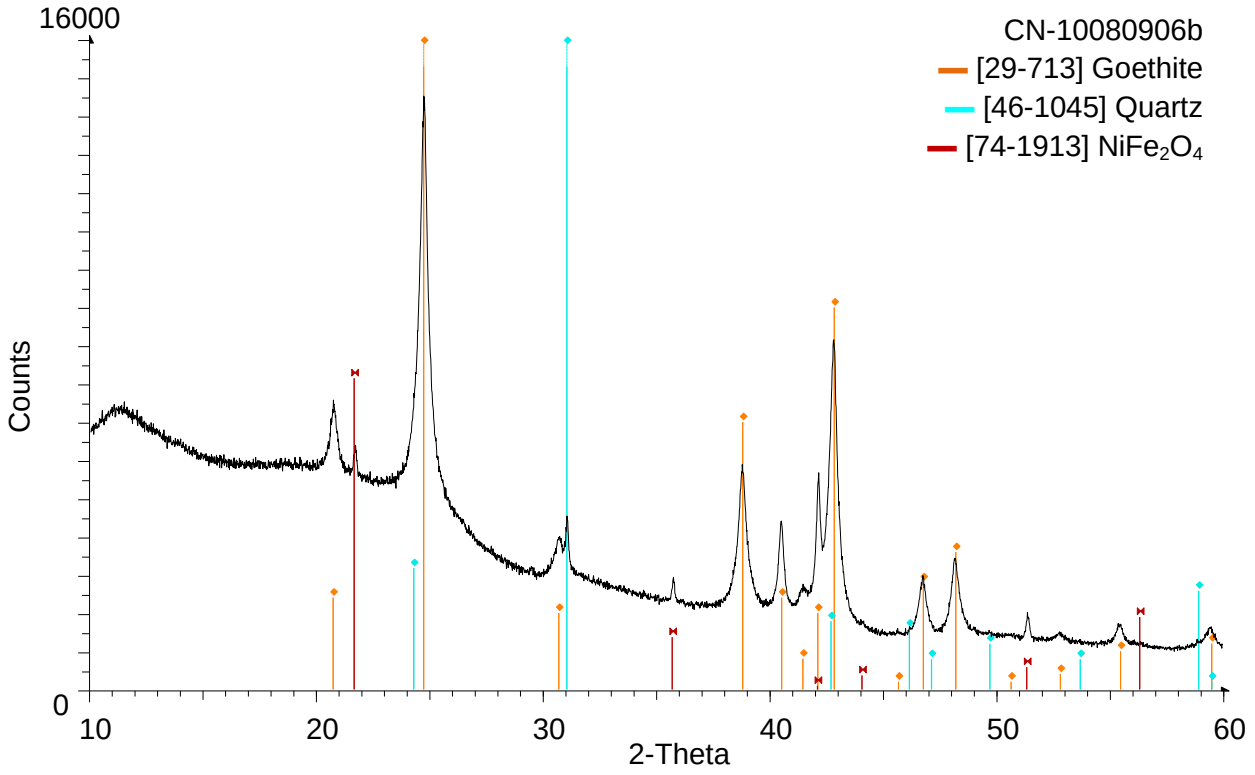

Figure 6.11: PXRD patterns collected for natural sample CN-10080906b. Data collected using Co $K_{\alpha 1}$ radiation.

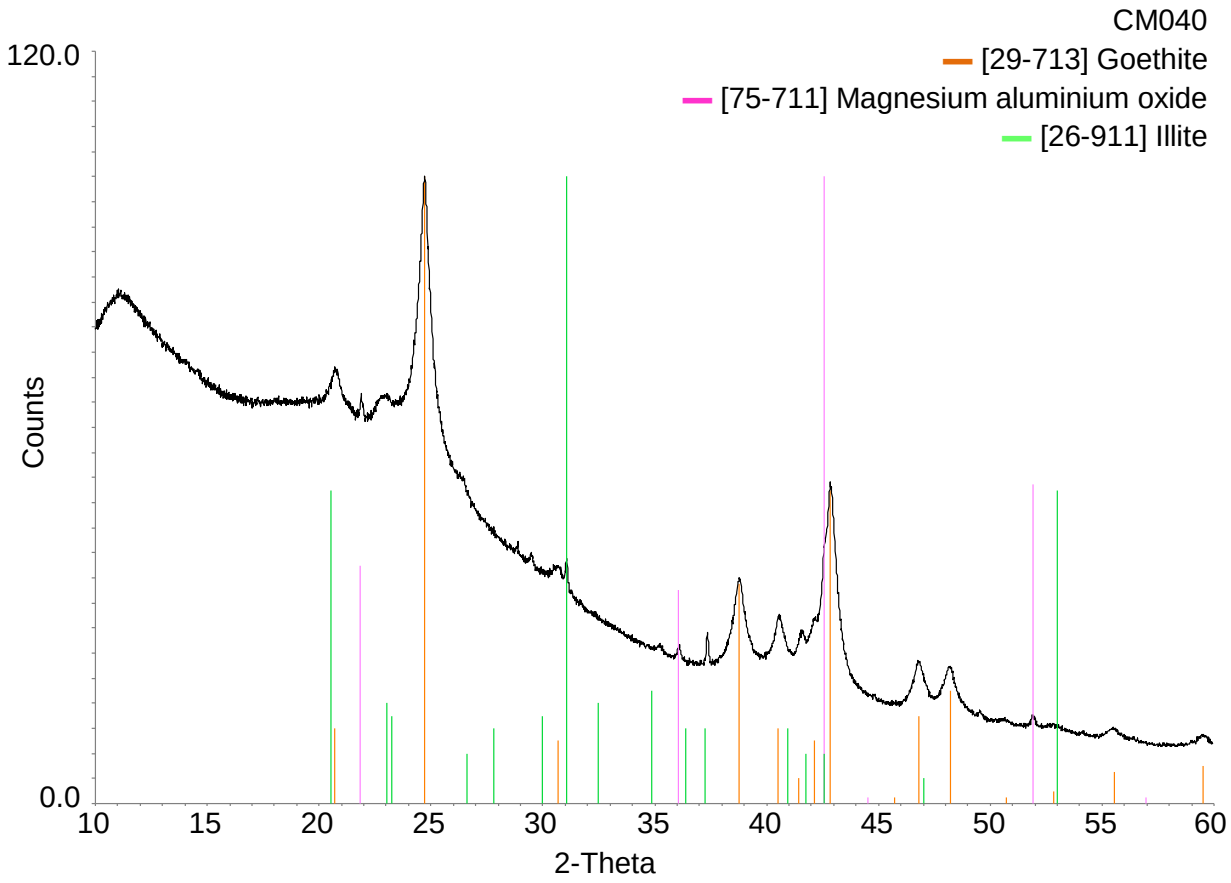

Figure 6.12: PXRD patterns collected for natural sample CM040. Data collected using Co $K_{\alpha 1}$ radiation.

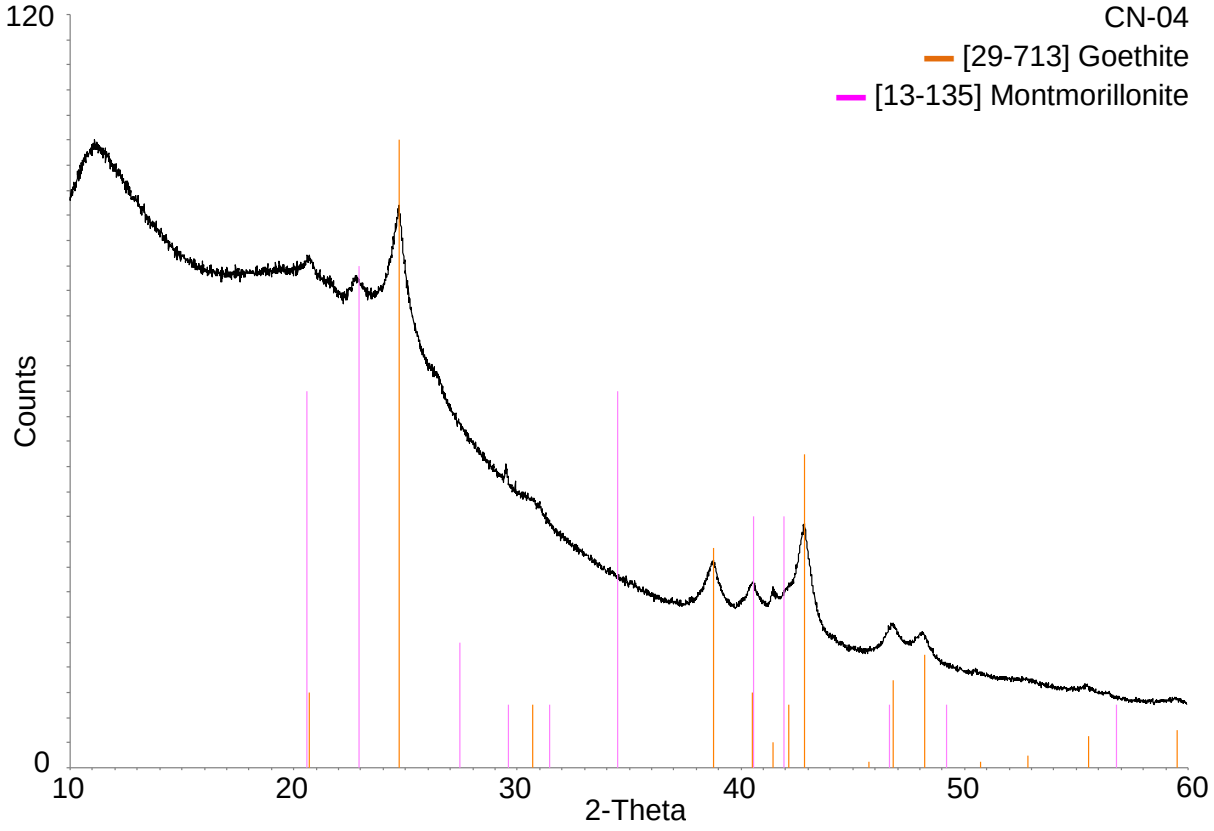

Figure 6.13: PXRD patterns collected for natural sample CN-04. Data collected using Co $K_{\alpha 1}$ radiation.

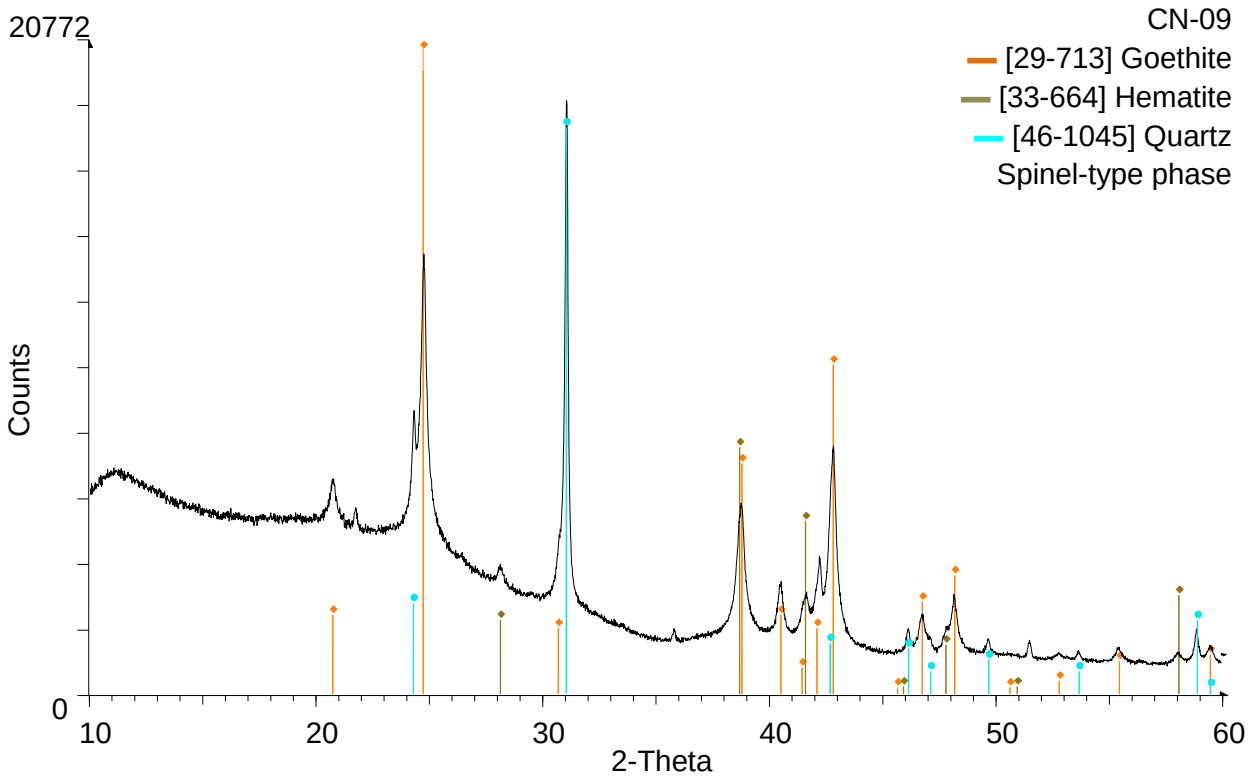

Figure 6.14: PXRD patterns collected for natural sample CN-09. Data collected using Co $K_{\alpha 1}$ radiation.

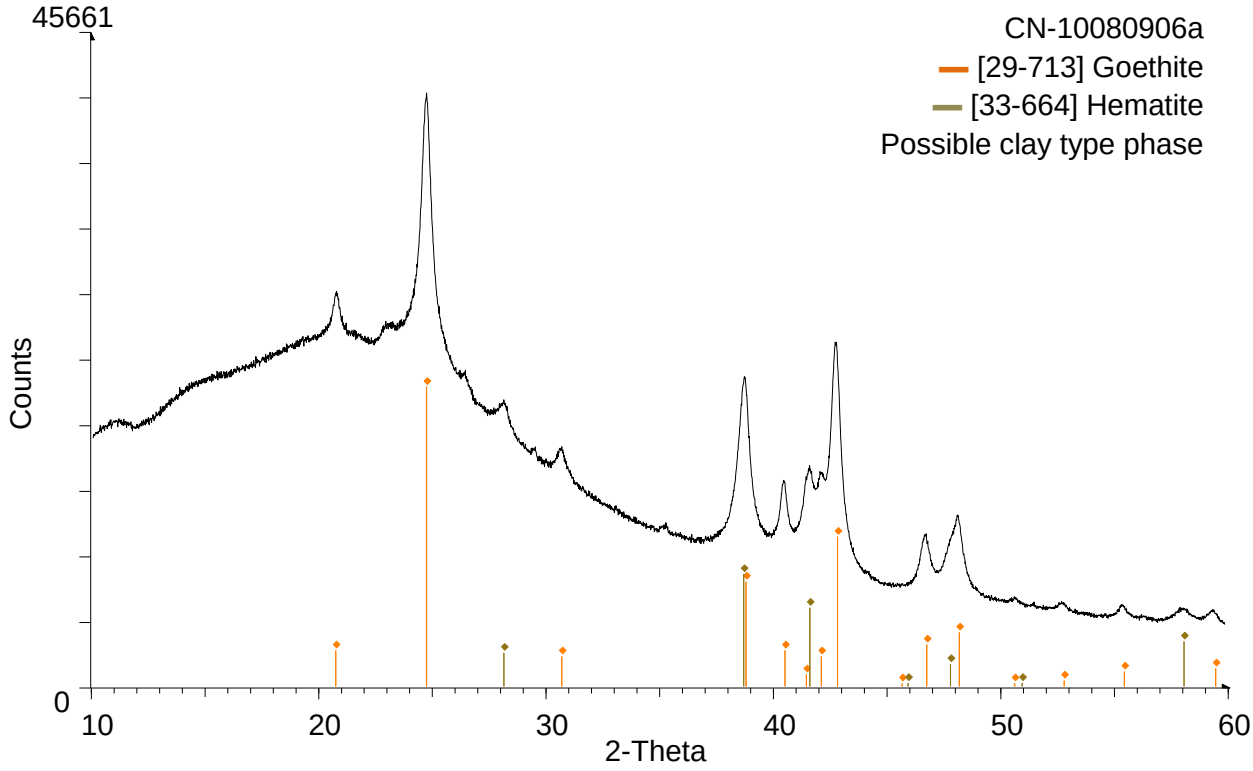

Figure 6.15: PXRD patterns collected for natural sample CN-10080906a. Data collected using Co $K_{\alpha 1}$ radiation.

6.3.2. Elemental Composition

The elemental composition of the natural laterite samples had been determined previously by staff at the Natural History Museum, using EPMA and/or ICP-AES.[11] The compositional information that was obtained is shown in Table 6.2. No data was available for samples BM18571 or BM1905,46, however these are used as goethite standards for PXRD and other measurements, so are assumed to be phase pure Fe-goethite. Data was also unavailable for sample CN-04.

Table 6.2: Elemental composition of natural goethite samples.

Sample Name	Elemental Composition (wt%) of Natural Goethite Samples							
	Mg	**Al**	**Si**	**Cr**	**Mn**	**Fe**	**Co**	**Ni**
BM18571	No data available.							
BM1905, 46	No data available.							
CM026	0.49	1.49	3.51	2.77	0.81	53.3	0.19	3.92
CM039	0.60	5.07	2.76	1.95	0.72	51.0	0.14	1.12
CN-10080902	0.02	0.33	1.27	2.75	0.01	53.1	0.01	0.13
CM043	0.43	4.80	2.61	2.46	0.31	57.2	0.03	1.96
CN-03	0.04	0.29	1.52	1.17	0.00	52.2	0.01	0.12
CN-08	0.08	0.11	4.70	0.01	0.18	49.7	0.05	1.53
CM040	0.63	2.77	6.90	0.83	0.20	50.1	0.06	2.74
CN-04	No data available.							
CN-10080906b	0.01	0.19	1.45	0.21	0.00	55.4	0.01	0.18
CN-05	0.09	0.62	3.70	0.04	0.05	50.7	0.07	2.03
CM022	0.68	4.41	1.01	2.11	0.76	54.0	0.19	1.94
CM038	0.42	5.37	0.79	1.25	0.15	60.0	0.04	0.88
CN-01	0.18	0.39	1.68	2.08	0.81	51.6	0.33	0.51
CN-07	0.03	0.20	1.51	0.78	0.01	56.3	0.00	0.05
CN-09	0.03	0.02	1.51	0.35	0.00	58.7	0.00	0.02
CN-10080906a	0.33	0.82	3.37	0.16	0.47	46.3	0.12	1.93

A wide variety of elements were identified in the natural laterite samples analysed, and the composition of the samples, with the Fe wt% excluded to enable better visualisation of the other elemental proportions, are shown in Figure 6.16. The major constituent of all of the samples was iron (46.3 - 60.0 wt%), which was expected as these samples were taken from the limonitic zone of the laterite ore and chosen as they were thought to consist mainly of goethite. The Mg and Mn content of the samples was low (≤1 wt%), as was the Co content (≤0.33 wt%). The Al content varies between the samples, ranging from 0 - 5.37 wt%, supporting the results of the PXRD characterisation as some of the samples (e.g. CM022, CM039, CM040) contained a $MgAl_2O_4$ (or other Al-rich) phase. The Si content of the natural samples also displays variation, ranging from 1 - 6.9 wt%, which

again is expected as quartz, as well as other Al-silicate phases were identified in some of the samples (e.g. CM026, CN-05, CN-10080906b, CN-09) by PXRD.

The natural laterite samples were also found to contain significant amounts of Cr – in some cases over 2 wt% (e.g. CM026, CN-10080902, CM043, CM022, CN-01), and the Ni content of the samples was found to range from ~0 - 4 wt%. This variation in the Ni content of the samples is vital for this work. All of the samples will be characterised using the range of techniques described and tested in previous chapters of this thesis and the results will be analysed taking into account the different Ni contents that have been determined. Working on the assumption that the Ni is incorporated into the goethite/ferrihydrite phase(s) will allow the effect that different Ni levels have on the proportions of goethite and/or ferrihydrite to be established.

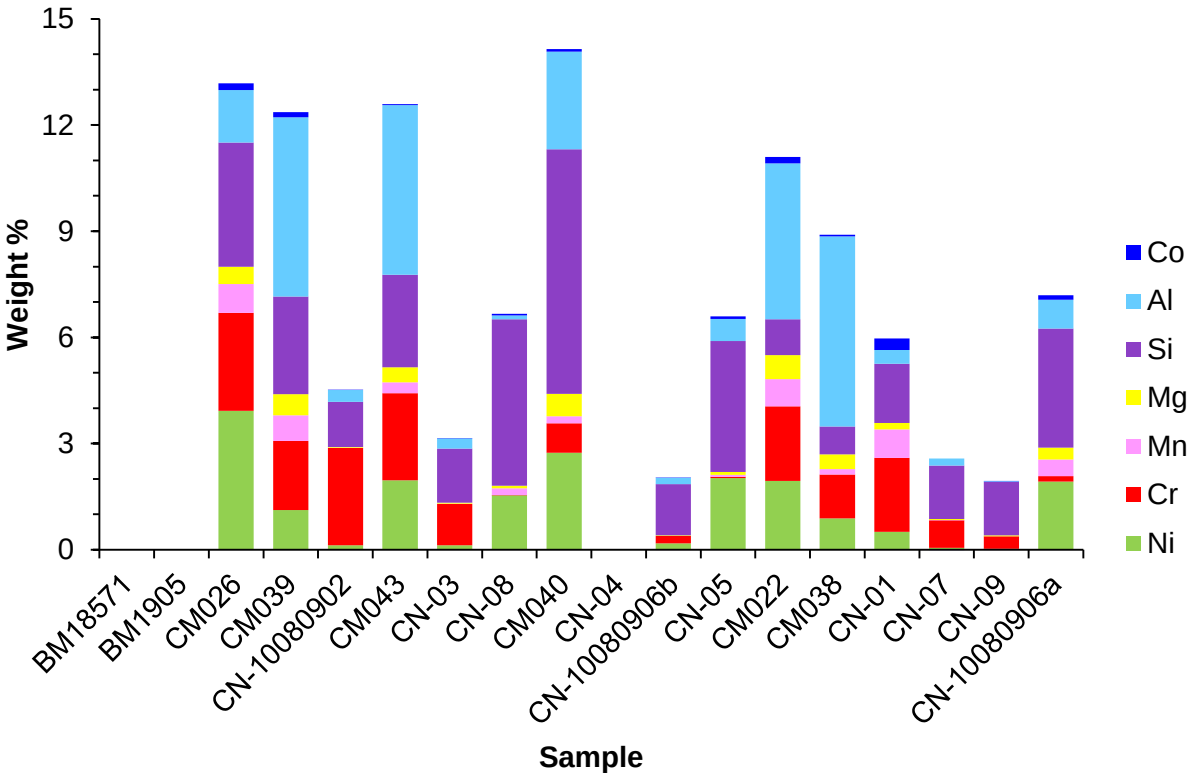

Figure 6.16: Elemental composition of natural goethite samples. Fe content omitted for ease of visualisation of the more minor elements.

6.3.3. TGA

The TGA weight loss profiles were recorded for the natural laterite samples (Figure 6.17). A lot of variation in the weight loss profiles for each of the samples was observed, particularly the weight loss which occurred below 40°C. Variation was also observed in the onset temperature and proportion of the total weight lost for the dehydroxylation of goethite to hematite. This variation was attributed to the multi-phase nature of the samples.

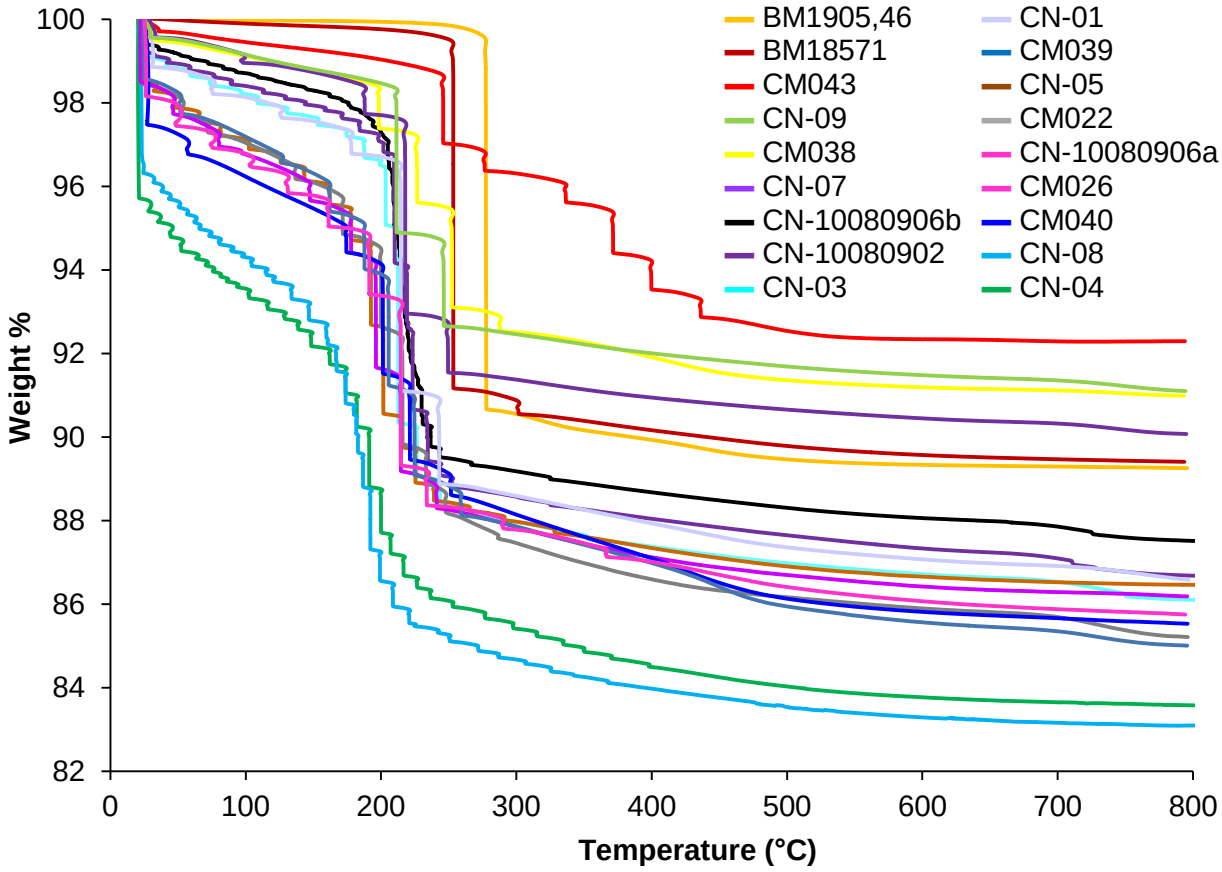

Figure 6.17: TGA weight loss profiles of natural laterite samples.

Throughout this thesis, the weight loss recorded below 40°C in the TGA profiles of the goethite samples has been used as an indicator to estimate the proportion of ferrihydrite that is associated with a goethite sample. Focusing on the weight loss in this temperature region, shown in more detail in Figure 6.18, there is a large amount of variation across the natural samples which were studied, with the weight loss ranging from 0 - 4.9 wt%. As has been discussed in previous chapters, and demonstrated here by the weight loss profiles of the PXRD standards BM1905,46 and BM18571, pure goethite should have no weight loss in this low temperature region.

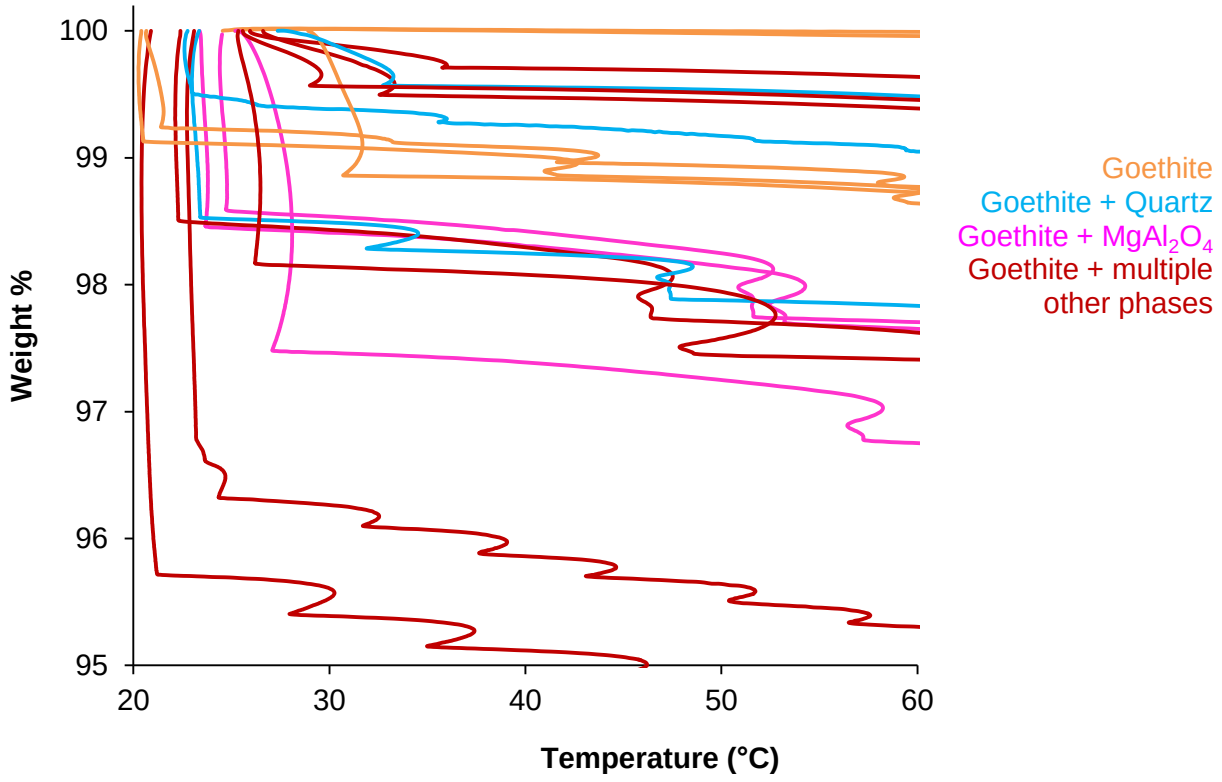

Figure 6.18: TGA profiles of natural goethite samples, showing the weight loss which occurs below 40°C.

The weight loss which occurs below 40°C results from the loss of physically adsorbed surface water, which has been reported as being as high as 15% in ferrihydrite samples.[12] However, as the PXRD characterisation showed, only five of the samples in this study have been identified as single phase goethite. It is, therefore, difficult to differentiate between the effect that the presence of these additional phases has on the weight loss profiles and the effects that result from either elemental substitution into the goethite structure or the presence of ferrihydrite.

In Chapter 5, the addition of Ni into the goethite synthesis was shown to increase the amount of ferrihydrite that was present in the samples. This was shown by a strong correlation between the target mol% Ni attempted to be incorporated into the goethite structure and the weight loss (wt%) which occurred below 40°C. This particular weight loss step was shown in Chapter 3 to be related to the proportion of ferrihydrite in a sample, suggesting that Ni is stabilising the ferrihydrite precursor phase, preventing it transforming to goethite. Based on the results that were gained in synthetic systems, it might be expected that increasing amounts of nickel in a laterite sample would also result in the presence of a stabilised ferrihydrite phase. A comparison between the wt% Ni in goethite

samples, both synthetic (see Chapter 5) and naturally occurring (discussed here), and the weight loss that occurs below 40°C when the samples are heated is shown in Figure 6.19.

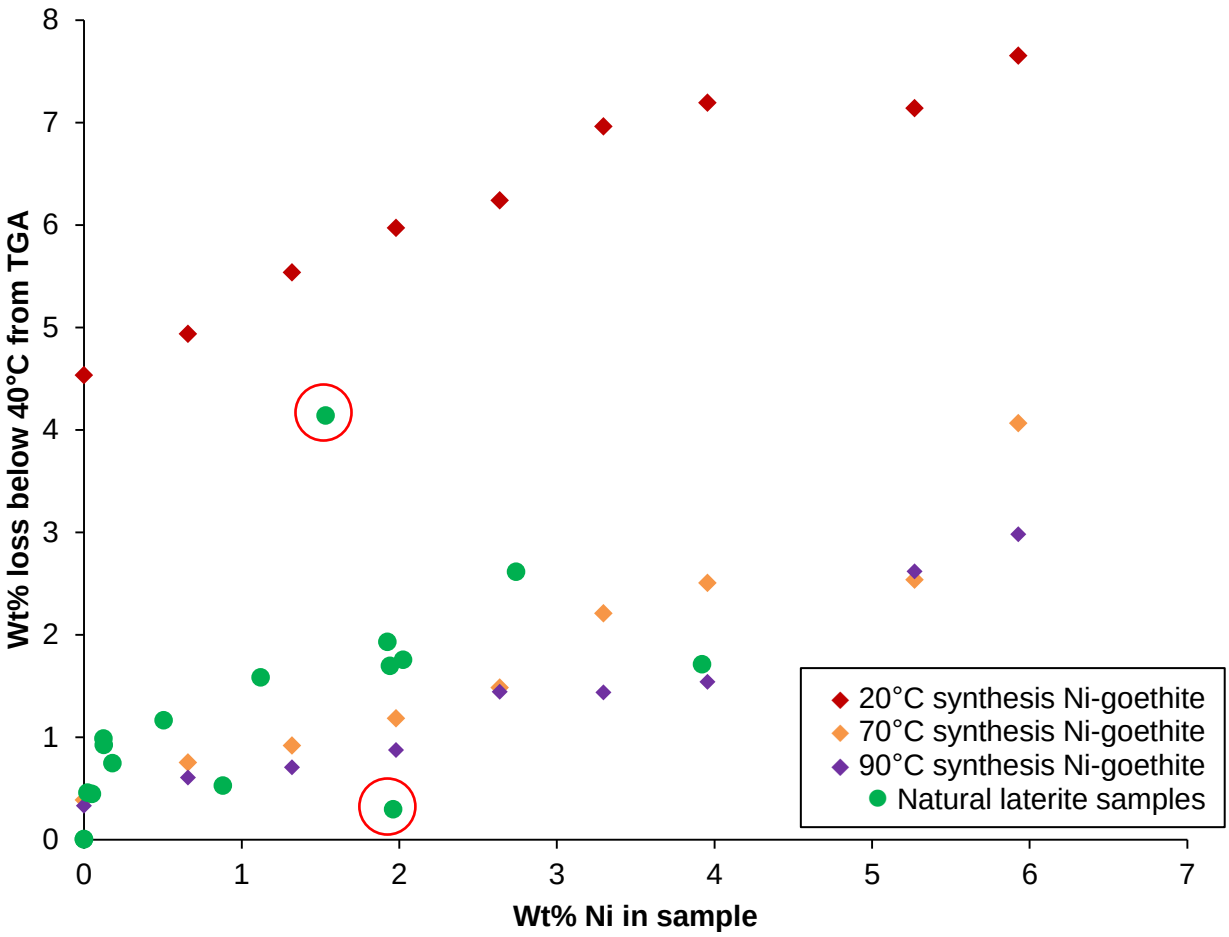

Figure 6.19: Comparison of the relationship between wt% Ni in goethite and wt% lost below 40°C from TGA profiles in natural and synthetic goethite samples (values shown for synthetic samples are target wt%). Outliers in red circles and discussed in the text.

Comparison of the data points for the natural goethite samples with those of the different sets of synthetic samples, shows that the weight losses occurring below 40°C most closely resembles those found in the synthetic 70°C Ni-goethite samples. Excluding the outliers (highlighted in red on the plot), which will be discussed in more detail shortly, there appears to be a correlation between the wt% Ni found in the natural samples and the weight loss which occurs below 40°C thus suggesting the presence of ferrihydrite in the samples. Generally, the weight loss below 40°C increased with increasing Ni content in the natural samples, mirroring the observations made for the synthetic Ni goethite samples.

In order to improve the correlation between the weight loss (assumed to be from the presence of ferrihydrite) and the amount of foreign cation present in the goethite/ferrihydrite system, further consideration of the cations present is needed. Characterisation of the natural samples has shown that the majority of them contain other mineral phases in addition to goethite (Table 6.1). Elemental analysis (Table 6.2) highlighted the presence of a variety of foreign cations in these natural samples. With the data available, it is impossible to ascertain whether these foreign cations are associated with secondary phases, or if the elements have also been incorporated into the goethite structure in addition to/instead of Ni, and may have also have a stabilising effect on a ferrihydrite phase.[13] In order to further this work, some assumptions about the natural laterite samples were made.

It is already widely known that aluminium [14], chromium [15], manganese [16], cobalt [17] and nickel [18] can substitute into the goethite structure, with the simultaneous incorporation of some of these cations into goethite also possible.[19, 20] Therefore, it cannot be confirmed from the data available here that Ni is the only element that has substituted into the structure of goethite. Other elements that have been confirmed as present from the elemental analysis (e.g. Co, Mn, Al, Cr) could be incorporated within the goethite structure, or alternatively present as a substituent of separate phases. Indeed, even the Ni may not all be present in the goethite/ferrihydrite system, some of it could be associated with other mineral phases.

Analysis of the PXRD data identified the presence of Al-rich phases ($MgAl_2O_4$, $Al(OH)_3$) in some of the samples, e.g. CM022, CM026, CM038, CM039, CM040. Al is assumed to be present in a separate (non-goethite) phase in all cases. The levels of Cr measured in the natural samples are, in some instances, quite high (>1.5 wt%), for example CM026, CM039, CN-10080902, CM043, CM022 and CN-01. With no evidence of a Cr-rich phase (e.g. chromite) from analysis of the PXRD patterns, it is difficult to know the nature of the Cr association with these materials, but it is assumed not to be associated with goethite/ferrihydrite.

Mn and Co were not identified as major substituents of any other phase from PXRD characterisation, although elemental analysis of the samples showed the presence of small amounts of each element (<1 wt%) in the natural laterite samples. Hunter *et al.* (2013) suggested the presence of nickeliferous asbolane, $(Co, Ni)Mn_2O_4(OH)_2.nH_2O$, in limonitic laterite ores from the Çaldağ deposit. This could be one explanation as to the origin of the Co and Mn, although it was not identified in the PXRD patterns collected in this study.[3] This does not necessarily mean that asbolane isn't in the samples though, as

phases of this type tend to be poorly crystalline so would be difficult to detect in small quantitites. Ni is known to be structuraly incorporated into goethite in these deposits, although, as previously mentioned, could also be associated with a nickeliferous asbolane phase. However it is possible that Mn and Co are both incorporated into the goethite structure, rather than being present as a separate phase. Cornell (1991) found that the structure of synthetic goethite samples could simultaneously incorporate 2-4 mol% of each of the three elements, Co, Ni and Mn, and that the presence of these elements also led to the formation of a secondary (Ni, Co, Mn)-ferrihydrite phase.[20]

Because Ni and Co are the two elements which are commonly assoicated (and extracted from) goethite in deposits of this type, it will be assumed that Ni and Co are both associated with the goethite/ferrihydrite system. To further investigate the relationship between the weight loss which occurs in the goethite samples below 40°C and the amount of foreign cation in the goethite structure, the weight loss below 40°C was re-plotted against the total wt% of Ni and Co that was measured, and compared to synthetic Ni-goethite prepared at 70°C (Figure 6.20).

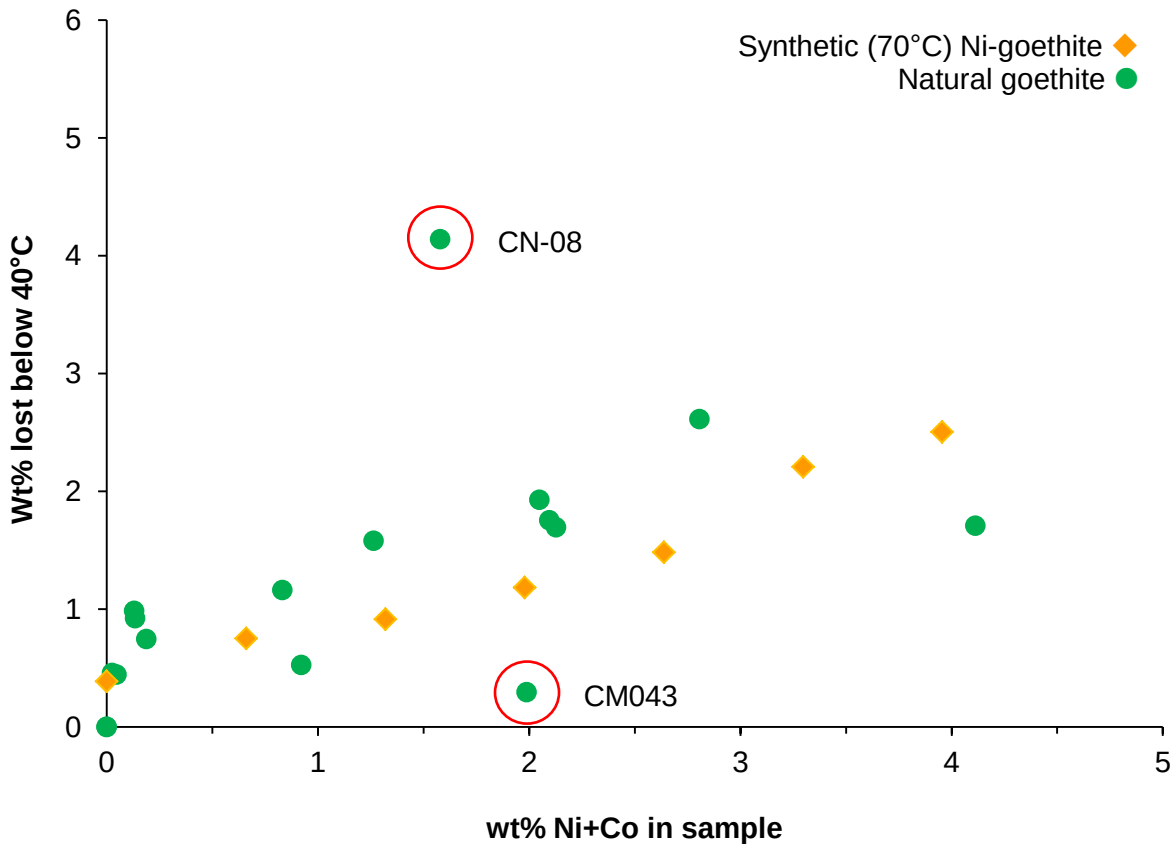

Figure 6.20: Comparison of the relationship between wt% Ni+Co in laterite samples and wt% lost below 40°C from TGA profiles in natural and synthetic goethite samples. Synthetic samples are plotted using their target wt% Ni. Outliers are shown in red circles.

There is reasonably good correlation between the total Ni+Co content of each laterite sample and the weight that is lost from the samples below 40°C. The samples CN-08 and CM043 deviated the most from the trend shown by the other samples with respect to their weight loss and Ni+Co contents (highlighted with red circles on Figure 6.20). The reasons for this are not immediately obvious, although all of these samples contained additional phases in significant enough quantities to be identified by PXRD. CN-08 has a larger weight loss below 40°C than might be expected from following the suggested trend shown in Figure 6.20. The sample was identified as containing maghemite, whilst the goethite phase appears to be relatively poorly crystalline as shown by the broad peaks in the PXRD pattern (Figure 6.10). The elemental analysis (Table 6.2) showed that the sample contained 4.7 wt% Si, although no Si containing phase was identified by PXRD. One possible explanation for this could be that the silicon is associated with a ferrihydrite phase.[21, 22] This would account for both the higher than expected weight loss observed, as Si is known to stabilise ferrihydrite, and the lack of any crystalline Si containing phases in the PXRD patterns. CM043 appears to have a lower weight loss than would be expected, based on its Ni+Co content. The PXRD pattern for this sample identified the presence of goethite, maghemite and a serpentine type phase. It is possible that the Ni could be contained within the serpentine phase, not associated with the goethite/ferrihydrite system, which would account for the weight loss not fitting with the suggested trends.

An important factor to consider when investigating the relationship between the weight loss which occurs below 40°C (related to the ferrihydrite content) and the proportion of foreign cations present in association with the goethite/ferrihydrite system, is that these natural samples do not just consist of goethite and ferrihydrite. The relationship that was established between the proportions of goethite and ferrihydrite present in a sample, and the weight loss below 40°C in Chapter 3, were based on the knowledge that goethite and ferrihydrite were the only two phases present in the system. The natural samples contain a number of different mineral phases, so therefore, depending on the proportions of these other phases that are present, the weight loss below 40°C may not be an accurate representation of the ferrihydrite proportion, complicating the estimation of the ferrihydrite content. Further to this, the total Ni (as well as the Co) present, as determined by elemental analysis, might not all be incorporated into the goethite/ferrihydrite system. Finally, because of the very small (~5 mg) sample sizes used for both the TGA and elemental analysis, it is possible that these results are not a fair representation of the bulk of the sample and, ideally, both the elemental analysis and the thermal analysis would need to be repeated multiple times.

Considering the possible problems with the technique described in the previous paragraph, TGA of goethite rich laterite samples still seems to be the best characterisation method to assess the ore material for the presence of Ni, and possibly Co, rich ferrihydrite phases in association with goethite.

6.3.4. EDTA washing

The presence of untransformed ferrihydrite, stabilised by the presence of foreign cations (e.g. Ni, Co), is suggested as an explanation for the high variability in the ease of extracting Ni via heap leaching from different goethite deposits in limonitic laterite ores.

Chapters 4 and 5, demonstrated how washing synthetic (Ni)-goethite samples with EDTA was an effective technique in removing associated ferrihydrite from goethite samples. The natural samples investigated in this chapter were prepared and treated with the EDTA solution as described in Chapter 4. After the washing procedure, the EDTA solutions (shown in Figure 6.21) were characterised by ICP-OES in order to determine the elements that were present in solution and hence ascertain what the EDTA washing process has removed. It is clear, visually, from the colours of the solutions (ranging from pale

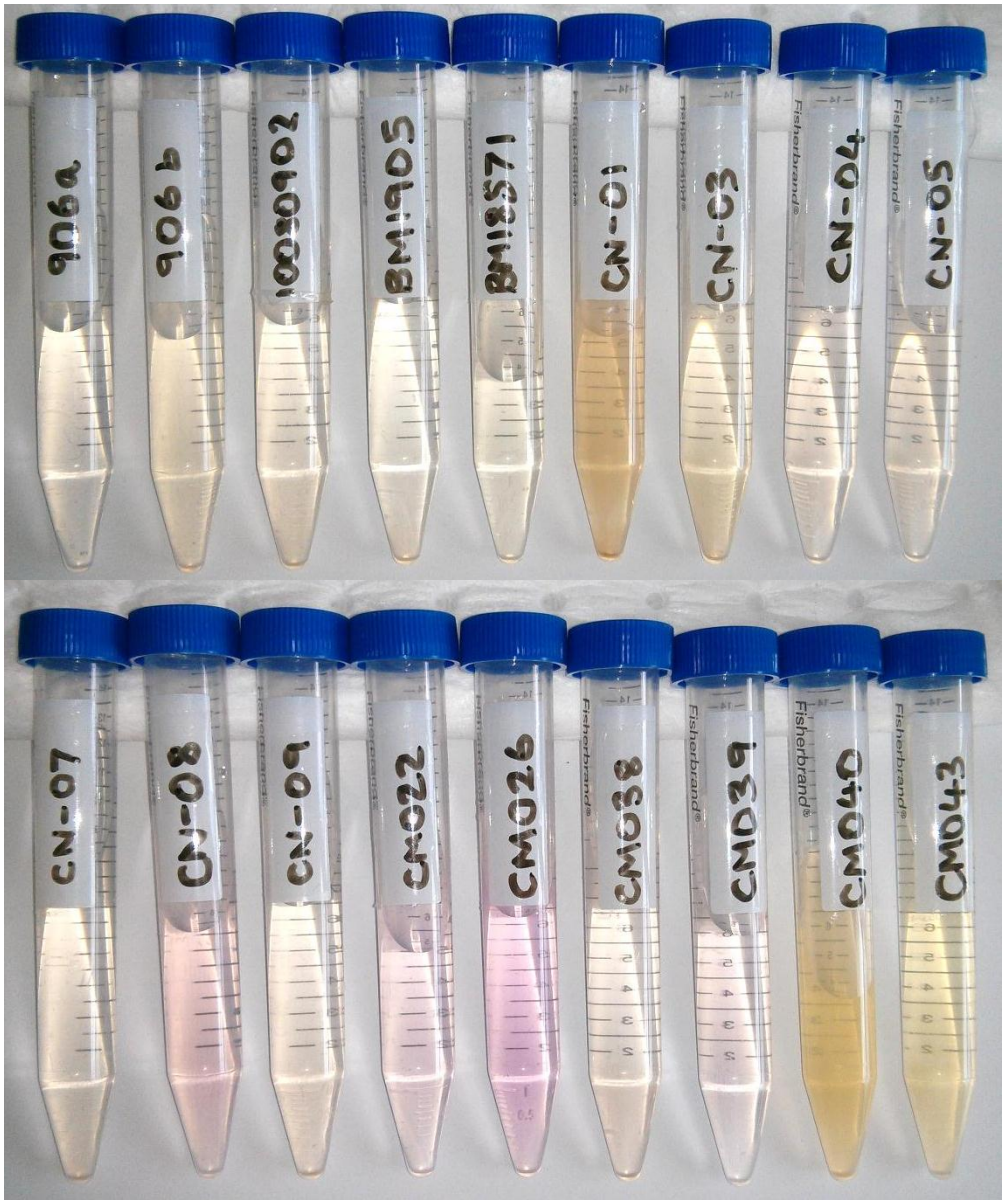

Figure 6.21: Appearance of EDTA solutions after natural goethite had been washed.

yellow/brown to pink) that, for the majority of the samples, the EDTA solution has removed something from the solid phase.

The compositions of the EDTA washing solutions after the natural goethite samples had been treated are shown in Table 6.3, with the quantity of each element expressed as the wt% of the total solid that was treated. The solutions were analysed for the presence of Al, Cd, Co, Cr, Cu, Fe, K, Mg, Mn, Ni, Pb and Zn. Cd, Cu, Pb and Zn were not detected in any of the samples and so are excluded from Table 6.3.

Table 6.3: Composition of EDTA washing solutions after treating natural goethite samples. Text in grey – values below limit of detection, text in blue – values below limit of quantification

Sample	Aluminum wt%	Cobalt wt%	Chromium wt%	Iron wt%	Magnesium wt%	Manganese wt%	Nickel wt%	Total wt% removed in EDTA wash
BM1905, 46	-0.06	-0.01	0.00	0.06	0.00	-0.01	-0.01	0.06
BM18571	-0.06	-0.01	-0.01	0.12	0.00	-0.01	-0.01	0.12
CM022	0.03	0.05	0.01	0.10	0.01	0.21	0.03	0.43
CM026	0.03	0.16	0.01	0.41	0.03	0.65	0.27	1.56
CM038	-0.01	-0.01	0.00	0.07	0.01	0.00	-0.01	0.07
CM039	0.02	0.04	0.02	0.09	0.04	0.25	0.05	0.51
CM040	0.03	0.00	0.00	0.80	0.12	0.04	0.14	1.14
CN-04	-0.06	-0.01	-0.01	0.02	-0.01	-0.01	-0.01	0.02
CM043	0.22	-0.01	0.01	2.05	0.03	0.09	0.11	2.51
CN-05	-0.05	0.05	0.00	0.26	0.02	0.32	0.12	0.75
CN-08	-0.05	0.14	0.00	0.64	0.02	0.43	0.21	1.43
CN-03	-0.05	-0.01	0.00	0.08	0.01	0.00	0.01	0.09
CN-10080906b	-0.06	-0.01	0.00	0.08	0.00	-0.01	-0.01	0.08
CN-10080902	-0.06	-0.01	0.00	0.05	0.00	-0.01	-0.01	0.05
CN-01	-0.01	0.02	0.00	0.08	0.04	0.05	0.02	0.20
CN-07	-0.06	-0.01	0.00	0.07	0.00	-0.01	-0.01	0.07
CN-09	-0.06	-0.01	0.00	0.09	0.00	-0.01	-0.01	0.09
CN-10080906a	-0.02	0.01	0.00	0.16	0.08	0.03	0.04	0.31

Only a very small amount of material appears to have been removed from each of the natural samples as a result of the EDTA washing procedure, ranging from ~0 – 2.5 wt% of the total. By comparison, the synthetic Ni goethite samples discussed in Chapter 5.5 with up to 5 mol% Ni-for-Fe substitution had ~14-22 wt% removed by EDTA washing for the (Fe+Ni) samples synthesised at 20°C, and 0-9 wt% removed for the samples (Fe+Ni)

synthesised at 70°C. The EDTA solutions resulting from the washing of synthetic samples comprised mainly of Fe, thought to be due to the large amounts of ferrihydrite present in association with the goethite phase.

Examining the composition of the EDTA solutions after washing natural goethite, shown in Table 6.3 and Figure 6.22, Fe is not always found to be the major component, for example CM026 has 0.41 wt% Fe and 0.65 wt% Mn. This raises questions about what the EDTA wash is removing from the natural samples. The experimental work presented in this thesis has demonstrated the capabilities of the EDTA washing technique in removing ferrihydrite whilst leaving goethite intact, however the effect that the EDTA wash may have on some of the other phases present in these natural samples is not known.

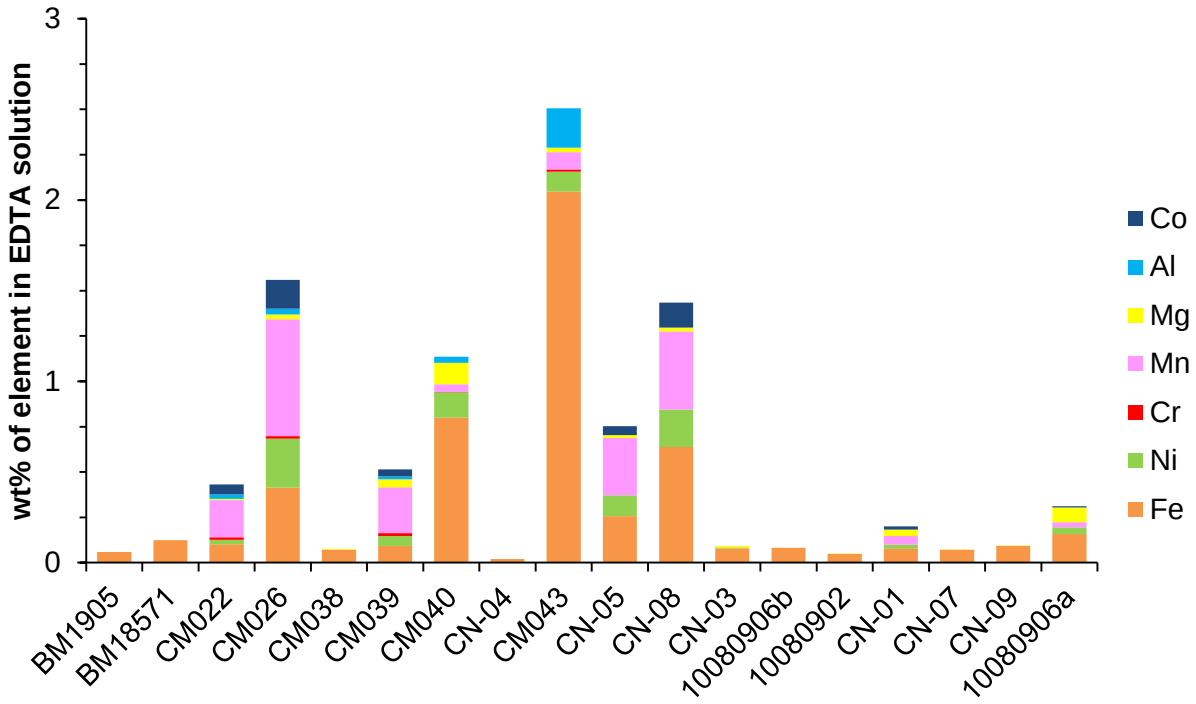

Figure 6.22: Composition of EDTA solutions after washing natural goethite.

The low amounts of Fe being removed from the natural goethite during the EDTA wash doesn't necessarily mean that there is no ferrihydrite associated with these samples. However, the natural laterite samples which have had thousands of years to form would probably contain far less ferrihydrite than synthetic samples prepared in the laboratory over one week, so less Fe would be washed away from them compared with their synthetic analogues. Furthermore, the EDTA washing technique may interact differently with natural samples than synthetic ones. Although the EDTA washing method developed by Borggaard (1992) was not identical to that developed in this work, he found that it took a minimum of 3 months for the removal of ferrihydrite from natural soil samples, so it is

possible that a longer washing time may result in more material being removed from the samples.[23]

In previous chapters of this thesis (e.g. Chapters 4 and 5), repeating the TGA analysis of the goethite samples after they had been washed with the EDTA solution demonstrated that ferrihydrite had been removed from the samples, by observation of a reduction (to less than 1 wt%) in the weight loss which occurred below 40°C. Comparing the weight loss which is measured in the natural samples before and after washing, (Figure 6.23 and Table 6.4), a decrease in the weight loss between the original and washed samples is observed in all cases.

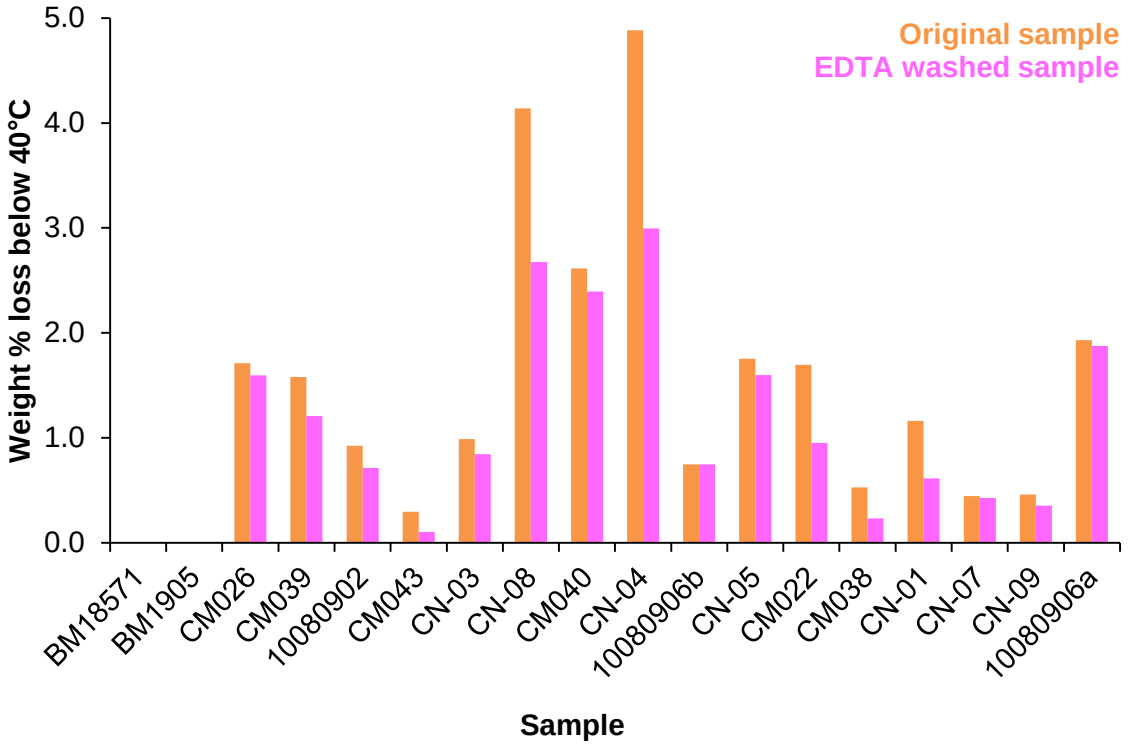

Figure 6.23: Comparison of weight % lost below 40°C in TGA analysis of natural samples before and after EDTA washing.

Although a reduction in the weight loss that occurs below 40°C is observed in all cases, it is not reducing to less than 1 wt%, as observed with the synthetic samples upon removal of the associated ferrihydrite phase, and the actual decrease in the weight loss is often very small (~0.2 wt%). There could be a number of reasons for this. As has been discussed already, the EDTA technique may not be removing all of the ferrihydrite from these natural samples in the timescales used in this study, therefore ferrihydrite remains in the samples even after the washing period, accounting for the weight loss observed. Alternatively, part of the weight loss occurring below 40°C could be attributed to the

decomposition behaviour of one of the other phases present in the sample, i.e. not due to ferrihydrite and therefore not being removed in the EDTA wash.

Table 6.4: Comparison of the weight loss measured below 40°C in natural goethite samples before and after EDTA washing.

Sample Name	Weight loss below 40°C (wt%)		Difference (wt%)
	Original Sample	EDTA washed sample	
BM18571	0.0	0.0	0.0
BM1905	0.0	0.0	0.0
CM26	1.7	1.6	0.1
CM39	1.6	1.2	0.4
CN-10080902	0.9	0.7	0.2
CM43	0.3	0.1	0.2
CN-03	1.0	0.8	0.2
CN-08	4.1	2.7	1.4
CM40	2.6	2.4	0.2
CN-04	4.9	3.0	1.9
CN-10080906b	0.7	0.7	0.0
CN-05	1.8	1.6	0.2
CM22	1.7	1.0	0.7
CM38	0.5	0.2	0.3
CN-01	1.2	0.6	0.6
CN-07	0.4	0.4	0.0
CN-09	0.5	0.4	0.1
CN-10080906a	1.9	1.9	0.0

6.3.5. Estimation of the Ferrihydrite Proportion in Natural Goethite Samples

In previous chapters of this thesis, a number of techniques have been demonstrated as possible methods to estimate the proportion of ferrihydrite associated with a goethite sample. Of these techniques, TGA was shown to be the most promising. Using the TGA data collected on the natural samples, the ferrihydrite content of the samples can be estimated using the methodology described in Chapter 3. However, the thermal analysis of the EDTA washed goethites (as discussed above), showed that in some cases there is still a relatively large weight loss occurring below 40°C. Two possible reasons were proposed for this; incomplete removal of ferrihydrite by the EDTA wash, or, the weight loss in this region is due to another mineral phase. To take into account all of these

factors, the estimated proportions of ferrihydrite in each of the natural samples have been calculated to account for the different possibilities, (Table 6.5).

Table 6.5: Amount of ferrihydrite estimated to be associated with natural goethite samples from TGA data.

Sample name	Estimated ferrihydrite proportion in laterite sample (wt%)		
	If all of the weight loss below 40°C is due to ferrihydrite		If the weight loss below 40°C is due to a number of phases
	Original Sample	After EDTA wash (assuming incomplete removal of ferrihydrite by EDTA technique)	Assuming EDTA wash removes ALL ferrihydrite
Column 1	*Column 2*	*Column 3*	*Column 4*
BM18571	-6	-6	-6
BM1905, 46	-6	-6	-6
CM26	10	9	-5
CM39	9	5	-2
CN-10080902	2	1	-4
CM043	-3	-5	-4
CN-03	3	1	-4
CN-08	33	20	7
CM40	19	17	-4
CN-04	41	23	12
CN-10080906b	1	1	-6
CN-05	11	9	-4
CM22	10	3	1
CM38	-1	-4	-3
CN-01	5	0	0
CN-07	-2	-2	-6
CN-09	-1	-2	-5
CN-10080906a	12	12	-6

Assuming that the weight loss below 40°C is fully attributed to the decomposition of ferrihydrite, the proportions of ferrihydrite estimated to be in the laterite samples ranges from 0-41 wt% (column 2 in Table 6.5). Some of the samples are estimated to have negative amounts of ferrihydrite associated with them. Clearly this cannot be true, and highlights the limitations of estimating the ferrihydrite content in this way. The quantification method was developed using synthetic goethites prepared at 70°C, where the fully formed goethite sample itself had ~0.6 wt% surface water associated with it. The amount of surface water physically adsorbed to goethite is affected by the particle size, and at present this method cannot take that into account. The natural laterite samples BM18571 and BM1905, 46 for example, are very well formed PXRD characterisation

standards, so it is likely they have very little surface water associated with them, hence the errors in quantification.

After the samples had been washed in EDTA, (column 3, Table 6.5), it is estimated that up to 23 wt% ferrihydrite remains in some samples. This could be because incomplete removal of ferrihydrite has taken place, i.e. the EDTA washing technique interacts differently with the natural samples and does not remove all of the ferrihydrite. An alternative explanation for the high estimated proportions of ferrihydrite after EDTA washing is that the weight loss occurring below 40°C is not due to ferrihydrite, but from the presence of one of the other secondary mineral phases that have been identified in the samples, e.g. maghemite, $MgAl_2O_4$ etc. Assuming that is the case, and that ferrihydrite is not wholly responsible for the weight loss occurring below 40°C, but the EDTA wash does remove all ferrihydrite from the samples, then the difference between the weight loss before and after washing can be used to estimate the ferrihydrite proportions that are present (column 4, Table 6.5). Using these results, with the exception of CN-08, CN-04 and CM022, the laterite samples are estimated to have no ferrihydrite associated with them at all. However, as has already been mentioned, the TGA quantification method does need to be modified, in order to take into account the amount of physically adsorbed surface water associated with the goethite itself. It is likely that doing this would change the proportions of ferrihydrite that were estimated to be present.

6.4. Summary

The aim of this chapter was to characterise goethite samples taken from laterite deposits, in order to find evidence to support the theory that ferrihydrite is present alongside goethite, hosting some of the nickel, and affecting the ease with which nickel is leached from these ore materials.

Studying goethites recovered from laterite deposits, rather than material produced synthetically, is inherently challenging. The samples that were provided for this research were believed to be single phase (goethite), however PXRD characterisation, carried out as part of this study, found that the majority contained significant amounts of other mineral phases. As a result of this, PXRD, which has been used with some success to identify and quantify ferrihydrite in synthetic samples (Chapter 3.3.4.), could not be used as a technique to identify associated ferrihydrite phases here.

Thermal analysis, which was very capable at characterising synthetic samples to allow quick and easy identification and quantification of ferrihydrite, showed promise when used to characterise the lateritic samples. The weight loss which was measured below 40°C (the indicator for ferrihydrite) ranged from ~0-5 wt%. To support the theory of the presence of an untransformed ferrihydrite phase (stabilised by foreign cations e.g. Ni) associated with the goethite samples, the weight loss was plotted against the wt% of foreign cation which had been measured in the samples by elemental analysis. The results of elemental analysis of the natural goethite samples showed a whole range of different elements to be present, and with the data available it was impossible to ascertain which foreign cations were associated with a goethite/ferrihydrite phase, and which were associated with separate, unrelated mineral phases. From analysis of the data available, the assumption was made that nickel and cobalt were associated with the goethite/ferrihydrite system. A trend, similar to that found in the synthetic samples made at 70°C, was observed when the weight loss was plotted against the wt% of Ni+Co that had been determined in the samples. These results showed an increase in weight loss with increasing foreign cation content, indicating greater amounts of ferrihydrite associated with the samples.

The EDTA washing technique, developed and shown to be successful for the synthetic systems, was tested on the natural samples. If ferrihydrite was present, as suggested by the thermal analysis, it should be removed by the EDTA wash and repeating the thermal analysis should show a reduction in the weight loss below 40°C, demonstrating its removal. Analysis of the EDTA washing solutions after treatment of the solid samples showed that elements had been removed into solution in all cases, however not as much

as might have been suggested from the thermal analysis results. Repeated thermal analysis showed that, although in all cases the weight loss below 40°C reduced after EDTA washing, it did not reduce as much as might have been expected, based on the results from the synthetic systems (shown in Chapter 5). As has been discussed in previous chapters, in its current form, the TGA ferrihydrite quantification methodology does not take into account the surface water associated with goethite, which is dependent on particle size. This could also be a factor in the weight loss measured below 40°C that remains even after EDTA washing.

Nickel and cobalt were assumed to be fully and completely associated with a goethite/ferrihydrite system, however, this may not be the case, and at least some of the Ni/Co may actually be associated with other mineral phases. Furthermore, the proposed goethite/ferrihydrite system may contain other elements apart from cobalt and nickel; the elemental analysis indicates the presence of a number of cations (e.g. Mn, Cr, Al) that could potentially incorporate into the goethite and/or ferrihydrite phases. It is also conceivable that some of the weight loss that occurs below 40°C results from other mineral phases, not ferrihydrite, and the thermal behaviour of the other minerals that were identified in the samples would need to be carefully examined to see what impact they may have in this temperature region. As the ferrihydrite quantification technique using thermal analysis data was developed with just two phases in the system, results from analysis of materials containing more than just ferrihydrite and goethite are likely to be less reliable as the relative proportions of each phase will be affected by the other minerals that are present. This does not rule out identifying the presence and estimating the proportion of ferrihydrite using this method, it is just another factor to consider when analysing the results.

The effectiveness of the EDTA wash on natural laterite samples cannot be resolved until further experiments have been carried out. Initially, the effect of the EDTA wash on the other mineral phases in the system needs to be determined, as its interaction has only been investigated on Fe and Ni originating from goethite and ferrihydrite. Also, longer term studies of the EDTA wash on natural laterite samples need to be conducted, as it is possible that they behave differently to the synthetic samples, and perhaps a longer treatment time is needed to fully remove ferrihydrite from these samples.

Given the complex nature of the natural samples investigated in this study, it is not possible to make definitive conclusions. However, trends were observed that could be compared with the results of experiments carried out on synthetic systems and suggestions as to the reasons for any differences in results have been made. From the

research presented and discussed here, conclusive proof for the presence or absence of ferrihydrite in the natural laterite systems cannot be shown. The results appear positive, and the use of TGA to determine the presence of ferrihydrite and (perhaps) other metastable Fe-oxyhydroxide phases in natural systems is certainly worth pursuing. This investigation needs to be continued using a larger set of samples with variations in the mineralogy, and the experimental work extended to account for the large number of mineral phases involved.

6.5. References

1 S. A. Gleeson, R. J. Herrington, J. Durango, C. A. Velasquez, G. Koll, *Economic Geology*, (2004) **99**, 1197-1213.

2 X. Wang, R. G. McDonald, R. D. Hart, J. Li, A. van Riessen, *Hydrometallurgy*, (2014) **141**, 49-58.

3 H.M.A. Hunter, R.J. Herrington, E.A. Oxley, *Minerals Engineering*, (2013) **54**, 100-109.

4 T. Norgate, S. Jahanshahi, *Minerals Engineering,* (2011) **24**, 698-707.

5 Poster Presentation, A. Karacar, H. Hunter, R. Herrington, An Infrared Spectral Reflectance Study of Nickeliferous Goethite and its Applications to Interpretation of Satellite Imagery.

6 Çaldağ Nikel, http://caldagnikel.com.tr/en/hakkimizda.php, last accessed August 2013.

7 R. Thorne, R. Herrington, S. Roberts, *Mineralium Deposita,* (2009) **44**, 581-595.

8 Google Maps, www.google.com/maps, last accessed February 2013.

9 http://www.bhpbilliton.com/home/businesses/aluminium_manganese_nickel/Pages/default.aspx last accessed August 2013.

10 http://www.mining-technology.com/projects/cerro-matoso/ last accessed August 2013.

11 Natural History Museum and Sardes Nikel Madencilik A.S.(SN), IAPP NICAL project, Secondment Report, March 2010.

12 H. Stanjek, P.G. Weidler, *Clay Minerals,* (1992) **27**, 397-412.

13 R.M. Cornell, R. Giovanoli, *Clays and Clay Minerals,* (1989) **37**, 65-70.

14 E. Wolska, W. Szajda, P. Piszora, *Journal of Thermal Analysis,* (1992) **38**, 2115-2122.

15 E.E. Sileo, A.Y. Ramos, G.E. Magaz, M.A. Blesa, *Geochimica et Cosmochimica Acta*, (2004) **68**, 3053-3063.

16 M.H. Ebinger, D.G. Schulze, *Clays and Clay Minerals,* (1989) **37**, 151-156.

17 U.G. Gasser, E. Jeanroy, C. Mustin, O. Barres, R. Nüesch, J. Berthelin, A. J. Herbillon, *Clay Minerals,* (1996) **31**, 465-476.

18 M.L.M. Carvalho-E-Silva, C.S.M. Partiti, J. Enzweiler, S..Petit, S.M. Netto, S.M.B. De Oliveira, *Hyperfine Interactions,* (2002) **142**, 559-576.

19 M. Alvarez, E.H. Rueda, E.E. Sileo, *Geochimica et Cosmochimica Acta*, (2007) **71**, 1009-1020.

20 R.M. Cornell, *Clay Minerals,* (1991) **26**, 427-430.

21 P.R. Anderson, M.M. Benjamin, *Environmental Science & Technology,* (1985) **19**, 1048-1053.

22 R.K. Vempati, R.H. Loeppert, *Clays and Clay Minerals*, (1989) **37**, 273-279.

23 O.K. Borggaard, *Zeitschrift für Pflanzenernährung und Bodenkunde,* (1992) **155**, 431-436.

Chapter 7.

Conclusions and Further Work

7.1. Conclusions and Further Work

This research project was funded by the mining company European Nickel plc, (later ENK plc), who developed an atmospheric heap leaching process for the extraction of Ni from limonitic (goethite-rich) laterite ores. This extraction process was originally developed for a laterite deposit in Çaldağ, Turkey and was hailed as an environmentally conscious method due to the low energy costs involved in the process, which was carried out at atmospheric pressures and temperatures. Further investigations by European Nickel into Çaldağ and other laterite deposits in their portfolio (e.g. Acoje in the Phillipines), found that ore materials with seemingly similar properties, showed large variations in their leachability, i.e. the ease with which Ni is extracted.

This PhD project aimed to investigate the reasons why goethite rich ores originating from laterite deposits display such variation in their leachability, with certain ores leaching Ni more favourably than others. The reasons behind the differences in the leachability need to be understood to enable mining companies to 'screen' the ore before processing. Development of simple characterisation techniques for the ore materials which could potentially be used on site, either at the mine or processing plant, would give a better idea of how to approach the extraction, or simply allow selection of the ores most amenable to the heap leach process.

In order to establish reasons for the variability in the ease with which nickel could be extracted from these ores, the precise way in which nickel was associated with goethite needed to be understood; i.e. whether the nickel was structurally incorporated via isomorphous substitution for iron, or associated in some other way with a separate phase or phases. The laterite systems in which goethite forms are inherently complex, containing multiple mineral phases. As the nickel is known to be associated with goethite (or iron oxyhydroxide phases), a synthetic study was conducted to investigate the formation of goethite, both in the pure Fe form (FeOOH) and in the presence of nickel ($Fe_{1-x}Ni_xOOH$). Studying the formation processes synthetically allows the conditions to be controlled, so the association between Ni and goethite (or other iron oxyhydroxide phases) can be investigated without the presence of other competing ions or mineral phases found in the natural ore body. Once the formation processes and the association between Ni and goethite is understood in simple, synthetic systems, the findings can be used to draw comparisons with the more complex laterite deposits.

From preliminary studies on the formation of goethite discussed in this thesis (Chapter 3), it was proposed that a nickel rich ferrihydrite phase could have formed in laterite deposits alongside goethite. Nickel and other foreign cations present in the system are known to

have a stabilising effect on the ferrihydrite precursor, inhibiting its transformation to goethite. This theory could account for the differences in the leachability of the ore material; nickel may be removed more easily from the poorly crystalline ferrihydrite phase than from the more crystalline goethite.

In order to find out if ferrihydrite is present in ore material, techniques to accurately and rapidly identify ferrihydrite in the presence of goethite, as well as to quantify the amount of ferrihydrite associated with a goethite phase, needed to be developed. Characterisation of ferrihydrite is often problematic, with its presence in natural systems often ambiguous, and it is thought that its true abundance in the environment is probably underestimated. To address this issue, a unique approach to identifying ferrihydrite was devised, by using a number of different and complimentary techniques to characterise goethite/ferrihydrite 'standards' (mixtures of the two phases where the exact proportions were known), to establish the best way to confirm the presence of ferrihydrite. Furthermore, a washing technique was developed using EDTA, which was able to remove ferrihydrite from goethite samples without affecting the goethite itself.

Analysis of synthetic goethite material to establish the presence of ferrihydrite using the characterisation methodology that was developed here was successful. Thermal analysis of the samples proved to be the most promising identification and quantification technique, whereby a strong relationship was observed between the weight lost due to surface adsorbed water in each sample and the amount of ferrihydrite that was present. Analysis of the goethite samples prepared with increasing levels of nickel demonstrated a linear relationship between the weight loss which occurred below 40°C and the amount of nickel added to the synthesis. This indicated that as the amount of Ni increased, the proportion of ferrihydrite also increased; supporting the theory that Ni has a stabilising effect on ferrihydrite and so could be present in lateritic material alongside goethite.

Estimations of the proportion of ferrihydrite present in samples from thermal analysis data was found to be most reliable for the samples that were synthesised at 70°C. This was thought to be due to the way in which the quantification method was developed, as the goethite standard that was used to create this technique was also synthesised at 70°C. The synthesis temperature used to prepare goethite samples affects the particle size of the resulting product. Goethite samples prepared at lower temperatures have smaller particles, and therefore a larger surface area, so more surface water is likely to be adsorbed on them than on those synthesised at higher temperatures. Due to the differences in the amount of surface water associated with the goethite samples, as a result of the particle size, the quantification method overestimated the amount of

ferrihydrite present in the samples prepared at lower temperatures, as it did not take into account the increased water associated with goethite itself.

In order to improve this methodology to enable more accurate quantification of ferrihydrite in a wider range of samples, further work needs to be carried out to refine the technique to enable it to account for the differences in the amount of surface water associated with goethite. One possible way to investigate this would be to prepare a range of goethites under different synthesis conditions, to produce samples with varying particle sizes. After ensuring all ferrihydrite was removed from the samples using the EDTA wash, the particle size for each goethite sample would need to be established (perhaps by an imaging technique, e.g. TEM). Finally, TGA should be carried out on the samples in order to relate the weight loss due to surface adsorbed water on the goethite itself to the particle size. With this information, it may be possible to adapt the ferrihydrite quantification methodology to factor in these differences.

After confirming that ferrihydrite was present in synthetic Ni-rich goethite systems, and that the amount increased with increasing nickel, the way in which nickel was partitioned between the two phases was investigated. ICP-OES analysis of the EDTA washing solutions, resulting from removal of the associated ferrihydrite from the goethite samples, and SEM of the solid samples, before and after washing, showed that Ni was mainly associated with the ferrihydrite phase. The maximum amount of nickel found to be structurally incorporated into the goethite samples prepared in this study was ~2.5 mol%, far lower than the 5.5 mol% maximum reported elsewhere.[1] The lower levels of Ni incorporation that have been achieved in the goethite samples prepared in this work compared to those described previously are likely to be due to differences in the synthesis procedures. To develop this work further, sets of samples prepared under different synthesis conditions, for example an increased duration or under hydrothermal conditions, are required. These samples would then be treated using the EDTA washing method and the presence and quantity of ferrihydrite determined using the characterisation techniques developed in this work. Finally the actual Ni incorporation levels in the goethite (and therefore the amount associated with ferrihydrite) could be established, enabling comparison between the different synthesis procedures.

A key result of this work was that samples prepared at 70°C, for 7 days with a target composition of 8 mol% Ni ($Fe_{0.92}Ni_{0.08}OOH$), had only ~2.5 mol% Ni incorporated into the goethite structure, i.e. only 35% of the Ni originally added to the synthesis. The majority of the nickel, therefore, is assumed to be associated with the ferrihydrite phase. The effect of increasing the synthesis duration, to see if, and how much, more of the Ni-

ferrihydrite transforms to Ni-goethite if left for a longer time period should be investigated. Furthermore, the nature of the relationship between nickel and ferrihydrite, whether it is adsorbed to the surface or structurally incorporated in some way, could be explored.

It is possible that some of the nickel removed by the EDTA wash and assumed to be associated with the ferrihydrite phase is actually adsorbed to the goethite surface. The extent of nickel adsorption to goethite was not investigated as part of this research, so the proportion that may be surface adsorbed, rather than associated with ferrihydrite, is not known. Further work is needed to assess the degree of nickel surface adsorption on goethite, and to investigate if its presence has any effect on the ferrihydrite detection and quantification techniques developed in this work.

The synthesis temperature was also shown to affect the ultimate residence of the nickel in the goethite/ferrihydrite system. In Chapter 5.4., experiments into the EDTA washing procedure showed that more nickel was removed in the washing process from the goethite synthesised at 70°C than was removed from the samples synthesised at 20°C. The opposite was found for the amount of iron removed, with less Fe extracted in the EDTA wash of the samples synthesised at 70°C than at 20°C. This suggests that at the lower synthesis temperature over the synthesis period investigated, more ferrihydrite remains in the sample, but more of the nickel is incorporated into the structure of goethite. At higher temperatures, although a higher proportion of the sample appears to transform to goethite (as less Fe was removed in the EDTA wash), a higher percentage of the nickel is retained in the precursor phase.

The techniques developed and tested on synthetic samples for the identification and quantification of ferrihydrite have been shown to work well. Using these same methodologies for characterisation of goethite recovered from laterite deposits, which are inherently more complex systems, proved more challenging. The main reason for this is that the samples that were provided for this study contained significant amounts of other mineral phases, alongside goethite. Furthermore, only a relatively small number of samples were made available for this research, and a much larger sample suite is needed to continue this work.

The thermal analysis technique to identify ferrihydrite showed great potential when used to characterise the lateritic goethite samples, with a positive correlation observed between the weight loss measured below 40°C and the amount of foreign cation assumed to be present in the goethite/ferrihydrite system. Elemental analysis of the natural goethite samples showed a whole range of different cations were present (e.g. Al, Co, Mn, Cr), but with the data available it was impossible to ascertain which foreign cations were

associated with goethite/ferrihydrite phases, and which were associated with separate, unrelated mineral phases. It is also possible that organic acids (e.g. humic acid), which may be found in deposits of this kind, could influence the stabilisation of the ferrihydrite phase in addition to the metal cations.

Elemental analysis of the laterite samples found that many contained Ni and Co; these elements are known to associate with goethite/ferrihydrite systems and are the two elements that mining companies extract from limonitic laterite ore in deposits of this type. To allow correlations between foreign metal cation content, weight loss and presence of ferrihydrite to be made, it was assumed that nickel and cobalt were associated with the goethite/ferrihydrite system. However, this may not have been the case. Further work needs to be conducted on the natural laterite samples, by separating the goethite/ferrihydrite from the other mineral phases present. This would allow accurate elemental analysis to be carried out to determine which elements (and the amounts of those elements) that were associated with the goethite/ferrihydrite system, rather than part of another mineral phase. This could be achieved in two ways; samples could be more carefully selected from the bulk ore material, to try and pick those which were wholly goethite/ferrihydrite, or the material could be processed in a way which would separate the goethite/ferrihydrite from the other mineral phases. Both of these methods would be challenging, but Carvalho-e-Silva *et al.* (2002) propose a method to isolate goethite from bulk ore material which should be attempted.[2]

Although a complete success when used on synthetic samples, the EDTA washing technique needs further development to establish its effectiveness at removing ferrihydrite from natural samples. It is possible that longer treatment times may be required, as analysis of the natural laterite samples after washing suggested that only very small amounts of ferrihydrite were being removed. Alternatively, perhaps only very small amounts of ferrihydrite are present in the natural samples, again highlighting the need for further characterisation work. It is also vital to establish the effect that the EDTA washing solution may have on the other mineral phases present in the laterite samples, as this study only investigated its interaction with the goethite/ferrihydrite system.

From the research presented and discussed in this thesis, proof of the presence or absence of ferrihydrite in laterite systems, causing variations in the leachability of the ore materials, could not be conclusively established. From the results of investigations on synthetic systems, it certainly seems that the presence of nickel (and possibly other cations) associated with ferrihydrite in laterite systems, may be the root cause for variations in the leachability observed in the ore materials. The thermal analysis

technique developed here successfully identified and quantified ferrihydrite in the presence of goethite in synthetic systems. With further refinement of the methodology, to enable a larger range of sample types to be accurately analysed, it could certainly be used as a screening tool for laterite ores.

7.2. References

1 B. Singh, D. Sherman, R.J. Gilkes, M.A. Wells, J.F.W. Mosselmans, *Clay Minerals,* (2002) **37**, 639-649.

2 M.L.M. Carvalho-E-Silva, C.S.M. Partiti, J. Enzweiler, S..Petit, S.M. Netto, S.M.B. De Oliveira, *Hyperfine Interactions,* (2002) **142**, 559-576.

Chapter 8.

Appendices

Appendix 1. ICP-OES

Calibration Standards

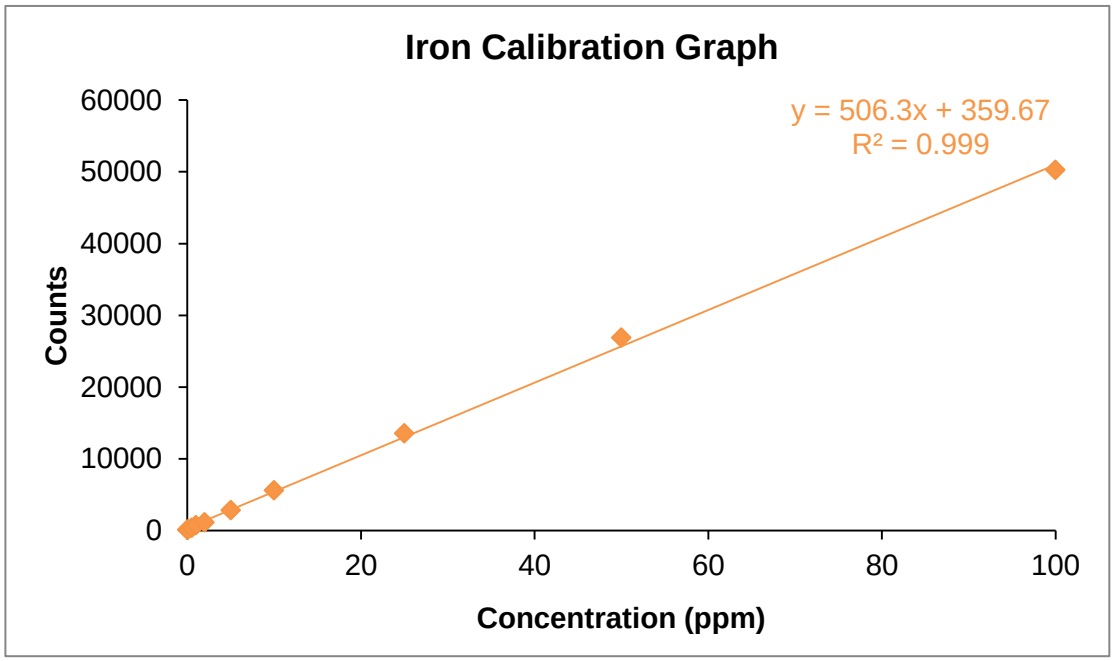

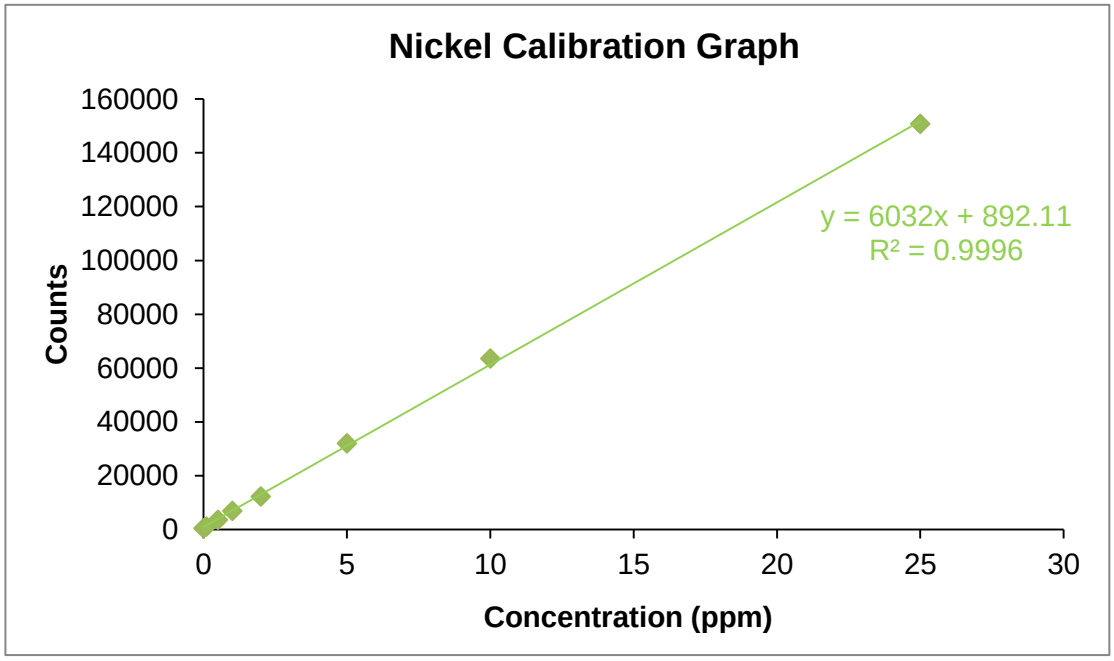

Limit of Detection (LOD) and Limit of Quantification (LOQ)

Iron calibration: $y = 506.3x + 359.67$

Nickel calibration: $y = 6032x + 892.11$

Blanks	Counts	
	Iron	Nickel
Blank 1	131.1	406.7
Blank 2	143.3	396
Blank 3	147	400.1
Blank 4	144.1	390.2
Blank 5	138.3	393.2
Blank 6	140.6	393.9
Blank 7	142	398.5
Blank 8	142.9	396.1
Blank 9	141.1	393.8
Blank 10	139.6	392
Average Counts	141.0	396.1
Standard Deviation	4.3	4.8
LOD (ppm)	**0.025**	**0.002**
LOQ (ppm)	**0.084**	**0.008**

Appendix 2. PXRD

Reproducibility of Ferrihydrite Estimation Technique

Repetition	Intensity of 110 goethite reflection	Average intensity of background ~39.2 – 40.1° 2θ
1	2674	70
2	2701	68
3	2706	68
4	2668	70
5	2641	70
6	2694	69
Average Intensity	2681	69
Range	65	2
% Variation	2.4	2.9

110 Goethite Reflection

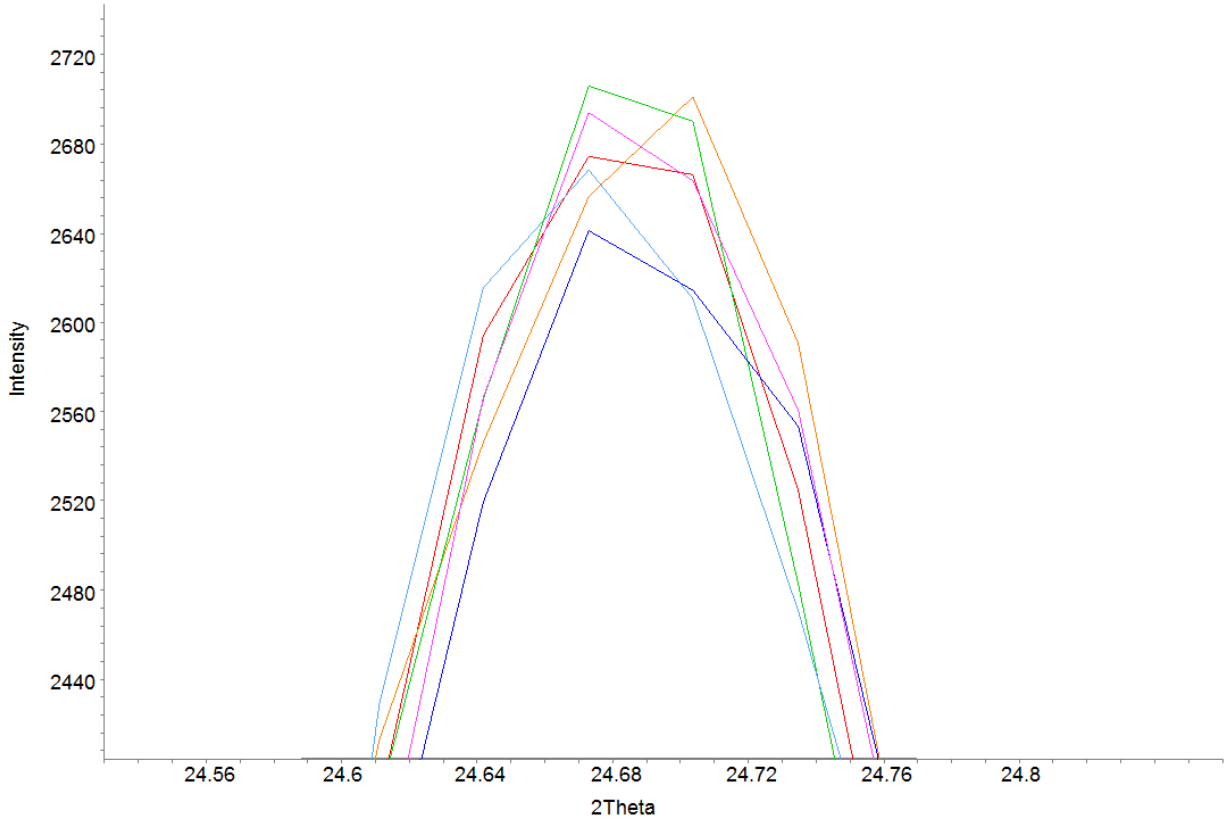

Background ~39.2 – 40.1° 2θ

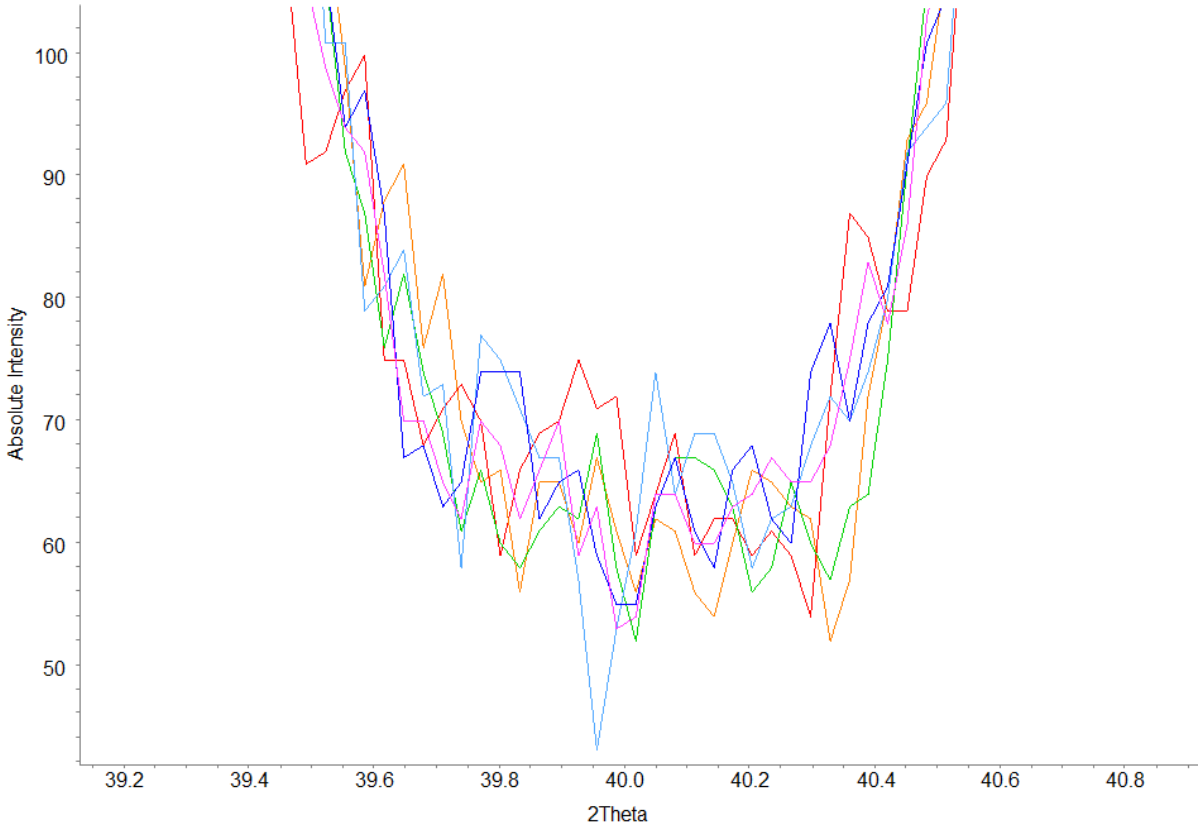

Appendix 3. TGA

Reproducibility of Ferrihydrite Estimation Technique

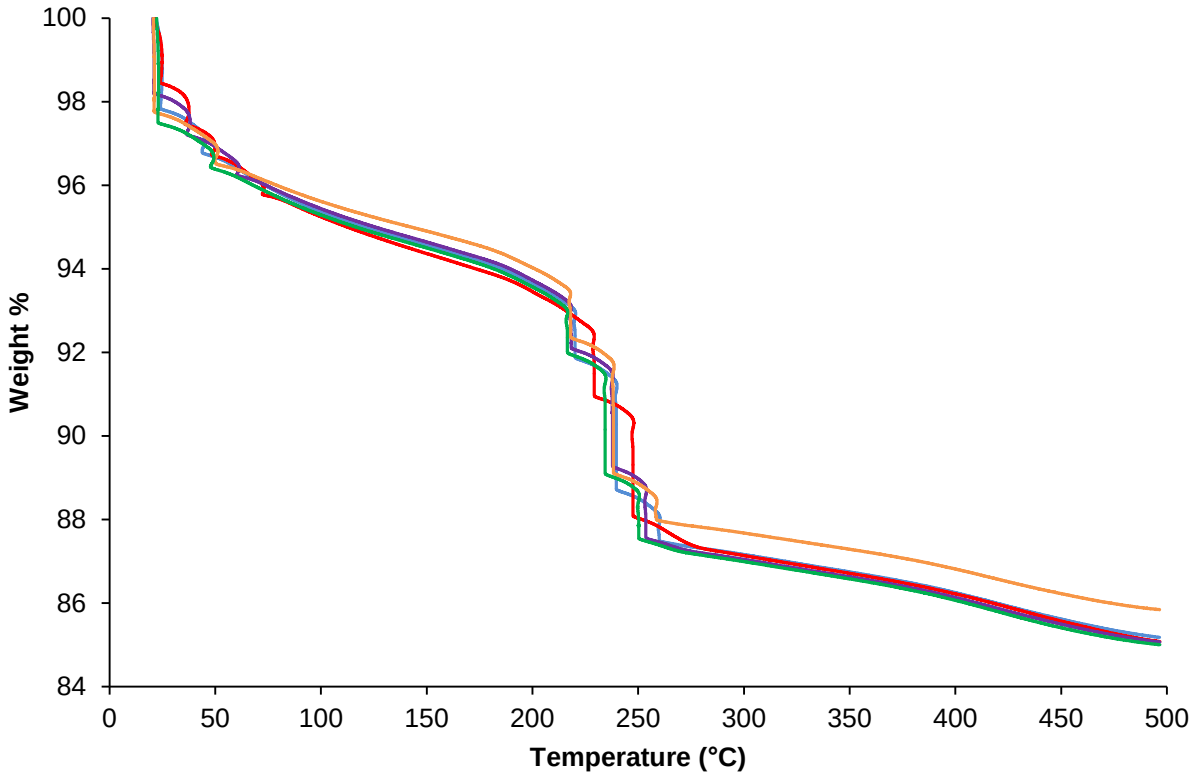

Sample	Weight loss below 40°C (wt%)	Estimated ferrihydrite content of sample(wt%)
1	2.6	18
2	2.6	19
3	2.8	21
4	2.7	19
5	2.9	21

Appendix 4. Conference Submissions

June 2013	Oral presentation – Minerals for Life, Edinburgh.
March 2013	Oral presentation – Natural History Museum Student Conference, London.
January 2013	Poster presentation – Mineral Deposits Studies Group Winter Meeting, Leicester.
April 2012	Oral presentation – Loughborough Chemistry Department Research Network Day.
March 2012	Poster presentation – Natural History Museum Student Conference, London.
December 2011	RSC Solid State Group Christmas Meeting, Liverpool.